The effect of the natural ageing process on vesicular release dynamics from an identified serotonergic neuron in the central nervous system of the pond snail, Lymnaea Stagnalis.

A thesis submitted in partial fulfilment of the requirements of the
University of Brighton for the degree of Doctor of Philosophy

March 2023

Nadezhda Velichkova

Abstract

Ageing is associated with cognitive decline, attributed to a decreased ability of neurons to transmit and sense signals. Despite this, little work has explored how ageing affects neurotransmitter release. This study explored how increasing age affected vesicular neurotransmitter content and release from the cerebral giant cell (CGC), a key neuron involved in long-term memory formation in the pond snail *L. stagnalis*.

Micro and nano-tip carbon-fibre electrodes in combination with single cell amperometry (SCA) and intracellular vesicle impact electrochemical cytometry (IVIEC) were used to monitor somatic vesicular 5-hydroxytryptamine (5-HT) release and intracellular vesicle content of the CGCs. Gaussian mixture clustering algorithm was applied to the collected data to identify different population of vesicles with different modes of release. CGCs of young and old snails were capable of spontaneous vesicular 5-HT release. The Ca^{2+} ionophore ionomycin was able to trigger release from the young CGCs but was less successful in the old. No significant differences were observed between spontaneous or ionomycin-evoked release events. Ageing significantly increased the number of serotonin molecules released per vesicle from the CGCs, due to increases in the width, rise and fall time of the events, but did not change their amplitude. The proportion of transmitter released by the CGCs increased from 46% in the young to 78% in the old. Cluster analysis suggested the existence of two different pools of intracellular vesicles releasing in two different modes with the number of molecules released increasing with age for both modes. The observed age-related differences in the kinetics of the release events and quantity of serotonin release from the CGCs could be due to changes in the lipids composing the neuronal membranes. Therefore, high-performance liquid chromatography-mass spectrometry was used to determine the effect of age on the lipids of the central nervous system. Age significantly increased the total concentration of sphingomyelin, cholesteryl esters, phosphatidylcholine, lyso-phosphatidylcholine and phosphatidylglycerol, but decreased the phosphatidylinositol. These findings suggest the age-related changes in the lipid composition may underly the changes in neurotransmitter release.

In conclusion, this thesis has shown for the first time that the natural ageing process not only increases the amount of serotonin release but that this occurs due to an increase in the proportion of serotonin released from an individual vesicle. These effects appear to be consistent for both pools of vesicle identified using cluster analysis and strongly suggest that plasticity at the level of the individual vesicle is reduced with increasing age.

Declaration

I declare that the research contained in this thesis, unless otherwise formally indicated within the text, is the original work of the author. The thesis has not been previously submitted to this or any other university for a degree and does not incorporate any material already submitted for a degree.

Signed: Nadezhda Velichkova

Dated: 31/03/23

Acknowledgements

Table of Figures

cytofacial leaflet. PI(4,5)P2 localized on the cytofacial leaflet is decreased, which is similar for cholesterol, which is spread between the two leaflets, rather than being concentrated at the cytofacial leaflet such as in mature membranes. Figure adopted form Ledesma et al. (2012). 216

List of Tables

Definitions

5-HT   5-hydroxytryptamine

AA   Arachidonic Acid

AHP   Afterhyperpolarization

AMPARs   α-amino-3-hydroxy-5-methyl-4-isoxazole   propionic   acid   (AMPA) receptors

AP   Action Potential

CE   Cholesterol Ester

CGC   Cerebral Giant Cell

CNS   Central Nervous System

CPG   Central Pattern Generator

DAG   Diacylglycerol

EPSP   Excitatory Postsynaptic Potential

I_{foot} The current of the foot

I_{max} Amplitude of the event

IP3   Inositol-1, 4, 5-triphosphate

IVIEC   Intracellular Vesicle Impact Electrochemical Cytometry

LD   Lipid Droplet

LDCV   Large Dense-core Vesicle

LTCC   L-type voltage gated Ca2+ channels

LTD   Long-term Depression

LTM   Long-term Memories

LTP   Long-term Potentiation

munc-18   Mammalian homologue of unc-18

NMDAR   N-methyl-D-aspartate (NMDA) receptors

PA   Phosphatidic Acid

PC 12   Phaeochromocytoma cells

PC   Phosphatidylcholine

PE   Phosphatidylethanolamine

PG   Phosphatidylglycerol

PI   Phosphatidylinositol

PKC   Protein Kinase C

PLA   Phospholipase A1/2,

PLC   Phospholipase C

PLD   Phospholipase D

PS   Phosphatidylserine

PSF   Pre-spike Foot

PUFA   Polyunsaturated Fatty Acids

SCA   Single Cell Amperometry

SCV   Small Clear Vesicles

SM   Sphingomyelin

SNAP-25   Synaptpsomal- associated protein of 25kDa

SYT1   Synaptotagmin 1

$t_{1/2}$ Width of the event at half of its amplitude

t_{fall} Peak to fall from 75% to 25% of its maximum

t_{foot} Lifetime of the foot

t_{rise} Peak to rise from 25% to 75% of its maximum

VAMP   Vesicle- associated Membrane Protein

1 General introduction

1.1 Ageing

In 2020 the UK's population had reached 67.1 million and it is predicted that by 2030 it will reach 69.2 million. The growth is accompanied by an increase of the percentage of old people. In 2020, people aged 65 years and older comprised 18.6 % of the population, a value predicted to increase to 21.7 % by 2030, and people aged 85 years and over comprised 2.5 % of the population, predicted to nearly double to 4.3 % by 2045. For comparison in 1996 the percentage of people aged 65 years and older was only 15.9 % of the population (Gilbert-Johns et al., 2022). Ageing in humans is accompanied by normal and pathological cognitive decline, which can affect the day-to-day life of people. This necessitates the provision of care, including medical treatments of diseases such as Alzheimer's and Parkinson's, therefore demanding more resources of the social care system. Understanding better the process of normal ageing and how it differs from disease states could provide us with better plans of how to keep older people healthier and independent for longer (Kennedy et al., 2014).

1.2 Effects of ageing on cognition in humans

Changes in cognition are observed in humans as an effect of normal ageing. Cognitive functions such as processing speed and psychomotor abilities start to decline in the beginning of the third decade of life (Salthouse, 2012). Slowed processing speed can influence a range of cognitive domains such as attention, memory, language, visuospatial abilities and executive function (Harada et al., 2013). The cognitive changes observed with age have been correlated to structural and functional changes in the brain, particularly to a decline of grey and white matter volume. Although one of the possible causes of loss of grey matter volume could be due to neuronal death, as it might be in the case of Alzheimer's dementia, where high levels of beta-amyloid are

associated with decrease of the volume of the hippocampus (Jack Jr et al., 2008), in normal ageing, loss of grey matter is better explained by structural changes of the neurons. Such changes usually include reduction of the length and the number of the neuronal dendrites, decrease of axon numbers, larger number of demyelinated axons and loss of synapses (Morrison and Hof, 1997, Pannese, 2011).

1.3 Effect of ageing on memory

Most commonly older adults complain of changes in memory and tend to perform worse than young people on a variety of learning and memory tests (Park et al., 2002, Park and Bischof, 2022). Memories are defined as the ability to recall explicitly or implicitly previously encoded information. Based on the duration for which memories are retained and the type of information retrieved, memories are classified as long-term memories, comprised of declarative and nondeclarative constituents, and short-term memories. Declarative (explicit) memories are memories of events (episodic memory), facts (semantic memory) or perceptual information (perceptual memory), which are consciously retrieved, whereas nondeclarative (implicit) memories are memories of learned skills or procedures, such as the knowledge to drive a car or to play an instrument, which are acquired gradually and slowly, but can be retrieved and used unconsciously. Contrary to long-term memories, which are usually stored for long periods of time (minutes to years), short-term memories, are memories held in storage, by a process termed working memory, for a very short periods of time (seconds) (Brickman and Stern, 2009). The performance of the distinct memory systems is differentially affected by the ageing process. Semantic, perceptual and procedural memories are usually relatively unaffected, but episodic and working memories suffer substantial losses, observed as difficulties in manipulation of information held in mind and the recollection of certain events (Craik and Rose, 2012).

The acquisition (encoding) storage (retention) and retrieval of memories is supported by numerous separate systems that include the hippocampus, the amygdala, the neostriatum and the cerebellum (Squire, 2004). Initially newly formed memories,

subject to disruption by interference, are stabilized into more resilient long-term memories by a process termed memory consolidation (Alberini et al., 2012). The consolidation of memories is possible due to the high plasticity of the neurons in memory relevant areas, which modify their function and structure following experience generated activity (Alberini et al., 2012, McGaugh, 2000). This is most noticeable at the synapses, where the efficacy of the synaptic transmission can be potentiated or depressed depending on the activity pattern generated by the experience (Korte and Schmitz, 2016). Activity dependent synaptic plasticity is observed in most brain regions. However, the most research so far has been performed on the hippocampus, which is considered essential for the formation of spatial, contextual and episodic memories (Eichenbaum, 2004, Eichenbaum et al., 1999), memories that are lost during the ageing process.

1.4 Mechanism of synaptic plasticity

A process associated with the generation of synaptic plasticity and believed to be one of the neural substrates for learning and memory is long-term potentiation (LTP), first described in two papers by Bliss & Lømo and Bliss & Gardner-Medwin in 1973 (Bliss et al., 1973, Bliss and Lømo, 1973). LTP, together with its counterpart LTD (long-term depression), have been predominantly studied in rodent hippocampal slices, at the excitatory synapse between the CA3 and CA1 regions. Experimentally, LTP is elicited by tetanic high frequency stimulation (100Hz per second) applied to the axons of pyramidal neurons projecting from the CA3 to the CA1 region of the hippocampus. Its effect on the synapse is measured as an increase of the slope of the excitatory postsynaptic potential (EPSP) recorded in the postsynaptic pyramidal cells of the CA1 region. In contrast, LTD is elicited by low frequency tetanic stimulation (5Hz for 3 min, applied twice with an interval of 3min) again applied to cells of the CA3 region, and its effect is measured as a decrease of the slope of the EPSP recorded in cells of the CA1 region. The postsynaptic response of the CA1 pyramidal cells to the tetanic stimulation is due to two major types of glutamate receptors - *N*-methyl-D-aspartate (NMDA)

receptors (NMDARs) and α-amino-3-hydroxy-5-methyl-4-isoxazole propionic acid (AMPA) receptors (AMPARs). Both receptors have channels but are permeable to different extents to different cations (Dingledine et al., 1999). The AMPA receptors involved in LTP in the hippocampus allow the inward movement of Na^+ cations responsible for the generation of most of the excitatory synaptic response observed in the postsynaptic cell. Contrary to them, the NMDA receptors are permeable to Ca^{2+} and Na^+, but they do not contribute as much to the excitatory postsynaptic response observed in the postsynaptic cell. Their limited contribution is because of magnesium ions that block the NMDA channel while the cell is at a negative hyperpolarizing membrane potential. Following stimulation and depolarization of the membrane potential, the magnesium ion dissociates from its binding site allowing the inward movement of Na^+ and Ca^{2+} ions. The increase in the intracellular Ca^{2+} concentration is thought to be the main activator of several molecular cascades leading to the generation of LTP, and therefore the activation of the NMDA receptors is considered necessary for LTP to occur (**Figure 1.1**) (Malenka and Nicoll, 1993).
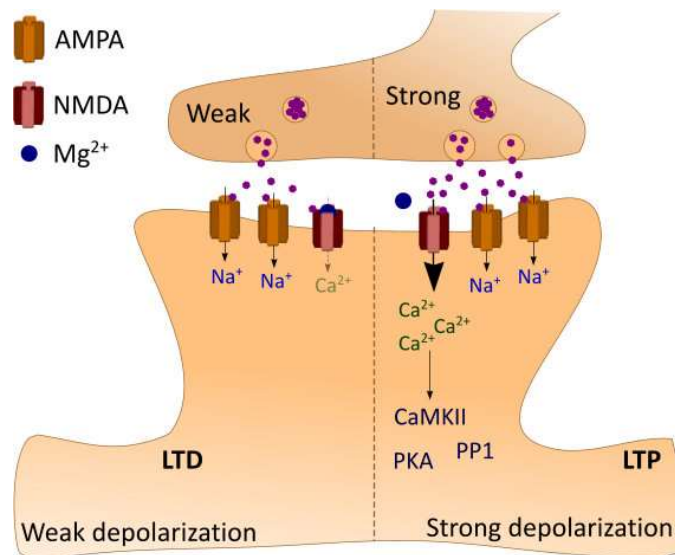
Figure 1.1 Postsynaptic expression of LTP and LTD. LTP is elicited by a high frequency stimulation, whereas LTD by a low frequency stimulation. LTP occurs as a result of intracellular increase of Ca^{2+} concentration through NMDA receptors, leading to the activation of molecular cascades causing AMPA receptors phosphorylation, new mRNA and protein synthesis and an improvement of synaptic connectivity.

Some of the molecules activated by the increase of the Ca^{2+} concentration at the postsynaptic cell are protein kinases such as calcium/calmodulin (CaM)-dependent protein kinase II (CaMKII) (Barria et al., 1997b, Fukunaga et al., 1995), cyclic adenosine monophosphate-dependent protein kinase (PKA) (Blitzer et al., 1998, Makhinson et al., 1999) and phosphatases such as protein phosphatase 1 (PP1). Their activity leads to the phosphorylation of AMPA receptors, which is correlated to the increase of the slope of the EPSP (Dingledine et al., 1999, Barria et al., 1997a, Soderling and Derkach, 2000). Together with an increase of activity of the channel, an increase in AMPA expression at the postsynaptic density, through changes in the trafficking of the channel (Bredt and Nicoll, 2003, Derkach et al., 2007), are the main mechanisms of LTP expression (**Figure 1.2**).
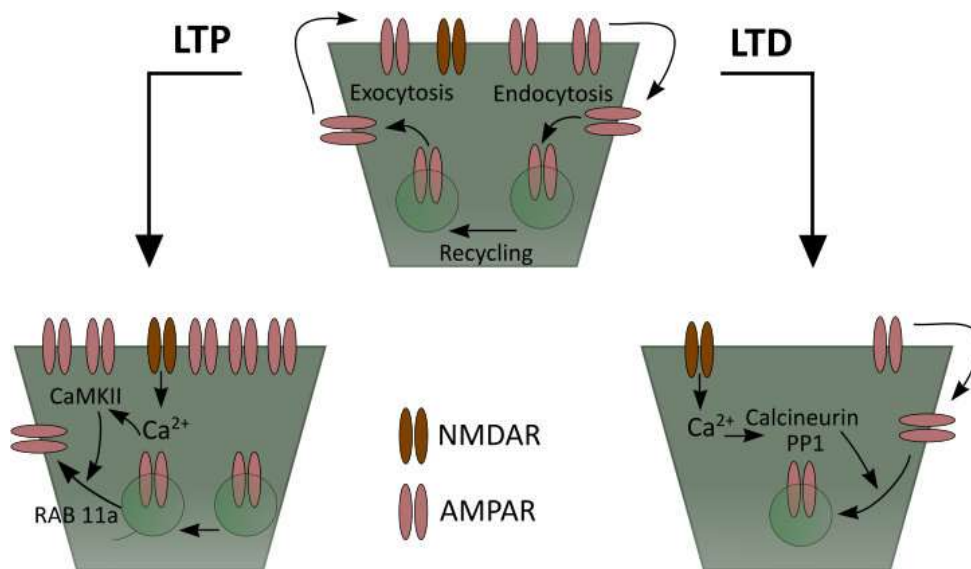
Figure 1.2 LTP and LTD induced trafficking of AMPA receptors at the postsynaptic density. *LTP leads to a raise in the number of AMPA receptors exocytosed to the synapse and LTD causes the raise in the number of AMPA receptors endocytosed and transferred for recycling.*

The maintenance of LTP following its initiation is enabled by the synthesis of new proteins (Reymann and Frey, 2007) at the local dendrite (Sutton and Schuman, 2006) as well as transcription of protein messenger RNAs in the nucleus (Zhou et al., 2006).

In addition to plastic changes observed at the postsynaptic dendrites, LTP is also observed at the presynaptic cells and such an example is seen at the axons of granule cell in the hippocampal dentate gyrus (DG) innervating the dendrites of neurons of the CA3 region (Nicoll and Schmitz, 2005). Like LTP in postsynaptic cells, presynaptic LTP at the DG – CA3 synapse, is considered to be a result of high-frequency tetanic stimulation eliciting increase of presynaptic calcium concentration, but in this case through voltage-dependent calcium channels (Nicoll and Schmitz, 2005, Zalutsky and Nicoll, 1990) and in some cases the activation of kainite receptors in particular the GluR6 receptor (Lauri et al., 2001, Schmitz et al., 2003). The influx of Ca^{2+} in the presynaptic terminal, leads to the triggering of the activity of downstream kinases and proteases. At the DG – CA3 synapse, the induction of presynaptic LTP is a result of the activation of PKA - cAMP signalling (Castillo, 2012). The expression of the presynaptic LTP is observed as an increase of the neurotransmitter released by the presynaptic neurons (Maeda et al., 1997, Weisskopf and Nicoll, 1995), but the exact process by which this happens is still not very well understood, mainly because of difficulties in visualizing and manipulating the axon and its presynaptic terminals (Monday and Castillo, 2017).

1.5 Effects of ageing on neurons and synaptic plasticity

The age-related cognitive decline attributed to changes in synaptic plasticity and disruption of neuronal connections has been assigned to alterations of intracellular Ca^{2+} homeostasis. Both presynaptic and postsynaptic plastic changes are dependent on Ca^{2+} release and therefore require its tight regulation. Age-related decreases in the ability of animals to learn and remember has been related to increased intracellular Ca^{2+} concentration ($[Ca^{2+}]_i$), and it is known as the Ca^{2+} hypothesis of brain ageing (Disterhoft et al., 1994, Khachaturian, 1989, Landfield et al., 1989, Verkhratsky and Toescu, 1998). This increase activates Ca^{2+} dependent K^+ currents and increases the amplitude and duration of the action potential afterhyperpolarization (AHP) as observed in the postsynaptic CA1 neurons, reducing their excitability (Landfield and

Pitler, 1984). The Ca^{2+} hypothesis of brain ageing has been based on the observations of excessive influx of Ca^{2+} through L-type voltage gated Ca^{2+} channels (LTCC) (Landfield and Pitler, 1984, Núñez-Santana et al., 2014, Oh et al., 2016, Proft and Weiss, 2015). The effect of ageing on synaptic plasticity has been predominantly investigated in studies looking at the effect of age on LTP and LTD in the hippocampus, which have demonstrated an increase of the threshold for inducing LTP and a decrease in the threshold for LTD (Barnes et al., 2000, Boric et al., 2008, Kumar et al., 2007, Twarkowski and Manahan-Vaughan, 2016). Thus, an age-associated increase in Ca^{2+} influx, through L-type Ca^{2+} channels reduce the excitability of post-synaptic CA1 neurons, reducing LTP and enhancing LTD.

The defects of postsynaptic LTP in aged rodents in regions of the brain such as the hippocampus and the striatum have been correlated to defects in spatial memory, evaluated with the use of the Barnes circular maze (Bach et al., 1999) and the Morris water maze (Clayton et al., 2002, Schulz et al., 2004), however there is not much information on the effect of age on presynaptic plasticity and how it might correlate to any age-related deficits of learning and memory. A group of messenger RNAs, encoding for proteins involved in exocytosis, such as synaptpsomal- associated protein of 25kDa (SNAP-25), vesicle-associated membrane protein 2 (VAMP-2), mammalian homologue of unc-18 (munc-18) are down regulated in the pituitaries of aged rats and this is paralleled by a decline in anterior pituitary hormone secretion (Jacobsson et al., 1998). Similarly, a reduction of the levels of the synaptic vesicle proteins SNAP-25 and synaptophysin are observed in the hippocampus of old rats (14-24months) (Canas et al., 2009). Such findings imply that age-related decrease of the presynaptic proteins involved in vesicular neurotransmitter release could be influencing the release probability of the presynaptic cell and therefore its contribution to synaptic plasticity and cognitive function.

Understanding the effect of age on the ability of the presynaptic cells to regulate the release of neurotransmitters would provide valuable information on possible interventions, which could restore any age-related changes of the release profile to configurations characteristic of young neurons. This could improve the plasticity of old neurons and their ability to undergo the processes of LTP and LTD. Subsequently this

could lead to improvement of the ability of aged individuals to acquire, store and retrieve new memories so they can continue to live independent healthy lives for longer.

Investigating the effect of ageing on neurotransmitter released from synapses is however a challenging task due to difficulties in the visualization and manipulation of axon buttons. Alternatively, detection of neurotransmitter release can also be achieved from neuronal cell bodies of neurons important in the process of learning and memory formation. A model system of ageing, which can provide a suitable platform for this type of study is the pond snail *Lymnaea stagnalis.* The central neurvous system (CNS) of *Lymnaea* is comprised of identifiable large neurons some of which are involved in plasticity mechanisms of learning and memory formation. A pair of well-studied neurons, involved in the modulation of the feeding behaviour of the snail (Yeoman et al., 1994a, Yeoman et al., 1994b), its ability to learn about new palatable foods (Kemenes et al., 2006b) and affected by ageing (Arundell et al., 2006, Hermann et al., 2007, Patel et al., 2006, Scutt et al., 2015), which also release serotonin from their cell bodies, provide a highly suitable model for the investigation of age-related changes of neurotransmitter release and how this might relate to learning and memory formation.

1.6 *Lymnaea stagnalis* as a model system of learning and memory formation and ageing

Acquisition and consolidation of short- and long-term memories in *Lymnaea* have been assessed using training paradigms such as appetitive classical conditioning (Alexander Jr et al., 1984, Alexander Jr et al., 1982, Audesirk et al., 1982), based on the feeding behaviour of the snail.

1.6.1 Neuronal circuitry underlying the feeding behaviour of Lymnaea

The feeding behaviour of the snail is a cycle of three active phases occurring in a sequence. The first phase is a protraction of a radula (a toothed tongue like structure), which is pushed out of the mouth towards a potential food substrate. This is followed by a rasp phase, during which the food is scraped by the radula and brought back into the mouth and the feeding cycle is completed with a swallow phase, during which the food substrate is swallowed into the oesophagus (Dawkins, 1974). The cycle is generated by the collective work of motor- and inter- neurons. The central pattern generator (CPG) interneurons fire in a three-phase sequence aligned to the three phases of the feeding cycle and the motor neurons stimulate a mass of muscles known as the buccal mass, which through series of contractions and relaxations generates the feeding behaviour (Elliott and Benjamin, 1985, Rose and Benjamin, 1979). The output activity of the CPGs is controlled and modulated by a group of cerebrobuccal interneurons (CBIs) together with a slow oscillator (SO) and the cerebral giant cells (CGCs) (Benjamin, 1989, Yeoman et al., 1994a, Yeoman et al., 1994b) (**Figure 1.3**).
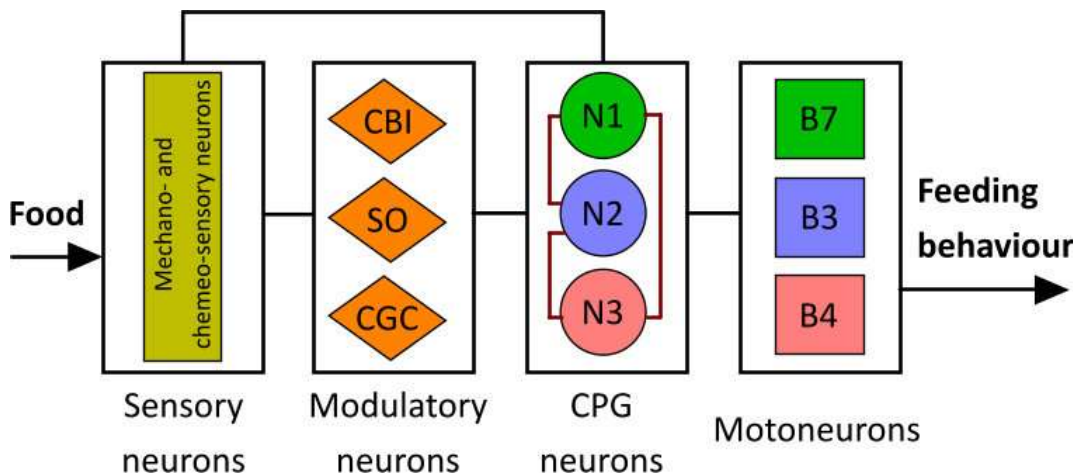
Figure 1.3 The neuronal network underlying the feeding behaviour of Lymnaea. Food is sensed by a combination of mechano- and chemosensory neurons located on the lips and the oesophagus. The sensory input is sent to the modulatory and CPG interneurons (N1, N2 and N3), which generate the feeding cycle through the activation of the buccal mass.

The SO is the cell that influences the frequency control and the maintenance of the feeding cycle (Rose and Benjamin, 1981), whereas the CGCs, through their tonic firing,

provide background excitation to the CPGs making them and the motoneurons, innervating the buccal mass, more likely to respond to excitation (Yeoman et al., 1994a, Yeoman et al., 1994b).

The CGCs are also the cells that show persistent changes following classical appetitive conditioning of the snails. This happens through a single training trail of pairing of an appetitive unconditioned stimulus (US) to a neutral conditioned stimulus (CS), which leads to the formation of short- and long-term memories of the conditioned stimulus (Alexander Jr et al., 1984). The long-term formation of these memories leads to the emergence of a persistent depolarisation of the CGCs soma between 16 and 24 hours after the training, which last for as long as the memory is detectable (Kemenes et al., 2006b) and is based on an increase of persistent sodium current (Nikitin et al., 2008).

1.6.2 Effects of ageing on *Lymnaea*

As humans and vertebrates, *Lymnaea's* ability to consolidate memories is also affected by age (Hermann et al., 2007, Watson et al., 2012, Watson et al., 2013). Old snails like old rodents perform poorer on tests measuring memory formation and consolidation and this is also related to decreases in neuronal excitability (Arundell et al., 2006, Hermann et al., 2007), an enhancement of the AHP (Patel et al., 2006) and intracellular Ca^{2+} dysregulation (Scutt et al., 2015). Several studies have explored the effects of age on snail feeding behaviour. Arundell et al. (2006) reported a decrease of the number of animals responding to sucrose with increasing age and an increase in the duration of the swallow phase of responding animals together with a reduction of the number of bites evoked by sucrose. Hermann et al. (2007) however, didn't observe any difference in sucrose- induced rasping responses between young, middle aged and old animals, but this could have been due to differences in the behavioural methods used, such as: time of starvation before testing, partial or full body exposure to the stimulus and control for novelty. Despite this dissimilarity, both studies noted that there was no difference in the electrical activity of the chemosensory pathway passing sensory information from the lips to the cerebral ganglia. However, Arundell et al., 2006 noted

a reduction in CGC activity in the nerve connecting the cerebral and buccal ganglia, suggesting that this might be related to memory impairments. Consistent with this finding was the observation that increasing age reduced the excitability of the CGCs (Arundell et al., 2006, Hermann et al., 2007). This observation has been confirmed by electrophysiological assessment of the CGCs of conditioned young and old animals, which has reported a more hyperpolarised membrane potential in old snails compared to young snails independent of training (Hermann et al., 2007). Furthermore, the resting membrane potential of CGCs of old snails is not depolarised by conditioning as it is in young snails, pointing out the failure of this mechanism as one of the main factors in the impairment of long-term memories (LTM) in old snails (Watson et al., 2012). The CGC cell body is necessary for LTM formation, and this has been confirmed by an experiment in which the soma of the cell has been ablated. The removal of the soma does not impair the ability of the snail to feed or learn, however it affects the consolidation of LTMs and their recall (Sunada et al., 2017).

The similarity of the age-related changes, in behaviour including the ability to learn and remember and in neuronal excitability, between molluscs such as *Lymnaea* and higher organisms, demonstrates the applicability of the animal model in the investigation of the processes underlying brain ageing. Moreover, *Lymnaea* offers a pair of unique large cells – the CGCs, which undergo somatic plasticity changes, encoding the information enabling the expression of LTM (Kemenes et al., 2006b). The important role the CGCs play in plasticity, the easy access to their large cell body and their ability to release neurotransmitters, makes them an optimal model in the investigation of the effect of age on the mechanism of neurotransmitter release.

1.7 Neurotransmitter detection from single cells

Different techniques have been utilized for the real-time detection and measurement of neurotransmitters released from single cells and neuronal cell bodies, dendrites and axons. Broadly these techniques can be classified into three groups – microdialysis, optical sensing and electrochemical sensing.

Microdialysis can be used for *in vitro* or *in vivo* measurements of a broad range of neurotransmitters. Detection is achieved using a semi-permeable membrane probe, inserted into the brain region of interest. An artificial cerebrospinal fluid is constantly perfused through the probe and membrane permeable neurotransmitters released by nearby cells are collected for analysis. The technique allows for the detection of a broad range of molecules, which currently cannot be detected by electrochemical techniques, however the sampling of the neurotransmitters is not directly from a single synaptic cleft or a cell body and therefore it is hard to judge if it reflects direct release from a specific neuron or if there is overflow from other sources (Chefer et al., 2009). In addition, the time limited diffusion of the used analytes from their release site to the dialysis probe which can be as high as 20s cannot provide the required milliseconds time resolution necessary to acquire detailed information of the dynamics of release (Ganesana et al., 2017) a pre-requisite of this thesis.

Optical sensing of neurotransmitters relies on the use of fluorescent molecules that can absorb and emit light of different wavelengths. A range of microscopy techniques and fluorescent probes can be utilised to investigate neurotransmitter release. Often used probes are optical indicators genetically encoded to vesicular proteins (Lin and Schnitzer, 2016) or styryl dyes loaded into vesicles following electrical stimulation of the neurons to mobilise vesicle exocytosis (Cousin and Robinson, 1999). Vesicles are observed as fluorescent spots and the number of spots is proportional to the number of exocytosed vesicles. A fluorescence microscopy technique that offers a very good spatial resolution for the detection of cellular membrane binding events is Total Internal Reflection Fluorescence microscopy (TIRF) (Combs and Shroff, 2017). When combined with presynaptic capacitance and postsynaptic currents (PSCs) measurements which offer a high temporal resolution, TIRF has been used in the monitoring of exocytosis at the mossy fibre buttons (Midorikawa and Sakaba, 2017). Despite the rich information that can be obtained on neurotransmitter release using optical sensing, the technique still cannot be used for precise measurements of the dynamics of the exocytotic process, and it does not allow for the precise quantification of released neurotransmitter.

The electrochemical sensing techniques are based on the measurements of current, potential or charge produced by the chemical reactivity of the measured molecules. The main electrochemistry detection techniques include voltammetry and amperometry and both utilise sensing electrodes. The voltammetric techniques measure currents generated by the rapid oxidation of oxidizable molecules evoked by a voltage ramp protocol. The applied voltage is started at a value lower than the oxidizing potential of the measured neurotransmitter, then gradually increased to a value above it and returned to the initial value. The resulting current is dependent on the concentration of the measured neurotransmitter. The rate at which the ramp voltage is changed can vary depending on the voltammetry technique e.g. cyclic voltammetry (CV; 100 mV/s) and fast-scan cyclic voltammetry (FSCV; 400 V/s). Both techniques generate a cyclic voltammogram, which is unique to the measured molecule due to the molecule's specific electron transfer rates and its chemical stability and therefore can be used in the identification of different neurotransmitters. Although FSCV is able to offer measurements in the order of 10 ms, this is still much slower than the time of release of single vesicles and therefore not sufficient to provide information of the dynamics of single vesicle release (Ganesana et al., 2017). In contrast to voltammetry, amperometry uses a constant potential that is set to a value above the oxidizing potential of the measured molecule and measures the current generated by the oxidation reaction. As the applied voltage is constant, no temporal limitations to the detection are observed unlike in voltammetry (Wang, 2006). The current transients recorded with amperometry are at a millisecond time scale providing the required time resolution needed to detect the kinetics of individual release events and the amount of neurotransmitter released by each event can be quantified from the area of each current transient using Faraday's law (Q = nNF, Q – integrated charge, n – number of electrons produced by oxidation, F -Faraday's constant and N – number of molecules oxidized). These features make the amperometry technique the most suitable for studies aiming to detect changes in release kinetics and quantify the exact amount of neurotransmitter that is released.

1.8 Thesis outline

As described above ageing often effects the ability of people to continue their lives as independent individuals able to perform normal cognitive functions such as memory, attention and executive function (Harada et al., 2013). This has been linked to a decline of grey and white matter volume, which has been explained by observations of reduced length and number of the neuronal dendrites, decrease of axon numbers, larger number of demyelinated axons, loss of synapses, and decreases in synaptic plasticity (Barnes et al., 2000, Boric et al., 2008, Pannese, 2011, Kumar et al., 2007, Morrison and Hof, 1997, Twarkowski and Manahan-Vaughan, 2016). Most work has focused on how the natural ageing process affects signalling in the postsynaptic neuron with no studies exploring the effects of age on the dynamics of vesicular release from the pre-synaptic cell and how age-related changes in lipids may contribute to this process.

This thesis focuses on the investigation of the effect of age on the vesicular release kinetics and internal neurotransmitter storage of the cell body of the CGCs of young and old snails utilising the high temporal and spatial resolution offered by the amperometry techniques.

Chapter two presents the fabrication and characterization of the micro and nano-tip electrodes used for the recordings of vesicular release and vesicular content.

Chapter 3 examines the ability of the CGCs to release serotonin from their cell bodies, using amperometry in combination with the 10 µm disc carbon fibre microelectrodes.

Chapter 4 examines the effect of age on the content and kinetics of vesicular release and utilizes gaussian mixture clustering to investigate possible modes of release.

Chapter 5 investigates the effects of age on the intracellular vesicular content and the fraction of release utilizing single cell amperometry and intracellular vesicle impact electrochemical cytometry (IVIEC) in combination with the nano-tip carbon fibre electrodes. Gaussian mixture clustering is utilized to investigate the existence of different pools of vesicles.

Lastly to identify possible age-related changes in membrane lipids composition that can influence the dynamics of vesicular release, chapter 6 utilises mass spectrometry to determine the effect of age on the lipids composition of membranes constructing the central nervous system (CNS) of young an old *Lymnaea*.

The hypothesis for the thesis is that ageing influences the intracellular vesicular content, the release content, and the dynamics of release from the CGCs and that this is related to changes in *Lymnaea's* CNS membrane lipids composition.

2 Fabrication and characterisation of carbon fibre micro and nano electrodes used for the detection of oxidizable neurotransmitters.

2.1 Introduction

The aim of this chapter is to describe the fabrication and characterisation of the micro and nano-tip carbon fibre electrodes necessary for the real-time electrochemical detection of intracellular vesicular content and extracellular release of serotonin from young and old CGCs.

2.1.1 Electrochemistry at the surface of charged electrodes.

Electrochemical detection is based on the movement of electrons between the conducting electrode and the molecules being detected. The detection is possibe due to the ability of certain molecules to undergo oxidaton or/and reduction reactions with the application of an electrical potential at the electrode. During oxidation, the molecule undergoing the reaction loses an electron from its highest occupied molecular orbit. The opposite is observed during reduction, where the reduced molecule receives an electron in its lowest unoccupied orbit. Schematically this is presented in **Figure 2.1.**, where R represents the reduced form of the molecule and O represents the oxidized form of the molecule. This reaction is usually written as: O + ne^- <=> R. A few processes can influence this reaction: 1) the transfer of the molecules between the bulk of the solution to the region at the surface of the electrode, 2) the ease with which the electrons are transferred between the molecule and the electrode, 3) the adsorption and desorption reactions at the electrode and 4) any other chemical reactions that may precede the oxidation/reduction reactions (Patel, 2021).
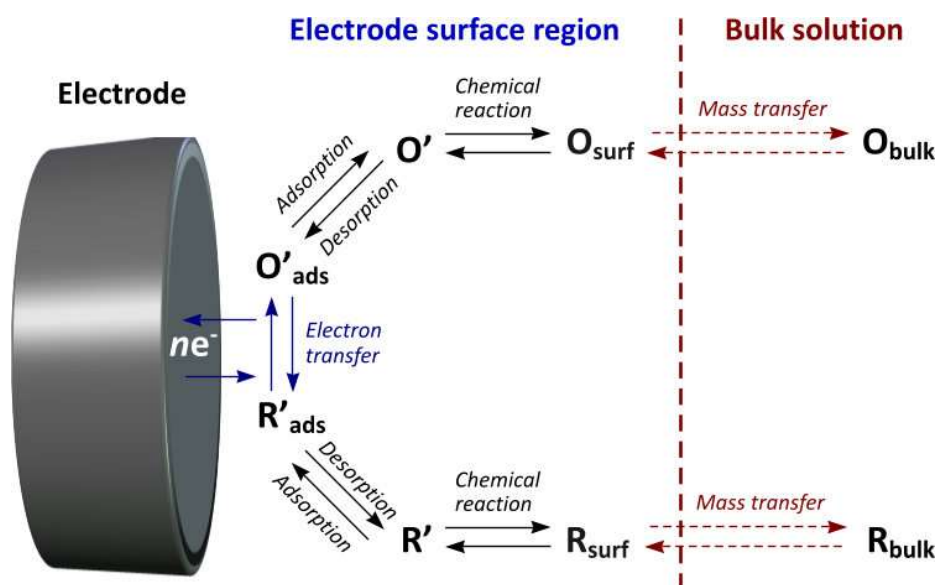
Figure 2.1 The electrochemical reactions taking place at the surface of the electrode.

Molecules undergoing the redox reaction are transferred between the bulk solution and the surface region of the electrode, where due to the application of electrical potential they undergo the redox reaction, either donating or accepting electrons.

2.1.2 Detection of neurotransmitter release from and content of single cells using amperometry.

Amperometry is the electrochemical technique currently offering the highest temporal and spatial resolution for the detection of neurotransmitter release from individual cells (Ganesana et al., 2017, Wang, 2006). In addition, it can also be used to measure the intracellular vesicular content of the cells (Gu et al., 2019, Larsson et al., 2020, Li et al., 2015b, Majdi et al., 2019, Majdi et al., 2017, Ren et al., 2017, Taleat et al., 2019, Zhu et al., 2019). In this technique, a fixed potential is applied to a working electrode causing the oxidation or reduction of the molecules of interest (**Figure 2.2 A**). The initial application of the fixed potential generates a charging current, which is due to the rearrangement of ions from the surrounding solution, around the surface of the electrode. Once the ions arrange, the current settles to a constant baseline (**Figure 2.2 B**) (Patel, 2021).
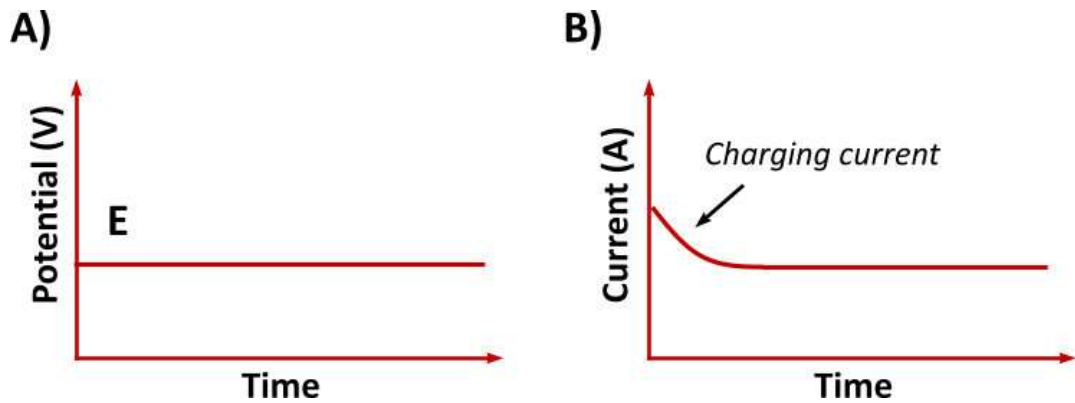
Figure 2.2 Amperometry. A) Applied waveform of a fixed potential E. B) Output current with an initial charging current.

When amperometry is used for the detection of oxidizable molecules released from single cells, a microelectrode is positioned on the surface of the cell and held at a constant potential more positive than the oxidation peak potential of the molecule of interest. Neurotransmitter released by the cell is oxidised, generating a current that is detected as a release event (**Figure 2.3 A**).
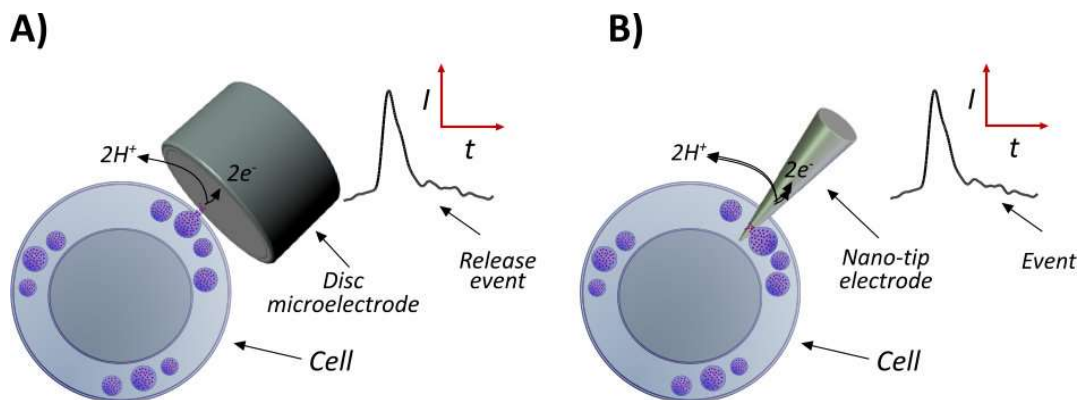
Figure 2.3 Cell-electrode set ups for the detection of extracellular release and intracellular content. A) A microelectrode is positioned on the cell membrane and a working fixed potential is applied to the electrode. Neurotransmitter released from single vesicles is oxidized generating currents observed as release events. B) A nano-tip electrode is positioned inside the cell and a working fixed potential is applied to the electrode. Vesicles inside the cell adsorb on the electrode and an electroporation force opens a pore on the vesicle, allowing for the oxidation of the vesicle content generating an event.

Similarly, for intracellular measurements of vesicular content, a nano-tip electrode is pushed inside of the cell. Again, a fixed potential sufficient to oxidize the molecule of interest is applied to the nano-tip electrode. In the cell, intracellular vesicles adsorb on the surface of the electrode, and due to the electroporation force generated by the charged electrode, open a pore allowing for the oxidation of their content. This generates an oxidation current peak that is observed as an event (**Figure 2.3 B**) (Lima et al., 2021).

Applied in this setup, the intracellular and extracellular amperometry measurements provide high temporal information about the dynamics of release from single vesicles, which is further described in chapters 3, 4 and 5.

2.1.3 Carbon fibre micro and nano electrodes for amperometric detection of neurotransmitters

Carbon based sensing electrodes, including carbon fibre electrodes, have been preferred for the majority of amperometry measurements of neurotransmitter release (Aref et al., 2020, Bertrand, 2006, Bruns et al., 2000, Chen and Ewing, 1995, Colliver et al., 2000, Dong et al., 2014, Gu et al., 2019, Hatamie et al., 2021, Jackson et al., 1995, Larsson et al., 2020, Li et al., 2016a, Li et al., 2015b, Li et al., 2016b, Majdi et al., 2019, Majdi et al., 2017, Ren et al., 2020, Taleat et al., 2019, Trouillon and Ewing, 2014, Wang and Ewing, 2021, Wang et al., 2021, Wang et al., 2022, Ye and Ewing, 2018, Ye et al., 2018, Zhu et al., 2019). The main advantages of these electrodes are the biological compatibility of the carbon fibre, their good electrochemical properties and the ability to measure rapidly (sub-millisecond range) when used with constant potential amperometry (Huffman and Venton, 2009). They have been extensively used for the detection of catecholamines from chromaffin cells (Jiang et al., 2019, Majdi et al., 2019, Wightman et al., 1991, Wightman et al., 1995) dopamine from phaeochromocytoma (PC 12) cells (Li et al., 2016b, Li et al., 2016a, Moore-Dotson et al., 2010, Ren et al., 2017, Westerink et al., 2002, Zhu et al., 2019) and serotonin from

beta cells (Hatamie et al., 2021) and from axonal and somatic sites of cultured leech Retzius neurons (Bruns et al., 2000).

Carbon fibre electrodes are usually made using commercially produced carbon fibres of different diameters and microstructure (Manocha, 2001). The fibre is sealed into a glass capillary and then connected to a conductive wire (Kawagoe et al., 1991, Kelly and Wightman, 1986). The electrodes can be made into a disc microelectrode by bevelling the protruding carbon fibre outside of the glass capillary (Kelly and Wightman, 1986), or into nano-tip electrodes by flame-etching the protruding fibre to form a sharp tip (Strand and Venton, 2008). Due to the nanometre sized tip of the flamed carbon fibre, nano-tip electrodes can penetrate the cell membrane without damaging the cell and therefore have been successfully used to measure the intracellular content of vesicles under different conditions in PC 12, chromaffin cells and neurons (Gu et al., 2019, Larsson et al., 2020, Li et al., 2015a, Majdi et al., 2019, Majdi et al., 2017, Ren et al., 2017, Taleat et al., 2019, Zhu et al., 2019).

The combination of extracellular and intracellular measurements made with carbon fibre microelectrodes and nano-tip electrodes has allowed researchers to determine that release from PC 12 cells is partial rather than full, as only a fraction of the content of the vesicles is exocytosed (Li et al., 2015b). Additional studies have shown that the fraction of release can be regulated by different pharmacological treatments such as cisplatin, zinc, tamoxifen, cocaine and methylphenidate (Li et al., 2016a, Ren et al., 2017, Taleat et al., 2019, Zhu et al., 2019). It has been shown that the fraction of neurotransmitter release can also be influenced by activity-induced plasticity (Gu et al., 2019). These studies have demonstrated that the combination of amperometry with carbon-fibre micro and nano-tip electrodes provides a great methodology that can be used to determine the effect of any condition on the contents of vesicles and release of neurotransmitter from single cells. This makes the method very suitable for the investigation of the effect of age on the neurotransmitter content and release from the CGCs.

2.1.4 Oxidation of Serotonin

The CGCs of *Lymnaea* contain serotonin (5-hydroxytryptamine (5-HT)) (Kemenes et al., 1989, McCaman et al., 1984, Yeoman et al., 1994a, Yeoman et al., 1994b), which is an oxidizable molecule. The oxidation of serotonin during an electrochemical measurement has been described by Dryhurs (Dryhurst, 1990). When serotonin is oxidised at low concentrations (20 µM) on a pyrolytic graphite electrode using cyclic voltammetry, two oxidation peaks are observed. Increasing the concentration to 0.1 mM, increases the amplitude of the second peak relative to the first peak. The oxidation leads to the initial formation of a radical cation (5-HT$^{+\cdot}$) because of the abstraction of a single electron. This is followed by a deprotonation of the radical cation and the production of the 5-HT$\cdot$ radical. The 5-HT$\cdot$ radical then reacts with another molecule of serotonin producing dimers 1 to 4 in **Figure 2.4**, making the reaction irreversible (Dryhurst, 1990).
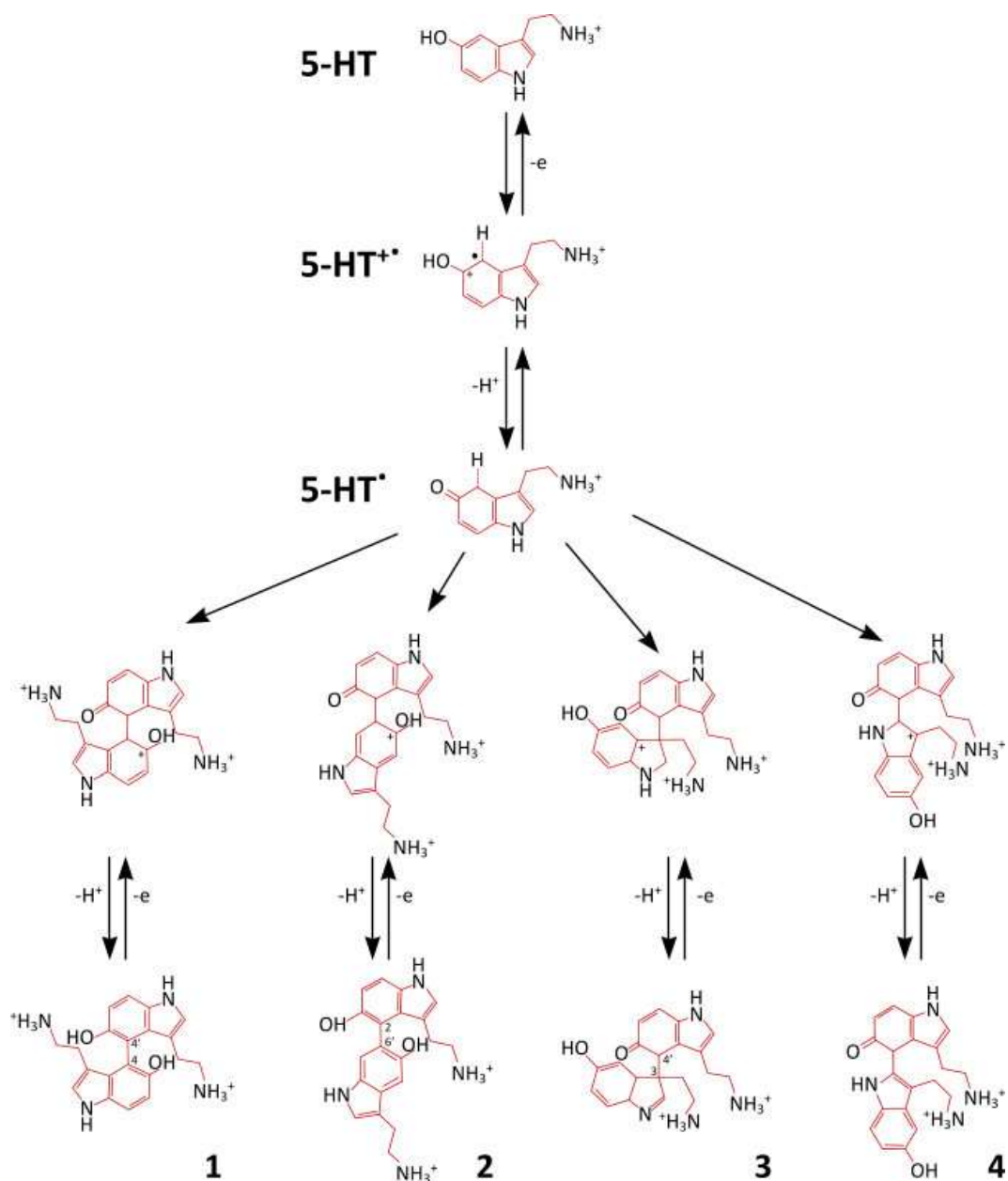
Figure 2.4 Oxidation of serotonin. *5-HT oxidation leads first to the formation of a radical cation 5-HT$^{+\cdot}$, which is deprotonated to the 5-HT$^{\cdot}$ radical. The radical further reacts with another serotonin molecule leading to the formation of 4 dimers (1, 2, 3, and 4), as final products of the reaction.*

The aim of this chapter was to fabricate and characterise carbon fibre micro and nano-tip electrodes that can be used for the detection of extracellular release and intracellular vesicular content of the CGCs of young and old *Lymnaea*.

2.2 Methods

2.2.1 Fabrication of 10 μm diameter carbon fibre disc electrodes

10 μm disc electrodes were developed to be used for extracellular recordings of neurotransmitter release.

10 μm (Goodfellow Cambridge Limited) diameter carbon fibres of lengths slightly longer than 15 cm, were inserted into a glass capillary (length 15 cm, OD 1.5 mm, ID 0.06 mm; Harvard Apparatus, UK), with the use of a suction pump. Following the insertion of the fibre, the capillary was heat pulled using a Dual-Stage Glass Micropipette Puller (model PC-10, Narishige, Inc., Japan) and the carbon fibre extending between the two microtips of the capillary was cut. Any protruding fibre at each microtip (**Figure 2.5 A**) was cut with a scalpel as close to the formed seal as possible under a light microscope (**Figure 2.5 B**). An additional seal between the carbon fibre and the glass capillary was fabricated by dipping the tips of the electrode in epoxy (301, 4 :1 Part A: Part B, EPO_TEC, Sweden) for approximately 60 s (**Figure 2.5 C**). The epoxy coated electrodes were then cured overnight in an oven at 100 °C. Once cured, the microelectrode tips were bevelled at ~45 ° angle using micropipette grinder (model EG-4, Narishige, Inc., Japan) to expose the carbon fibre (**Figure 2.5 D**).

A)
Protruding tip
Carbon fibre
Glass capillary

B)
Close cut
Carbon fibre
Glass capillary

C)
Epoxy coating
Carbon fibre
Glass capillary

D)
Silver paint
Bevelled tip
Silver wire
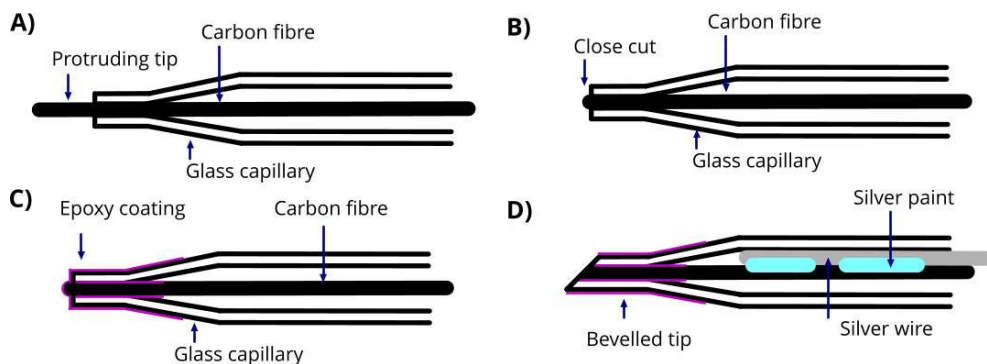
Figure 2.5 Schematics of epoxied, sealed and bevelled microelectrodes. A) Microelectrode with protruding carbon fibre tip B) Microelectrode with carbon fibre cut close to the tip. C) Microelectrode sealed with epoxy and cured overnight. D) Microelectrode with bevelled tip connected to silver wire with silver paint.

The fabrication process was completed with the formation of a connection between the carbon fibres inside the microelectrode tip and a silver wire (0.25 mm Advent, UK) soldered to 1 mm gold pin (RS Components Ltd) with the use of conductive silver paint (RS Components Ltd). The silver paint was spread onto the silver wire with the use of a paint brush and the silver wire was then inserted into the glass capillary. Following the insertion of the silver wire into the glass capillary the gold pin was sealed to the capillary with the use of shrink heat tubing (RS Components Ltd) (**Figure 2.6**).
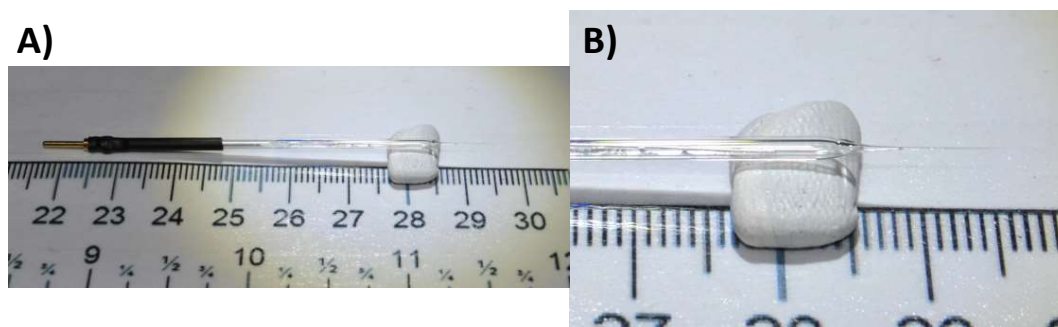
Figure 2.6 Carbon fibre microelectrode. *A) Carbon fibre microelectrode made with 10 µm diameter carbon fibre inserted into glass capillary and connected to a silver wire and gold pin sealed with shrink heat tubing. B) Closer view of the tip of the carbon fibre microelectrode.*

2.2.2 Fabrication of carbon fibre nano-tip electrodes

Carbon fibre nano-tip electrodes were fabricated following the methodology described by Strein and Ewing (1992) and (Li et al., 2015b). Five micrometre diameter carbon fibre (Goodfellow Cambridge Limited) were used to make the electrodes. As with the 10 µm disk electrodes, a carbon fibre of length slightly longer than 15 cm, was inserted into a glass capillary (length 15 cm, OD 1.5 mm, ID 0.06 mm; Harvard Apparatus, UK), with the use of a suction pump. The glass capillary was heat pulled using a Dual-Stage Glass Micropipette Puller (model PC-10, Narishige, Inc., Japan) and the carbon fibre extending between the two produced microtips was cut using scissors. The carbon

fibre protruding at each tip was then cut such that ~200 to 300 µm of fibre was left outside of the glass capillary tip. The protruding fibre was then flamed using butane gas micro blow torch (Brand: AK, Amazon, UK) until it formed a conical nano-tip, which was determined by checking under a light microscope (**Figure 2.7**). Nano-tip electrodes were sealed and connected to silver wires in the same way as disc microelectrodes as described in 2.2.1 (Fabrication of 10 µm diameter carbon fibre disc electrodes)(Li et al., 2015b, Strein and Ewing, 1992).
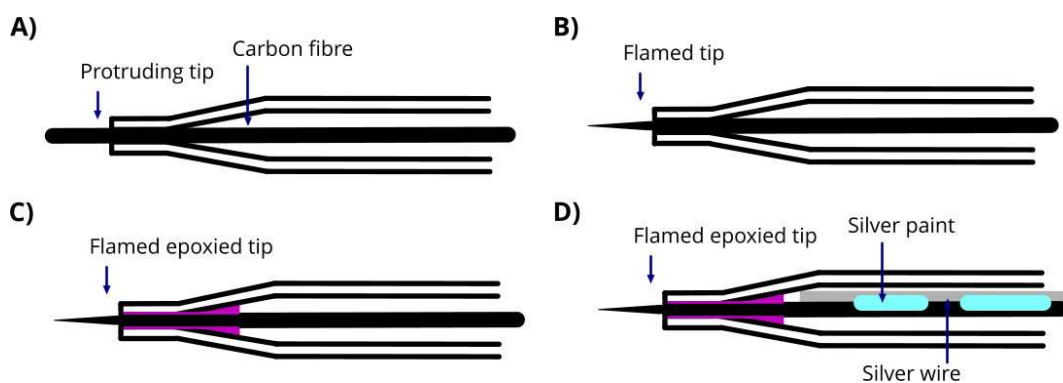
Figure 2.7 Schematics of carbon fibre nanotip electrode. *A) Microelectrode with protruding carbon fibre tip B) Nano-tip electrode with flamed tip. C) Nano-tip electrode sealed with epoxy and cured overnight. D) Nano-tip electrode connected to a silver wire.*

2.2.3 Characterisation of the micro and nano-tip electrodes

The carbon fibre micro and nano-tip electrodes were characterised using cyclic voltammetry of a redox probe. To reduce or oxidize the probe, a potential is swept from a lower to higher or a higher to a lower value, resulting in a current potential curve, which is characterised by a sigmoidal shape. Due to the small size of the micro and nano-tip electrodes, the diffusion of the redox molecules to the surface of the electrode is limited leading to the observation of steady-state currents. Theoretically, the diffusion limited steady state current (I_{dif}) of a disc microelectrode can be calculated using the formula (Kovach et al., 1985, Saito, 1968, Singleton et al., 1989):

$I_{dif} = 4nFDc^{b}r$

where *n* is the number of electrons transferred during the redox process, *F* is Faraday's constant, c^b is the bulk concentration of the redox species, *D* is the diffusion coefficient and *r* is the radius of the disc electrode.

2.2.3.1   Cyclic voltammetry in ruthenium hexamine

As the oxidation of serotonin leads to the generation of oxidation products, that can absorb on the surface of carbon fibre electrodes and therefore reduce the reusability and reproducibility of the electrodes, other molecules that absorb less to the electrodes are used to determine the functionality of the electrodes (Sharma et al., 2018). Such a molecule is the reversable redox couple ruthenium hexamine, used to characterise carbon based electrodes (Chen and Kucernak, 2002).

To characterise the new micro and nano-tip electrodes, all electrodes were cycled from 0.1 V to -0.5 V at a scan rate of 0.1 V/s in 1 mM ruthenium hexamine dissolved in 1 M KCl using a CHI 630B Potentiostat (CH Instruments, Austin, TX 78738, USA). A Ag|AgCl (KCl (3 M)) electrode was used as the reference electrode and an electrode made of platinum wire was used as the counter electrode. Testing was performed before and after the experimental use of the electrodes. The applied voltage waveform causes the ruthenium hexamine to undergo a redox reaction, producing a cyclic voltammogram (CV), plotted as current response versus applied potential. The diffusional limited steady state current (I_{dif}) of the microelectrodes is calculated as the difference between the residual current (a small measurable current flowing through the electrochemical cell in the absence of analyte) and the limiting current of the microelectrode identified by the CHI associated software (**Figure 2.8 A, B**).
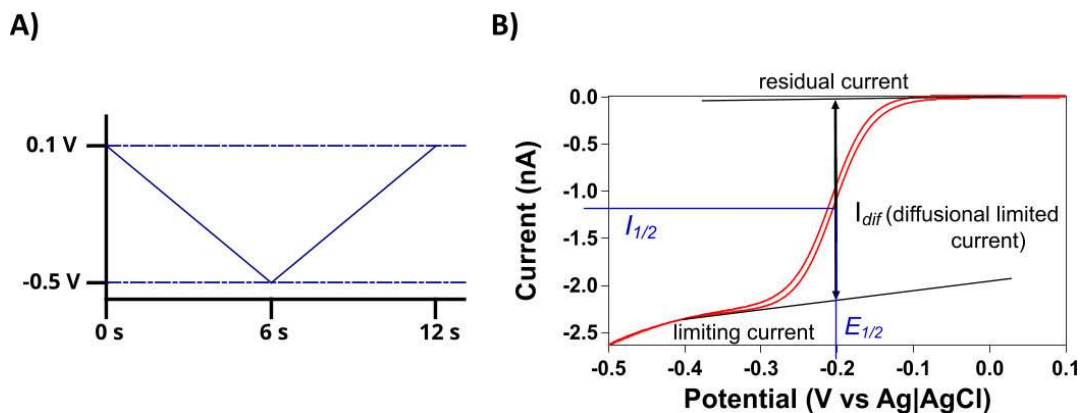
Figure 2.8 Cyclic voltammetry waveform and a cyclic voltammogram using a 10 μm carbon fibre disc electrode. A) Applied potential as a function of time. The applied potential was varied between +0.1 and -0.5 V over a 12 second period. B) Example of a cyclic voltammogram of bevelled microelectrode ($I_{1/2}$ – half wave-height current, $E_{1/2}$ – half wave potential). From the produced cyclic voltammograms a diffusional limited current of the microelectrode (I_{dif}) is calculated by the CHI associated software, which is later used to determine the usability of the microelectrode.

2.2.3.2 Differential pulse voltammetry (DPV)

Differential pulse voltammetry is an electrochemical technique used to determine the peak current at which the maximum number of electroactive molecules is oxidised. In this technique, short duration voltage pulses of small amplitude (+50 mV), superimposed on a short ramp, are applied to the electrode and currents are measured at the start and the end of each small amplitude pulse (**Figure 2.9 A**). The difference between the two currents is calculated and plotted on a DPV voltammogram (**Figure 2.9 B**) (Patel, 2021).
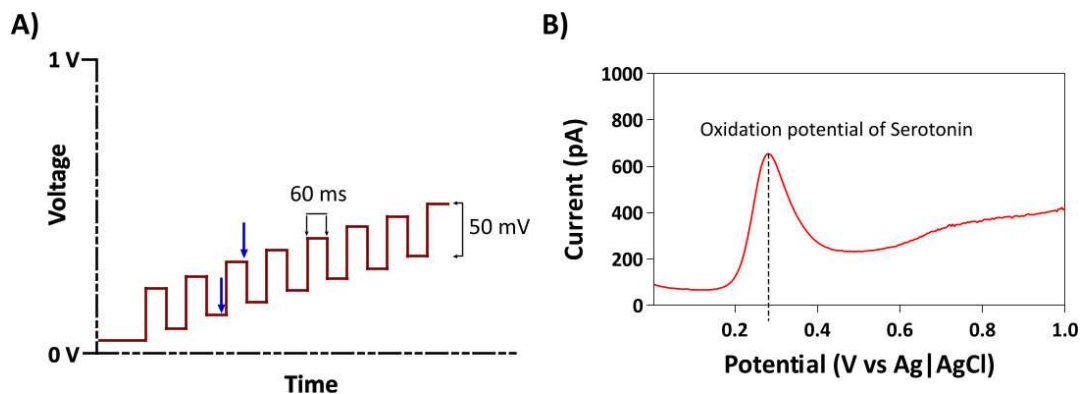
Figure 2.9 Differential pulse voltammetry waveform and voltammogram. *A) Diagram of a DPV waveform, blue arrows show the measured interval of the differential current. B) DPV voltammogram of 50 μM serotonin.*

Although the CGCs are known to be serotonergic cells (Kemenes et al., 1989, McCaman et al., 1984, Yeoman et al., 1994a, Yeoman et al., 1994b), the CNS of *Lymnaea* also contains a number of other electroactive neurotransmitters such as dopamine and octopamine (Audesirk, 1985, Magoski et al., 1995, Elekes et al., 1996, Vehovszky et al., 2005). To determine the peak potential of serotonin on the carbon-fibre based electrodes (10 μm disc and nano-tips) and to confirm that 5-HT is the molecule that is oxidised when released by the CGCs, differential pulse voltammetry was used to determine the oxidation peaks of the three neurotransmitters (serotonin, dopamine and octopamine, (Sigma Aldrich, UK)). The DPV was applied between 0 and 1 V, with amplitude of 50 mV, pulse width of 60 ms and pulse period of 0.5 s, using a CHI 630B Potentiostat (CH Instruments, Austin, TX 78738, USA). A Ag|AgCl (KCl (3 M)) electrode was used as the reference electrode and an electrode made of platinum wire was used as the counter electrode.

2.2.4 Cleaning of carbon fibre microelectrodes used in amperometry experiments

Used 10 μm diameter microelectrodes were cleaned by bevelling the electrode tip after use. 2-propanol was used as a lubricant as suggested by Machado et al. (2008).

2.2.5 Imaging of the micro and nano electrodes

Scanning electron microscopy images of the micro and nano-tips were taken using Zeiss Sigma Field Emission Gun scanning electron microscope (FEG-SEM), equipped with secondary electron detector. The FEG-SEM working conditions used were 0.750 kV accelerating voltage and 3.2 mm working distance.

2.2.6 Fast-step perfusion stability analysis

A fast-step perfusion set up (SF 77 Perfusion Fast-Step, Warner instruments, UK) was used to determine the stability of the 10 μm carbon fibre microelectrodes for recordings lasting for ≥ 50 min. Two joined glass capillaries (length 15 cm, OD 1.5mm, ID 0.06mm; Harvard Apparatus, UK) were connected to the arm of the fast-step perfusion system and 10 μM serotonin (5-HT), made up in 4-((2-Hydroxyethyl)piperazine-1-ethanesulfonic acid (HEPES))-buffered saline (containing in mM NaCl 50; KCl 1.5; $CaCl_2$ 4; $MgCl_2$ 2; HEPES 10) and HEPES-buffered saline were constantly perfused through the capillaries. The sensor was kept in the HEPES-buffered saline stream (**Figure 2.10 A**). Brief changes of the HEPES-buffered saline stream with the 5-HT stream were made with the application of a 10 ms current pulse, which moved the capillary containing the 5-HT opposite the microelectrode (**Figure 2.10 B**).
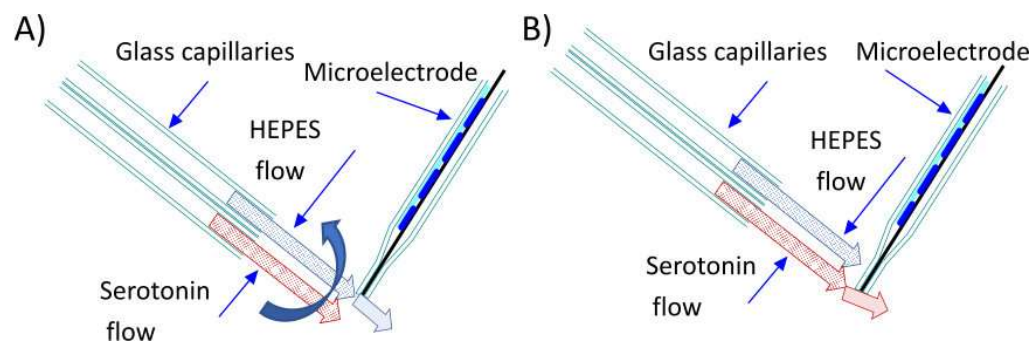
Figure 2.10 Flow and microelectrode set up of the fast-step perfusion bath. A) HEPES-buffered saline and 5-HT were constantly perfused through two joined glass capillaries and the tip of the carbon fibre microelectrode was positioned in the HEPES-buffered saline stream. B) A 10 ms voltage pulse was applied to move the glass capillaries, briefly shifting the serotonin flow in the direction of the microelectrode.

Initially, HEPES-buffered saline and red-food dye (The Pantry Red Food Colouring, 38 ml, Aldi Stores Ltd, UK) were perfused through the first and the second capillaries (**Figure 2.11 A**). The dye was used to facilitate the positioning of the microelectrode tip. The microelectrode was held in the HEPES-buffered saline stream at a constant potential of +750 mV and 10 ms current pulses were generated using the fast-step perfusion system to adjust the positioning of the stream so that the electrode was perfused by the red food dye (**Figure 2.11 B**). Each time red food dye hit the electrode (**Figure 2.11 B**) an oxidation peak was observed (**Figure 2.11 C**).
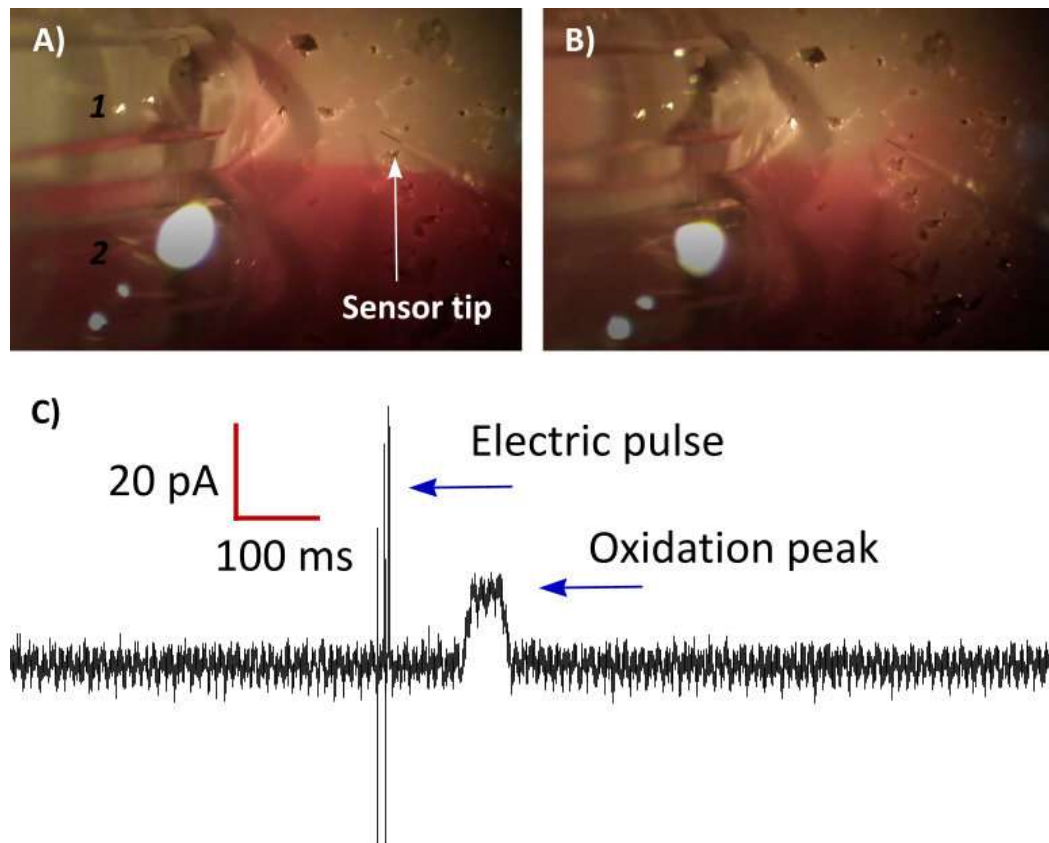
Figure 2.11 Two glass capillary set up used for fast-step switch perfusion of HEPES and Serotonin. *A) Initially HEPES and red dye are perfused through two joined glass capillaries – 1 and 2 so the separation of the flow can be visualised, while the sensor is positioned in the HEPES flow. B) Fast step switch moves the dye flow briefly over the sensor. In the experiments, the dye is swapped with 10 μm serotonin. C) An oxidation peak of the food dye is observed on the trace following the electric pulse.*

Following the adjustment of the microelectrode, the red dye was replaced with the serotonin. Application of 10 μM serotonin for 10 ms to the microelectrode generates reproducible current transients with defined rise time, amplitude, fall time, half time and base time (**Figure 2.12 A, B**).

A)   B)
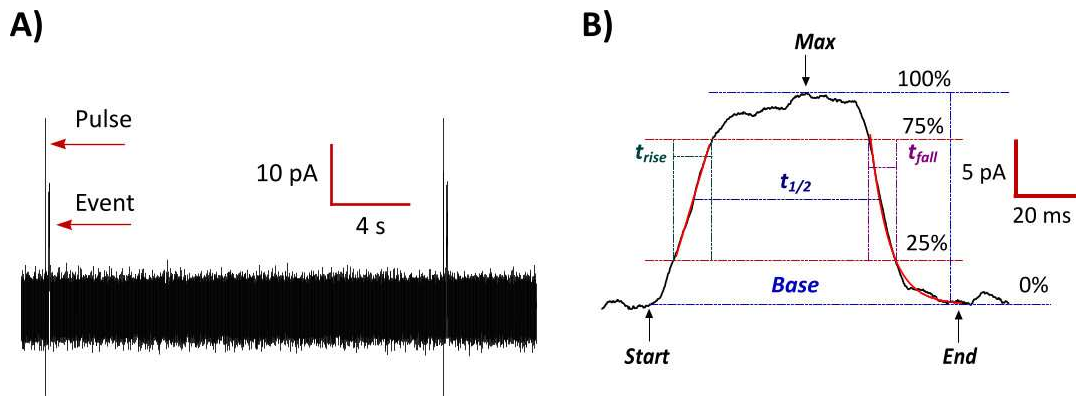
Figure 2.12 Example of a trace with events generated by a pulse and an example of a recorded event with the measured parameters. *A) Sample of a recording showing a pulse generated by the fast step switch and the event generated by the serotonin pulse. B) An example of a recorded event and the parameters analysed.*

To determine the stability of the carbon fibre microelectrodes over time, the 10 ms pulses were introduced in three bouts of 8 pulses each. These bouts were initially repeated with a 10 min gap between the first and second group of pulses and subsequently with 15 min gaps between the second and third and third and fourth groups (**Figure 2.13**).
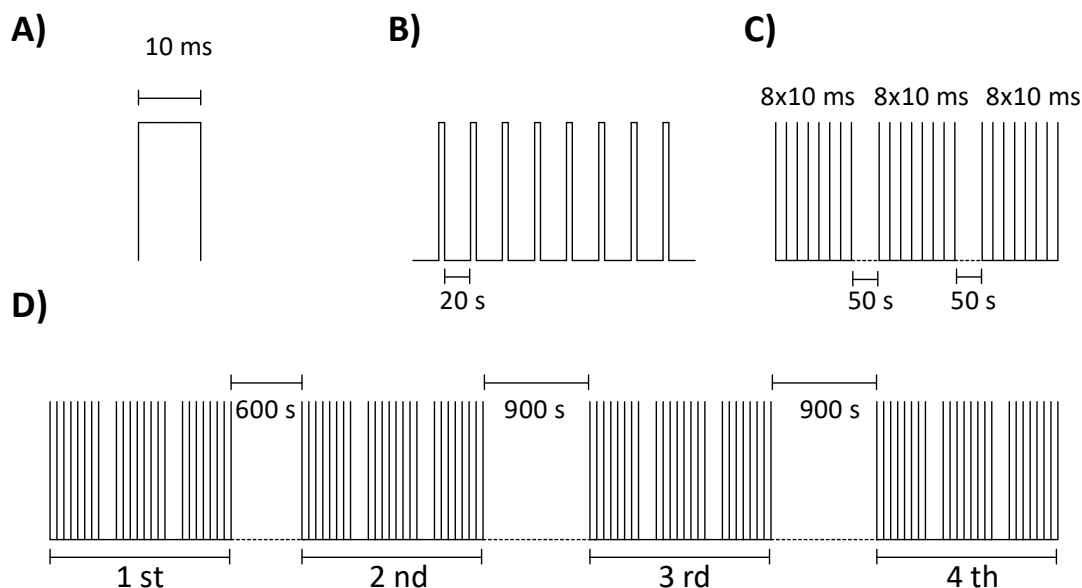
Figure 2.13 Experimental set up for fast-step perfusion switch. *10 ms pulses (A) with a space of 20 s between each 8 pulses (B) were generated in a group of 24 pulses, spacing each 8 pulses by 50 s(C). This was repeated 4 times with a pause of 10min between the first and the second bouts and 15 min between the second and the third and the third and fourth bouts (D).*

Signals were recorded using Axopatch 200B amplifier (Molecular Devices, U.S.A.). Data was sampled at 10 kHz and filtered at 1 kHz using a 4 pole Bessel filter prior to digitisation using a Micro 1401 A/D converter (CED, Cambridge, UK). The data was recorded on a PC using Spike 2 software (CED, Cambridge, UK).

2.2.7 Data analysis

Cyclic voltammetry and differential pulse voltammetry data were collected and analysed with CH Instruments Model 630B electrochemical analyser software. All statistical analysis were performed using GraphPad Prism vs9.0. Normality of the data distribution was tested with Kolmogorov-Smirnov test. Steady state diffusional currents of the different carbon fibre microelectrodes, calculated by the CHI associated software, were compared using a Wilcoxon t-test, when comparing between treatments of the same electrodes or a Mann-Whitney t-test, when comparing

between groups of different electrodes. Data are presented as scatter plots with range with the line in the middle representing the mean for normally distributed data and the median for not normally distributed data or a scatter plot bar with mean and SEM, $p < 0.05$ is taken as significant. All p-values are shown above the graphs.

2.2.8 Analysis of the electrochemistry recordings

Amperometric events were analysed using IgorPro 6 routine from David Sulzer laboratory (Mosharov and Sulzer, 2005). The differentiated trace was filtered at 300 Hz, but no filtering was applied to the current trace. The chosen threshold for the peak detection was 3.5 * SD (dI/dt). The software allows for the analysis of event parameters such as: the base of the event from the start to the end of the event (*Base*), the amplitude of the event (I_{max}); the time it takes for the peak to rise from 25% to 75% of its maximum (t_{rise}); the width of the event at half of its amplitude ($t_{1/2}$); the time it takes for the peak to fall from 75% to 25% of its maximum (t_{fall}); the number of molecules released per event (Q); The number of moles of oxidized serotonin is determined using Faraday's law:

Q = nFN

where Q is the integrated charge under the individual event, n is the number of electrons produced by the oxidation of serotonin ($n = 2$), F is Faraday's constant and N is the number of moles of oxidised serotonin.

2.3 Results

2.3.1 Fabrication and characterisation of the 10 µm disc microelectrodes

2.3.1.1 Fabrication of the 10 µm disc microelectrodes

To determine the surface texture of the disc electrodes and how it changes following coating with epoxy, bevelling and use, scanning electron microscope (SEM) images were taken of the tips of the 10 µm disc microelectrodes. The SEM images of the disk electrodes show an 'onion skin' transverse texture of the new carbon fibre (**Figure 2.14 A**). The use of epoxy to form a seal between the fibre and the glass capillary does not appear to change the surface architecture (**Figure 2.14 B**). Bevelling the electrode down to the level of the glass capillary smooths out small variations in the surface of the fibre (**Figure 2.14 C**).
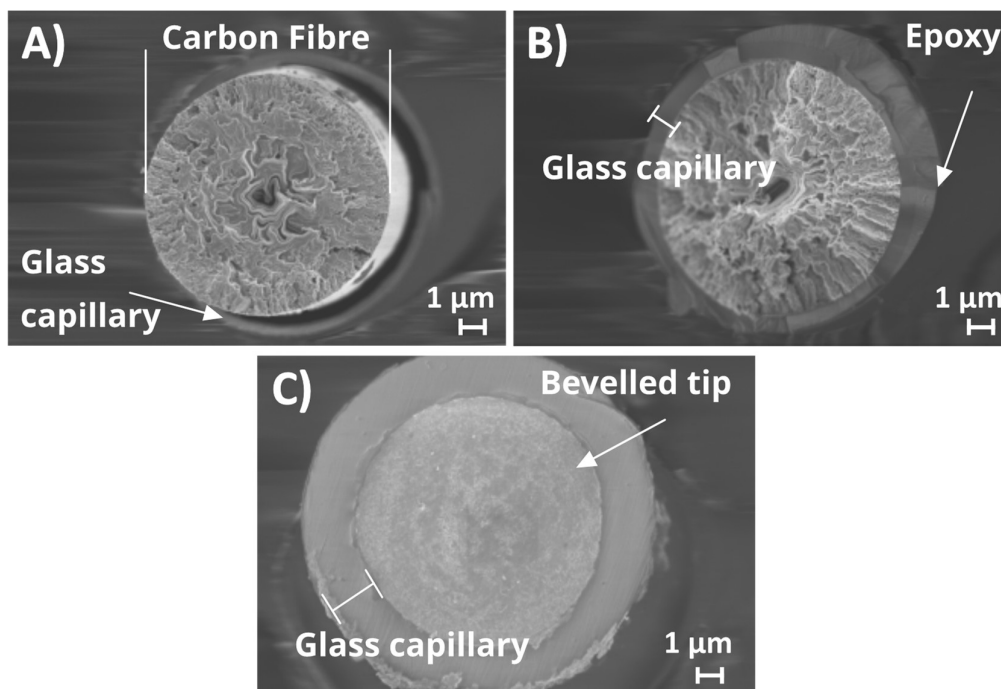
Figure 2.14 SEM of 10 µm disc electrode at different fabrication stages. A) New carbon fibre microelectrode into a glass capillary. B) New carbon fibre microelectrode sealed with epoxy. C) Bevelled and buffed carbon fibre.

Determining connectivity and conductivity of the 10 μm diameter disc microelectrodes with cyclic voltammetry.

To ensure that only suitable electrodes were chosen to record transmitter release from CNS neurons, the connectivity and conductivity of all new fabricated disc electrodes were tested in 1 mM ruthenium hexamine diluted in 1M KCl using cyclic voltammetry. The disc microelectrodes produced clear cyclic voltammograms, from which the diffusion limited current of the microelectrodes was calculated (**Figure 2.15 A**). The mean diffusion limited steady state current of the disc microelectrodes was 1.906 nA (**Figure 2.15 B**).
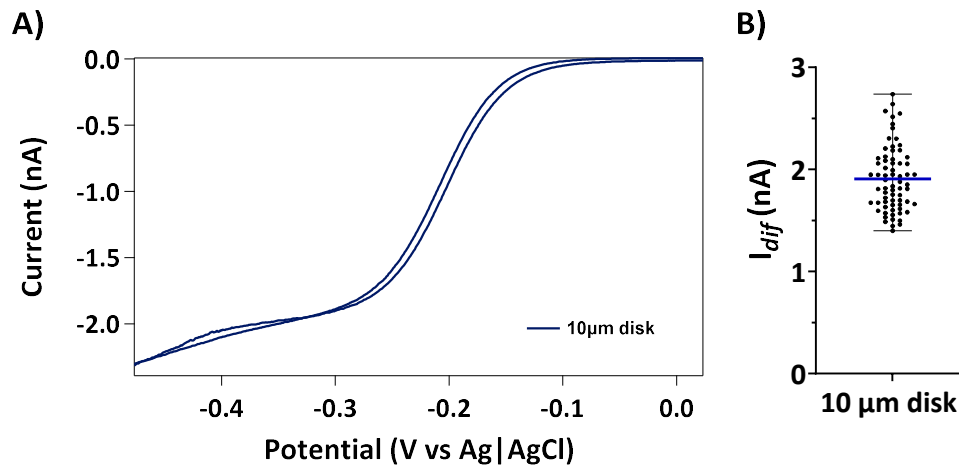
Figure 2.15 Cyclic voltammograms and measurements of steady state currents of new 10 μm disc microelectrodes. A) Sample cyclic voltammogram of 10 μm disc microelectrode. B) Steady state currents of 10 μm disc microelectrodes produced in 1 mM ruthenium hexamine (n = 69, mean = 1.906 nA).

Determining the oxidation peaks of serotonin, dopamine and octopamine on the 10 µm diameter disc microelectrodes.

DPV measurements of dopamine on the 10 µm disc microelectrodes yielded an oxidation peak with a mean at +125.3 mV (±2.667 SEM) (**Figure 2.16 A and D**). The oxidation peak for serotonin occurred at a mean of +283 mV (±1.333 SEM) (**Figure 2.16 B and D**) and at a mean of +633 mV (± 5.333 SEM) for octopamine (**Figure 2.16 C and D**).
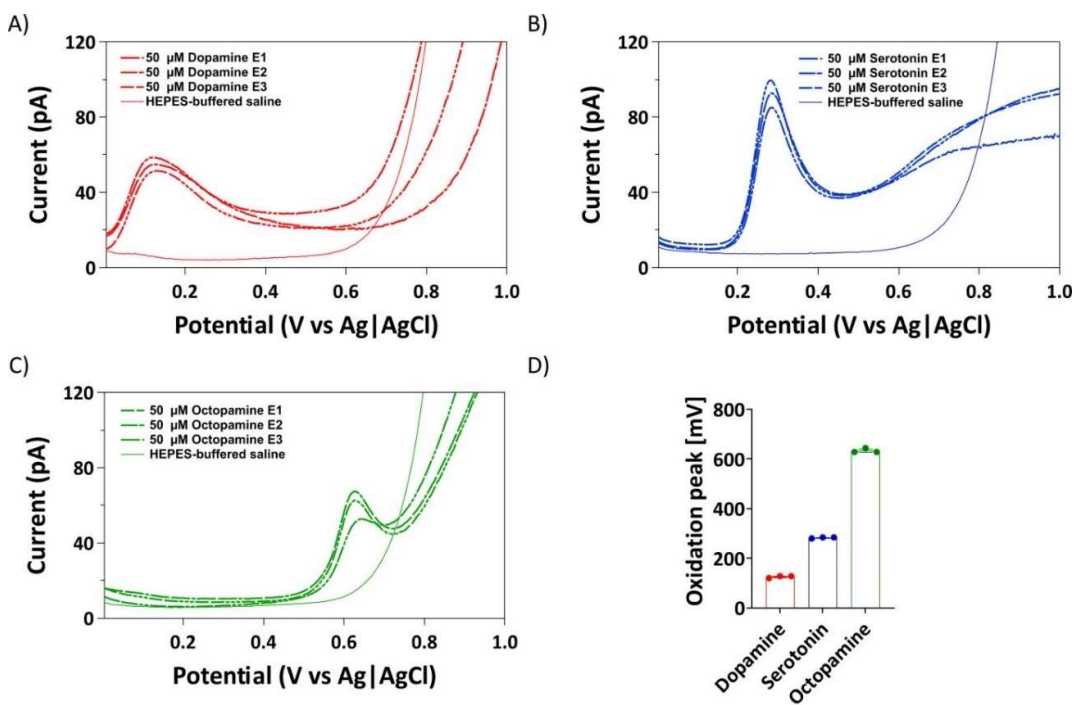
Figure 2.16 Oxidation peaks of dopamine, serotonin and octopamine determined using DPV. *DPVs with oxidation peaks for A) dopamine, B) serotonin and C) octopamine on 10 µm microelectrodes. E) Oxidation peaks of dopamine, serotonin and octopamine.*

2.3.1.3 Effects of use and cleaning on the surface properties and electrochemical properties of the 10 µm disc microelectrodes.

The effects of use and cleaning after use, on the surface properties and electrochemical properties of the 10 µm disc microelectrodes were established using a combination of SEM imaging and cyclic voltammetry.

SEM images of the 10 µm disc microelectrodes taken before (**Figure 2.17 A**), and after use (**Figure 2.17 B**) and following cleaning (**Figure 2.17 C**) show that with use a layer of biological material builds on the exposed carbon fibre tip, which is removed by the cleaning process.
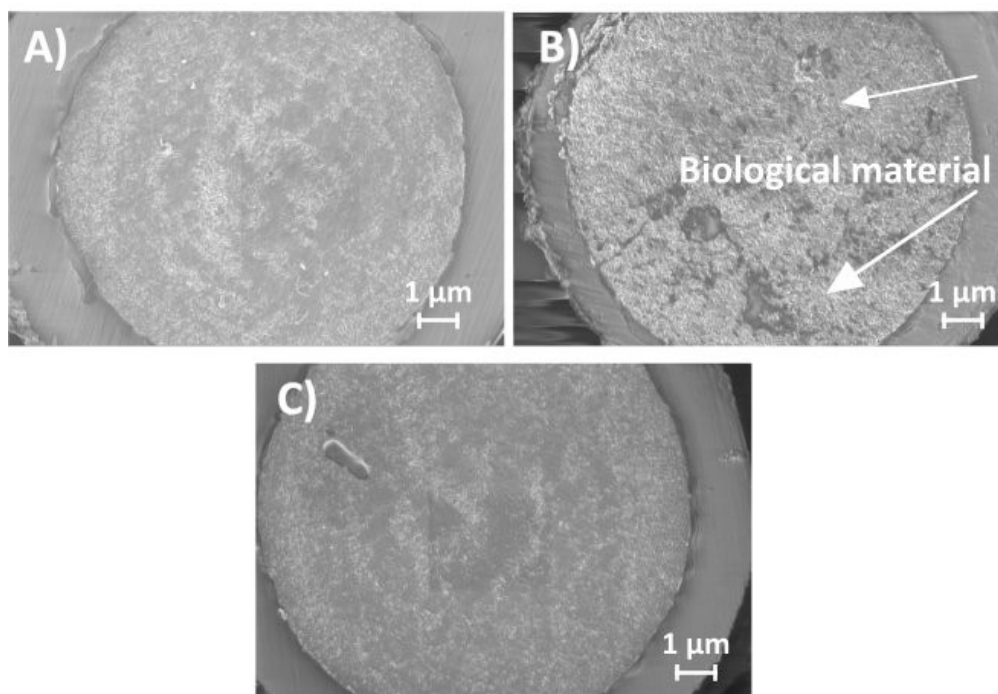
Figure 2.17 SEM of new, used and cleaned 10 µm disc microelectrodes. *A) New, B) Used, C) cleaned after use illustrating the build-up of surface material after use and its subsequent removal following cleaning.*

Testing of the 10 μm disc microelectrodes in 1 mM ruthenium hexamine showed that used microelectrodes have a significantly lower diffusional limited current (I_{dif}) compared to the new electrodes (**Figure 2.18 A, B**; $p < 0.0001$), consistent with the observed surface build-up of material shown in **Figure 2.17 B**. Cleaning of the carbon fibre surface however did not significantly change the diffusional limited currents of the electrodes (**Figure 2.18 B**).
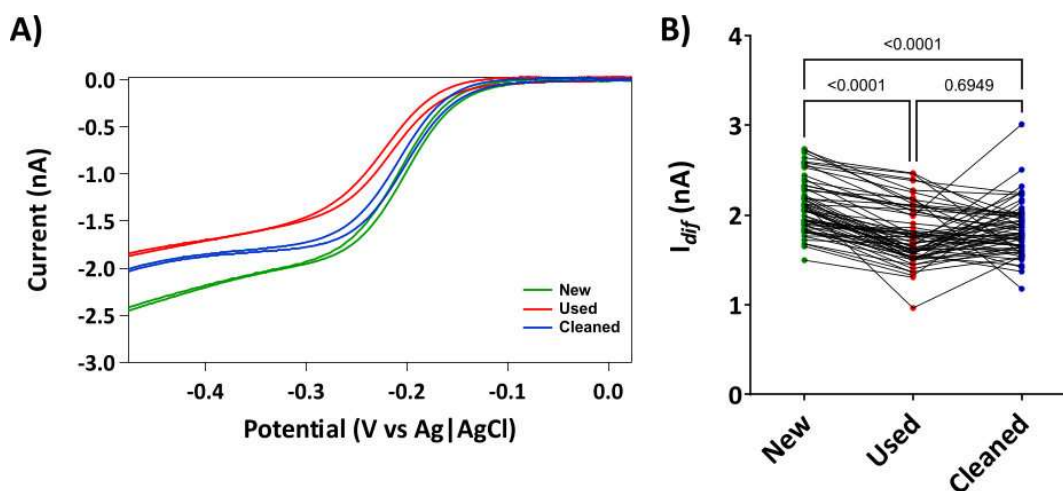
***Figure 2.18 Cleaning of the microelectrodes conductive surface following use does not restore their electrical properties.** A) Cyclic voltammograms of new, used, and cleaned microelectrodes. B) Comparison of the steady state currents recorded from new, used and cleaned microelectrodes (new n = 66, used n = 63, cleaned n = 61, repeated measures, Kruskal-Wallis test, followed by Dunn's multiple comparisons post-hoc test, p-values shown above the graph).*

2.3.1.4 Analysis of fast perfusion experiments performed with the 10 μm disc microelectrodes.

Fast perfusion experiments were run to determine the stability of the 10 μm carbon fibre disc microelectrodes for recordings lasting for 50 min. Repeated applications of 10 μM serotonin for 50 min time period failed to alter the parameters of the recorded oxidation events (**Figure 2.19**).
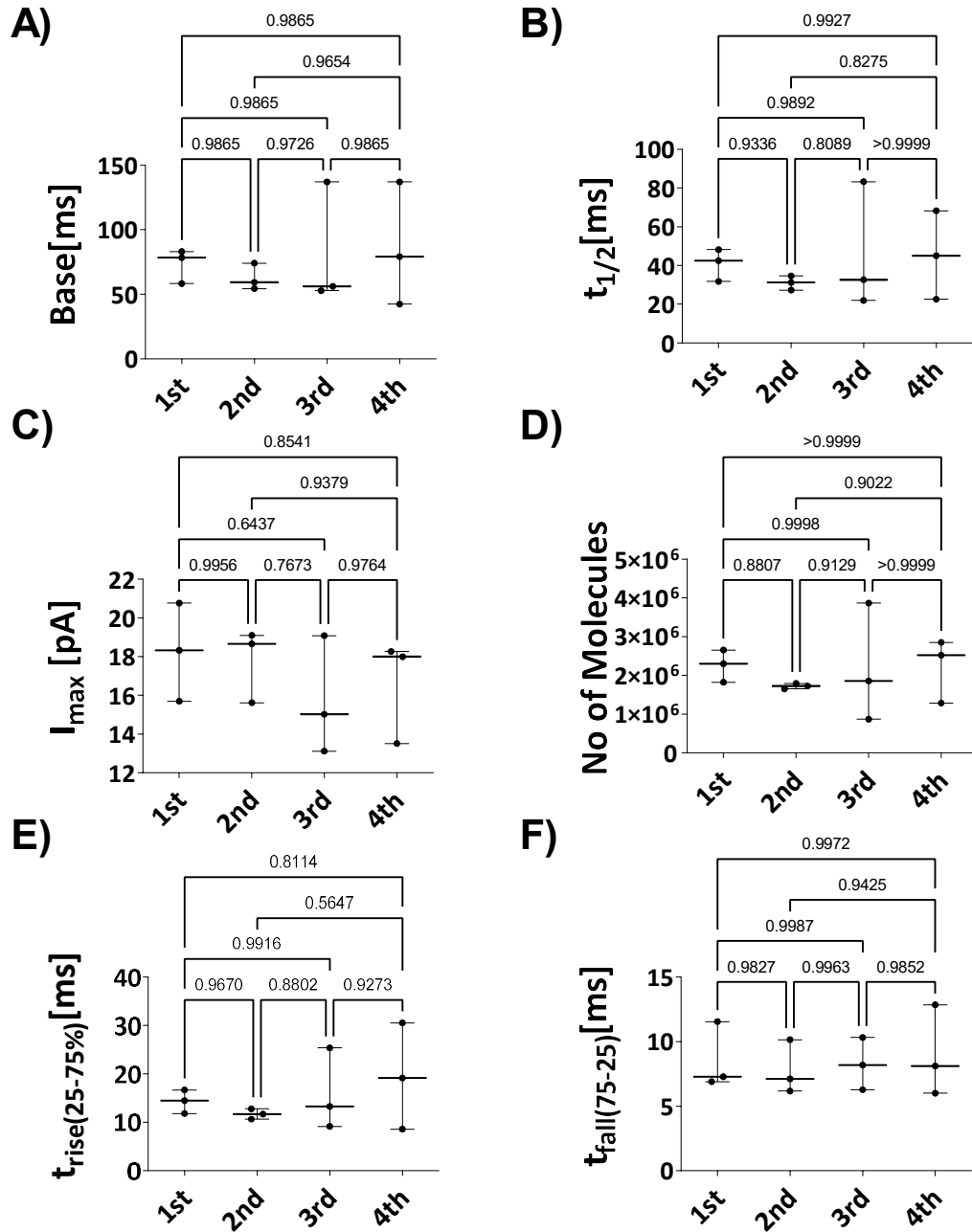
Figure 2.19 The parameters of the events, generated in bouts of 24, by 10ms pulses of serotonin, does not change with time. A) Base, B) t1/2, C) Imax, D) Molecules, E) Rise time, F) Fall time (n = 3, ordinary one-way ANOVA, p-values shown above the graph).

2.3.2 Fabrication of the nano-tip electrodes.

Nano-tip electrodes were developed to allow the measurement of the neurotransmitter content of intracellular vesicles. SEM images of typical electrodes were taken at different stages of production to determine the surface texture of the 5 µm fibre and confirm the nanometre size of the tips. The 5 µm diameter carbon fibre has a flat layer transverse texture (**Figure 2.20 A**). Before the fibre is flamed ~200 µm of the fibre is left to protrude outside of the glass capillary (**Figure 2.20 B**). Flaming of the fibre etches the cylindrical tip to form a conical shape (**Figure 2.20 C**), of a nanometre size at the sharp end (**Figure 2.20 D**).
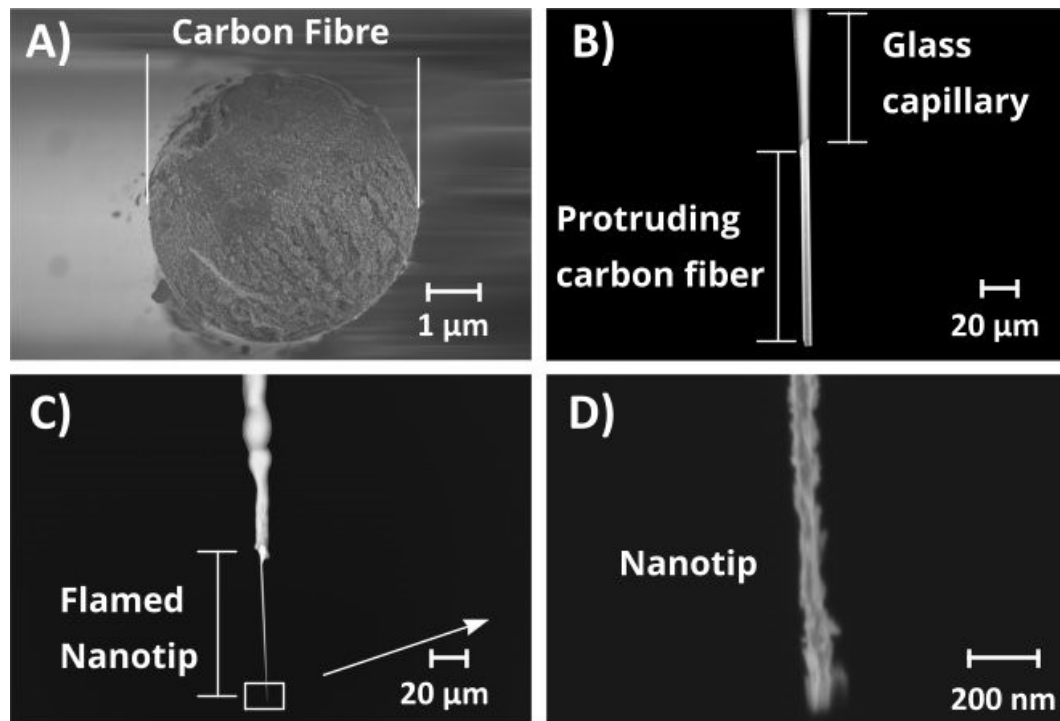
Figure 2.20 SEMs of 5 µm disc fibre tip before flaming and a nano-tip after flaming. *A) Cut tip of 5 µm carbon fibre, B) protruding carbon fibre sticking out of the glass capillary, C) Flamed protruding nano-tip. D) The end tip of the nano-tip.*

As with the disc microelectrodes, the conductivity of the new nano-tip electrodes was assessed using cyclic voltammetry applied in 1 mM ruthenium hexamine (**Figure 2.21 A**). New electrodes have a mean steady state diffusion current of 15.16 nA, which decreases to 13.54 nA after use (**Figure 2.21 B**).
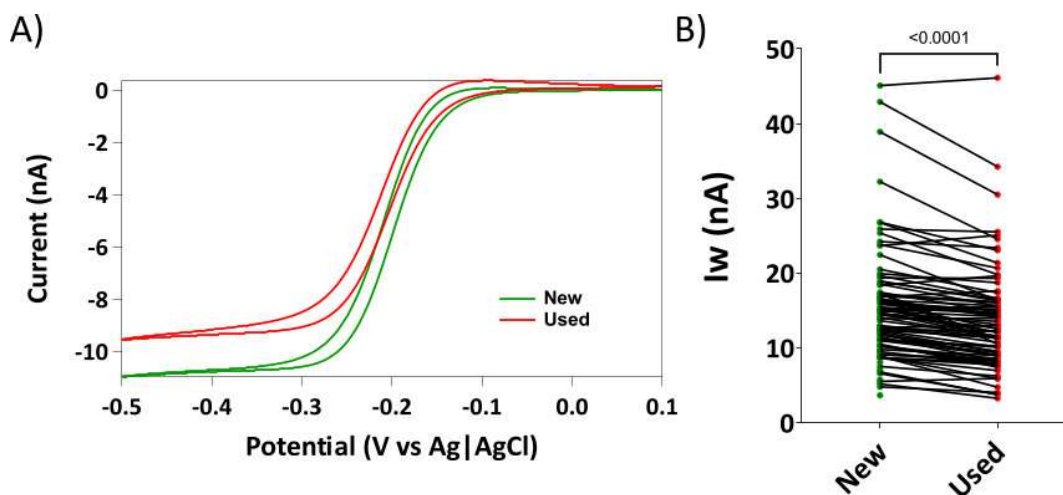
Figure 2.21 Cyclic voltammograms and measurements of steady state currents of new and used nano-tip electrodes. A) Cyclic voltammograms of new and used nano-tip. B) Comparison of the steady state currents recorded from new and used nano-tips (New n = 95, Used n = 83, paired t-test, p-values shown above the graph).

All nano-tip electrodes are a single use, as often the nano-tip is damaged with use and therefore there is not simple way of reconstituting their tip to close to their original state.

DPV measurement of 50 µM dopamine (**Figure 2.22 A**), serotonin (**Figure 2.22 B**) and octopamine (**Figure 2.22 C**) using the nano-tip electrodes showed mean oxidation peaks at +342.7 mV (±26.77 SEM), +308 mV (±4.619 SEM) and +637.3 mV (±1.333 SEM) for dopamine, serotonin and octopamine respectively (**Figure 2.22 D**).
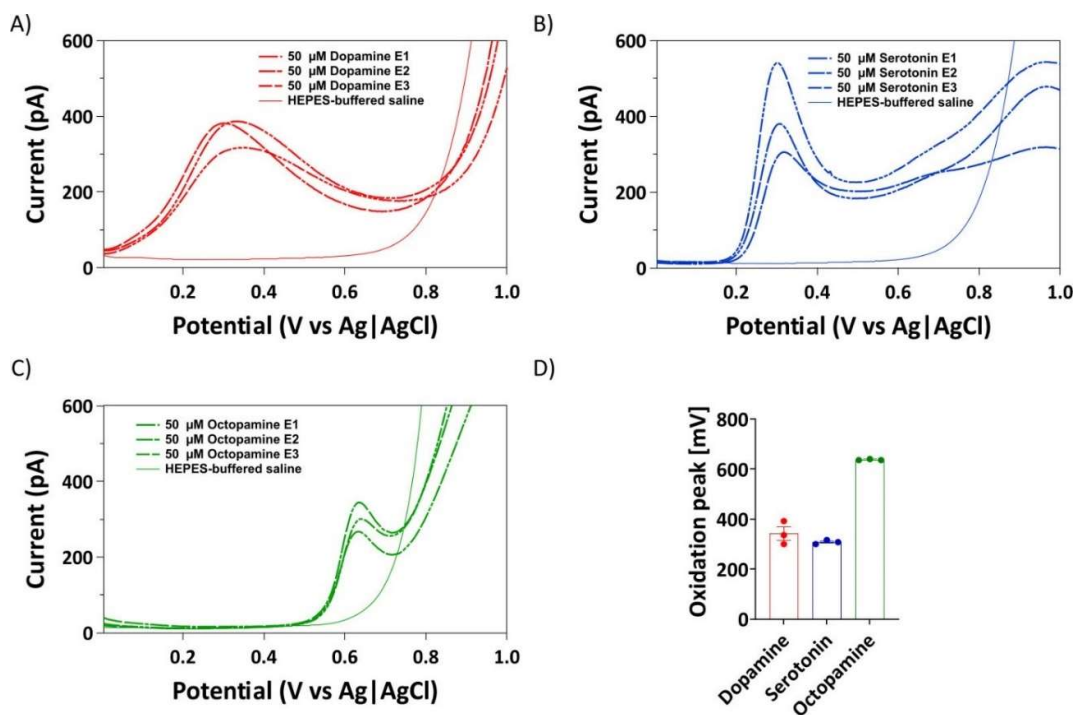
Figure 2.22 Oxidation peaks of dopamine, serotonin and octopamine determined using DPV. *DPVs with oxidation peaks for A) dopamine, B) serotonin and C) octopamine on nano-tip electrodes. D) Oxidation peaks of dopamine, serotonin and octopamine.*

2.4 Summary and discussion

Functional 10 µm diameter disc microelectrodes and nano-tip electrodes were fabricated for the measurements of the kinetics of extracellular vesicular release and intracellular vesicle content. Representatives of the fabricated electrodes were imaged using a SEM to determine the structure of the carbon fibres and the effect that the fabrication process and use had on the surface of the electrodes. SEM images of the carbon fibre used in the fabrication of the 10 µm disc electrodes showed an 'onion skin' structure. The 5 µm diameter carbon fibre used for the fabrication of the nano-tips showed a 'flat layer' structure. The differences in the fibre structures of the carbon fibre can influence the electrochemical performance of the electrodes made with the fibres. However, due to the large number of carbon fibre manufacturers and types of carbon fibres manufactured, there is still no clear relationships established between the electrochemical activity of the fibres and their structure (Patel, 2021, Uslu and Ozkan, 2007). Images of the bevelled newly fabricated 10 µm disc electrodes showed an even surface to the disc.

Flaming of the protruding 5 µm diameter carbon fibre used for the fabrication of the nanotip electrodes produces a sharp tip with conical shape of a nanometre size at the end. These nano-tips appear very similar to the nano-tip electrodes made and used by Li et al. (2015b).

Typically, carbon fibre microelectrodes and nano-tips are tested in the analyte they will be used to measure, which in most cases has been dopamine (Li et al., 2015b, Mundorf and Wightman, 2002). However, unlike dopamine, serotonin can reduce the reproducibility and reusability of the electrodes due to the generation of oxidation products that tend to absorb on the surface of the electrode (Sharma et al., 2018). Therefore, to avoid alterations of the carbon fibre electrodes, all fabricated micro and nano-tip electrodes were tested in 1 mM ruthenium hexamine using cyclic voltammetry. All electrodes produced cyclic voltammograms with typical sigmoidal curves, as those observed when carbon fibre electrodes have been tested in dopamine or ruthenium hexamine (Li et al., 2015b).

The 10 μm disc microelectrodes produced mean diffusional limited currents of 1.906 nA. The mean diffusional limited current of the nanotips was 15.16 nA.

Applying the formula described by Wightman and J. Osteryoung groups (Kovach et al., 1985, Singleton et al., 1989),

$$I_{dif} = 4nFDc^b r$$

determined that the theoretical diffusional limited steady state current (Idif) of a perfect 10 μm disc microelectrode is 1.760 nA. The calculated theoretical diffusional limited current is smaller than the experimentally measured current. Such a difference can be explained by a larger surface area of the tips of the electrodes. As the tips of the disc electrodes were bevelled at an angle of ~ 45°, the bevelling process would produce an electrode with and larger ellipsoidal surface area, rather than a perfect disc, which would lead to a larger diffusional limited currents measured experimentally. In addition, it is also possible that bevelling does not completely remove all the protruding tip again increasing the surface area of the electrode.

Following use, all electrodes were retested in 1 mM ruthenium hexamine and representative electrodes were imaged with the SEM. This was done to determine if they can be reused. For all electrodes, testing following use showed a decrease of the diffusional limited currents. In addition, the SEM images of representative electrodes showed a build-up of a biological layer on the surface of the electrodes.

Used 10 μm disc microelectrodes were cleaned using 2-propanol and by rebevelling the surface of the tip as suggested by Machado et al. (2008). Overall, cleaning of the electrodes did not show a statistically significant reversal of the decreased diffusional steady state currents to the values measured before use. SEM imaging of the representative electrodes showed almost complete removal of the built-up biological layer on the surface of the imaged electrodes. Even though there was not a statistically significant reversal of the decreased diffusional steady state currents of all electrodes taken together, for some of the electrodes, the measured diffusional steady state currents were closely reversed to the currents measured before use and therefore only these electrodes were used in further experiments.

The inability to reverse the diffusional steady state currents of all electrodes to their initial values could be explained by a reduction of the surface area of the electrodes with the rebevelling. This could occur if the surface area of the electrode was initially larger due to protrusion of the carbon fibre, which is then reduced by the rebevelling process. In addition, reduction of the electrode surface area could occur with the repositioning of the electrode for re bevelling. Changes to positioning orientation, which are hard to control for due to the small size of the electrode, could create different angles of bevelling and therefore different size surface areas. Alternatively, the used cleaning procedure of the electrodes might have not been enough to completely remove the serotonin oxidation products that might have adsorbed on the surface of the carbon fibre on all electrodes, (Jackson et al., 1995).

In addition to electrochemical characterisation in ruthenium hexamine, the 10 µm disc microelectrodes were also tested for stability using multiples of serotonin pulses. Repeated application of 10 µM serotonin for ~ 50 minutes showed that no significant changes occur to the parameters of the events detected by the electrodes, therefore showing that the electrodes are stable when used in experiment lasting for at least 50 minutes.

As all electrodes were fabricated to be used for the amperometric recordings of electrochemical neurotransmitters, specifically the release of serotonin from the CGCs of *Lymnaea*, representatives of all types of electrodes were tested using DPV to determine the potentials needed to oxidise serotonin and the other two most common neurotransmitters (dopamine and octopamine) in the CNS of the snail. DPVs conducted using 10 µm disc microelectrodes showed mean oxidation peaks at +125.3, +283 and +633 mV for dopamine, serotonin and octopamine respectively. DPVs conducted using the nanotips showed mean oxidation peaks at +342.7 mV, +308 mV and +637.3 mV for dopamine, serotonin and octopamine respectively. Based on these results, on all electrodes serotonin is maximally oxidized at potentials of +308 mV or slightly lower, similar to oxidation peak potentials observed in rat brains (Martin et al., 1988). These measurements and the recommendation that oxidation potentials used to measure molecules of interest should be ~ 50 mV higher than the peak potential at which the molecules are oxidised, indicate that a minimum potential of +358 mV

should be used for the detection of serotonin release from the CGCs (Patel, 2021). The oxidation potentials used in other studies measuring serotonin using carbon fibre electrodes, have been in the range of +650 to +750 mV (Bruns et al., 2000, Patel et al., 2010, Hatamie et al., 2021, Marszalek et al., 1997). Therefore, an oxidation potential of +750 mV would generate data comparable to the data collected by previous studies.

Overall, working carbon fibre micro and nano-tip electrodes able to detect serotonin were manufactured. All electrodes showed typical steady state current responses in ruthenium hexamine. The 10 µm disc microelectrodes exhibited stable responses to multiple applications of serotonin pulses over long period of time, demonstrating suitability to measure serotonin released from the CGCs.

3 Detection of spontaneous and triggered neurotransmitter release from the soma of the CGCs

3.1 Introduction

3.1.1 Neurotransmitter release

The first indirect measurements of vesicular release were observed by Fatt and Katz in 1952 (Fatt and Katz, 1952). Initially, in earlier studies Fatt and Katz described local discharges at the surface of isolated muscle fibres from the frog neuromuscular junction (NMJ), termed end plate potentials (EPPs; (Fatt and Katz, 1950, Fatt and Katz, 1951)). Following these investigations, they later used intracellular microelectrodes at the NMJ to record spontaneous postsynaptic responses in the form of small membrane depolarizations of similar waveforms to the EPPs, which they named miniature end-plate potentials (mEPPs) (Fatt and Katz, 1952). Statistical analysis of these recordings, conducted by Del Castillo and Katz in 1954 (Del Castillo and Katz, 1954) showed that the recorded mEPPs are built-up of small quanta ('quantum content'), which represents the smallest number of neurotransmitter molecules that can be released by a nerve cell. A few years later Katz and Miledi managed to affirm that the release of these quantal contents of neurotransmitter is governed by the availability of Ca^{2+} ions in the Ringer's solution. They demonstrated this in experiments in which the sodium ions were removed from the Ringer solution and mEPPS are still recorded, or when the nerve endings are locally depolarised with the use of micropipettes filled with calcium chloride and quantal release is observed (Katz and Miledi, 1967).

3.1.2 Types of neurotransmitter release

3.1.2.1 Synaptic neurotransmitter release

Three different modes of neurotransmitter release have been described: synchronous (occurring within milliseconds of the action potential arrival), asynchronous (persisting for tens of milliseconds to seconds after the action potential arrival), or spontaneous (occurring in the absence of an action potential) (Kaeser and Regehr, 2014) and they can occur at multiple sites on the nerve cells. Neurons predominantly communicate by the release of neurotransmitters at synapses. The neurotransmitters can be packed into vesicles of two main types, small clear vesicles and large dense core vesicles, which differ by the type of content. The clear vesicles contain predominantly small molecules, whereas the dense core vesicles also contain neuropeptides and intravesicular proteins forming a matrix (Pellegrino de Iraldi, 1992, Salio et al., 2006). In addition to the synapse, dense core and small clear vesicles are also observed and released at non-synaptic sides such as axonal varicosities, dendrites and the soma of the neurons (Agnati et al., 1986, Bruns et al., 2000, Dun and Minota, 1982, Leon-Pinzon et al., 2014, Taber and Hurley, 2014).

At the synapse, vesicles packed with neurotransmitters are seen either localized at membrane regions rich in proteins, perceived on micrographs as electron-dense zones, known as active zones (AZs) or are seen in larger groups scattered around the active zone (Alabi and Tsien, 2012, Schikorski and Stevens, 1997). The organisation of the vesicles either at the plasma membrane of the AZ or their scattering into groups throughout the rest of the synaptic bouton area and the difference in the ease with which they are released, has led to the classification of the vesicles as belonging to distinct pools. Vesicles attached or seen closely adjacent to the plasma membrane of the AZ are assigned to a pool known as the readily releasable pool (RRP) which is comprised of ~ 1% of all vesicles at the synapse and can undergo fast exocytosis. Vesicles, which are observed very close to the plasma membrane, but take slightly longer to get mobilised and released are classified into a recycling pool (RP), which comprises ~ 10-15% of all vesicles at the synaptic terminal. The rest of the vesicles throughout the bouton (~80-90%) are assigned to a reserve pool, which sometimes is referred to as the silent pool (SP) or the resting pool (**Figure 3.1**) (Rizzoli and Betz, 2005, Fernandez-Alfonso and Ryan, 2008, Ashton and Ushkaryov, 2005).
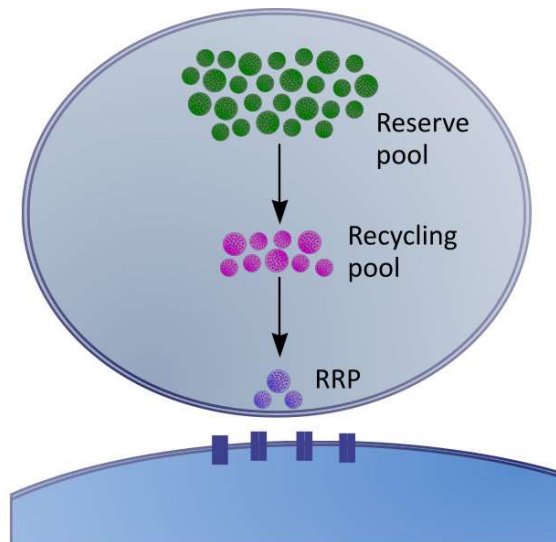
Figure 3.1 Classical model of three pools of vesicles. *The reserve pool is ~ 80-90 % of total pool, the recycling pool ~ 10-15 % of vesicles and the readily releasable pool (RRP) ~ 1%.*

Synaptic release of neurotransmitters from vesicles in the RRP is initiated with the arrival of the action potential (AP) at the end of the nerve terminal. The depolarization of the terminal caused by the arrival of the AP activates the opening of voltage-gated calcium channels (VGCC) leading to the influx of Ca^{2+} ions in the intracellular space around the channels (Llinas, 1977, Llinas and Nicholson, 1975, Südhof, 2012). The increased concentration of Ca^{2+} ions in the AZ of the synapse can be sensed by specific Ca^{2+} sensor proteins, such as calmodulin, visin-like protein (VILIP-1), neuronal calcium sensor 1, CaBP1, and Munc 13. However, the most prominent protein, which binds Ca^{2+} ions and instigates the fusion of the vesicle with the plasma membrane leading to the release of the neurotransmitter is the vesicle protein synaptotagmin 1 (SYT1) (de Jong and Fioravante, 2014). Although having a main role in neurotransmitter release, SYT1 is only one of a group of proteins, known as SNAREs, forming a complex machinery, which facilitates the attachment of the synaptic vesicle (SV) to the plasma membrane (PM) and the formation of a fusion pore through which the neurotransmitter is discharged into the synaptic cleft (**Figure 3.2**) (Rizo and Xu, 2015, Rodrigues et al., 2016).
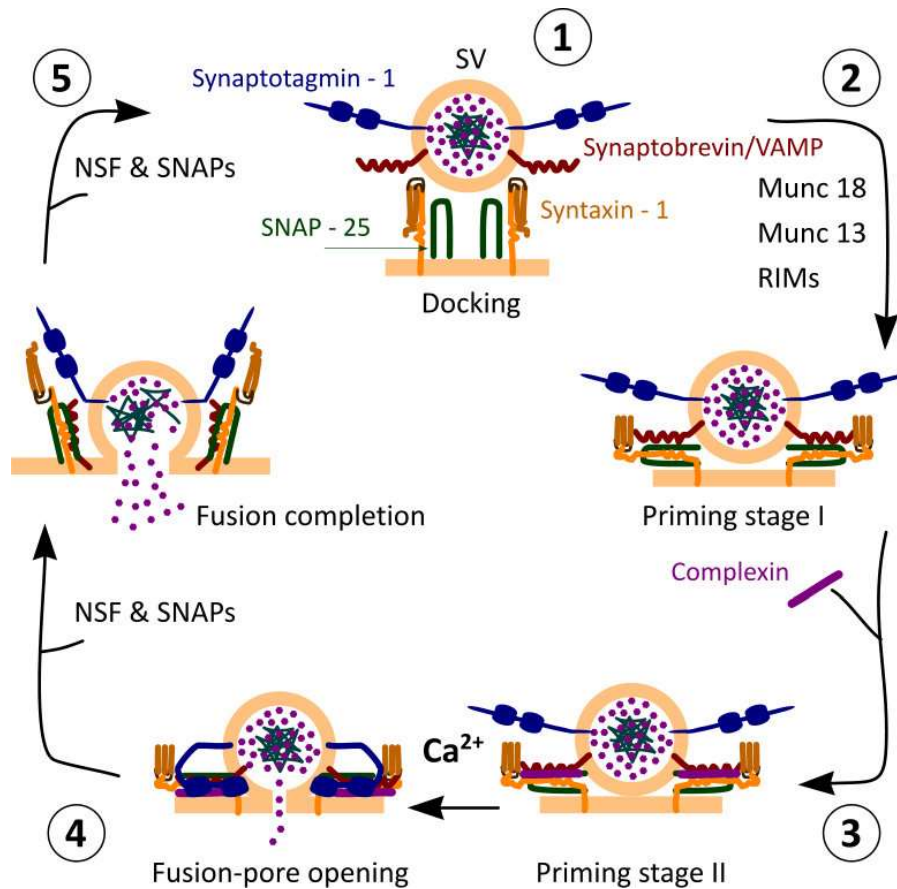
Figure 3.2 Vesicular release machinery and the SNARE – Sec1/Munc18 (SNARE- SM protein) cycle. *The release of neurotransmitters at the synapse is governed by a complex of proteins. Synaptic vesicles are docked at the cell membrane and primed for release by the assembly of a SNARE complex composed of the synaptosome-associated protein (SNAP-25), Syntaxin 1, and Synaptobrebin/Vesicle- associated membrane protein (VAMP) proteins. The assembly of the SNARE complex is catalysed by Munc18, Munc13 and RIMs proteins leading to the priming of the SV at the PM (Priming stage I), which is further regulated by a protein known as Complexin (Priming stage II). Once primed to the PM the vesicle is ready to form a fusion pore with the PM and this is triggered by the Ca^{2+} influx or spontaneously causing the release of the vesicle content. The vesicular release process could be followed by the disassembly of the SNARE complex facilitated by the N-ethyl-maleimide-sensitive factor (NSF) and SNAP proteins allowing for the recycling of the vesicle, or the vesicle might remain primed to the PM and undergo subsequent release until its completely empty. Figure adopted from Rodrigues et al. (2016).*

The mode of neurotransmitter release is dependent on several factors. Synchronous neurotransmitter release, occurring within several milliseconds of the arrival of the AP, depends greatly on the availability of the RRP of vesicles, the brief and fast opening and closing kinetics of voltage-gated Ca^{2+} channels, a Ca^{2+} sensor which can respond quickly to the action potential-gated Ca^{2+} signals and the coupling or proximity of the voltage-gated Ca^{2+} channels to the vesicular release machinery. Low-frequency stimulation predominantly induces synchronous release, whereas continuous moderate to high-frequency stimulations can additionally evoke asynchronous release (Kaeser and Regehr, 2014). As in the case of synchronous release, asynchronous release is dependent on Ca^{2+}, however findings suggest that the source of Ca^{2+} might be located further away from the calcium sensor of the vesicular release machinery (Atluri and Regehr, 1998, Cummings et al., 1996, Van der Kloot and Molgó, 1993), therefore explaining the persistence of release after the end of the stimulus. SYT1, -2 and -9 are identified as the main Ca^{2+} sensors involved in synchronous release in mammals (Fernández-Chacón et al., 2001, Geppert et al., 1994, Pang et al., 2006, Sun et al., 2007, Xu et al., 2007), whereas SYT7 and Doc2 proteins are hypothesized to be the sensors mediating asynchronous release (Maximov et al., 2008, Wen et al., 2010, Yao et al., 2011). Spontaneous neurotransmitter release at the synapse is observed at much slower rates ($<10^{-3}$ vesicles per second) compared to AP evoked release ($>10^3$ vesicles per second) (Kaeser and Regehr, 2014). As with synchronous and asynchronous release, spontaneous release is also thought to be Ca^{2+} dependent, however a Ca^{2+} independent component might also exist (Meffert et al., 1994). Various sources of Ca^{2+} have been linked to spontaneous release, such as voltage gated Ca^{2+} channels (Williams et al., 2012), cation channel subfamily V member 1(TRPV1) channels (Shoudai et al., 2010) and in some synapses release from internal Ca^{2+} stores (Llano et al., 2000). There is also a variability in the molecular machinery facilitating the spontaneous release. In addition to the molecular complex mediating AP dependent release, alternative SNARE proteins such as VAMP4, VAMP7 and vesicle transport through interaction with t-SNAREs homologue 1A (VTI1A) are observed to participate in spontaneous release (Bal et al., 2013b, Ramirez et al., 2012).

3.1.3 Somatic neurotransmitter release

Neurotransmitter release is also observed from the dendrites and the cell bodies of neurons. Peptides such as vasopressin and oxytocin are released by the soma and dendrites of hypothalamic neurons (Landgraf and Neumann, 2004, Leng and Ludwig, 2008, Ludwig and Leng, 2006) and dopamine is released from dendrites and the soma of neurons in the substantia nigra (SN), pars compacta (SNc) and pars reticulata (SNr) (Jaffe et al., 1998, Ludwig et al., 2016, Robertson et al., 1991). The vasopressin and oxytocin neuropeptides are released from large dense-core vesicles (LDCVs), observed within the dendrites and the soma of the magnocellular neurosecretory cells (MCNs)(Pow and Morris, 1989). It is suggested that the control of release of these LDCVs might be exerted by the cytoskeletal elements, such as F-actin, which could either restrict secretory vesicles from moving to the plasma membrane or by reorganising itself it might facilitate the organization of the molecular machinery needed for exocytosis (Dillon and Goda, 2005, Tobin and Ludwig, 2007, Vitale et al., 1995). As in synaptic release, some evidence suggests that release of the LDCVs is catalysed by the participation of SNARE proteins, but this is predominantly supported by experimental observations in the dopaminergic neurons (Witkovsky et al., 2009). Although several proteins, such as VAMP-1 and syntaxin 1a are absent from the somatodendritic compartments of the dopaminergic cells, alternative protein isoforms including VAMP-2, syntaxin 3b and the high Ca^{2+} affinity sensors such as synaptotamin 4 and 7, are expressed in these neurons (Mendez et al., 2011, Witkovsky et al., 2009). Conversely to synaptic neurotransmitter release, somatodendritic release can occur independently of the action potentials and in addition to inflow of extracellular Ca^{2+} ions, it can be facilitated by Ca^{2+} mobilised from intracellular stores (Chen et al., 2011, Ludwig et al., 2002, Ludwig et al., 2005, Patel et al., 2009, Rice et al., 1994, Rice et al., 1997).

In addition to neuropeptides and dopamine, serotonin is another transmitter released by the soma and dendrites of neurons. In the mammalian brain, serotonin is released by a collection of serotonergic neurons located in midline structures of the brainstem, known as the Raphe nuclei (Jacobs and Azmitia, 1992). A subregion of the nuclei, the

dorsal raphe nucleus (DRN) is the place at which most serotonergic innervation of the cerebral cortex originate. Neurotransmitter release from serotonergic raphe neurons is triggered by two different mechanisms depending on the site of release. At synapses, the soma and proximal dendrites, release is triggered by the arrival of the action potential (de Kock et al., 2006, Héry and Ternaux, 1981). In contrast, vesicular release from the distal dendrites is action-potential independent and facilitated by the activation of NMDA receptors and dendritic L-type Ca^{2+} channels (Colgan et al., 2012). As in other neurons, the trafficking, fusion, and release of vesicles filled with neurotransmitter, from the serotonergic neurons is most likely carried out by the formation of alternative synaptic and somatodendritic SNARE complexes (Quentin et al., 2018).

Along with the studies of somatic serotonin release in mammalian brains, a system, which has contributed substantially to the understanding of the mechanism of somatic serotonin release is the giant leech Retzius neurons. The neurons synthesize and package serotonin in clear synaptic and dense-core synaptic and somatic vesicles (Bruns and Jahn, 1995, Kuffler et al., 1987). Quantal release of serotonin, triggered with the ionophore ionomycin, has been directly recorded using amperometry from axonal and somatic sites of cultured Retzius neurons (Bruns et al., 2000). Consecutively, fluorescently labeled vesicles have been observed to undergo exo/endocytosis following high-frequency stimulation with a stimulus of 10 action potentials at 20 Hz. Blocking of different Ca^{2+} channels and incubation with caffeine has shown that the process is dependent on the entry of Ca^{2+} through L-type Ca^{2+} channels and has suggested the contribution of Ca^{2+} induced Ca^{2+} release from intracellular stores (Trueta et al., 2003). The dependence of the somatic vesicular release mechanism, in the Retzius neuron, on multiple sources of calcium and its latency were further unraveled in a study by Leon-Pinzon et al. (2014). Simultaneous imaging of the dynamics of intracellular Ca^{2+} and exocytosis, combined with blocking of L-type Ca^{2+} channels with nimodipine and manipulation of internal calcium stores with ryanodine and thapsigargin, have facilitated the decomposition of the calcium current and it sources. High frequency stimulation (10 action potentials at 20Hz) caused a fast transient Ca^{2+} increase through L-type Ca^{2+} channels, which spreads to nearby regions

triggering the exocytosis of vesicles located close to the plasma membrane, inducing the further release of Ca^{2+} through ryanodine receptors from intracellular stores (presumably the endoplasmic reticulum) (**Figure 3.3 A**). The Ca^{2+} induced Ca^{2+} release together with the fast transient Ca^{2+} are thought to spread further to vesicular clusters, attached to microtubules close to the periphery of the plasma membrane, and to mobilize an ATP-dependent transport of the somatic vesicles towards the plasma membrane (**Figure 3.3 A**) (De-Miguel et al., 2012). Reaching the plasma membrane, the vesicles fuse with it and release their serotonin content, which in turn activates 5-HT_2 autoreceptors. The activation of the 5-HT_2 autoreceptors evokes an additional large transient Ca^{2+} current close to the membrane, which sustains the exocytosis until all nearby vesicles are released. The large transient Ca^{2+} current observed following the activation of the 5-HT_2 autoreceptors is a result of the activation of phospholipase C (PLC) leading to the production of inositol 1,4,5-triphosphate (IP_3), which acts on IP_3 receptors (**Figure 3.3 B**). With the completion of the vesicular release process from the soma of the Retzius neuron, the neurotransmitter vesicles are endocytosed and relocated back to inner region of the cell, where they can be recycled for further use (Leon-Pinzon et al., 2014, Trueta et al., 2012).
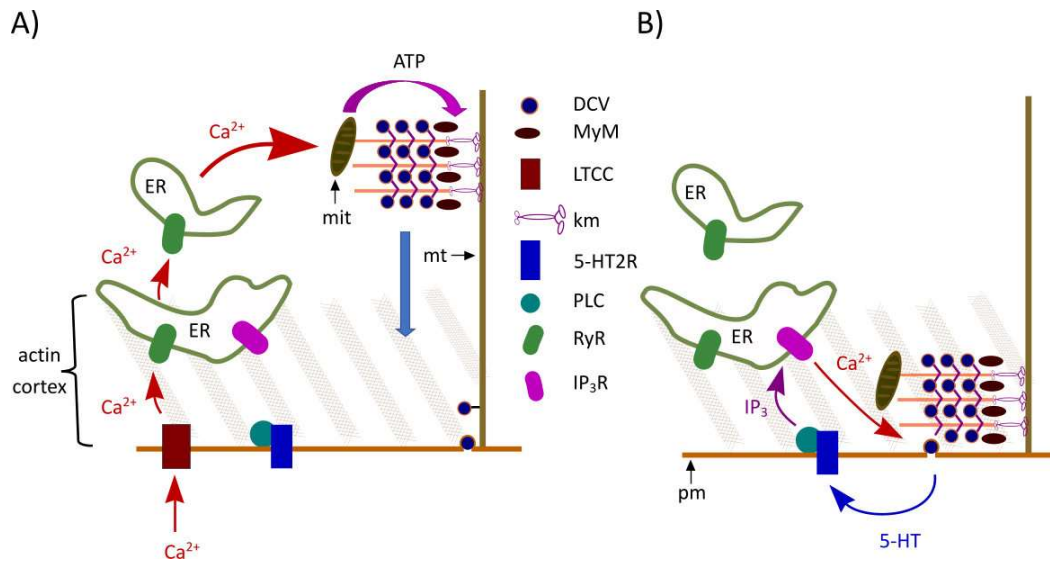
Figure 3.3 Schematic representation of the vesicular release mechanism of serotonin from the soma of the Retzius neurons. A) L-type calcium channels (LTCC) open following a train of action potentials, letting extracellular calcium, which activates ryanodine receptors (RyR) on the Endoplasmic Reticulum (ER). Following activation of RyR, calcium is released from the ER invading the cell soma and stimulating the synthesis of ATP in mitochondria (mit). Kinesin motors (km), activated by ATP move on microtubules (mt) transporting dense core vesicles (DCV) towards the plasma membrane (pm). B) The transportation of the vesicles through the actin cortex is additionally facilitated by myosin motors (MyM). Serotonin from newly released vesicles provides a feedback loop by activation of 5-HT2 receptors, which in turn activate phospholipase C (PLC). The activation of PLC produces IP3, which activates IP3 receptors (IP3R) leading to additional release of intracellular calcium maintaining exocytosis until all vesicles are released.

3.1.4 Control and dynamics of neurotransmitter release

Neurotransmitter release is accomplished through the formation of a fusion pore between the vesicle carrying the neurotransmitter and the plasma membrane. The dynamics of pore formation, its structure and size can determine what neurotransmitters are released, the rate at which they are released and therefore their

extracellular concentration (Chang et al., 2017). Two main structural models of the fusion pore have been proposed. The first model suggests that fusion pores are formed by the lining of 24 transmembrane domains (TMD) of the SNARE proteins synaptobrevin and synaptophysin into a ring-like structure forming a gap junction (Adams et al., 2015, Han and Jackson, 2005, Han et al., 2004). However, such a model proposes a very large pore and is contradicted by studies showing that fusion pores can be formed with as little as one SNARE complex and kept open with only three SNARE complexes (Shi et al., 2012). An alternative model suggests a fusion pore made solely of lipids but formed remotely by surrounding proteins (Chanturiya et al., 1997, Nanavati et al., 1992). Although, such a model supports fusion pores with a conductance similar to experimentally observed values, it is more plausible that the fusion pore is composed of both lipids and proteins as both mutations of the transmembrane domains of proteins of the SNARE complex and changes in membrane lipid composition influence neurotransmitter release. Mutations of the transmembrane segment of syntaxin, in phaeochromocytoma (PC 12) cells, shows alterations to the pore conductance and the flux on neurotransmitter through the pore (Han et al., 2004). Similarly, changes to the transmembrane domains of synaptobrevin 2 also alters the fusion pore conductance and parameters of the amperometrically recorded release from chromaffin cells (Chang et al., 2015). Changes is cellular cholesterol in chromaffin cells have an effect of the prespike foot of the release events and nano-injections of phospholipids to the same type of cells alters the number of released catecholamines (Aref et al., 2020, Wang et al., 2010). The effect of different changes in membrane lipids and protein expression are summarised in **Table 3-1**.

Lipid/Protein	Molecules	i-max	t-half	t-rise	t-fall	foot parameters	Cell type, study
cholesterol (*reduction*)	–	–	–	NR	–	foot duration ↓	Chromaffin cells, (Wang et al., 2010).
cholesterol (*overload*)	–	–	–	NR	–	foot duration ↑, % release during foot ↑	
PE injection	↑	↑	↑	↑	↑	NR	PC12 cells, (Aref et al., 2020).
PC injection	↓	↓	↓	–	–	NR	
LPC injection	↓	↓	↓	–	–	NR	
LPC *(3 min)*	↑	↑	NR	↓	NR	NR	Chromaffin cells, (Amatore et al., 2006).
AA (arachidonic acid)	↓	↓	NR	↑	NR	NR	
PS *(3 days)*	–	–	–	–	–	NR	PC12 cells, (Uchiyama et al., 2007).
PI	–	–	–	–	–	NR	
PC	↓	↓	↑	–	↑	NR	
PE	–	↑	↓	–	↓	NR	
SM	–	↓	↑	↑	–	NR	
AA *(30 min)*	↑	↑	–	↓	↑	NR	Chromaffin cells, (García-Martínez et al., 2013).
sphingomyelinase	↑	↑	–	↓	–	NR	
Actin (*inhibition*)	↑	↑	↑	–	↑	NR	PC12 cells, (Trouillon and Ewing, 2014).
Dynamin (*knock-out*)	↑	↑	↑	NR	NR	foot charge ↑, foot duration ↑	Chromaffin cells, (Wu et al., 2019)
Syntaxin (*modifications*)	NR	NR	NR	NR	NR	foot current ↑, foot amplitude ↓	PC12 cells, (Han et al., 2004).
Synaptobrevin (*knock-out*)	NR	NR	NR	NR	NR	foot amplitude ↓	Chromaffin cells, (Chang et al., 2015)

Table 3-1 Summary of the effect of changes in lipids and proteins on the release characteristics of the amperometry events (↑ - significant increase, ↓ - significant decrease, '–' - not significant, NR – not reported).

3.1.5 Phases of the fusion pore

Simultaneous measurements of changes in cell capacitance, using whole cell patch clamp, and the flux of neurotransmitter release of oxidizable catecholamines, using amperometry, has allowed for the distinction of the different phases the fusion pore goes through to facilitate neurotransmitter release. The dynamics of the vesicular release process are described by the kinetics of the individual release events, recorded using amperometry. Analyses of these recordings have provided information about the size of the pore, its conductance and the concentration of the transmitters released (Albillos et al., 1997, Dernick et al., 2005).

The first phase of neurotransmitter release is characterised by the initial formation of a fusion pore, through which there is still no flow of molecules (**Figure 3.4 B, Fusion pore opening**). This phase is followed by a slow expansion phase, with is characterised by an increase of the cell membrane capacitance, initiation of pore conductance and a slow outflux of neurotransmitters (Tabares et al., 2003). On the amperometry trace the neurotransmitter outflow is observed as a small current step, known as a pre-spike foot (PSF) (Chow et al., 1992, Wightman et al., 1995) (**Figure 3.4 B: Fusion pore opening; A: Change in membrane capacitance, amperometric current step, pore conductance**). In the final step of the pore formation, the vesicle fully merges with the plasma membrane following fusion pore expansion, which leads to an increase of neurotransmitter outflow, observed as a full current spike on the amperometry trace (**Figure 3.4 B: Fusion pore expansion; A: Amperometry spike**)(Álvarez de Toledo et al., 2018). The expansion of the fusion pore could continue until the membrane of the vesicle fully fuses with the plasma membrane, leading to the complete release of the neurotransmitter content of the vesicle, or the fusion pore expansion could be reversed and closed, leading to partial release of the neurotransmitter. In both cases this is usually observed as a slow decay of the amperometric spike to the initial level of the trace (**Figure 3.4 A: Amperometry**) (Harata et al., 2006). However, detailed examinations of the decay phase of the amperometric peaks recorded from PC12 cells have also revealed the existence of feet on the descending part of the peak, a feature

that is predicted by the closure of the vesicle (Mellander et al., 2012). It is believed that the shape of the decay of the spike is determined by the dissociation and diffusion of the neurotransmitter from a polyelectrolyte matrix, which occupies the interior of the vesicle, through the fusion pore (Wightman et al., 2002). An increasing number of studies support the notion of partial release, which has been initially referred to as 'kiss-and-run' (Elhamdani et al., 2006, Fesce et al., 1994, Larsson et al., 2020, Mellander et al., 2012, Omiatek et al., 2010, Ren et al., 2016, Sulzer and Edwards, 2000, Wang and Ewing, 2021). This suggests that the amount of neurotransmitter released by the vesicles could also be determined by the mechanism of pore closure.
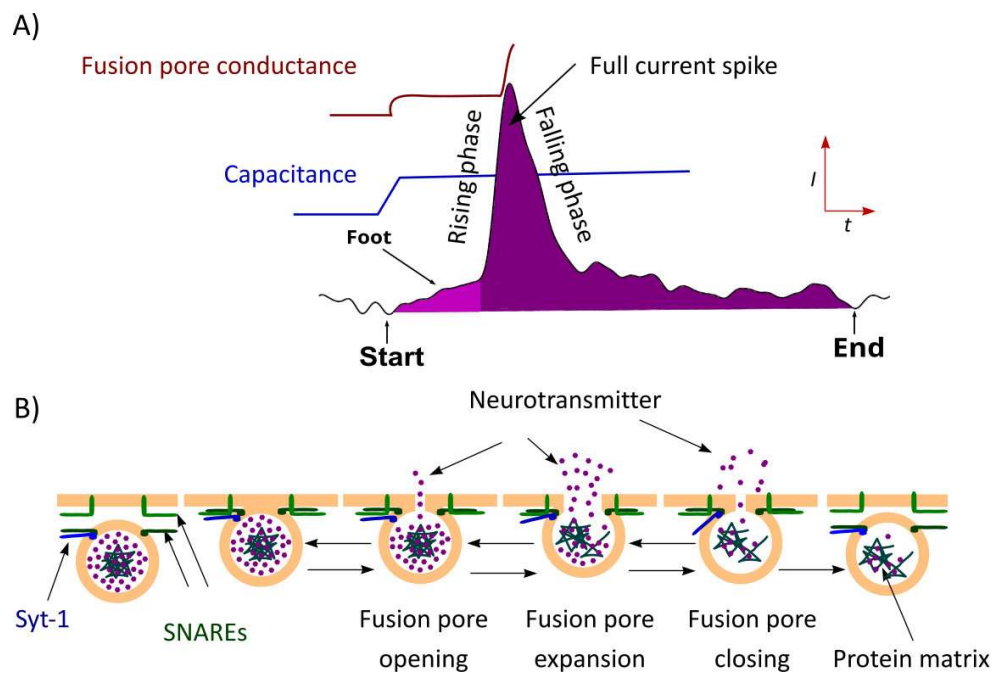
Figure 3.4 Model of vesicular pore formation along with amperometric spike, fusion pore conductance and cell membrane capacitance traces. *A) The exocytosis process is observed as an increase of cell membrane capacitance (blue trace) following the initial pore opening, a small current step (foot) on the amperometry trace (black trace) and the initiation of a fusion pore conductance (red trace). Following full membrane merging, there is no additional change in the capacitance, but a full current spike is observed on the amperometry trace and there is a large increase in the pore conductance. B) Vesicle containing protein matrix and neurotransmitter docking at the plasma membrane via SNARE complex and undergoing exocytosis through the forming an opening (fusion pore), which undergoes expansion and closure.*

Not much is known about how the fusion pore closes, however inhibition of actin, using latrunculin A in PC12 cells has shown an increase of the neurotransmitter released and a slowing of the falling phase of the amperometric events, suggesting its involvement in the regulation of the pore closure (Trouillon and Ewing, 2014). Similarly, a role of dynamin 1 in pore closure is supported by observations of increased transmitter release in dynamin knockouts in naïve adrenal chromaffin cells (Wu et al., 2019).

The aim of this chapter is to use carbon fibre microelectrodes to probe release of serotonin from the CGCs of young and old *Lymnaea*. Previously, only spontaneous release has been detected from the soma of the cells (Patel et al., 2010). However, in other studies that have looked at release from cell bodies of endocrine cells and neurons a range of triggers have been used. These include high K+ salines (Li et al., 2016b, Ren et al., 2017, Wang et al., 2021), neuronal depolarisation via an intracellular microelectrode (Leon-Pinzon et al., 2014, Trueta et al., 2003, De-Miguel et al., 2012) and ionomycin (Bruns et al., 2000). Therefore, similar triggers will be used in an attempt to stimulate release from the CGCs.

3.2 Experimental methods

3.2.1 Animals used in the experiments

Pond snails *Lymnaea stagnalis,* between 3- and 12-months old were used in the experiments. 3 to 4 months old snails represent young sexually mature animals. By fitting the survival curves of batches of snails to a Weibull function, snails representing the last 20% of surviving animals were typically between 10-12 months old and are classed as old (Arundell et al., 2006, Hermann et al., 2007, Patel et al., 2006). The breeding and maintenance of the animals were done at the University of Brighton facilities, where animals were kept in tanks of copper-free water at temperatures of 18 – 20 °C. A 12 h light and dark cycle was maintained, and the animals were fed every other day on an alternating diet of round lettuce and fish food (Sera Flora, Germany).

3.2.2 CNS Preparations

The CNS preparations used in the electrophysiological recordings were made by dissecting the CNS from the snail and pinning it dorsal side up in a Sylgard-lined dish filled with normal HEPES-buffered saline (mM concentration stated below). The CGCs were exposed by cutting the cerebral-cerebral commissure and pinning the two cerebral ganglia laterally (**Figure 3.5**). The outer connective tissue sheath covering the cerebral ganglia was removed with the use of fine forceps and the inner sheath digested with Protease (Type VIII, lyophilized powder, Sigma-Aldrich, UK) 1 mg mL^{-1} in HEPES-buffered saline by keeping the CNSs of young snails in the protease for ~45 min and the CNSs of old snails for ~ 55 min due to their thicker connective tissue. Once proteased, the connective tissue was carefully removed with fine forceps.
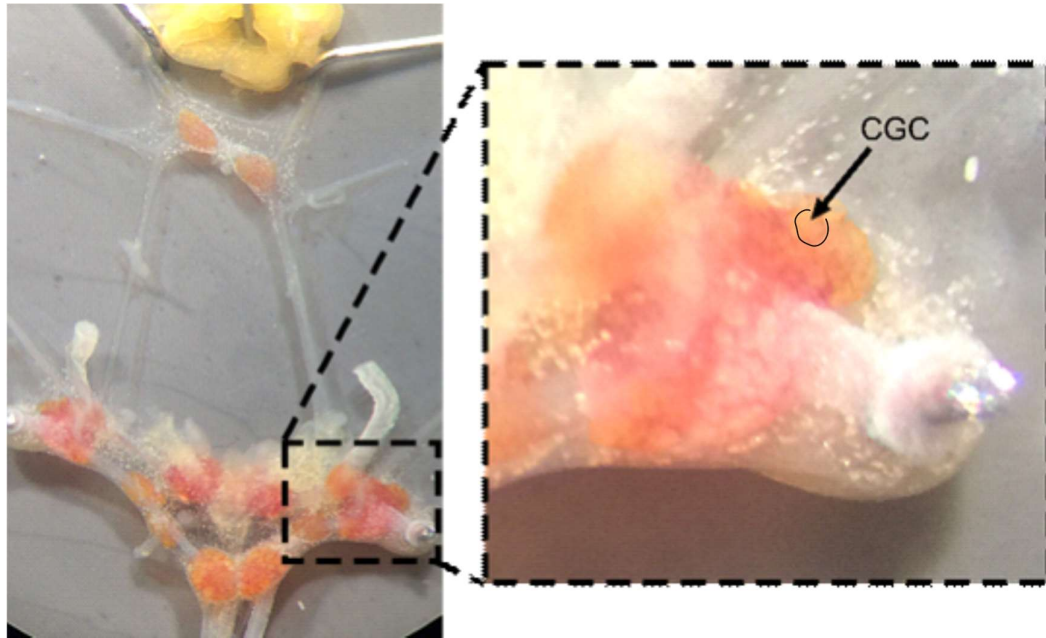
Figure 3.5 CNS of Lymnaea pinned down dorsal side up, in a Sylgard lined dish with the CGC on the right.

During the electrophysiology/electrochemistry recordings the bath containing the CNS was constantly perfused with normal HEPES-buffered saline through a gravity fed perfusion system at a rate of ~1 ml min^{-1}. Spontaneous serotonin release was recorded by placing the carbon fibre microelectrode on the soma of the CGC.

3.2.3 Solutions used in the electrochemistry experiments.

All chemicals used in the making of different saline were obtained from Sigma-Aldrich, UK.

Saline	Content in mM
Normal HEPES-buffered saline	NaCl 50; KCl 1.5; CaCl$_2$ 4; MgCl$_2$ 2; N-(2-Hydroxyethyl)piperazine-N'-(2-ethanesulfonic acid) (HEPES) 10
5 mM KCl HEPES-buffered saline	NaCl 46.5; KCl 5; CaCl$_2$ 4; MgCl$_2$ 2; N-(2-Hydroxyethyl)piperazine-N'-(2-ethanesulfonic acid) (HEPES) 10
5 mM KCl, 10 mM CaCl$_2$ HEPES-buffered saline	NaCl 40.5; KCl 5; CaCl$_2$ 10; MgCl$_2$ 2; N-(2-Hydroxyethyl)piperazine-N'-(2-ethanesulfonic acid) (HEPES) 10
10 mM KCl HEPES-buffered saline	NaCl 41.5; KCl 10; CaCl$_2$ 4; MgCl$_2$ 2; N-(2-Hydroxyethyl)piperazine-N'-(2-ethanesulfonic acid) (HEPES) 10

The pH of all salines was adjusted to 7.9 with 1 or 10M NaOH.

The Normal HEPES-buffered saline was exchanged by either the 5 mM KCl HEPES-buffered saline for 3 min, the 5 mM KCl & 10 mM CaCl$_2$ HEPES-buffered saline for 3 min or the 10 mM KCl HEPES-buffered saline for 4 min.

3.2.4 Pharmacological agents used in the electrochemistry experiments.

3.2.4.1 Ionomycin

Ionomycin was used to evoke serotonin release from the CGCs.

Stock solution was prepared by dissolving the Ca^{2+} ionophore, ionomycin free acid (Bio-Techne Ltd) at 2.5 mM in DMSO. For use in the experiments the stock solution

was diluted in HEPES-buffered saline to final concentration of 2.5 µM yielding a final concentration of DMSO of 0.1 %. Preliminary experiments showed that this concentration of DMSO did not affect vesicular release from the CGCs. 2.5 µM ionomycin was perfused through a gravity fed focal perfusion system (1 ml min^{-1}) added to the bath on the right side of the CNS ~300 to 400 µm away from the right CGC. Before ionomycin was used, HEPES-buffered saline was perfused for 2 min from the same perfusion tube to determine if the introduction of additional flow of solution close to the CGC has any effect on the CGC's release pattern.

3.2.5 Electrophysiology recordings

CGCs' firing activity was recorded with the use of sharp intracellular glass microelectrodes (10 to 50 MΩ resistance), backfilled with 3 M potassium acetate/0.5 mM potassium chloride and marked with black ink (Windsor and Newton, UK) at the tip for better visualization. Signals were recorded and amplified with the use of Axoclamp 2B (Molecular Devices, U.S.A.) amplifier and digitised with Axon Digidata 1440A (Molecular Devices, U.S.A.). Data were sampled at 25 KHz. All recordings were made with the use of pClamp 10.0 (Clampex, Molecular Devises, U.S.A.) software.

3.2.6 Electrochemistry recordings

Electrochemical recordings of serotonin release were carried out with the use of the 10 µm bevelled carbon fibre microelectrodes positioned on the CGC cell body. The carbon fibre microelectrodes were held at +750 mV vs. Ag/AgCl reference electrode and signals were recorded using Axopatch 200B amplifier (Molecular Devices, U.S.A.) and digitised with Axon Digidata 1440A (Molecular Devices, U.S.A.). Data were sampled at 25 KHz and filtered by a lowpass 4-pole BESSEL filter at 5 KHz. All recordings were made with the use of pClamp 10.0 (Clampex, Molecular Devises, U.S.A.) software.

The CGCs have been identified to have serotonin as their main neurotransmitter (McCaman et al., 1984, Kemenes et al., 1989, Morgan et al., 2021, Yeoman et al., 1994a, Yeoman et al., 1994b), however a single study has also shown the coexistence of serotonin and dopamine in the CGCs (Boer et al., 1984). Therefore, a couple of recordings were used to confirm the nature of the neurotransmitter released, in which the holding potential of the used carbon fibre microelectrode was first lowered from their initial holding potential of + 750 mV to + 200 mV and ~ 100 s latter increased to + 400 mV for another 100 s and then returned to +750 mV. These values were selected according to the DPV experiments conducted in Chapter 2, which showed that on 10 μm disc microelectrodes dopamine reaches peak oxidation at + 125.3 mV, serotonin at +283 mV and octopamine at +633 mV.

3.2.7 Analysis of the electrochemistry recordings

Amperometric events were analysed using IgorPro 6 routine from David Sulzer laboratory (Mosharov and Sulzer, 2005). The differentiated trace was filtered at 300 Hz, but no filtering was applied to the current trace. The chosen threshold for the peak detection was 3.5 * SD (dI/dt) and 1.5 * SD(I) for the foot. All detected events were visually confirmed before any analysis was performed. The software allows for the analysis of event parameters such as: the amplitude of the event (I_{max}); the time it takes for the peak to rise from 25% to 75% of its maximum (t_{rise}); the width of the event at half of its amplitude ($t_{1/2}$); the time it takes for the peak to fall from 75% to 25% of its maximum (t_{fall}); the number of molecules released per event (Q); the current of the foot (I_{foot} or Foot$H$); the lifetime of the foot (t_{foot} or Foot$W$) and the number of molecules released during the time of the foot (Foot$Q$) (**Figure 3.6**). The number of moles of oxidized serotonin is determined using Faraday's law:

Q = nFN

where Q is the integrated charge under the individual event, n is the number of electrons produced by the oxidation of serotonin (n = 2), F is Faraday's constant and N is the number of moles of oxidised serotonin.
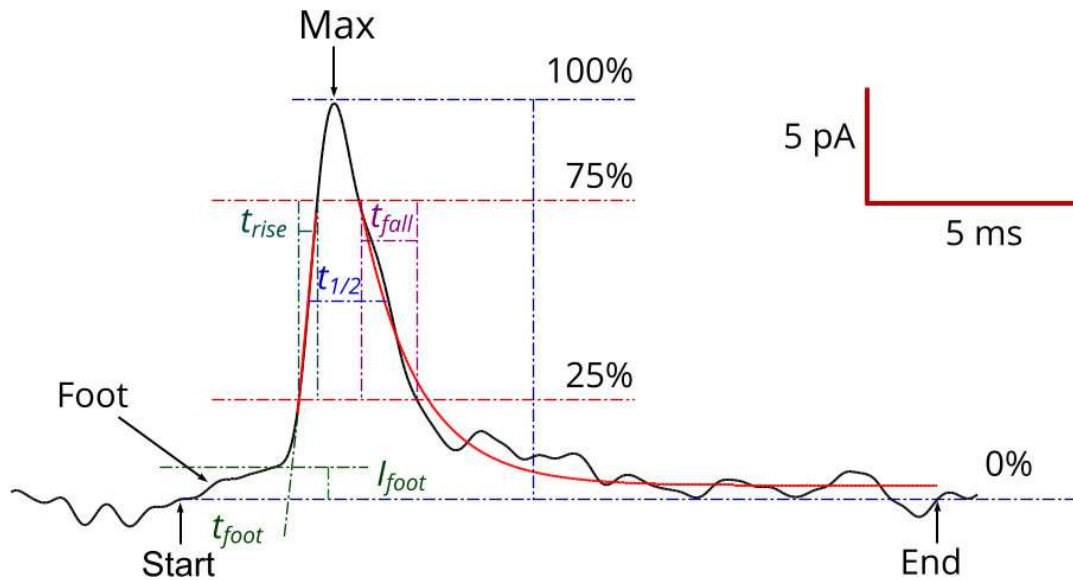
Figure 3.6 Parameters of release events. *Sample release event detected using the Sulzer software showing how the different parameters of the release event were determined.*

3.2.8 Analysis of the electrophysiological recordings

Electrophysiology recordings were analysed offline using pClamp 10.0 (Clampfit, Molecular Devices, U.S.A.) and were not filtered. The Clampfit's® functions 'Event detection' and 'Template search' were used to identify and measure the action potential firing frequency and the membrane potential of the CGCs. For the recordings in which the CGCs were perfused with the High KCl HEPES-buffered saline, the action potential firing frequency and membrane potential were analysed for 300s before the exchange of the normal HEPES-buffered saline with the High KCl HEPES-buffered saline, and 60s after the start of the High KCl HEPES-buffered saline, they were analysed for another 300s. For the recordings in which the CGCs were perfused with ionomycin, the action potential firing frequency and membrane potential were analysed for 180s before the ionomycin perfusion and for 180s, 120s after the start of the ionomycin perfusion. In the recordings in which AP were triggered by injection of

current, action potential firing frequency and membrane potential were analysed for 300s before the trigger and then for as long as the trigger lasted.

The analysed values were averaged for each recording and used to determine a population mean ± SEM.

3.2.9 Statistical analysis

GraphPad Prism 9 (GraphPad Software, La Jolla California USA) was used for all statistical analysis of the amperometry data. Normality of the data distribution was tested with Kolmogorov-Smirnov test. Data are displayed as individual values or as scatter plots with range and mean value for normally distributed data or a median value for not normally distributed data. The statistical analyses were performed on the mean of the median values obtained from each individual cell-recording and only recordings with more than 10 events were used. The event parameters between two groups were compared using Student's t-test for normally distributed data and Mann-Whitney test for data that was not normally distributed. More than two groups of data were compared using one-way ANOVA with a post hoc Tukey's multiple comparisons test. Compared groups were considered significantly different if $p < 0.05$. All p-values are shown above the graphs.

3.3 Results

3.3.1 Detection of somatic vesicular release events

Initially, spontaneous somatic vesicular release was recorded by positioning the 10 μm carbon-fibre microelectrode held at +750 mV, on the soma membrane of the right CGC of young and old snails. If vesicular release was not present and given that the soma was 50-75 μm in diameter, the carbon-fibre microelectrode was relocated to other locations on the soma membrane to find an active vesicular release site. Initial attempts were made to record release from the cells with the inner connective tissue still intact, but as no release was observed, the sheath was removed, allowing vesicular release events to be recorded (**Figure 3.7 B**). The events had a classical shape with a steep rise phase and an exponential decay (**Figure 3.7 A**).
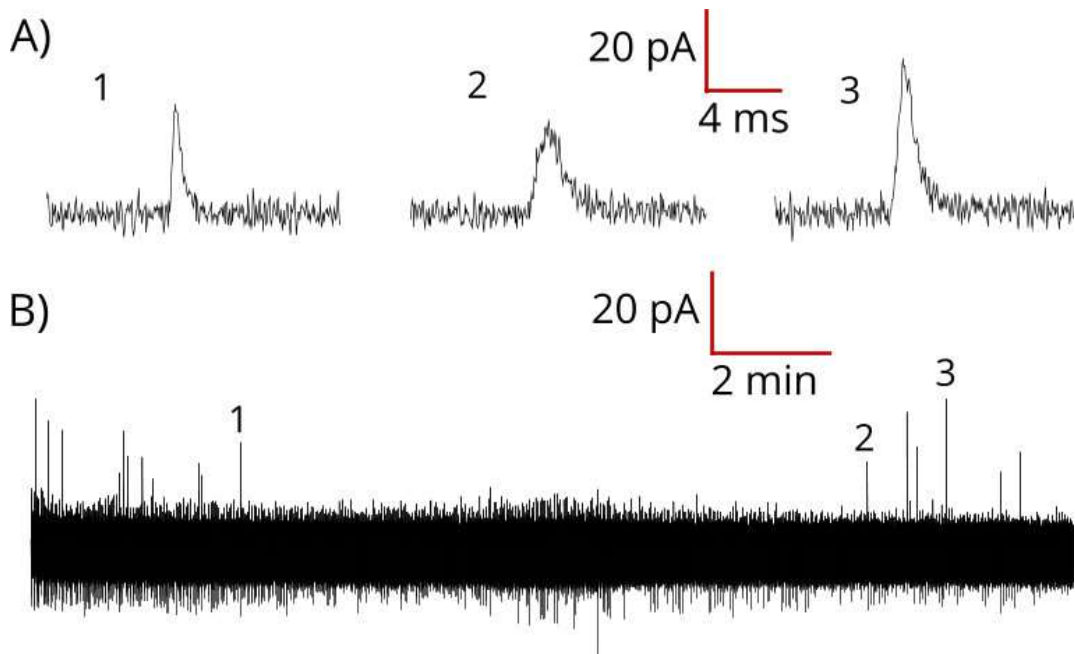
Figure 3.7 Sample trace showing spontaneous vesicular release from the soma of the CGC. A) Example of individual events on expanded time base and B) sample trace with multiple vesicular events.

In addition to the release events, the action potentials fired by the CGCs could also be recorded simultaneously using the sensor (**Figure 3.8**). The CGCs are a single pair of cells with one cell of the pair located in each of the left and right cerebral ganglia. The pair fire synchronously and are the only large cells in the ganglia that have this property. Therefore, when an intracellular recording of the left CGC is combined with the amperometric recording from the right CGC, synchronous action potentials from both cells could be observed (**Figure 3.8 A and B**). The action potentials on the amperometry traces are observed as an initial negative peak followed by a positive going waveform which then returns to baseline. A typical action potential waveform is compared to a vesicular event waveform in **Figure 3.8 C**, showing that the two waveforms are easily distinguishable.
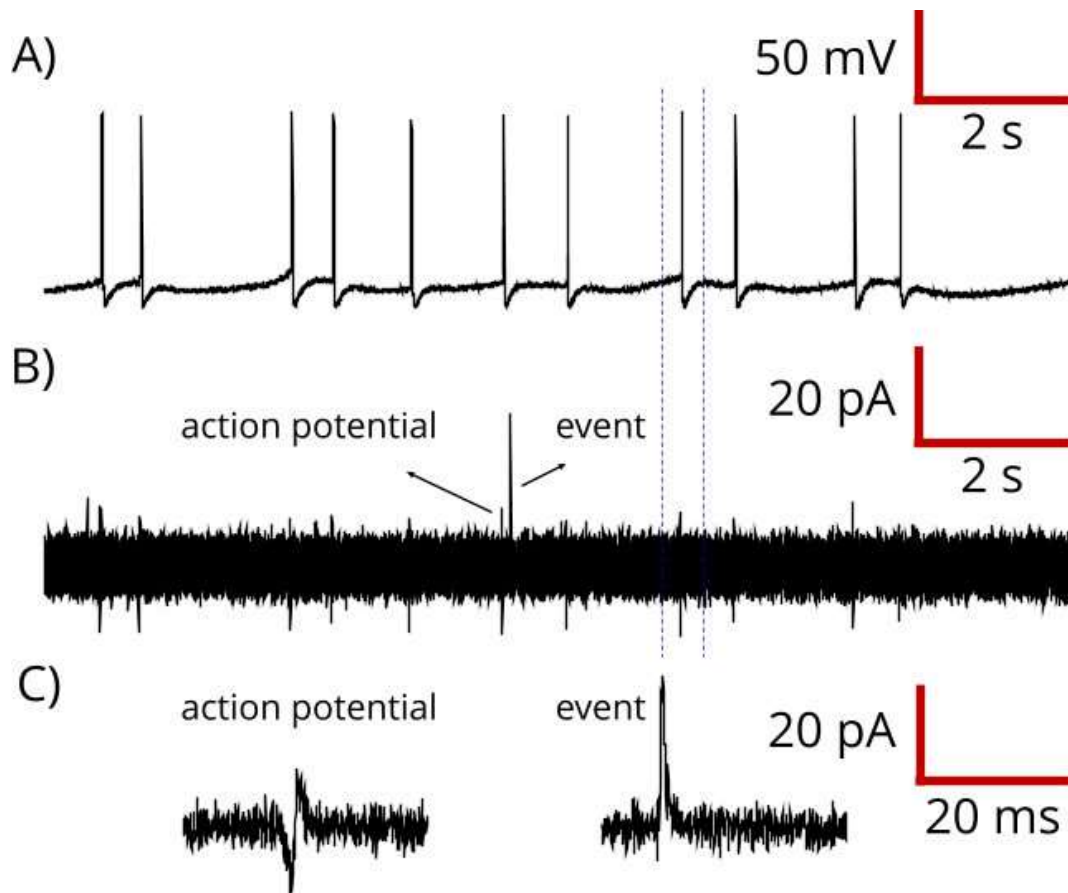
Figure 3.8 Example of a trace showing a spontaneously release event and an action potential. A) Electrophysiological trace of the CGC firing action potentials recorded from the left CGC. B) Amperometry trace recorded from the right CGC with an example of event and action potentials. The blue dotted lines show the synchronous action potential recorded with an intracellular electrode in A and extracellularly using the carbon fibre microelectrode in B. C) Action potential and release event shown on expanded time base.

During some of the experiments, relocation of the carbon fibre microelectrodes on the cell surface membrane to find a release site, appeared to alter the electrical activity of the CGC recorded using the intracellular microelectrode (**Figure 3.9 A**) and these changes were associated with multiple vesicular release events (**Figure 3.9 B**). In these experiments the carbon fibre microelectrode appeared to have adhered to cell membrane and when pulled to be moved, it pulled on the cell membrane, possibly causing transient damage to the membrane.
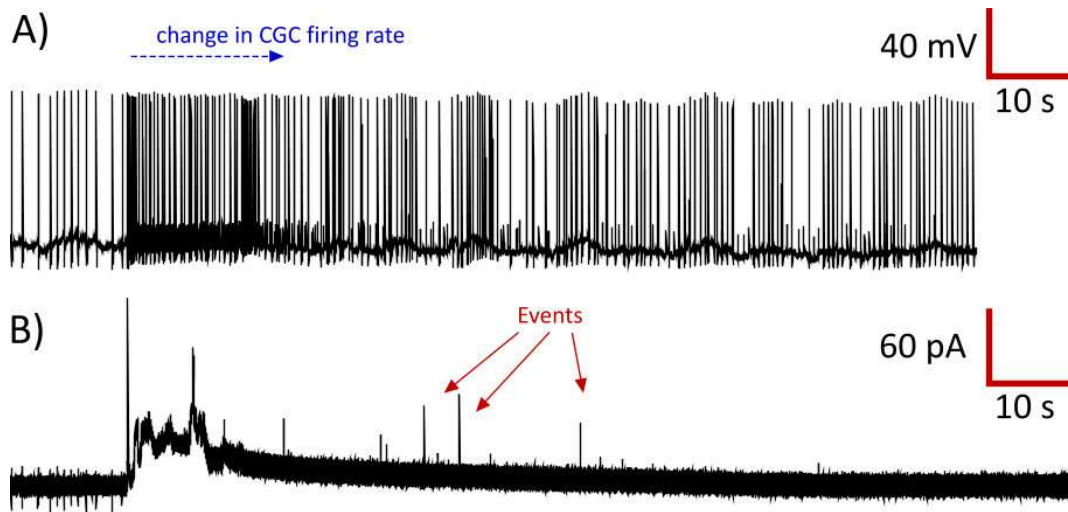
Figure 3.9 Vesicular release caused by the electrode re-placement. *A) Example of an electrophysiological trace of the CGC firing action potentials recorded from the lCGC. B) Example of the corresponding amperometric trace recorded from the rCGC with events triggered by the electrode re-placement.*

As the two neurotransmitters, serotonin and dopamine, are oxidized by different positive peak potentials, + 125.3 mV for dopamine and +283 mV for serotonin as shown in Chapter 2, in this experiment different positive potentials were used to determine the neurotransmitter oxidized during vesicular release. In the two experiments used for these investigations, the holding potential of the carbon fibre microelectrodes was first lowered from their initial holding potential of + 750 mV to + 200 mV and ~ 100 s latter increased to + 400 mV for another 100 s and then returned to +750 mV (**Figure 3.10 A**). The number of events occurring during each interval were counted and compared. Lowering the holding potential to + 200 mV significantly decreased the number of recorded events per second. Increasing the holding potential

back to +400 mV and then to +750 mV restored the number of release events back to initial values recorded at the start of the experiment (**Figure 3.10 B**).
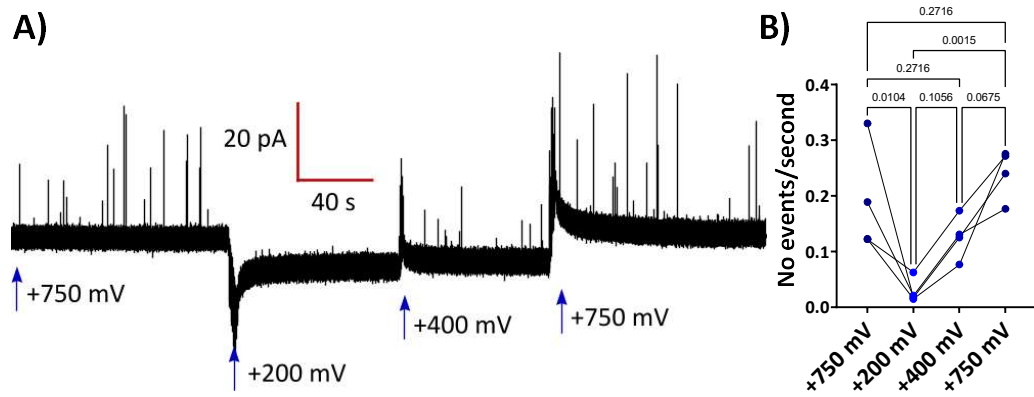
Figure 3.10 Most neurotransmitter oxidation of events released by the CGCs occurs at potentials higher than + 400 mV. *A) Example of an amperometry trace with release initially recorded at + 750 mV, then at +200 mV, +400 mV and +750 mV. B) Comparison of the number of oxidized vesicular event at different holding potentials (One-way ANOVA with Holm-Sidak multiple comparisons test, p-values shown above the graph).*

3.3.2 Triggering of somatic vesicular release from the CGCs.

A range of different methods were utilised to evoke transmitter release from the CGC soma. Previous studies have shown that perfusing cells with a high K$^+$ saline can evoke transmitter release. Normal HEPES-buffered saline containing 1.7 mM KCl, was therefore exchanged with a 5 mM KCl HEPES-buffered saline for 3 minutes to try to evoke release. Observations of the recorded electrophysiological and amperometric traces showed that the high K$^+$ perfusion depolarised the CGCs from a mean of -57.15 mV to a mean of -54.26 mV, and increased AP firing of the CGCs from a mean of 0.56 Hz to a mean of 0.70 Hz (**Figure 3.11 A, C and D**), however it only evoked one event in one of the 3 CNS preparations used (**Figure 3.11 B**).
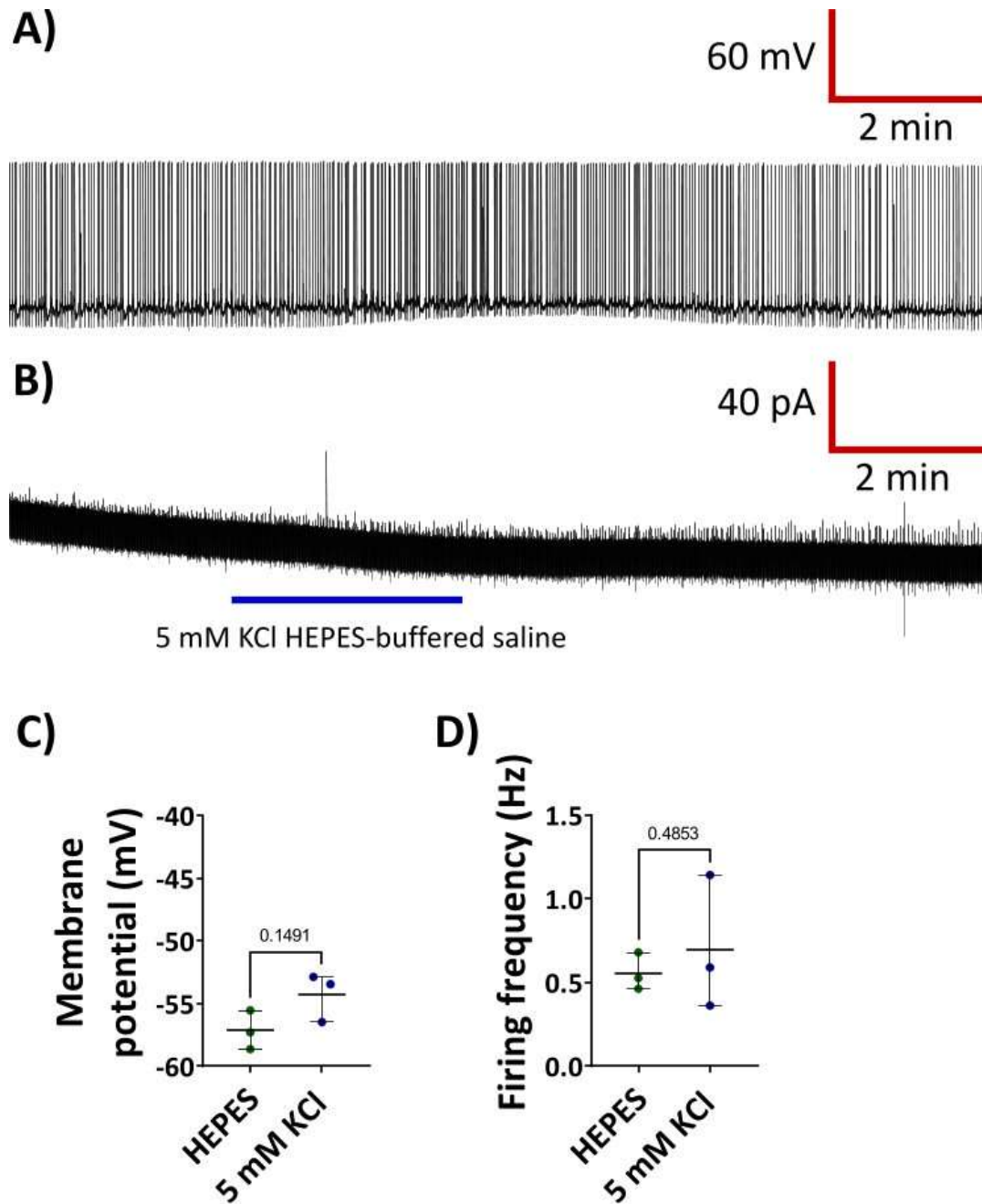
Figure 3.11 5 mM KCl HEPES-buffered saline could not trigger vesicular release from the CGCs. *A) Example of an electrophysiological trace of the CGC firing action potentials recorded from the left CGC. B) Example of the corresponding amperometric trace recorded from the right CGC. C) Membrane potential of the CGCs in normal HEPES-buffered saline and 5 mM KCL HEPES-buffered saline (n = 3, paired t-test). D) Firing frequency of the CGCs in normal HEPES-buffered saline and 5 mM KCL HEPES-buffered saline (n = 3, paired t-test).*

Given that Ca^{2+} is a trigger for vesicular release, experiments were performed in which normal HEPES-buffered saline was exchanged with HEPES-buffered saline containing 5 mM KCl and 10 mM $CaCl_2$ to both depolarise the CGCs and increase the flux of Ca^{2+} into the CGC soma. Similar to the observations above, the change of saline depolarised the CGCs from a mean of -57.15 mV to a mean of -52.06 mV but decreased AP firing rate from a mean of 0.56 Hz to a mean of 0.41 Hz (**Figure 3.12 A, C and D**), and it did not trigger vesicular release (**Figure 3.12 B**).
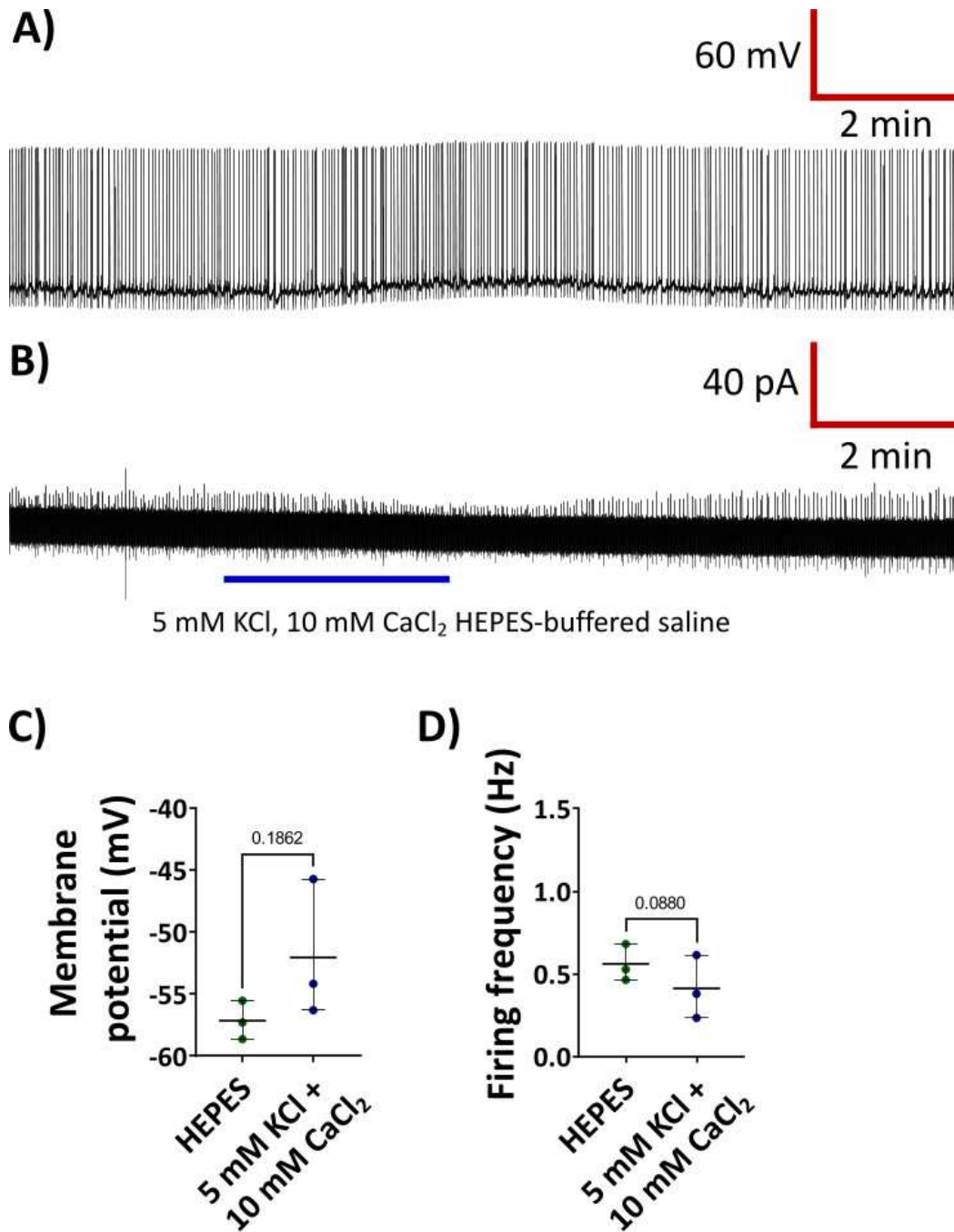
Figure 3.12 5 mM KCL, 10 mM CaCl₂ HEPES-buffered saline could not trigger vesicular release from the CGCs. *A) Example of an electrophysiological trace of the CGC firing action potentials recorded from the left CGC. B) Example of the corresponding amperometric trace recorded from the right CGC. C) Membrane potential of the CGCs in normal HEPES-buffered saline and 5 mM KCl 10 mM CaCl₂ HEPES-buffered saline (n = 3, paired t-test). D) Firing frequency of the CGCs in normal HEPES-buffered saline and 5 mM KCl 10 mM CaCl₂ HEPES-buffered saline (n = 3, paired t-test).*

An additional five experiments were carried using 10 mM KCl in a HEPES-buffered saline as a possible stimulus of vesicular release. Perfusing the CGCs for 5 min with a higher concentration of K^+ ions first depolarised the cells from a mean of -57.88 mV to a mean of -50.82 mV, and then decreased the firing of APs from a mean of 0.52 Hz to a mean of 0.24 Hz (**Figure 3.13A, C and D**), but like the previous experiments, it did not trigger vesicular release (**Figure 3.13 B**).
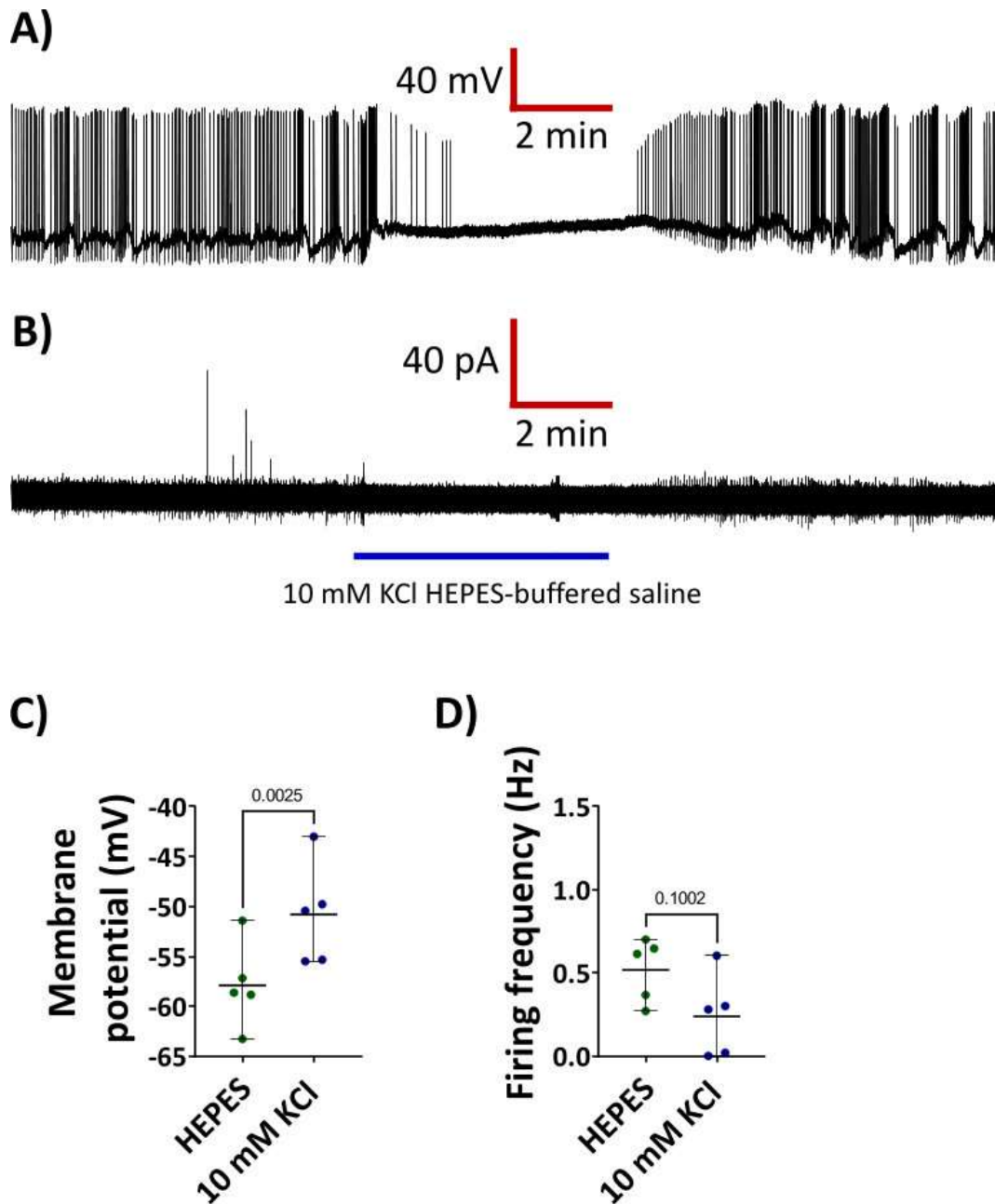
Figure 3.13 10 mM KCl HEPES-buffered saline could not trigger vesicular release from the CGCs. *A) Example of an electrophysiological trace of the left CGC firing action potentials recorded before, during and after perfusion with 10 mM KCl HEPES-buffered saline. B) Example of the corresponding amperometric trace recorded from the right CGC. C) Membrane potential of the CGCs in normal HEPES-buffered saline and 10 mM KCl HEPES-buffered saline (n = 5, paired t-test). D) Firing frequency of the CGCs in normal HEPES-buffered saline and 10 mM KCl HEPES-buffered saline (n = 5, paired t-test).*

High frequency action potential firing was able to drive vesicular release of 5-HT from the cell soma of cultured leech Retzius neurons. This stimulus was explored in the *Lymnaea* CGCs by the injection of depolarising current pulses for ~20 s into the left CGC through an intracellular recording electrode while recording release from the right CGC using the microelectrode sensor (**Figure 3.14 A**). The experiments were attempted on 4 different CNS preparations and although the current injection increased the firing frequency of both the left (from mean of 0.57 to 3.19 Hz, **Figure 3.14 C**) and the right CGCs, no transmitter release was triggered from the right CGCs (**Figure 3.14 B**).
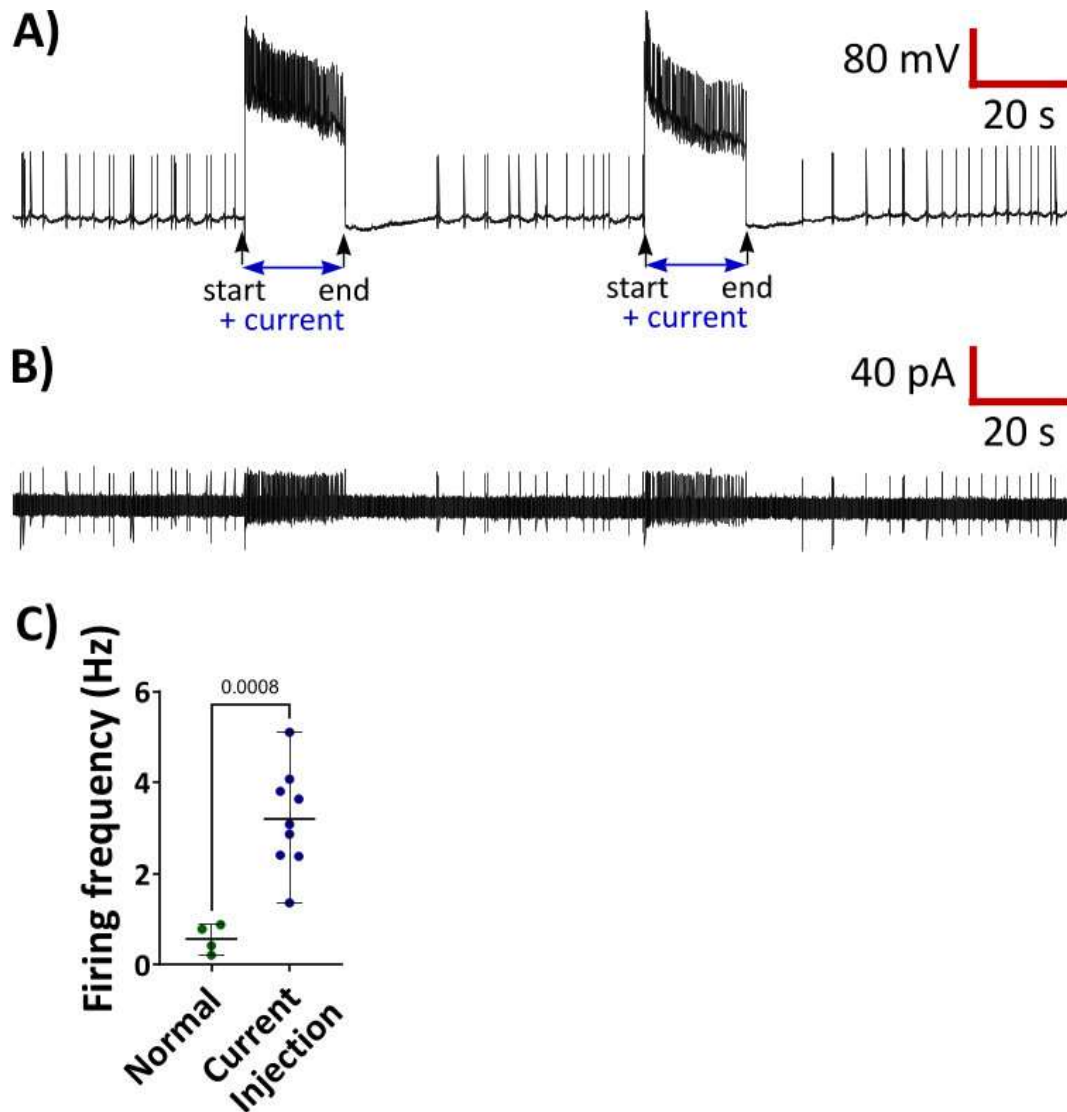
Figure 3.14 Injections of constant positive current to the left CGC did not trigger release from the right CGC soma*. A) Example of an electrophysiological trace of the left CGC showing the current injection and the increase in CGC firing rate B) Example of the corresponding amperometric trace recorded from the right CGC showing the corresponding increase of action potential firing. C) CGC Normal firing frequency and firing frequency during the current injection (normal n = 4, current injection n = 9, unpaired t-test).*

In addition to a constant current pulse injection, 5 or 10 groups of trains of current pulses were also used in 10 CNS preparations, in an attempt to trigger vesicular release as high frequency pulses had been shown to evoke somatic release in the Retzius neuron of the leech (Trueta et al., 2003) (**Figure 3.15 A and B**). Twenty milliseconds current pulses were injected every 90 ms such that each current pulse can trigger an action potential (**Figure 3.15 B**). This would yield a firing frequency of approximately 10 Hz like that utilised in the leech. During the first group of current pulses injected into the left CGC (**Figure 3.15 C**), action potentials were triggered by each pulse, which could be seen on the amperometry trace (**Figure 3.15 D**), however further pulse injections appeared unable to continue to reliably trigger action potentials. No vesicular release was observed during the first or subsequent trains of current injection pulses.
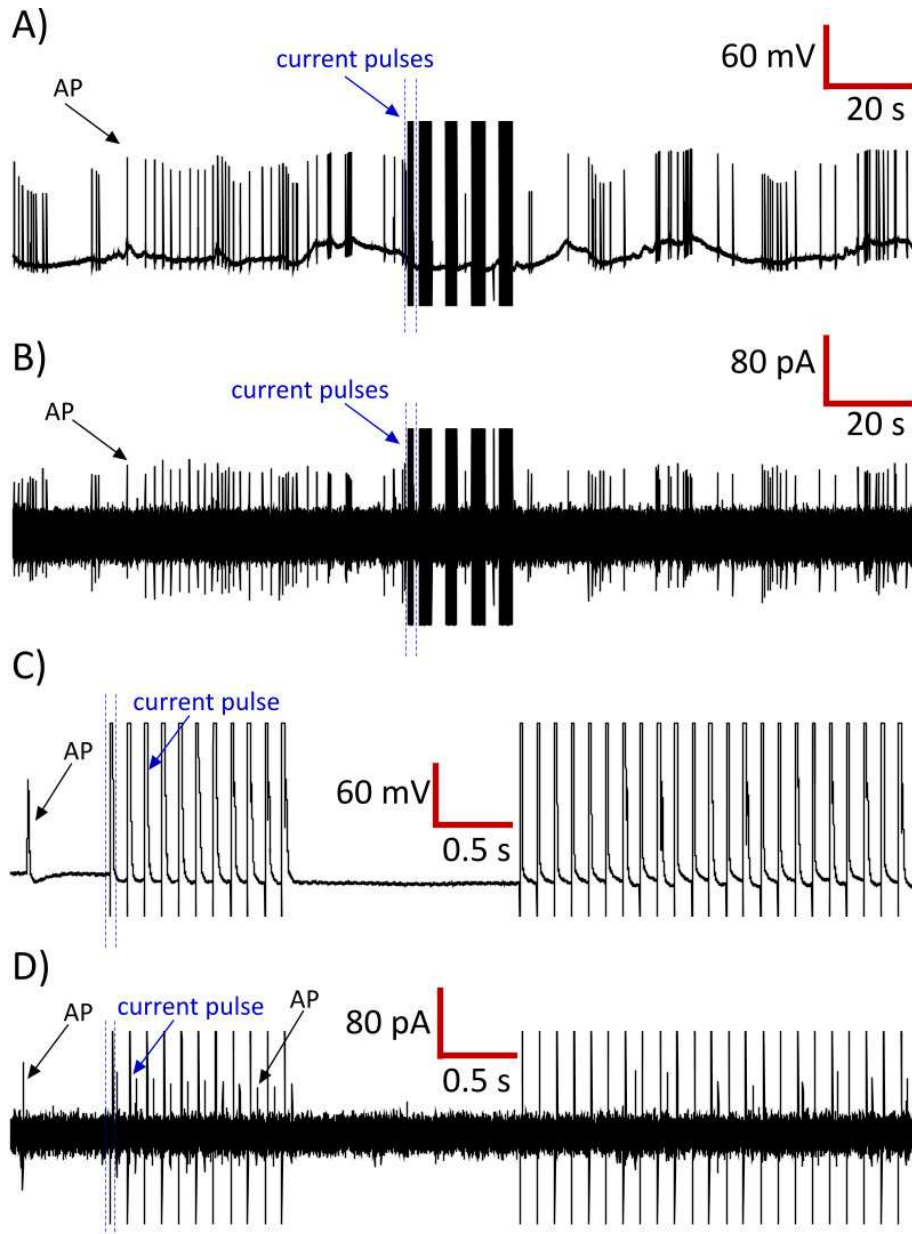
Figure 3.15 Injection of trains of current pulses into the Left CGCs could not trigger vesicular release from the CGCs. *A) Example of an electrophysiological trace of the lCGC showing its firing and the injection 5 groups of 20 ms duration current pulses. B) Example of the corresponding amperometric trace recorded from the rCGC. C) Section of the first and second train of current injections to the lCGC on a faster timebase. D) The corresponding amperometric trace showing that an AP is triggered after each pulse injection during the first train of injections and the decrease of APs triggered during the second train of pulse injections.*

Attempts were also made to trigger release by stimulating the left parietal dorsal 4 (PD4) neuron. This neuron has previously been shown to drive high frequency action potentials in the CGC soma (Price, 2019). Injection of positive depolarising current pulses via an intracellular microelectrode in the left PD4, evoked a high frequency burst of action potentials in PD4 (**Figure 3.16 A, lower panel**). This burst of PD4 action potentials excited the CGCs (**Figure 3.16 A, top panel left CGC and bottom panel right CGC**), depolarizing the cell and increasing its firing frequency (**Figure 3.16 C and D**). The experiments were repeated on 4 CNS preparations and in two of them several events were observed following PD4 stimulation (**Figure 3.16 A, bottom panel**). However, PD4 evoked release was not consistently observed and therefore this method was not used in further experiments.
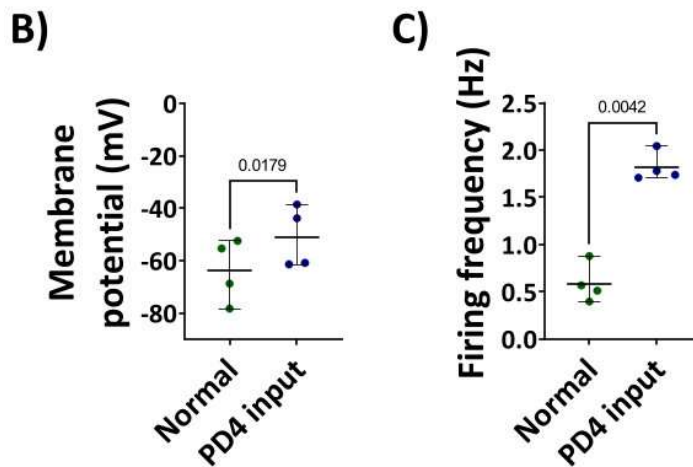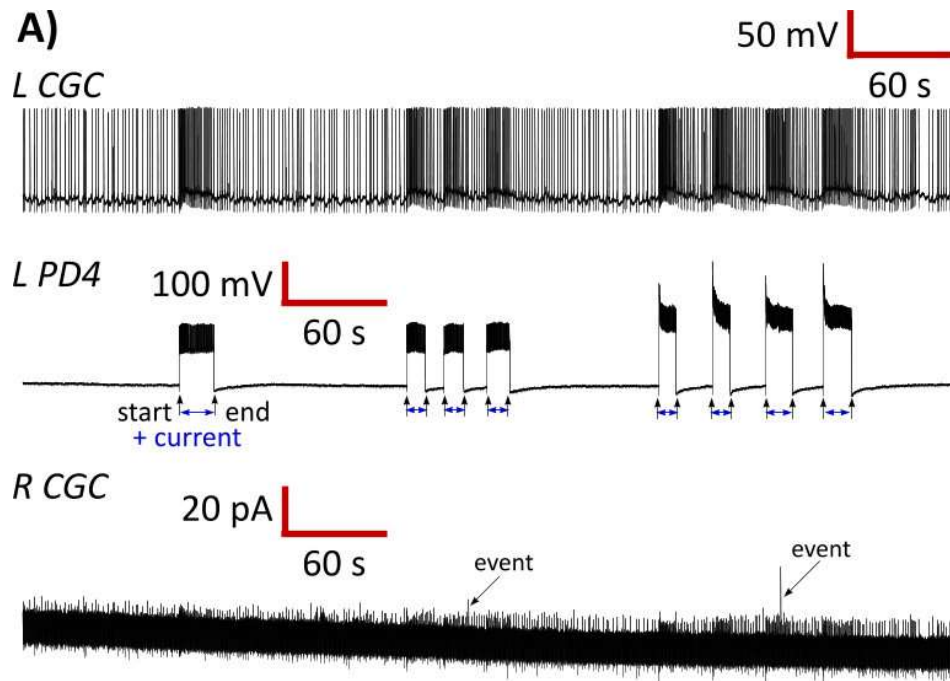
Figure 3.16 Activation of the CGCs by depolarising PD4 neuron did not consistently trigger vesicular relese from the CGCs. *A) Top panel, example of an electrophysiological trace of the left CGC showing its spontaneous firing frequency and those following the activation of the PD4 neuron. Middle panel, the corresponding electrophysiological trace of the PD4, which is initially inactive and artificially activated by the injection of constant depolarising current. Bottom panel, the corresponding amperometry trace of the right CGC with two events occurring during and after the excitation of the CGCs. C) Membrane potential of the LCGCs before and during PD4 excitation (n = 4, paired t-test). D) Firing frequency of the left CGCs LCGCs before and during PD4 excitation (n = 4, paired t-test).*

As previously noted, somatic vesicular release from another serotonergic neuron, the leech Retzius neuron has been triggered using ionomycin (Bruns et al., 2000). Perfusing HEPES-buffered saline through the superfusion pipette did not influence the CGCs firing rate or cause vesicular release (**Figure 3.17 A and B**). Administration of ionomycin to a young CGC soma evoked several release events (**Figure 3.17 A and B bottom panels**). In addition to triggering release from the left CGC, ionomycin also affected the synchronised firing of the CGCs, first influencing the right CGC, the closest to the perfusion system, and later the left CGC causing a transient desynchronization of the action potentials in the two neurons. However, it did not significantly change the membrane potential or the firing frequency of the left CGC (**Figure 3.17 C and D**). As ionomycin successfully triggered release from the CGC, the ionophore was used as a release stimulus in preparations from young and old snails.

A)

L CGC

40 mV

3 min

R CGC

30 pA

3 min

HEPES-buffered
saline

Ionomycin
(2.5 μM)

B)

L CGC

40 mV

30 s

R CGC

30 pA

30 s

Ionomycin (2.5 μM)

C)

0.7001

D)

0.8231
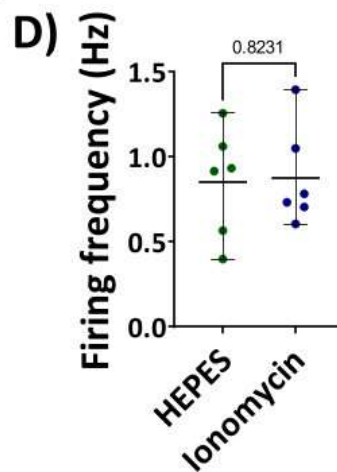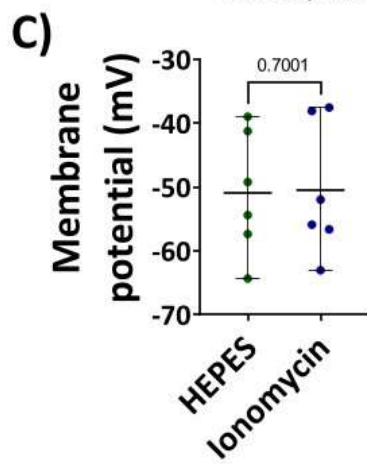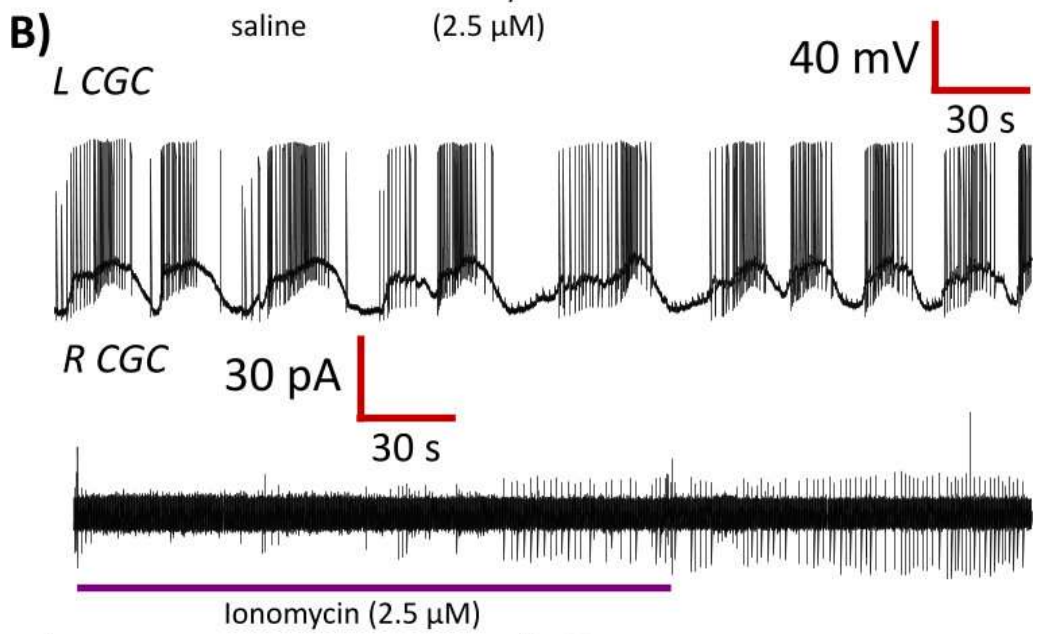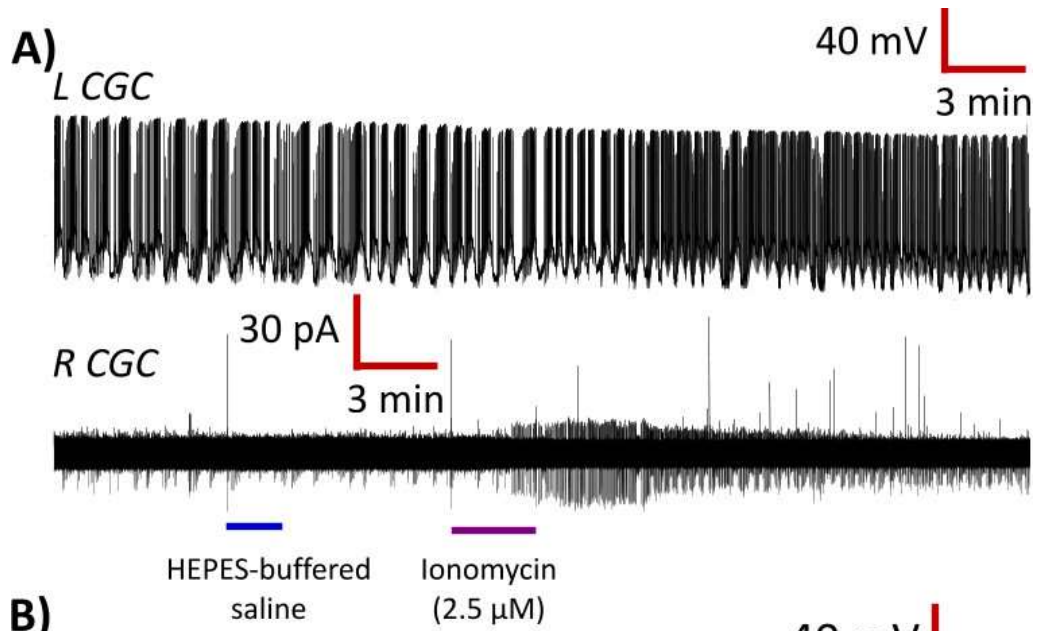
Figure 3.17 2.5 μM Ionomycin successfully triggered neurotransmitter release from the CGCs. A) Top panel, example of an electrophysiology trace of the left CGC before, during and after ionomycin perfusion. Bottom panel, the corresponding amperometric trace recorded from the right CGC. B) Speed up section of the same electrophysiological trace of the left CGC, top panel and the corresponding amperometric trace recorded from the rCGC showing increased firing activity of the cell. C) Membrane potential of the left CGC before and after Ionomycin perfusion (n = 6, paired t-test). D) Firing frequency of the left CGC before and after Ionomycin perfusion (n = 6, paired t-test).

3.3.3 Effect of Ionomycin on somatic vesicular release

3.3.3.1 The effect of ionomycin on the release events from young CGCs

Spontaneous or ionomycin triggered vesicular release events were recorded from the right CGCs of young and old snails.

To determine the effect of the ionomycin perfusion on the young CGCs, first the number of events occurring during the first 10 minutes of ionomycin perfusion was compared to the number of events occurring during the 10 minutes immediately before the start of the ionomycin perfusion (**Figure 3.18 A**). Ionomycin perfusion triggered the release of events increasing their number significantly from a median of 0 to 24 events (**Figure 3.18 B**).

Figure 3.18 Ionomycin increases the number of events released from the soma of the CGCs in young snails. A) Examples of 10-minute amperometric traces showing spontaneous (Ai) and ionomycin (Aii) triggered release events from the CGC soma of a young snail. B) Quantification of the number of released events showing increase of the number of released events following ionomycin perfusion. N=7 for spontaneous release and N=7 for ionomycin, paired t-test.

Given the low numbers of spontaneous release events observed in the 10-minute period immediately before ionomycin perfusion and to allow a statistically valid comparison of their kinetics with those of the ionomycin evoked release events, all spontaneous events that occurred prior to ionomycin perfusion were analysed. No significant differences were observed in the median half width (**Figure 3.19 A**), amplitude (**Figure 3.19 B**), rise time (**Figure 3.19 C**), fall time (**Figure 3.19 D**) or the number of molecules released per event (**Figure 3.19 E**) between the spontaneous and iononmycin-evoked release.
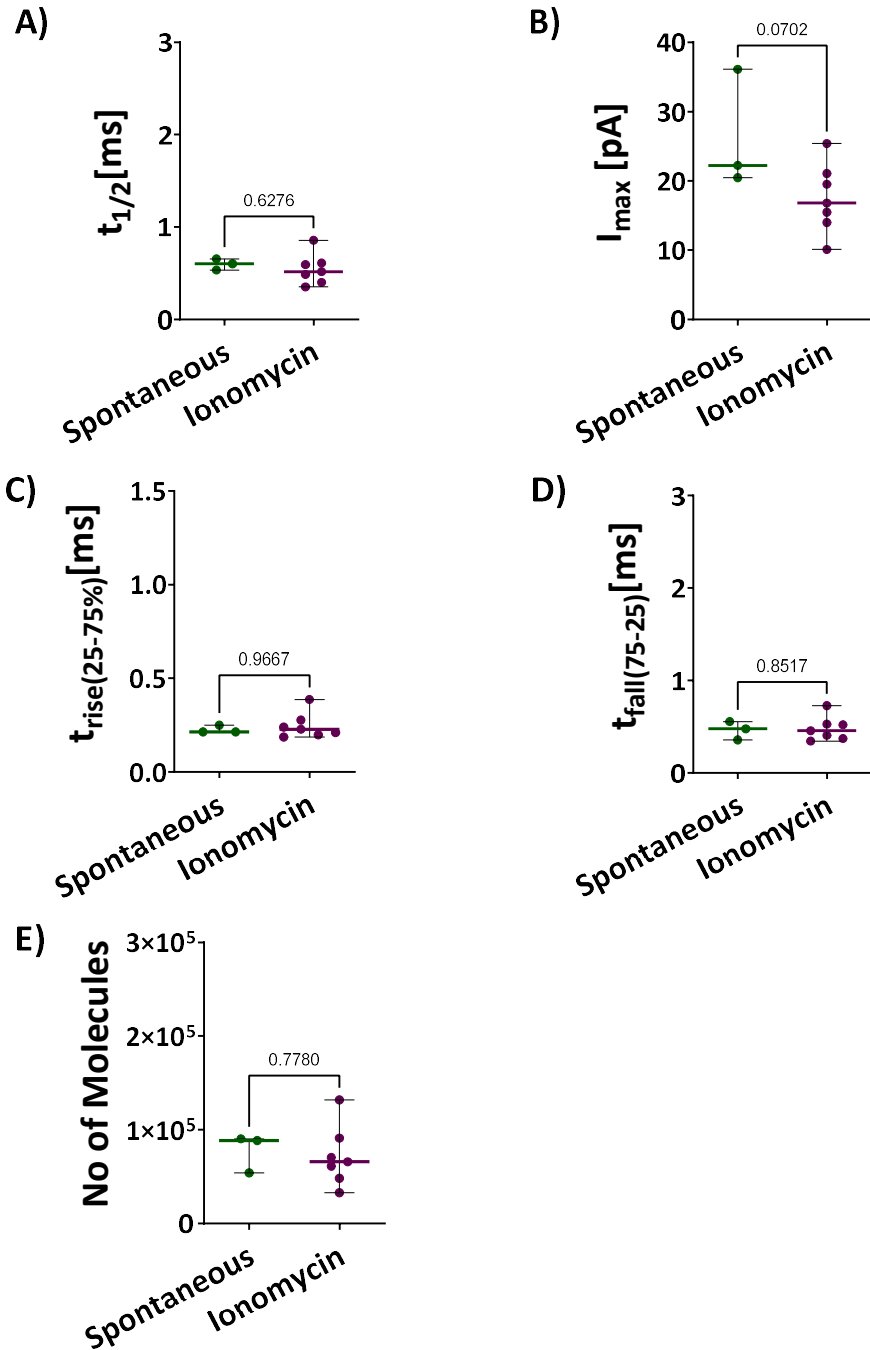
Figure 3.19 Ionomycin does not have a significant effect on the parameters of the release events from the soma of the CGC of young snails. *Bar graphs showing a comparison of the A) Half width, B) Imax, C) Rise time (Mann-Whitney test), D) Fall time and E) Number of molecules were all non-significant. N=3 for spontaneous release and N=7 for ionomycin, unpaired t-tests. Data presented as median with range.*

Application of 2.5 µM ionomycin to old CGCs failed to significantly increase the number of release events recorded using the sensor (**Figure 3.20 A**). Overall, the median number of spontaneous events recorded in the 10 minutes period before ionomycin perfusion was 1 and it was not significantly changed by the ionomycin perfusion, which increased it to 6 (**Figure 3.20 B**).
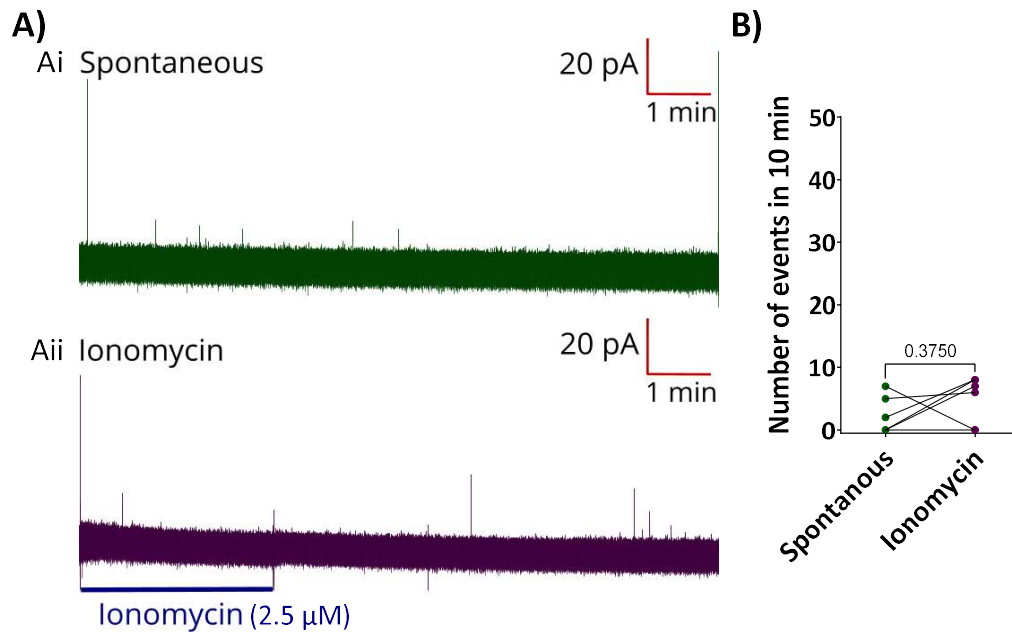
Figure 3.20 Ionomycin does not significantly change the number of events released from the soma of the CGCs in old snails. *A) Examples of sample 10-minute amperometric traces showing spontaneously release events (Ai) and ionomycin evoked events (Aii) from the CGC soma of an old snail. B) Quantification of the number of release events showed a slight, but not significant increase of the number of released events following ionomycin perfusion. N=6 for spontaneous release and N=6 for ionomycin, paired t-test.*

Comparison of spontaneous versus ionomycin-evoked old release events demonstrated that there were no significant differences of the parameters of the release events (**Figure 3.21 A, B, C, D, E**).
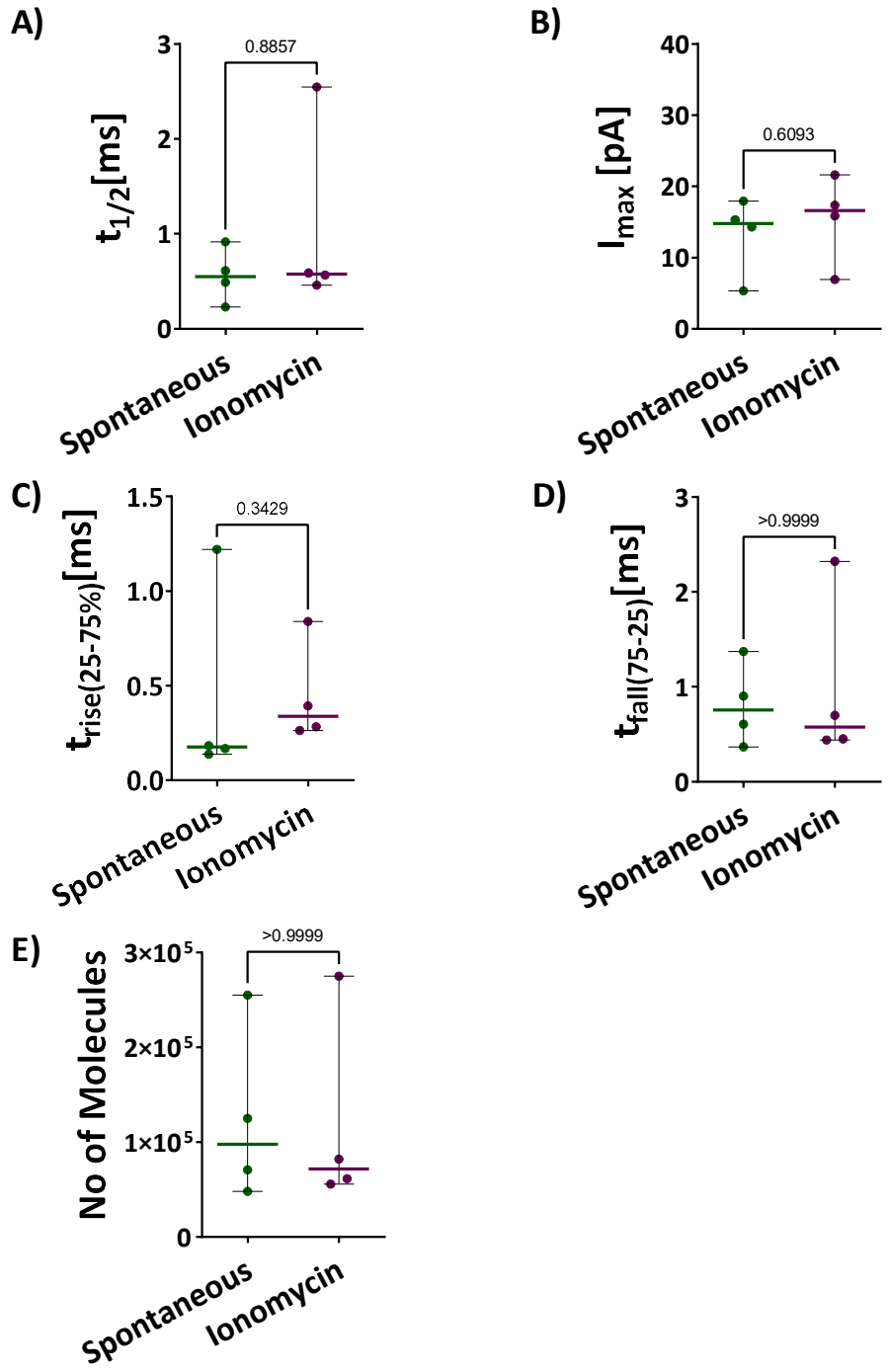
Figure 3.21 Ionomycin does not have a significant effect on the parameters of the release events recorded from the soma of the CGC of old snails. *Bar graphs showing the effects of ionomycin on A) half width, B) Imax (unpaired t-test), C) Rise time, D) Fall time and E) number of molecules. N=4 for both groups, Mann-Whitney tests. Data presented as median with range.*

Although Ionomycin had no effect on any of the parameters of the events released from the young or old CGCs, it significantly increased the frequency of the events released from young snails compared to old snails (**Figure 3.22**).
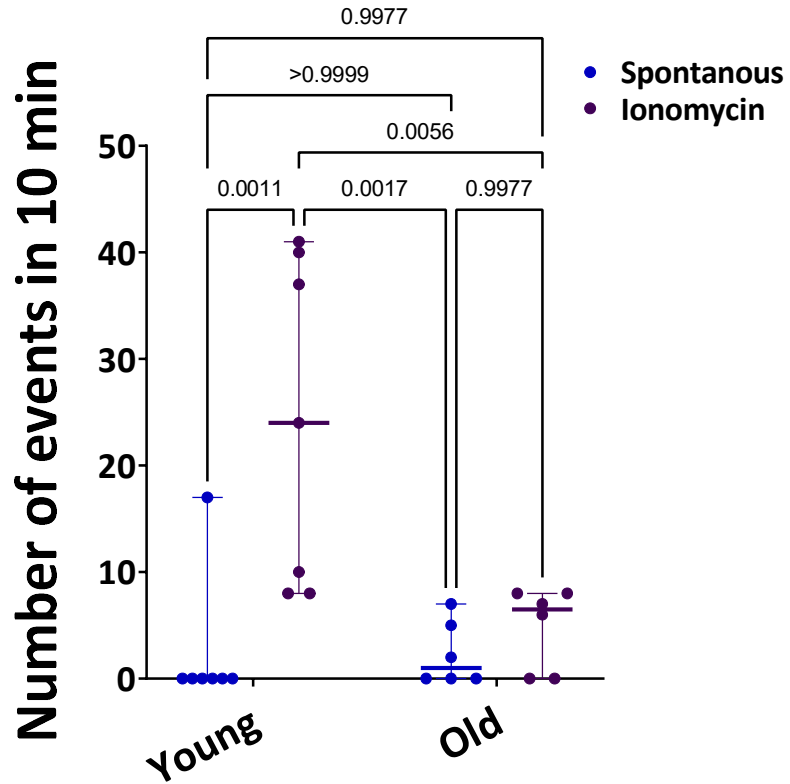
Figure 3.22 *Ionomycin significantly increases the number of events released from the young CGCs, compared to old CGCs. Young n = 7, old n = 6, data presented as median with range. Two-way ANOVA with Sidak multiple comparisons test, p-values are shown above each comparison.*

3.4 Summary and discussion

The aim of this chapter was to see whether it was possible to record vesicular release events form the cell soma of the CGC's in an intact ex vivo preparation and to explore the potential triggers that drive release in both young and old CGCs. Neurotransmitter release was recorded using 10 µm disc electrodes in combination with amperometry. Both CGCs of young and old *Lymnaea* showed spontaneous release. Attempts were made to trigger release using a range of stimuli, however, only ionomycin could reproducibly trigger release in the young CGCs but was without a significant effect in the old cells. No significant differences were observed in the number of molecules released by the events or the kinetics of the events (half time, amplitude, rise time and fall time) between the spontaneous and ionomycin triggered release.

3.4.1 Spontaneous release of young and old CGCs.

As mentioned above, both CGCs from young and old *Lymnaea* showed spontaneous release. The detection of spontaneous release is not unusual and has been observed at synapses (Alten et al., 2022, Bal et al., 2013a, Deitcher et al., 1998, Kavalali, 2015, Pang et al., 2011, Xu et al., 2009) and cell bodies, which include the serotonergic raphe neurons in the rat (de Kock et al., 2006) and the cell soma of the leech Retzius neuron (Trueta et al., 2003). At the synapse, spontaneous release is important for the development of connections between neurons (Andreae and Burrone, 2018) and the formation of dendritic arbors (Andreae and Burrone, 2015). Cell body release of 5-HT from the raphe neurons has been shown to be important for stimulating GABA-ergic signalling onto the dorsal raphe nuclei (de Kock et al, 2003). Release from the cell body of the Retzius neurons of the leech have been shown to regulate escape swimming behaviour (De-Miguel et al., 2015). Both studies show that cell body release is physiologically relevant, although currently the role of somatic 5-HT release in *Lymnaea* is unclear. Although the release from the CGCs was classed as spontaneous, the observations that the CGCs fire tonically in the isolated but intact CNS strongly suggest that intracellular Ca^{2+} concentrations will also be oscillating (Scutt et al 2015)

and therefore this release could, in some circumstances be linked to this stimulus. Additionally, given the intact nature of the preparation used in this study, it is not possible to exclude that an input from other cells is not driving the release. To further explore this, a range of stimuli designed to increase intracellular Ca^{2+} concentrations were examined for their ability to evoke somatic 5-HT release from the soma of the CGCs.

3.4.2 Evoked release of young and old CGCs

High potassium and high potassium/high calcium HEPES-buffered saline were used as indirect stimuli of membrane depolarization and activation of voltage gated Ca^{2+} channels. Depolarizing current pulses, via an intracellular microelectrode, were used in attempt to trigger action potentials at high frequencies allowing possible summation of the calcium transients that would occur with each action potential. Even though both stimuli had a depolarizing effect on the CGCs membrane potential, and some led to the increase of their firing rate, neither was able to reliably trigger and sustain vesicular release from the cell soma. These observations strongly suggest that action potential evoked Ca^{2+} entry through voltage-gated Ca^{2+} channels is not a direct driver of somatic 5-HT release from the CGCs.

Keeping the CGCs in the intact CNS allows the probing of the hypothesis that release could be stimulated through the activity of cells with monosynaptic connections to the CGCs. Such a cell is the parietal dorsal 4 (PD4) neuron, which when artificially activated can excite both the ipsilateral and contralateral CGCs (Price, 2019). Excitation of the CGCs by the PD4 neuron increased the firing rate of the CGCs from a mean of 0.59 (±0.103 SEM) Hz to 1.82 (±0.077 SEM) Hz, similar to observations made by Price (2019). The used protocol evoked low numbers of release events in a minority of preparations suggesting that it alone was not the main driver of the CGC somatic 5-HT release.

Previous work has shown that somatic release from the leech Retzius neurons is dependent on an initial entry of Ca^{2+}, which in turn evokes a larger Ca^{2+} release from intracellular stores (De-Miguel et al., 2012). Therefore, in the Retzius neurons, release

has been triggered by a train of action potentials of 10 and 20 Hz (Trueta et al., 2003), firing frequencies that this cell can reach as a response to mechanical pressure applied to the skin of the leech (Velázquez-Ulloa et al., 2003). Attempts to increase the firing frequency of the CGCs and therefore stimulate somatic release, by injection of constant positive current or pulses of current, that trigger trains of action potentials, was not able to stimulate release from the CGCs. In comparison to the Retzius neuron, the maximum rates at which the CGCs have been observed to fire *in vivo* are around 0.34 Hz during feeding and around 0.15 Hz during locomotion (Yeoman et al., 1994b) and although they are higher in the *in vitro* preparations reaching up to 0.9 Hz (Staras et al., 2002) and were increased to a mean of 3.2 Hz by the injection of positive current, none of them are as high as that observed in the Retzius neurons. These observations suggest that if the mechanism of release from the CGCs was similar to the one in the Retzius neurons, the initial trigger that drives Ca^{2+} entry into the soma of the CGCs is probably different. It is possible that the inability of increased firing frequency to elevate intracellular Ca^{2+} to a level that is sufficient to drive release is due to the sparse expression of voltage activated Ca^{2+} channels on the soma of the CGCs on sites near the ER, and or a requirement of another voltage independent channel such as the NMDA receptor or nicotinic ACh receptor that can provide additional Ca^{2+} influx. Initial attempts to utilise these stimuli were also unsuccessful.

Another stimulus consistently used in a range of cell types to evoke release is ionomycin. Ionomycin is an antibiotic that acts as an ionophore allowing Ca^{2+} to enter cells. It was therefore interesting to note that ionomycin was capable of evoking release from the CGCs soma of young snails and this appeared to be independent to changes in membrane potential or firing frequency of the CGCs and no significant changes were observed in these parameters for at least the first 5 minutes following ionomycin application. The ability of ionomycin to evoke release from the CGCs strongly suggests that somatic neurotransmitter release from the cell body of the young CGCs is calcium dependent.

In addition to its action as a Ca^{2+} ionophore, ionomycin is also capable of releasing Ca^{2+} from internal stores (Dedkova et al., 2000, Morgan and Jacob, 1994, Müller et al., 2013). It has been previously shown that this mechanism is important for the somatic

release of 5-HT from the Retzius neurons of the leech (De-Miguel et al., 2012). In the Retzius neurons intracellular Ca^{2+} must be increased sufficiently to activate ryanodine receptors on the ER, which in turn would lead to a further increase in intracellular Ca^{2+}. This additional Ca^{2+} can drive the synthesis of ATP from mitochondria therefore facilitating the active transport of the vesicles to the plasma membrane (De-Miguel et al., 2012).

Interestingly, ionomycin was not able to evoke somatic 5-HT release from old CGCs. An explanation for this could be a decline of the Ca^{2+} concentration in the ER with age (Puzianowska-Kuznicka and Kuznicki, 2009) or a decline in the levels of ryanodine receptor channels mRNA or protein, as observed in the superior cervical ganglia in rats aged 12 to 24 months, compared to rats aged 6 to 12 months (Vanterpool et al., 2006). In addition to this, if vesicular release from the CGCs requires active vesicular transport dependent on ATP, as it does in the Retzius neuron (**Figure 3.23**), then this would require the production of ATP by the mitochondria. As the ability of the mitochondria to generate ATP is dependent on Ca^{2+} ion uptake in the mitochondria (Carafoli, 2010, McCORMACK et al., 1990), a decline of Ca^{2+} release from intracellular stores could lead to a reduction of ATP production. Similarly, reduced production of ATP in neurons is observed with age and as a result of mitochondrial dysfunctions (Błaszczyk, 2020, Grimm and Eckert, 2017). In all cases the reduced ATP would in turn hinder the transport of vesicles toward the plasma membrane, therefore leading to less vesicles being released by the old CGC, in response to ionomycin.
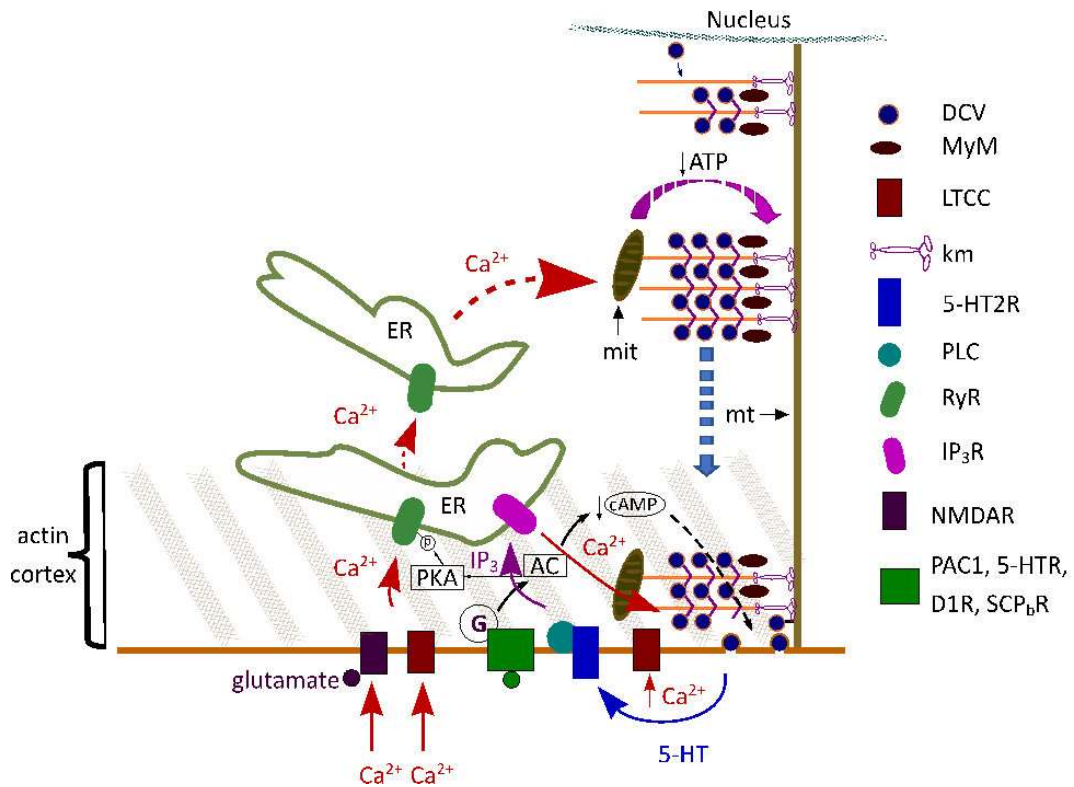
Figure 3.23 Possible mechanisms of serotonin release from the CGCs soma. *Newly formed vesicles located in the perinuclear region are filled up with extravesicular serotonin from the cytoplasm and the nucleus as observed in the rat raphe neurons and the leech Retzius neurons (Colgan et al., 2009, Kaushalya et al., 2008, Trueta et al., 2012). Transport of the vesicles is possibly facilitated by myosin (MyM) and kinesin motors (km) similar to the Retzius neuron. Initial calcium influx trough L-type calcium channels (LTCC) and or NMDAR with concurrent activation of AC, via PCA1, 5-HT or D1 receptors and ryanodine receptors (RyR) phosphorylation, could lead to the induction of calcium release from ER. This would facilitate the production of mitochondrial ATP and the transport of the vesicles towards the membrane. Further release could be sustained by the activation of 5-HT2 autoreceptors, IP₃ production and IP₃ receptors activation.*

Another possible explanation for the inability of ionomycin to increase release from the old CGCs could be that the ryanodine receptors have to be first activated by phosphorylation by protein kinase A (PKA) to release Ca^{2+} from the ER (Hain et al., 1995, Witcher et al., 1991). In *Lymnaea* PKA activation plays a major role in the formation of short- and long-term memories (Michel et al., 2008) and it is activated indirectly by an activation of adenylate cyclase (AC). AC on its turn can be activated

132

either by the binding of the pituitary adenylate cyclase-activating polypeptide (PACAP) to a PAC1 receptor (Shen et al., 2013) or by other G-coupled receptors such as $5HT_4$ (Bockaert et al., 1992), D1 (Undieh, 2010) or receptors for the small cardioactive peptide b (SCP_b) (Ferretti et al., 1996, Ocorr and Byrne, 1986). The presence of PACAP and its receptors in the CNS of Lymnaea are confirmed (Pirger et al., 2010a) and it has been shown that PACAP is necessary for the formation of long-term memories in the cerebral ganglia, where the CGCs are located (Pirger et al., 2010b). With age, there is a significant reduction of the PACAP levels in the cerebral ganglia of *Lymnaea* (Pirger et al., 2014), which could be a reason for a lower levels of activity of AC and PKA and therefore lower levels of phosphorylated ryanodine receptors leading to less release of Ca^{2+} from the ER, which in turn would influence the transport and release of vesicles.

While ionomycin did increase the number of release events from young CGCs, the kinetics of the events (their half time, amplitude, rise time and fall time) or the number of molecules released per events were not significantly influenced by the ionomycin application. This strongly suggests that spontaneous release events and those evoked by ionomycin come from the same population or pool of vesicles and that ionomycin-evoked elevations in intracellular Ca^{2+} do not affect the kinetics of the release events but merely the number of release events.

In summary, release of 5-HT from the soma of the CGCs can be triggered by ionomycin in young CGCs strongly suggesting that somatic CGC release is calcium dependent. The events evoked by ionomycin were not significantly different to those recorded spontaneously suggesting they arose from the same pool of vesicles. The lack of a consistent effect of ionomycin in the old CGCs is interesting and could reflect changes in the vesicular release pool, or age-related impairments to the processes that drive release. The next chapter focuses on whether the natural ageing process affects the dynamics of release from young and old snails.

4 Age-related changes in vesicular neurotransmitter release

4.1 Introduction

The aim of this chapter is to determine the effects of ageing on the content and the kinetics of vesicular neurotransmitter release from the CGCs.

4.1.1 Effect of age on neurotransmitter release

A range of studies have looked at the effect of age on neurotransmitter release from different brain regions. Age-related decrease in storage capacity and release of acetylcholine from cholinergic neurons, preloaded with radioactive choline and measured at rest or following field stimulation, is observed in the striatum of male and female Wistar rats (Zsilla et al., 1994). Decrease in acetylcholine release induced by depolarizing of synaptosomes is also seen with age in mouse cortex (Tanaka et al., 1996). Age-related changes in evoked release of acetylcholine (reduction), noradrenaline (reduction) and serotonin (increase) from hippocampus and cortex slices preloaded with the radioactive neurotransmitters, are observed in Long-Evans female rats (Birthelmer et al., 2003a, Birthelmer et al., 2003b). Age-related decrease of electrically evoked release of preloaded radioactive dopamine in the striatum is observed in Long-Evans female rats (Rutz et al., 2009).

Nevertheless, not much is known about the effect of age on the dynamics of neurotransmitter release at the level of the single vesicle. Direct observations of the effect of age on neurotransmitter release and its kinetics from single neurons, the CGCs in *Lymnaea,* have been made by Patel et al. (2010). The study showed a significant increase in the molecules released by the neuron in aged snails, facilitated by an increase of the time constant of decay of the vesicular release events.

4.1.1.1 Factors influencing the dynamics of neurotransmitter release

The formation of the fusion pore, its expansion and closure can be determined by a range of factors, such as the number of SNARE copies, the intracellular Ca^{2+} concentration, the Ca^{2+} sensor, the lipid composition of the vesicles and the plasma membrane and the content of the vesicles (Sharma and Lindau, 2018, Chang et al., 2017).

The formation of the fusion pore is facilitated by the SNARE proteins (synaptobrevins, syntaxins and SNAP-25 with the cooperation of accessory proteins synaptotagmins, complexins, Munc18 and Munc13). It is believed that the initiation of the fusion pore formation is commenced by the zippering of the SNARE proteins, which pulls the C terminus of the synaptobrevin transmembrane (TM) domain deeper into the membrane of the vesicle, disrupting the membrane and inducing the formation of the pore (Ngatchou et al., 2010).

Stabilising or destabilizing the TM domain of synaptobrevin could either delay or accelerate the formation of the fusion pore (Dhara et al., 2016). Efficient pore fusion seems also to be dependent on the number of SNARE complexes facilitating the formation of the pore and it is suggested that an increase of their number could lead to an increase of the fusion rate (Mostafavi et al., 2017). Additionally, the expansion of the fusion pore could be modulated by the clustering of the SNAP25 SNARE protein, which leads to the production of amperometric spikes with no feet, whereas amperometric spikes with feet are produced at sites where such clusters are not seen (Zhao et al., 2013).

Fusion pore formation can further be regulated by the accessory proteins, participating in its formation. Different isoforms of the calcium sensor synaptotagmin, can regulate the dynamics of the fusion pore. The time it takes for the fusion pore to dilate can be prolonged by the overexpression of the synaptotagmin 1, which in PC12 cells is observed as an increase of amperometric foot duration, however the opposite is observed with the overexpression of synaptotagmin IV (Wang et al., 2001). Mutations of the synaptotagmin 1 linkers to the SNARE proteins reduce the binding of the protein

to the SNARE complex destabilizing the pore formation and decreasing the duration of the prespike foot of events recorded from PC 12 cells (Bai et al., 2004). Munc 18-1 and complexin II have also been implicated in the regulation of the fusion pore duration (Archer et al., 2002, Cai et al., 2008, Fisher et al., 2001, Gulyás-Kovács et al., 2007).

Another set of proteins that participate in the regulation of the release of neurotransmitters are actin, myosin and dynamin. In chromaffin granule exocytosis, F - actin and myosin II disruption leads to the increase of the half-width of amperometric spikes and a reduction of the spike amplitude, without changing the quantal size (Berberian et al., 2009). Direct imaging of the dynamics of the release pore in bovine adrenal chromaffin cell culture combined with pharmacological manipulations has suggested that pore expansion is facilitated by the membrane tension provided by F-actin and pore constriction is facilitated by dynamin (Shin et al., 2018). Confocal and stimulation emission depletion imaging of the chromaffin cells' dense-core vesicles have shown pore closure mediated by dynamin following strong calcium influx (Chiang et al., 2014). Knockout of dynamin I in naïve adrenal chromaffin cells from mice, increases release of transmitter by 250%, strongly supporting its role in maintaining subquantal release, by rapidly resealing open fusion pores, before all neurotransmitter is released from the vesicles (Wu et al., 2019).

As well as proteins, the observations that lipid bilayers of secretory vesicles and neuroendocrine granules can become continuous with the plasma membrane following transient exocytosis (Taraska and Almers, 2004) and that membrane topology can change prior to fusion pore formation (Anantharam et al., 2010a) or following exocytosis of dense core granules in chromaffin cells (Anantharam et al., 2010b) strongly supports the notion of the involvement of lipids in the dynamics of the exocytotic pore. An evident example is the effect of altering cholesterol, in rat chromaffin cells, on the pre-spike foot recorded using constant potential amperometry. Reduction of cholesterol shortens the duration of the prespike foot, whereas increases in cholesterol has the opposite effect (Wang et al., 2010). Other membrane lipids that have been observed to influence the kinetics of the vesicular release are phosphatidylcholine (PC), phosphatidylethanolamine (PE) and sphingomyelin (SM). In amperometric recordings of dopamine release from PC12 cells,

incubation of the cells with PC reduced neurotransmitter release, by reducing the amplitude and slowing the rise time of the spike, while increasing its half width and decay time. Supplementation with PE decreased the half-width of the amperometric spike but increased its amplitude and incubation with SM increased the rise time and half width of the peak (Uchiyama et al., 2007).

In addition to the regulation of the pore dynamics by the SNARE protein, the accessory proteins, and the lipids, a factor that can indirectly determine the dynamics of the fusion pore is the intracellular concentration of Ca^{2+}. Elevations of intracellular Ca^{2+} have shown shifts of the exocytosis from kiss-and-run to full fusion in calf adrenal chromaffin cells (Elhamdani et al., 2006). In rat PC12 cells, elevation of intracellular Ca^{2+} reduces the lifetime of the fusion pore and accelerates its opening and dilation (Wang et al., 2006). Conversely, increasing of the calcium concentration near membrane fusion sites in rat chromaffin cells, shifts the mode of exocytosis from full fusion to kiss-and-run (Alés et al., 1999). These observations suggest that for different cell types, different levels of intracellular Ca^{2+} are optimal for different modes of release.

4.1.1.2 Effect of age on the factors influencing the content and dynamics of neurotransmitter release

Many of the factors that can influence the content and dynamics of neurotransmitter release, such as the SNARE proteins, lipids and intracellular Ca^{2+} concentration, can also be affected by age and therefore contribute to age-related changes observed in the dynamics or the content of release, although the link between the changes described and the dynamics of transmitter release have not been explored.

Age-related down regulation of a group of messenger RNAs, encoding for proteins involved in exocytosis, such as synaptpsomal- associated protein of 25kDa (SNAP-25), vesicle-associated membrane protein 2 (VAMP-2), mammalian homologue of unc-18 (munc-18) are observed in the pituitaries of aged rats and this is paralleled by a decline in anterior pituitary hormone secretion (Jacobsson et al., 1998). In other studies, decreases of the levels of synaptophysin, synaptobrevin and SNAP-25 in both the

brains of aged rats and humans have been observed (Hatanpää et al., 1999, Shimohama et al., 1998). However, no effect of age was observed in the levels of synaptotagmin-1, synaptophysin and syntaxin in synaptosomes prepared from the cerebral cortex of male Wister rats (Iwamoto et al., 2004).

Age-related decrease in neurotransmitter release at the synapse have been related to a decrease in the levels of the α1A (P/Q-type) and α1B (N-type) subunits of the VDCCs (Iwamoto et al., 2004) and an increase in intracellular free Ca^{2+} concentration observed in peripheral and central neurons in rats (Verkhratsky et al., 1994). Calcium dysregulation either due to altered function of VDCCs (Navakkode et al., 2018) or other proteins regulating intracellular calcium homeostasis, such as the sodium/calcium exchanger (Scutt et al., 2015) are not uncommon with age, therefore any of these alternations could contributed to changes of calcium dependent neurotransmitter release observed with age.

In addition to proteins, it has been shown that age has also an effect on the lipid composition of different neurons and brain regions (Ledesma et al., 2012), and therefore, any age-related changes to neurotransmitter release could also be a result of these changes.

4.1.2 Different pools of vesicles

Neurons can release neurotransmitters packaged either in small clear vesicles (SCV) or large dense-core vesicles (LDCV) (Salio et al., 2006). These two types of vesicles are usually differentiated by the type of transmitter molecules they contain and release. SCVs tend to contain smaller molecule transmitters such as dopamine, serotonin and norepinephrine, whereas LDCV, in addition to small molecule transmitters, also store neuropeptides, which together with intravesicular proteins form a matrix with a dense core (Pellegrino de Iraldi, 1992, Reigada et al., 2003). Under an electron microscope, the SCVs appear electron-lucent, whereas the LDCVs appear electron-dense, due to the dense packaging of the protein matrix (Rabasco et al., 2022, Pellegrino de Iraldi, 1992).

In addition to differences in vesicular content and translucency, neurotransmitter vesicles have also been divided into pools based on their spatial positioning to the plasma membrane and the context under which they are exocytosed (Crawford and Kavalali, 2015). Depending on the proximity of the vesicles to the release site (active zone), synaptic neurotransmitter vesicles have been grouped into pools such as the readily releasable pool (RRP, vesicles docked to the active zone and immediately available for release (~1% of all vesicles)), the recycling pool (vesicles primed for release under moderate stimulus (~10-15% of the vesicle population) and the reserve pool (vesicles released following an intense stimulus and accounting for ~80-90% of the vesicle pool) (Rizzoli and Betz, 2005). The frequency and the strength of stimulation can also differentially influence the release of SCVs and LDCVs from different neuronal compartments, where SCV undergo exocytosis more frequently than LDCV when Retzius cells are stimulated with action potentials, possibly due to differences in spatial organization of the different vesicle types (Bruns et al., 2000, Bruns and Jahn, 1995). Furthermore, release from LDCV, which typically contain more than one neurotransmitter can be differentially regulated by the size of the fusion pore formed between the vesicle and the plasma membranes and the mode of release – 'quantal', complete release or no release and 'sub-quantal' – partial release (Li et al., 2015b, Li et al., 2016a, Omiatek et al., 2010, Zhang et al., 2019, Zhou et al., 1996).

In cultured serotonergic Retzius neurons of adult leeches, neurotransmitter vesicles have been differentiated into two populations - small synaptic vesicles (SSV) and LCDVs. This has been achieved using a combination of morphological and amperometric analysis, demonstrating that small release events correspond to the SSV, which are released from the axons of the neuron and that larger events correspond to the LCDVs released from both the axon and the cell body (Bruns and Jahn, 1995, Bruns et al., 2000). Similarly, amperometric and morphological analysis have also been used to classify the type of vesicles released by PC12 cells, a dopaminergic cell line. Using clustering analysis of the amperometric data, the authors of the study determined that PC12 cells store and release three major sub pools of vesicles – a single pool of SCV and two pools of LDCVs- which they have termed 'large

dense core vesicles (lgDCV) and small dense core vesicles (smDCV) (Adams and Harkins, 2014).

As outlined in chapter 1, the CGCs of *Lymnaea* offer a unique model of a cell directly involved in the encoding of information that enables the expression of long-term memories (Kemenes et al., 2006a), which is also affected by age (Hermann et al., 2007, Watson et al., 2012). As the main neurotransmitter of the CGCs is serotonin (Kemenes et al., 1989, Morgan et al., 2021, Yeoman et al., 1994a, Yeoman et al., 1994b), which is electro - oxidizable by the application of positive potential (Sharma et al., 2018), the release dynamics from the cell body can be detected using amperometry (Patel et al., 2010) and the effect of age on release can be investigated. Therefore, in this chapter serotonin release from CGCs of young and old *Lymnaea* will be recorded using amperometry in combination with the carbon fibre disc microelectrodes fabricated in house as described in chapter 2, to determine the effect of age on the kinetics of vesicular release.

This chapter tests the hypothesis that ageing alters the dynamics of vesicular release from the CGC, an identified serotonergic neuron in the pond snail, *Lymnaea*.

4.2   Experimental methods

4.2.1   Animals used in the experiments

The animals used in this section are the same as the animals described in section 3.2.1 Animals used in the .

4.2.2   CNS Preparations

The CNS preparations used for the data collection in this section are the same as described in 3.2.2 CNS Preparations.

4.2.3   Electrochemistry recordings

The electrochemical recordings in this section were the same as the recordings described in section 3.2.6 Electrochemistry recordings.

4.2.4   Analysis of the electrochemistry recordings

The electrochemistry recordings in this section were analysed as described in 3.2.7 Analysis of the electrochemistry recordings.

4.2.5   Cluster analysis

Clustering is a process used to group data sets based on similarities between certain measures into a homogenous group. The aim of the clustering is to partition data points such that points belonging to one cluster (which would represent one of the possible pools of vesicles) are more like each other compared to points belonging to another cluster (another possible pool of vesicles). This is achieved by determining a similarity measure. This deduces the similarity between data points and implements an

algorithm/method that can discover similar clusters (Ahmad and Dey, 2007, Jain et al., 1999).

As each release event is described by five features – its rise time, fall time, half width, amplitude, and the number of molecules, when data is clustered, one or more of the available features can be taken into consideration depending on the desired outcome. Clustering using one or more or all features would provide different clustering outcomes. Clustering using only the number of molecules would provide information on clusters/pools of vesicles releasing different amounts of neurotransmitter. However, such clustering would not take into consideration the kinetics of the release events. As the number of molecules released by an event is calculated based on the area of the event the same amount of neurotransmitter could be observed in a release event with fast kinetics and a large amplitude and in an event with a slower kinetics but a small amplitude.

In order to determine which kinetic measures of the release events contributed significantly to the number of molecules released by an event an ordinary multiple linear regression model can be applied (Casson and Farmer, 2014).

As the sub-pools of vesicles are modelled as gaussian functions (Adams and Harkins, 2014, Bruns et al., 2000, Grabner et al., 2005, van Kempen et al., 2011, Zhang et al., 2011), the release events recorded by amperometry would include release events from all possible pools and therefore be a mixture of gaussian distributions. A clustering model, that is suitable for performing clustering analysis on a mixture of gaussian distributions is the gaussian mixture model. To estimate the parameters of each gaussian distribution (mean and variance) from the mixture, the model applies the expectation-maximization (EM) algorithm. The algorithm iterates between two steps, known as expectation (E-step) and maximization (M-step). Initially, the parameters of each Gaussian distribution from the mixture are guessed. During the E-step, each data point is assigned to one of the gaussians, by calculating the probability of the point coming from each gaussian. Following assignment, the parameters of each gaussian are recalculated based on the points assigned to the gaussian. These two steps are repeated until there is little change in the calculated parameters (Do and Batzoglou, 2008).

To perform the clustering, the gaussian mixture model requires an input of the most likely number of gaussians in the data. This is determined using the bayesian information criterion (BIC) (Fonseca and Cardoso, 2007).

Bayesian information criterion

The Bayesian information criterion is a statistical selection information criterion, used to help to determine the most suitable model from a collection of possible candidates. In the case of clustering analysis when assuming a mixture of Gaussian populations, it is used to advise on the most suitable number of gaussian populations.

It is defined by the equation:

$$BIC = -2\log(\hat{L}) + \log(N)d$$

where $\hat{L}$ is the maximum likelihood of the models, N is the number of samples and d is the number of parameters. Log-likelihood for linear gaussian model is defined as:

$$\log(\hat{L}) = -\frac{n}{2}\log(2\pi) - \frac{n}{2}\ln(\sigma^2) - \frac{\Sigma_{i=1}^{n}(y_i - \hat{y}_i)^2}{2\sigma^2},$$

where σ^2 is the noise variance estimate, y_i and $\hat{y}_i$ are the true and the predicted targets and n is the number of samples. The absolute value of the BIC is considered not to be important, however the model with the lowest values is considered the best candidate. The difference between the BICs of all possible candidates is used to determine if any of the other candidates are also likely, therefore a ΔBIC is calculated such that ΔBIC = $BIC_{of\ candidate}$ − BIC_{best}. Models with ΔBIC higher than 10 are considered unlikely and models with ΔBIC smaller than 10 are considered to be potential true fits of the data (Neath and Cavanaugh, 2012).

Implementation of the Gaussian mixture model and the BIC method

The open-source Python *scikit-learn* library was used to implement the clustering algorithm (Pedregosa et al., 2011). The library contains the *sklearn.mixture* package, which enables the estimation of gaussian mixture models from given data. The *GaussianMixture* object was used to implement the expectation- maximization algorithm. The BIC was implemented using *GaussianMixture.bic()* method.

Ordinary linear regression

The ordinary linear regression model was implemented from the *statsmodels* python library (Seabold and Perktold, 2010) using the *statsmodels.OLS* function.

4.2.6 Statistical analysis

The statistical analyses were performed as described in section 3.2.9 Statistical analysis. Histograms were made and plotted using GraphPad Prism 9 (GraphPad Software, La Jolla California USA). Gaussian functions were fitted using the nonlinear regression Gaussian model implemented in GraphPad Prism 9. All p-values are shown above the graphs.

4.3 Results

4.3.1 Effect of age on the vesicular release events

As outlined in the preceding chapter, although ionomycin had an effect of the number of events released from CGCs of young and old snails, there was no significant difference in the parameters of the release events. Therefore, in the following section all spontaneous and ionomycin evoked events were analysed to enable a comparison of young and old event parameters.

Ageing in the snail significantly affected the kinetics of the events released by the CGCs (**Figure 4.1 A**). Ageing increased the half-width (**Figure 4.1 C**), rise time (**Figure 4.1 E**), fall time (**Figure 4.1 F**) and number of molecules released per event (**Figure 4.1 B**), but did not change the amplitude of the events (**Figure 4.1 D**).
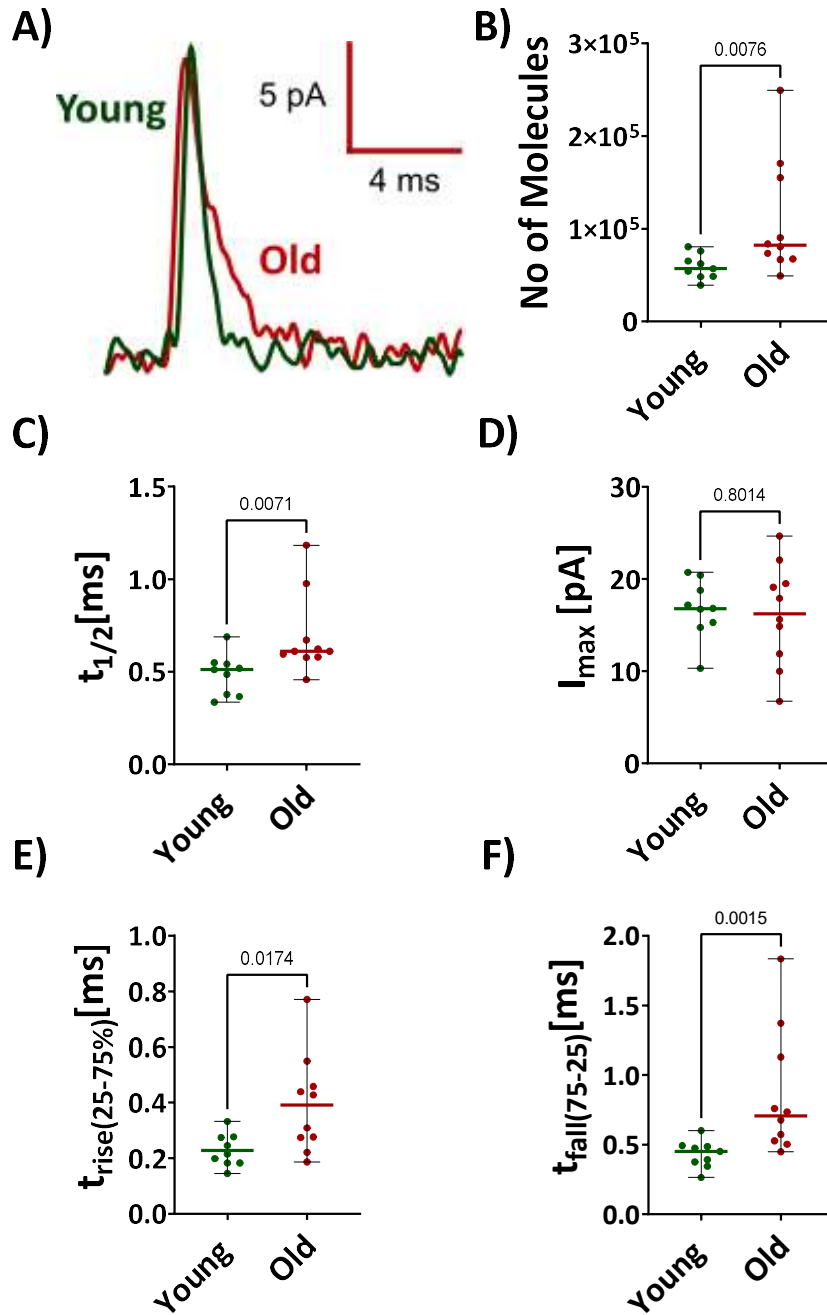
Figure 4.1 Age significantly slows the kinetics and increases the number of molecules per release event from the cell body of the CGCs. *A) Sample events released from a young and an old CGC. Graphs showing the effects of age on B) Number of molecules, C) Half width, D) Imax, E) Rise time and F) Fall time. N = 9 for young and N = 10 for old, Mann-Whitney (molecules, half width, fall time) and unpaired t-tests (Imax and rise time), data presented as median with range.*

The effect of age on the foot parameters of the released events (**Figure 4.2 A**) was also compared. No significant difference was observed in the percentage of events with a foot released from young and old CGCs (**Figure 4.2 B**). No significant age-related differences were observed in the current of the foot (**Figure 4.2 D**), time of the foot (**Figure 4.2 E**), however there was a borderline significant increase of the number of molecules released during the foot with age (**Figure 4.2 C**).
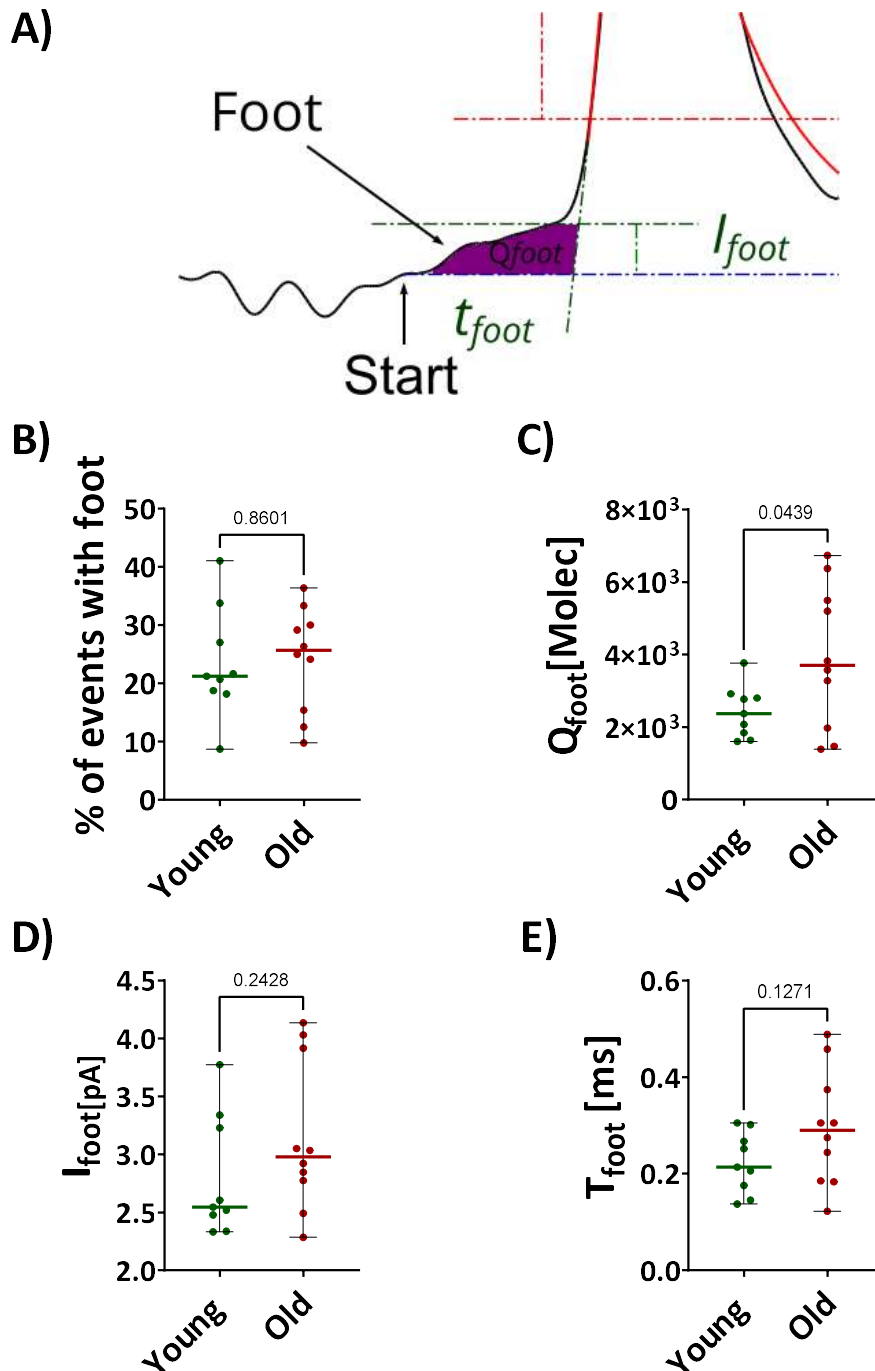
Figure 4.2 Age has no effect on the % of events with foot or on the foot parameters of the events. *A) Schematic diagram of the foot and its parameters. B) Percentage of events with foot. C) Molecules released during the foot (unpaired t-test). D) Current of the foot (Mann-Whitney test). E) Time of the foot (Mann-Whitney); n = 9 for young and n = 10 for old, data presented as median with range.*

The results describing the effect of age on the number of molecules released per release event and on the kinetics of the vesicular release events are summarised in **Table 4-1**.

	Molecules	I_{max} [pA]	$t_{1/2}$[ms]	$t_{rise(25-75\%)}$[ms]	$t_{fall(75-25)}$[ms]	Q_{foot}[Molec]	I_{foot}[pA]	T_{foot} [ms]
Young	59024 ± 13440	16.78 ± 3.188	0.4862 ± 0.1110	0.2282 ± 0.05880	0.4314 ± 0.09854	2417 ± 714.0	2.795 ± 0.5175	0.2225 ± 0.06298
Old	108694 ± 63088 ↑	16.24 ± 5.555	0.6885 ± 0.2187 ↑	0.3912 ± 0.1767 ↑	0.8555 ± 0.4513 ↑	3929 ± 1966 ↑	3.148 ± 0.6520	0.2939 ± 0.1192

Table 4-1 Summary of the effect of age on the vesicular release events recorded with the 10 µm disk electrodes *(mean ± SD, ↑ - significant increase, ↓ - significant decrease).*

4.3.2 Identification of distinct clusters based on the cube root of the number of molecules.

To identify possible sub-pools of vesicles, the vesicular release events from young CGCs formed one group denoted as Young, and the vesicular release events from the old CGCs formed second group denoted as Old. In total 399 events released by the young CGCs, and 258 events released by the old CGCs were used. Using amperometric data, sub-pools of vesicles have been previously identified by fitting Gaussian curves over the histograms of the cube root of number of molecules released per vesicle. This has been done for events released by the large dopaminergic neuron of the *Planorbis corneus* snail (Chen and Ewing, 1995), mouse chromaffin cells (Grabner et al., 2005), PC 12 cells (Zhang et al., 2011) and leech Retzius cell (Bruns et al., 2000). Similar analysis aiming at the investigation of vesicular pools, based on cube root of content of release, have also been performed using versions of the expectation maximization algorithm (Westerink et al., 2000, Adams and Harkins, 2014). All these analyses have been carried out with the assumptions that vesicular release leads to the complete emptying of the vesicle and therefore the cube root of vesicular content directly relates to the volume of the vesicle.

Therefore, to investigate the existence of multiple sub-pools of vesicles based on the content of the release events, the number of molecules released by the young and old CGCs were converted to the cube root of number of molecules and plotted against the number of events (**Figure 4.3 B**). This conversion transformed the skewed distributions (**Figure 4.3 A**), into gaussian-shaped distributions (**Figure 4.3 B**). In the case of both the young and old datasets, these distributions were best fitted by a sum of two gaussians suggesting the existence of two pools of vesicles in both the young and the old CGCs.
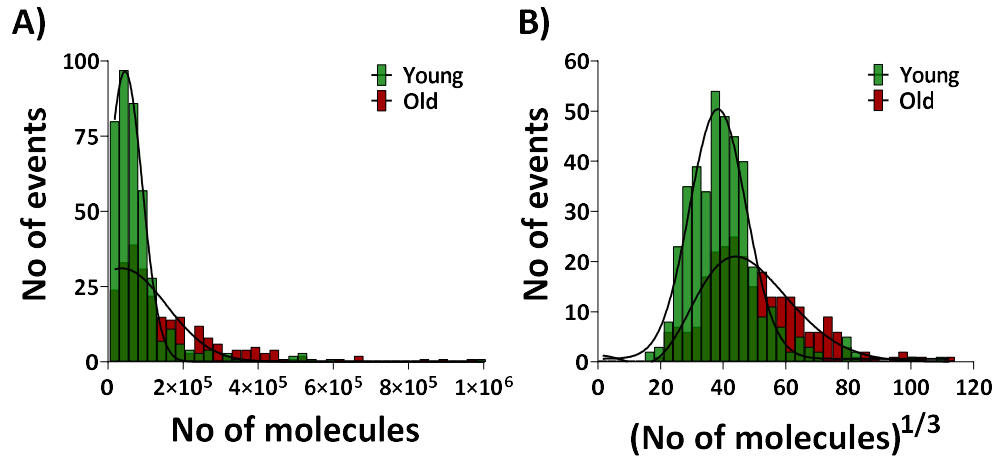
Figure 4.3 The skewed distribution of number of molecules of both young and old, when presented as a cube root of number of molecules to account for the volume of the vesicles is unskewed distribution, best fitted by a sum of two gaussians. *A) Histograms of number of molecules vs number of events. Data from the young and old were fitted separately with a single gaussian fit. (Young n = 399, mean = 85 275; Old n = 258, mean = 169 659). B) Histograms of cube root of number of molecules vs number of events. Data from the young and the old CGCs fitted best with a sum of two gaussians. (Young n = 399, R2 = 0.9582 for sum of two vs R2 = 0.9574 for single gaussian fit; Old n = 258, R2 = 0.9250 for sum of two vs R2 = 0.8941 for single gaussian fit).*

To determine if two clusters are also observed when the data is clustered using the gaussian mixture model, based on the expectation maximization algorithm, ΔBIC were calculated for each possible mixture of gaussian models, which could be describing the young and old datasets. The model with the lowest ΔBIC in the young was 2 (**Figure 4.4 A**), making this the best candidate and there were no other models with a ΔBIC < 10 that could also be considered potential candidates. The model with the lowest ΔBIC in the old was also 2 (**Figure 4.4 B**), and again there were no other models with a ΔBIC < 10 that could be considered potential candidates.

A)

B)
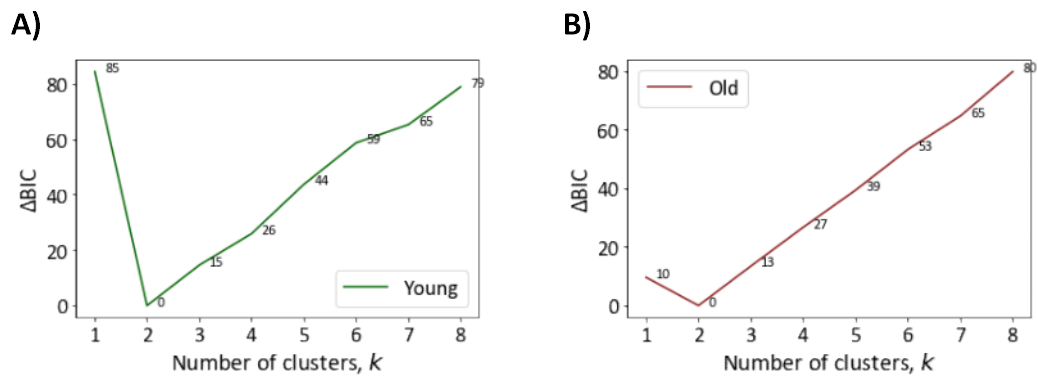
Figure 4.4 ΔBIC suggests that the events released by both the young old CGCs are best described as coming from two clusters/populations of vesicles. *Using the cube root of the number of molecules of the release events the ΔBIC of young (A) and old (B) shows that a model of 2 clusters best describes the data and no other models falls into the ΔBIC < 10 criteria for likeliness.*

Based on the ΔBIC recommendations, using the cube root of molecules, both the release events from young and old CGCs were clustered using the gaussian mixture model, described in the methods section, into two clusters. 93% of the release events from the young CGCs were assigned to one cluster, denoted as Cluster 1 and 7% of the release events were assigned to another cluster, denoted Cluster 2 (**Figure 4.5 A**). In the old dataset, 74% of the events were assigned to the first cluster, Cluster 1, and 26% to the second cluster, Cluster 2 (**Figure 4.5 B**).
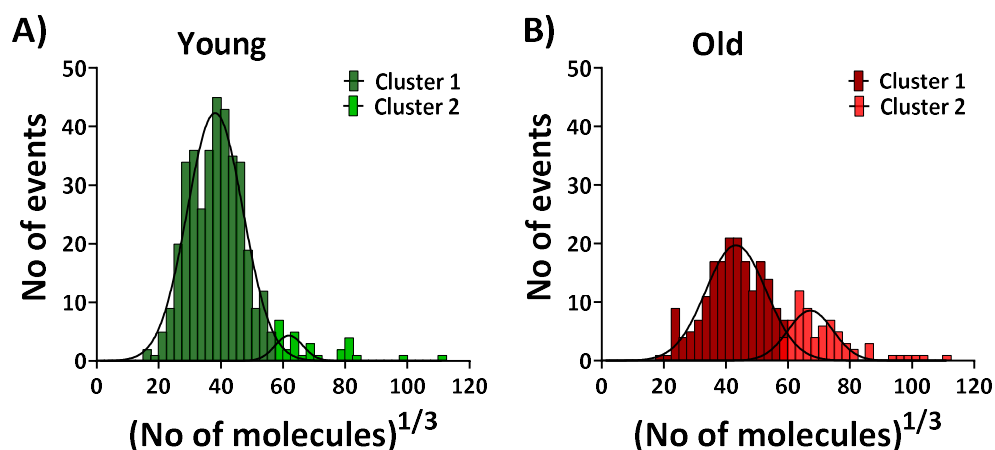
Figure 4.5 Cluster analysis of the release events from young and old CGCs shows that increasing age decreases the percentage of events in the first cluster and increases the percentage of events in the second cluster. A) Histogram plot of the two clusters of events released by (A) the young CGCs (93% in cluster 1 (371 events, mean = 62 563 molecules), 7% in cluster 2 (28 events, mean = 386 214 molecules)) and (B) the old CGCs (73% in cluster 1 (190 events, mean = 86 958 molecules), 27% in cluster 2 (68 events, mean = 400735 molecules)).

Typical events within Cluster 1 and Cluster 2 in both young (green) and old (red) release events are shown in **Figure 4.6 A**. For both the young and the old release events, significantly more molecules are released by the events in Cluster 2, compared to Cluster 1 (**Figure 4.6 B**). The events in Cluster 2 in both the young and old CGCs are of a significantly larger amplitude, half width and fall time when compared to Cluster 1 (**Figure 4.6 C, D and F**). In addition, in the old, the events of Cluster 2 have also a significantly larger rise time, compared to the events of Cluster 1 (**Figure 4.6 E**).

Comparing the two clusters of release events from the young CGCs to the two corresponding clusters of release events from the old CGCs showed a significant increase in the cube root of number of molecules released with age in the first cluster, Cluster 1 (**Figure 4.6 B**), whereas there is no significant change in the second, Cluster 2. These changes correspond to a significant increase in the rise and fall times of the events released by the old CGCs in this cluster (**Figure 4.6 E and F**).
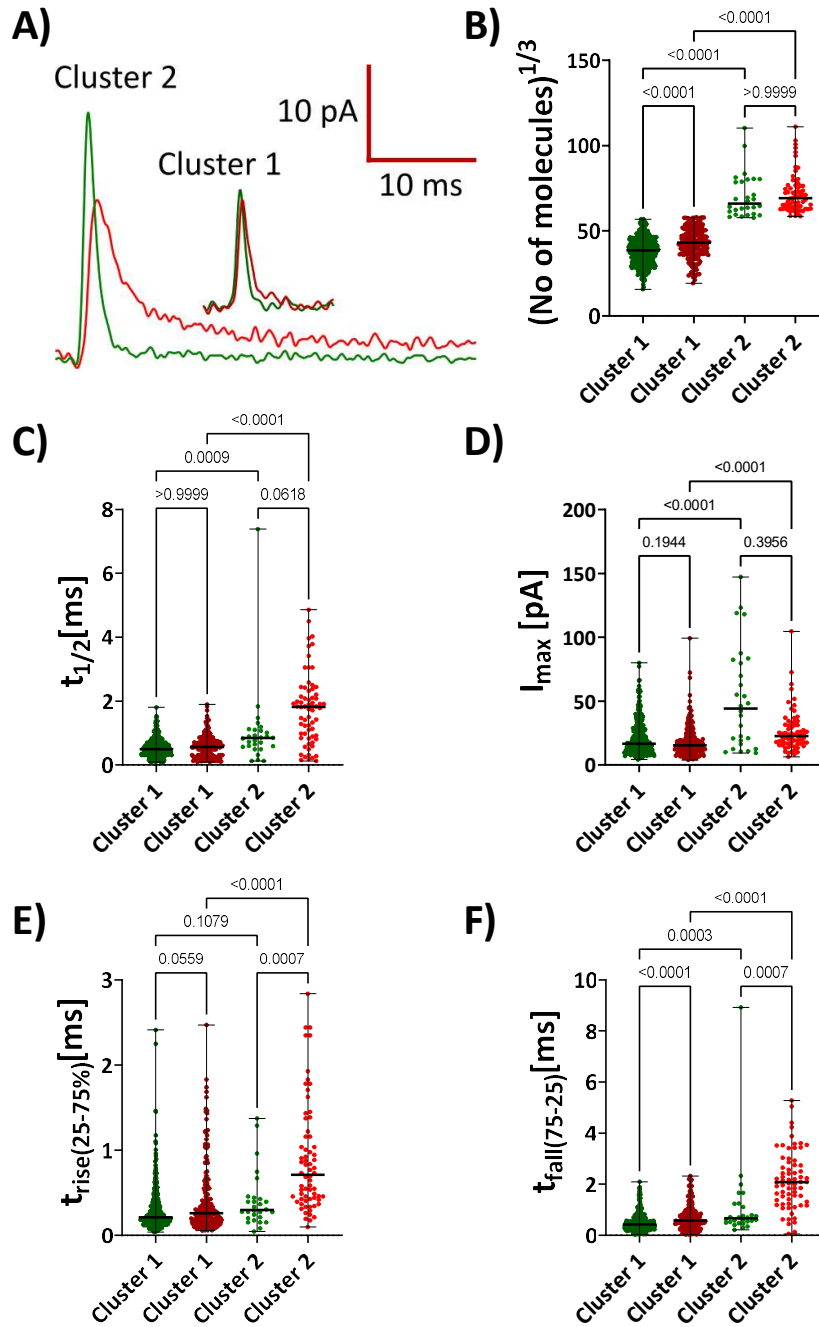
Figure 4.6 Both clusters of release events are differentially affected by age. *A) Sample release events from young (green) and old (red) for each of the two clusters. (B-F) Plots comparing the effect of age on the properties of the release events from each of the clusters. BYoungber of molecules, C) Half width, D) Imax, E) Rise time and F) Fall time. Young cluster 1 n = 371, cluster 2 n = 28; old cluster 1 n = 190, cluster 2 n = 68, Kruskal-Wallis tests.*

4.3.3 Identification of distinct release clusters based on the kinetics of the release events.

To refine the cluster analysis and to provide information about potential release modes of the vesicle and how they change with age, clustering was also performed utilizing the parameters describing the release events (amplitude, fall time, rise time and half width). For these types of analysis, the event parameters were log-transformed to normalise the distributions of the variables (Sokal, 1995) and to negate variables with very large magnitude dominating the regression equation.

To determine which parameters of the release events best described the number of molecules in a release event, an ordinary linear multiple regression model was run. Implementing the ordinary linear regression model showed that in both the young and old datasets, all event parameters (half width, the amplitude (I max), rise and fall times) can significantly predict the values of the molecules released by the events (**Table 4-2**).

	Young (p – value)	Young β-coefficient	Old (p – value)	Old β-coefficient
t1/2[ms]	< 0.0001	-1.6804	<0.0001	-1.3992
Imax [pA]	< 0.0001	3.5298	<0.0001	4.1070
Rise (25-75) [ms]	0.037	0.3190	<0.0001	0.8547
Fall (75-25) [ms]	0.005	0.4145	<0.0001	0.6095

Table 4-2 The results of the Ordinary linear regression model showed that all parameters of the events can account significantly for the number of molecules released per event. The algorithm was applied on the log-transformed values of the parameters.

Based on the result of the ordinary linear regression analysis, to determine the best model that can describe possible differences in release modes in the young and old CGCs, the ΔBIC was run separately on the event's parameters data (t-half, I-max, t-rise and t-fall) from the young and old CGCs. For both the young and old groups of release events, the ΔBIC showed that the most likely candidate model consists of 2 clusters (**Figure 4.7 A and B**). As there were no other ΔBIC values smaller than 10, no other models were considered as potential candidates.
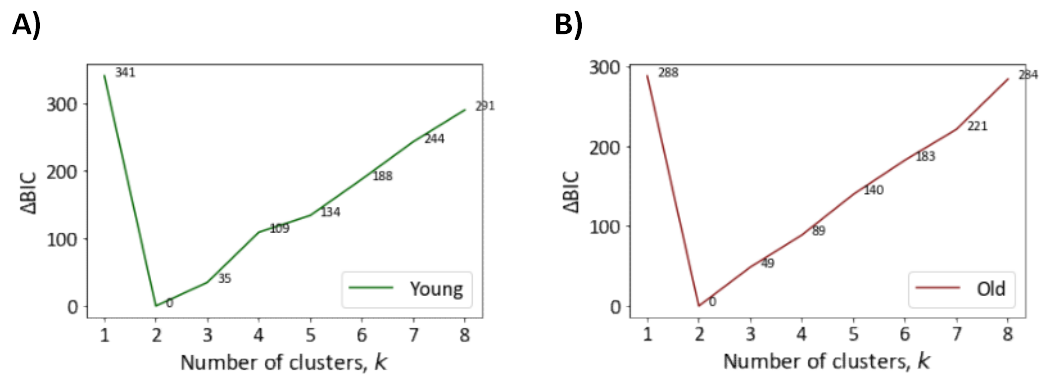
Figure 4.7 ΔBIC on the log-transformed combined data of t-half, I-max, t-rise and t-fall suggests two modes of release events in both the young old CGCs. Using the log-transformed data of the kinetics of the release events the ΔBIC of young (A) and old (B) shows that a model of 2 clusters/release modes best describes the data and no other models fall into the ΔBIC < 10 criteria for likeliness.

Based on the ΔBIC recommendations, the release events from both young and old CGCs were clustered using the gaussian mixture model. The clustering showed that in the young 66% of the events fit in one cluster (Cluster 1) and 34% of the events fit in another cluster (Cluster 2). Similarly, in the old 67% of the events fit in one cluster (Cluster 1) and 33% in another (Cluster 2) (**Figure 4.8 A and B**).
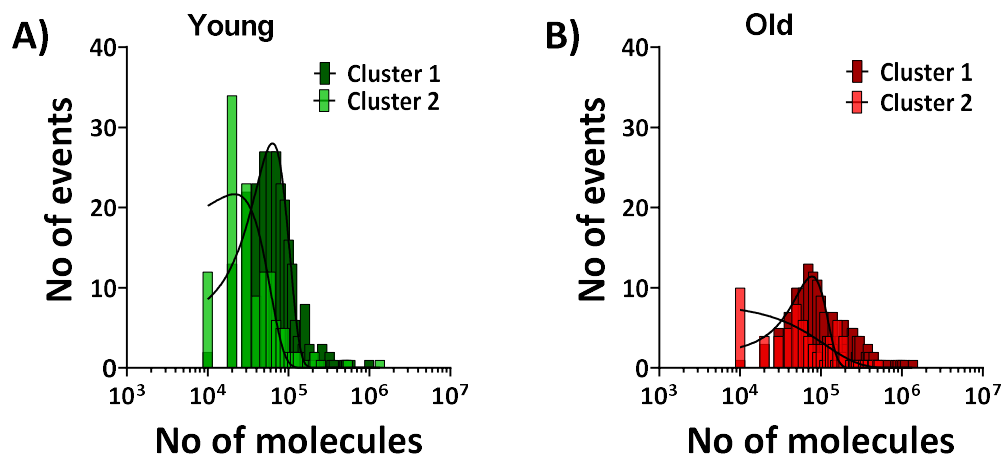
Figure 4.8 Cluster analysis of the release events from young and old CGCs in two distinct clusters/modes of release. *A) Histogram plot of the two clusters of events released by (A) the young CGCs (64 % in cluster 1 (264 events), 34 % in cluster 2 (135 events)) and (B) the old CGCs (67 % in cluster 1 (173 events), 33 % in cluster 2 (85 events)).*

Typical events representing the two identified release modes in both the young and old CGCs are shown in **Figure 4.9 A**. The events of Cluster 1 in both young and old CGCs are of larger amplitude and half width and faster rise and slower fall times when compared to cluster 2 events. Statistical comparison of the events in each cluster shows that in both young and old CGCs, significantly more neurotransmitter is released by events fitted in Cluster 1 than Cluster 2 (**Figure 4.9 B, Young Cluster 1 vs Cluster 2 and old Cluster 1 vs Cluster 2**). This is due to significant increases in Imax (**Figure 4.9 D**) and half-width (**Figure 4.9 C**). In the old differences between cluster 1 and cluster 2 events were also due to a significant increase in the rise time (**Figure 4.9 E**) and a decrease of the fall time (**Figure 4.9 F**). For both clusters of events, age significantly increased the number of molecules released by the CGCs. In cluster 1 this increase was due to a significant increase in the half width (**Figure 4.9 C**) the rise time (**Figure 4.9 E**) and fall time of the events (**Figure 4.9 F**). In Cluster 2, the age-related increase of the number of molecules was due to a significant increase in the rise time (**Figure 4.9 E**) and fall time (**Figure 4.9 F**) of the events.
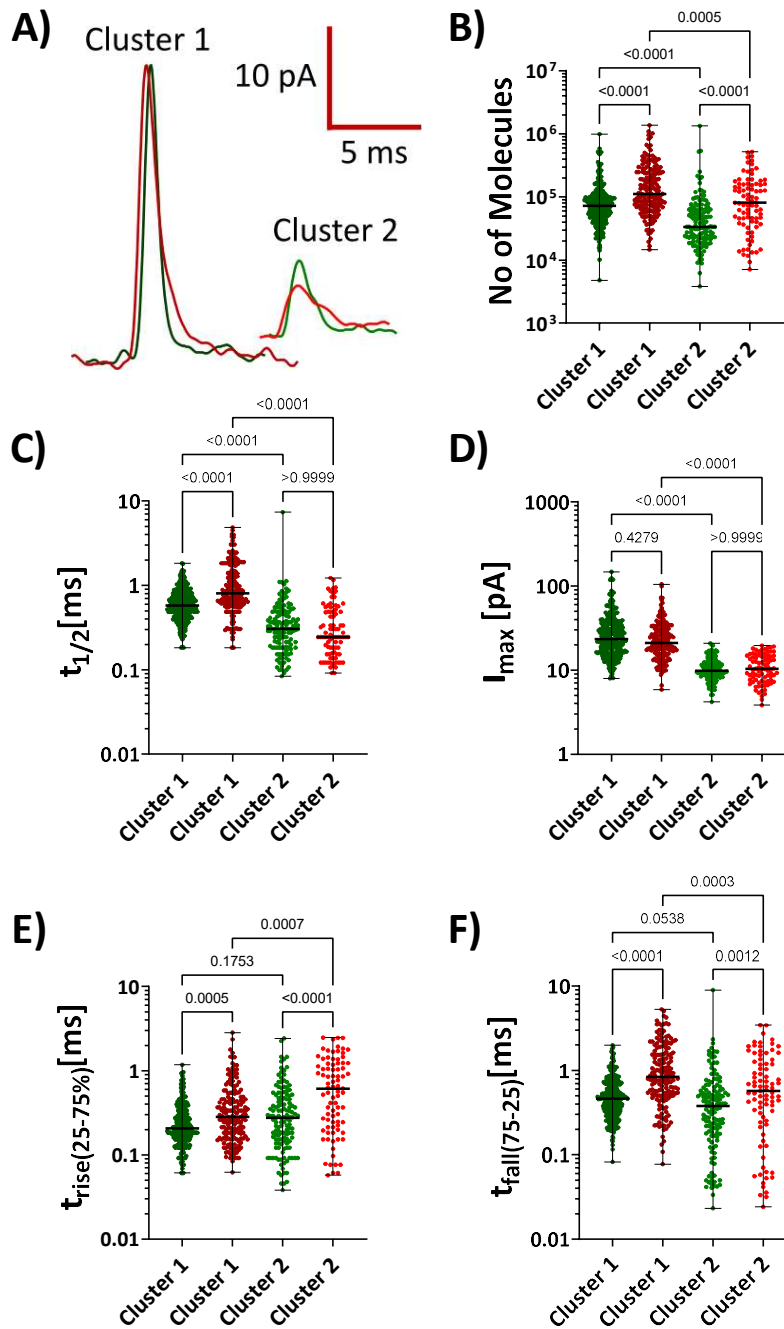
Figure 4.9 Both modes of release are differentially affected by age. *A) Sample release events from young (green) and old (red) for each of the two clusters. (B-F) Plots comparing the effect of age on the properties of the modes of release from each of the clusters. B) Number of molecules, C) Half width, D) Imax, E) Rise time and F) Fall time (young cluster 1 n = 264 dark green, cluster 2 n = 135 light green, old cluster 1 n = 173 dark red, cluster 2 n = 85, light red, Kruskal-Wallis tests).*

Strong positive corelations between the number of molecules in the release events and their half width have been inferred to describe partial release due to closure of the fusion pore before full emptying of the vesicle, whereas a poor or no corelation between the two parameters is suggested to indicate full release (van Kempen et al., 2011). Data from the two clusters identified in both the young and old CGCs are plotted in **Figure 4.10**. For both young and old release events there is a significant positive correlation between the molecules released by the events and the half with of the events in cluster 1 (**Figure 4.10 A; young cluster 1, r = 0.4588, p < 0.0001 and B; old cluster 1, r = 0.8371, p < 0.0001**). For cluster 2 events, only the correlation of the young data is significant (**Figure 4.10 C; young cluster 2, r = 0.7926, p < 0.0001**) but not in the old (**Figure 4.10 D; old cluster 2, r = 0.0822, p = 0.4547**).
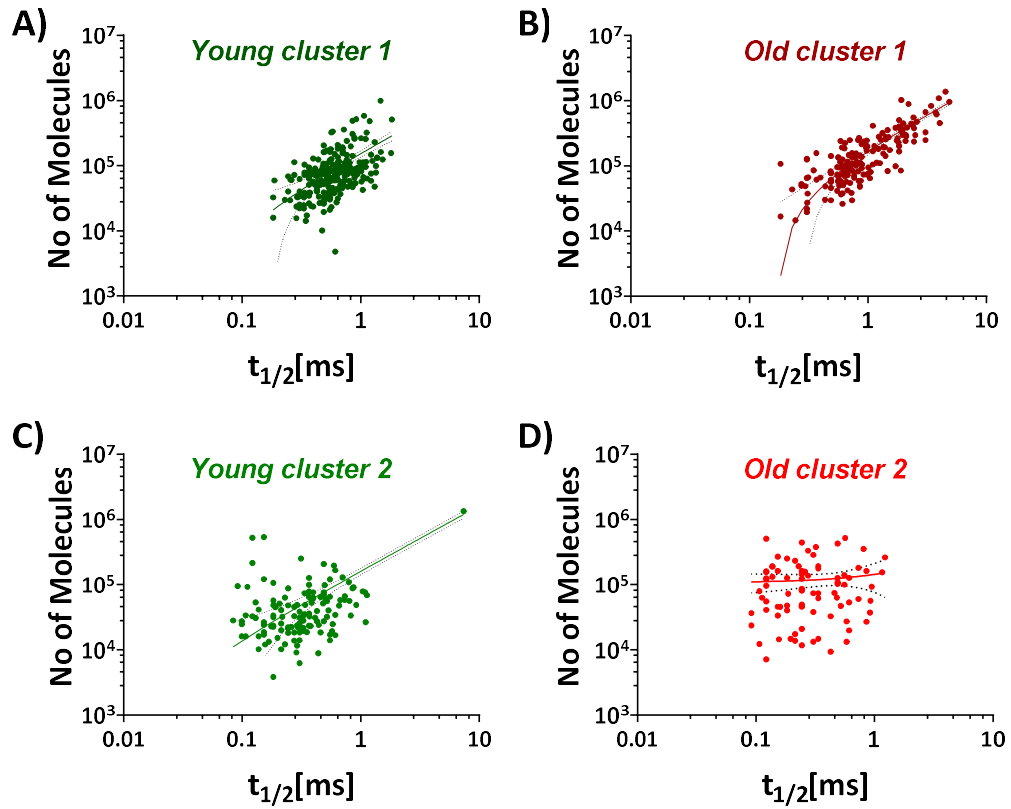
Figure 4.10 Changes in the relation between number of molecules and half width (t-half) are observed in the cluster 2 with age. *A) Young Cluster 1 (dark green) and C) young Cluster 2 (light green) and B) Old Cluster 1 (dark red) and D) Old Cluster 2 (light red), Spearman correlations.*

The relationship between the amplitude of the events and their fall time can provide information on the properties of the fusion pore. It is predicted that events coming from pores with varying conductance will exhibit an inverse correlation between the amplitude and the fall time of the events (van Kempen et al., 2011). Data shown in **Figure 4.11** shows an inverse correlation between amplitude and fall time for both young and old cluster 1 events which is significant for the young (**Figure 4.11 A, r = -0.3025, p < 0.0001**), but not for the old (**Figure 4.11 B, r = -0.09271, p = 0.2251**). Correlations for cluster 2 events in both the young and the old are positive (**Figure 4.11 C; young, r = 0.3813, p < 0.0001, Figure 4.11 D; old, r = 0.2801, p = 0.0094**).
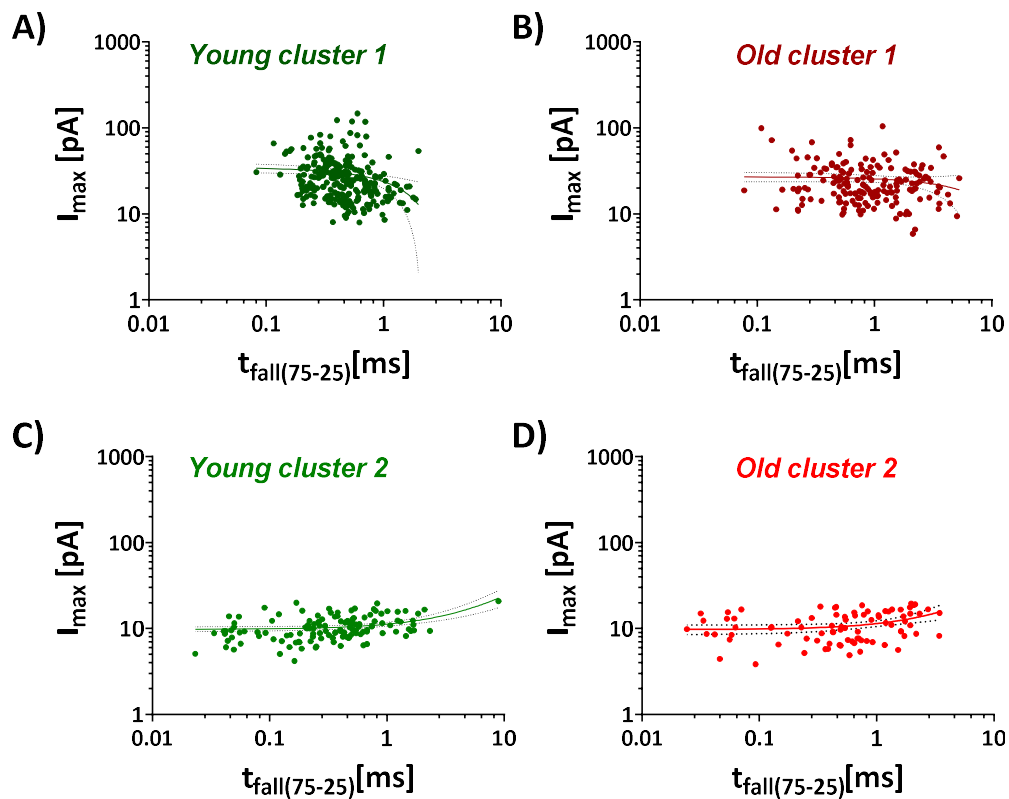
Figure 4.11 An inversely proportional relationship is found between the amplitude (Imax) and the fall time of the events (t-fall) in cluster 1 in both young and old. A) Young Cluster 1 (dark green) and C) young Cluster 2 (light green) and B) Old Cluster 1 (dark red) and D) Old Cluster 2 (light red), spearman correlations.

4.4 Summary and discussion

The aim of the current chapter was to determine the effect of increasing age on neurotransmitter release from the cell body of the CGCs. All events recorded as spontaneous release or triggered by ionomycin were used in the analysis, as it was shown in the previous chapter that ionomycin had no effect on the kinetics of the events or the number of molecules released by the events. Increasing age altered the kinetics of the release events by increasing the rise time, fall time, half width, and numbers of molecules of 5-HT released per event. An age-related significant increase was also observed in the number of molecules released in the foot of the events. Cluster analyses were applied to investigate the possible existence of different pools of release events. Cluster analysis predicted two clusters of release events, with one of the clusters releasing more molecules of 5-HT regardless of age. In addition, ageing increased the amount of transmitter released by each of the two clusters.

4.4.1 Effect of age on serotonin release from the CGCs soma.

Ageing had a significant effect on the kinetics of the release events and the number of molecules released per event. It increased the half width of the events their rise and fall time and the number of 5-HT molecules released per event. However, there was no obvious effect on the amplitude of the events (Imax).

A previous study by Patel et al. (2010) on the effect of age on neurotransmitter release from the soma of the CGCs of young and old snails reported an increase of the size of the vesicular release events with age. This increase in the number of serotonin molecules released per event was due to an increase of the time constant of decay of the events, a parameter linked to the fall time measured in this current study. These findings were confirmed by the experiments described in this chapter, however, in addition the current study also showed an age-related increase in the half width and rise time of the recorded release events. A complex release machinery of proteins and its interaction with the lipids of the plasma and vesicle membrane facilitate the formation of a fusion pore and the neurotransmitter release. Both the SNARE proteins

and the lipids of the membranes can be influenced by age. The age-related increase of the release events duration could be due to age-related downregulation in the expression of the SNARE proteins (VanGuilder et al., 2010), as observed in hippocampal synaptoproteome of rats, leading to decrease of their number and therefore to a decrease of the fusion rate (Mostafavi et al., 2017). In addition, an age-related elevation of intracellular Ca^{2+}, due to decrease of calcium clearance, as previously observed in the CGCs of *Lymnaea* (Scutt et al., 2015), could shift the exocytosis from kiss-and-run to full fusion (Elhamdani et al., 2006), which would be observed as an increase of the duration and an increase in the number of molecules of transmitter released per event. However, the observation that ionomycin does not affect the kinetics of release suggests that this is not the case. Changes in the lipid composition of the plasma and the vesicle membranes can also influence the kinetics of neurotransmitter release (Ledesma et al., 2012). Age-related changes in cholesterol and SM could affect the distribution and concentration of the SNARE proteins on the plasma membrane (Chamberlain et al., 2001, Lang et al., 2001, Chamberlain and Gould, 2002). Additionally, alterations in these lipids can affect the stability of the TM domain of synaptobrevin, which in turn could either delay or accelerate the formation of the fusion pore (Dhara et al., 2016). In relation to this last point, it is interesting to note that the charge of the pre-spike foot, which reflects the duration and conductance through the fusion pore is larger in events from old CGCs. Similarly, age-related changes in the availability of any of the sphingolipids and phospholipids, which have an effect on the curvature of the plasma membrane (Piomelli et al., 2007) can influence the kinetics of vesicular release (Uchiyama et al., 2007). In particular, an increase of SM concentration can lead to an increase in the rise time and the half width of the amperometric spikes, as seen in spikes recorded from the PC 12 cells (Uchiyama et al., 2007). The observed increase of the half width and number of molecules released per event from the CGCs could also be due to the increased production of free fatty acids such as AA (García-Martínez et al., 2013), evoked by an age-related increase of the activity of phospholipase A2 in the CNS of *Lymnaea* (Farooqui and Horrocks, 2006, Watson et al., 2013).

4.4.2 Populations of vesicular sub-pools of the CGCs and vesicular modes of somatic exocytosis from the young and old CGCs.

Neurotransmitters are packed into lipid-encapsulated vesicles, which, based on size and appearance, have predominantly been classed into two different pools. Small clear vesicles (SCV), called small synaptic vesicles (SSV) are located in axons and synapses of neurons, and large dense core vesicles (LDCV) located in the cell soma, dendrites and synapses, in both vertebrate and invertebrate neurons (Persoon et al., 2018, Bruns et al., 2000). In addition to this classification, release has also been described as either 'full fusion' release, during which the releasing vesicle fully fusses with the cell membrane letting all its content out or as 'kiss-and-run' release, during which only a fraction of the vesicular content is released through the formation of a pore between the vesicle and the plasma membrane (Elhamdani et al., 2006, Fesce et al., 1994). Partial vesicular release has been reaffirmed by experiments utilizing single cell amperometry (SCA) and intracellular vesicle impact electrochemical cytometry (IVIEC) (Larsson et al., 2020, Li et al., 2016a, Ren et al., 2016, Wang and Ewing, 2021). Therefore, there are at least two distinct modes by which cells can release neurotransmitters.

Previous studies have used different methods to classify or cluster release events recorded using amperometry to determine the existence of possible sub-pools of vesicles, that could represent the SCV and the LDCV. Histograms have been utilized to classify events into sub-pools based on the cube root of the integrated charge of the events recorded from a neuron in the pond snail *Planorbis corneus* (Chen and Ewing, 1995). Gaussian mixture analysis applied to the integrated charge of the recorded events and the diameter of the vesicles measured from EMs have been used to distinguish between three sub-pools of vesicles in PC 12 cells (Adams and Harkins, 2014). Different release modes have been proposed by cluster analysis utilizing 1D and 2D Gaussian mixture analysis applied to the charge and the kinetics of events recorded in PC 12 and chromaffin cells (van Kempen et al., 2011). Therefore, in this study, cluster analysis on the release data was performed to elucidate more about the potential vesicular pools in the CGC soma and their release mechanisms.

In this Chapter, clustering of the data was performed using the Gaussian mixture analysis model, implemented in Python. An advantage of using the Gaussian mixture analysis for clustering is that this type of analysis does not only fit one or more gaussian curves to the analysed data, but it considers the likelihood for each data point of coming from a specific gaussian cluster. In addition, cluster analysis using the gaussian mixture models can be performed on a multidimensional data, therefore it can include more than one parameter. In the case of clustering based on the amperometric release data, all relevant recorded parameters of the release events can be used. This allows to not only determine clusters representing vesicles of different size, but also to determine clusters that could be representing different modes of release.

As outlined above, clustering of the young and old datasets based solely on the cube root of molecules data generated two clusters of events with the majority of events in both age groups fitting in Cluster 1, which had the smaller number of molecules (93% in the young and 74% in the old). The remaining events contained the larger number of molecules and fitted in Cluster 2 (7% in the young and 26% in the old). This clustering method is based on the cube root of the number of molecules in the events, which corresponds to the size of the vesicle. Therefore, if release from the cell body of the CGCs is full, it is possible that the two observed clusters correspond to the two sub-pools of vesicles observed in neurons - the SSV and LDCV or to SCV and LDCV observed in neuroendocrine cells such as PC 12 and chromaffin cells. Both SSV and LDCV have been observed in the soma of the large serotonergic Retzius neurons in the leech, that are like the CGCs in Lymnaea. However, only LDCVs have been shown to be released from the cell soma of these cells (Bruns et al., 2000). Amperometric recordings of the release from the Retzius neurons have shown that the events corresponding to the SSV had a mean charge of 3 fC (~ 9358 molecules) and a mean amplitude of 3 pA, whereas the events corresponding to the LDCV seen in the soma had a mean charge of 47 fC (~ 146623 molecules) and a mean amplitude of 20 pA. In comparison, both clusters in the CGCs had events with a much larger mean amplitude (Cluster 1, 21 pA and 18 pA, Cluster 2, 52 pA and 26 pA in the young and the old, respectively) and more molecules released per event (Cluster 1 – 55002 (18 fC) and 76495 (25 fC), Cluster 2 – 349369

(112 fC) and 370610 (119 fC) in the young and the old, respectively). These observations suggest that the release events observed in the CGCs are less likely to correspond to a mix of SSV and LDCV, but more likely to correspond to two types of LDCV. Two types of dense core vesicles, large and small are observed in mouse chromaffin cells (Grabner et al., 2005) and PC 12 cells (Adams and Harkins, 2014). In the chromaffin cells, the mean neurotransmitter content of the small-DCV is 64 fC (199657 molecules) and the content in the large-DCV is 329 fC (1024832 molecules) (Grabner et al., 2005). In the PC 12 cells, events correlating to two DCV types have been described in addition to a cluster of SCV. The mean contents of the different types of events corresponding to the different types of vesicles have been determined to be 42 fC for the SCV, 104 fC for the small DCV and 205 fC for the large DCV (Adams and Harkins, 2014). Based on these observations, the two clusters in the CGCs could be either two types of DCV or an SCV and small DCV.

Alternatively, if release from the soma of the CGCs is partial, as it has been observed for other neurotransmitter releasing cells, the two clusters of release events could emerge from a single population of vesicles that is undergoing different modes of release (full fusion and partial release). Indeed, in support of this is the observation that ageing increases the number of molecules per release event in both clusters, strongly suggesting that in the young release is partial. Although all options are possible, currently there is no available electron microscope imaging data that can provide us with information about the size and appearance of the vesicles in the CGCs, therefore it is not possible to say if the observed clusters of release events correspond to populations of vesicles of different type and sizes. However, the mode of release from the CGCs can be determined by investigating the intracellular content of the vesicles using IVIEC and comparing it to the released amount, which will be presented in the next chapter.

Given the wealth of dynamic information available from the analysis of the release events it was possible that using this information could provide a more relevant model of clustering of the release events, that could be related to different modes of release. Therefore, clustering was also performed using the log-transformed data of all event parameters that contributed significantly to the observed content of release, as

determined by the ordinary linear regression model. As described above this clustering model also predicted the existence of 2 separate clusters of events in each age group, with similar percentage distributions (66 % of the events in young and 67 % of the events in old in Cluster 1, and 34 % of the events in young and 33% of the events in old in Cluster 2). Based on this clustering model, the events in a specific cluster in both the young and the old had similar kinetics and showed similar correlations between the molecules released by the events and the half width of the events and between the amplitude and fall time of the events. They did however differ significantly in the number of molecules, i-max and $t_{1/2}$ between the two clusters.

The observed difference in the kinetics of the release and the content of neurotransmitter released by the two distinct clusters (Cluster 1 and Cluster 2) could be dictated by a range of factors, including:

1) Vesicle size (small vs larger) and type (clear vesicles or dense core).
2) Different rates of diffusion of the neurotransmitter, determined by differences in the size or conductance of the fusion pore.
3) Differences in the intravesicular content, which could be free to diffuse or obstructed by interactions with the dense core matrix.
4) Whether fusion is full or partial.

Therefore, it is possible that these two clusters represent either one pool of a single type of vesicles (SCV or DCV) releasing into two different modes (fast and slow or partial and full), or two pools of different vesicles (SCV and DCV, or two types of DCV) each with its own release mode.

Assuming release is generated by a single homogenous population of vesicles either SCV or the LDCV, the observed difference in the two clusters of release could be ascribed to differences in the size and/or the conductance of the pore formed between the vesicle and the plasma membrane and how long it stays open for. Differences in the size and conductance of the pore could generate release of different rates (slow vs fast), and differences in the time for which the pore stays open can restrict release to partial or allow full release.

If the two clusters are representing release from two different types of vesicles, SCV and DCV then the differences in the kinetics of the release events could be caused by differences at the diffusion rate of the neurotransmitter, where free to diffuse neurotransmitter is released at a faster rate (**Figure 4.12 A**) compared to neurotransmitters interacting with the matrix of the dense core (**Figure 4.12 B**).
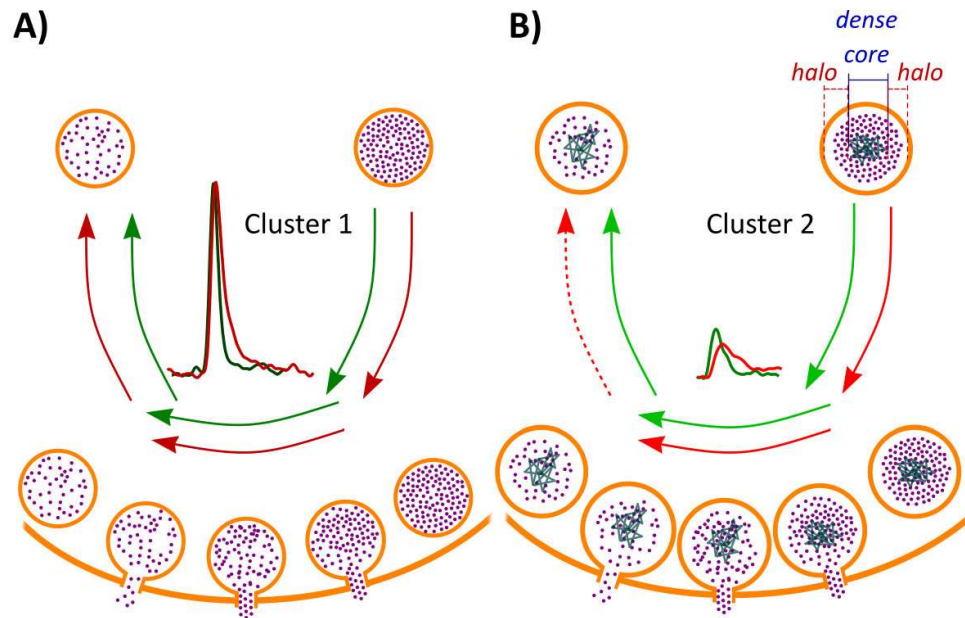
Figure 4.12 Two different pools of vesicle lead to two different modes of release. A) Vesicular release from a freely diffusing neurotransmitter. B) Vesicular release of a neurotransmitter, some of which is free to diffuse and some of which interacts with the dense core of the vesicles and takes longer to release.

Similar to the previous model, differences of the mode of release could be due to two different populations of DCVs with different size and internal composition. As in the previous model, the events with the higher rate of release (i-max) could be coming from vesicles which have more freely available for release neurotransmitter (**Figure 4.13 A**), whereas the events with lower rates of release might be generated by vesicles in which the majority of neurotransmitter is interacting with the matrix and therefore diffusing at slower rates (**Figure 4.13 B**).
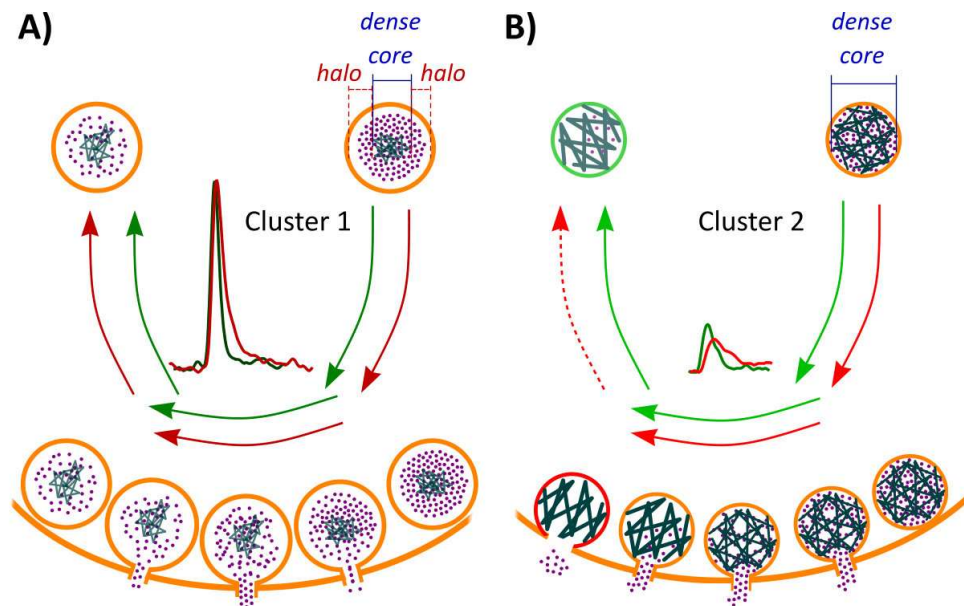
Figure 4.13 Two vesicle populations with different size and content organization. A) Release from vesicles with varying halo:matrix ratio, facilitated by a pore of varying size or conductance leading to release events of varying amplitude, inversely proportional to the fall time of the events. B) Release from DCV with a matrix completely filling up the vesicle, facilitated by a pore of a constant size or conductance, which ability to close is disturbed with age.

Independent of the cluster and the release mode, a significant age-related increase of the number of molecules released by the events in each cluster is observed. For both clusters this is a result of a significant increase in the rise and fall time of the events and in Cluster 1 a significant increase in the half width of the events. This suggests that the effect of age on the release from the CGCs extends to all modes of release. However, a difference within the clusters between the two age groups is observed in

the correlation between the molecules released by the events and the half width of the events in Cluster 2. In the young the two parameters show a significant positive correlation, which disappears with age. Such change could represent a shift of the release mode from partial to full, as suggested by van Kempen et al. (2011). As the mode of release from the CGCs has not been investigated up to now and in order to refine the model of how age affects vesicular release dynamics from the CGC soma, the next chapter will use single cell amperometry in combination with intracellular vesicle impact electrochemical cytometry to explore the number of clusters of vesicles in the young and old CGC soma and the fraction of transmitter released following their fusion with the plasma membrane.

5 Age-related changes to intracellular neurotransmitter vesicular content and the proportion of transmitter released from vesicles in the CGC cell soma.

5.1 Introduction

In chapter 4 ageing was shown to affect the kinetics of vesicular release in the CGCs in *Lymnaea*. Specifically, the natural ageing process increased the half width, rise time, fall time and the number of molecules of serotonin in each release event from the CGC soma. It is possible that these differences reflect an increase in intravesicular serotonin concentration, change in the pool of vesicles being released with increasing age or that the changes reflect alterations in the release profile of one or more pools of vesicles. To start to answer these questions this chapter characterised the vesicular pool in the CGC soma and explored whether the natural ageing process changes the vesicular pool and the proportion of transmitter released from the vesicles following fusion with the soma membrane. Characterization of the content of the vesicular pool can be determined using intracellular vesicle impact electrochemical cytometry (IVIEC) method, first developed, and used by Ewing's group (Li et al., 2015b). Changes in the proportion of transmitter released from an average vesicle can be calculated by quantifying the neurotransmitter content of individual vesicles in their intracellular environment using IVIEC and comparing it to the content released into the extracellular environment using single cell extracellular amperometry. The two methods can be combined due to the development of sharp flame-etched carbon-fibre nanoelectrodes, which can be inserted in the intracellular environment without causing permanent damage to the cell. In single cell amperometry, release is detected as an oxidation current transient when the vesicles bind to the cell membrane under the carbon-fibre electrode (**Figure 5.1 A**). Similarly, IVIEC also detects current transient peaks when a vesicle from the intracellular environment adsorbs and ruptures on the inserted nano-tip (**Figure 5.1 B**).
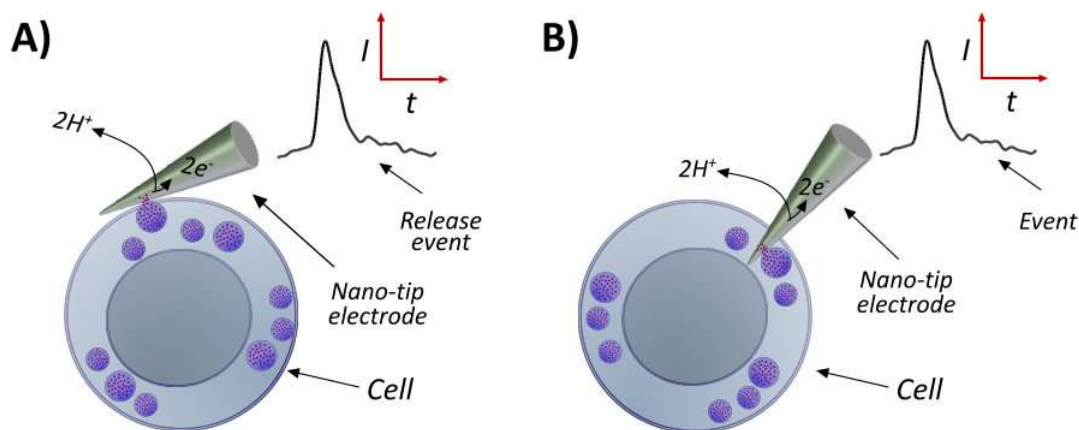
Figure 5.1 Schematic illustration of extracellular single cell amperometry (SCA) and intracellular vesicle impact electrochemical cytometry (IVIEC). A) Measuring extracellular release using carbon fibre nano-tip positioned on the cell membrane and SCA. B) Measuring individual vesicles content by inserting the carbon fibre nano-tip inside of the cell using IVIEC.

The combination of IVIEC and single cell amperometry have been used to measure intracellular vesicular content and vesicular release in a wide range of cell types. The first application of the two techniques in PC12 cells revealed that release is partial as only a fraction of the intra vesicular content (~64%) is seen to undergo exocytosis (Li et al., 2015b). Similar observations are made for serotonin release from mouse pancreatic beta cells, which releases only ~34% of its content (Hatamie et al., 2021).

Various studies, which have employed IVIEC and single cell amperometry, have made observations that a range of molecules and drugs can regulate the proportion of transmitter released. Zinc treatment (100 µM) of PC12 cells increased the proportion of release from ≈ 64 % in control cells to ≈ 100 % in Zn^{2+} treated cells, although it should be noted that Zn^{2+} also reduced the vesicle content (Ren et al., 2017). Conversely, treatment of the cells with a barbiturate did not affect vesicular content, but did affect the kinetics of the release events reducing the proportion of transmitter released (Ye and Ewing, 2018). Similarly, the local anaesthetic lidocaine also had no effect on vesicular content, but had a biphasic effect on the proportion of transmitter released, increasing it at low concentrations (0.1 mM) and decreasing it at high concentrations (5 mM) (Ye et al., 2018). Cultured PC12 cells have also been used to determine the effect of the anticancer drug tamoxifen on the transmitter storage and

release from the cells. Observations have shown that at high concentrations (10 µM) tamoxifen can decrease the proportion of transmitter released and significantly decrease the intracellular content, whereas low levels (100 nM) can increase the proportion of transmitter released and increase intracellular content (Taleat et al., 2019). Further studies applying the combination of the two techniques on PC12 have also shown the opposing effects of cocaine and methylphenidate, which decrease and increase the fraction of released transmitters (Zhu et al., 2019), the effect of plasticity (short-interval repetitive stimuli), which increases the amount neurotransmitter released (Gu et al., 2019), and the effect of iron deficiency during plasticity (Wang et al., 2022), which significantly decreases release, without changing vesicular content. The combination of IVIEC and single cell amperometry, have also been successfully applied to investigate the release kinetics and intra vesicular content of bovine chromaffin cells. Incubation of these cells with dimethyl sulfoxide (DMSO; > 0.4 %) increases the proportion of transmitter released from 53 % up to 92 % (at 0.6 % DMSO) (Majdi et al., 2017). Another set of experiments using extracellular application of ATP suggested a possible role of purinergic receptors in altering vesicular fusion. Incubation of bovine chromaffin cells with extracellular ATP shifted vesicular fusion events from partial fusion to full fusion as ATP was shown to increase the fraction of catecholamines released by the cells without influencing the intracellular vesicular content (Majdi et al., 2019). A role of different lipids (PC, PE and LPC) introduced to the chromaffin cells via intracellular injections or extracellular incubation of cells maintained in culture, have also been determined using IVIEC and single cell amperometry and will be discussed in more detail in the following chapter (Aref et al., 2020).

In this chapter the nano-tip carbon fibre electrodes were used in combination with IVIEC and single cell amperometry to first measure the serotonin released by young and old CGCs and then measure the intracellular content of the vesicles. The aims of the chapter are to determine how many pools of vesicles there are inside the cell and to explore how ageing changes the proportion of transmitter released by a given vesicle pool. The chapter tests the hypothesis that release from both the young and old CGCs is partial but is increased by the natural ageing process.

5.2 Methods

5.2.1 CNS preparations

The CNS preparations were prepared using the method describe in the chapter 3 (3.2.2 CNS Preparations).

5.2.2 Electrochemistry recordings

Electrochemical recordings of release and intracellular content were performed using the in-house fabricated nano-tips (see Chapter 2). Extracellular recordings were carried out in the same ways as described in Chapter 3 (3.2.6 Electrochemistry recordings), with the nanotip electrodes held at +750mV versus Ag/AgCl reference electrode. For IVIEC, the electrodes were inserted inside of the CGC cell body. In some experiments, the holding potential of the nano-tip electrodes was increased to +850 or +950 mV (see section 5.2.4 for rationale). Recordings were carried out in the same way as extracellular recordings (3.2.6 Electrochemistry recordings).

5.2.3 Pharmacological agents

5.2.4 DPV of serotonin in high KCL HEPES-buffered saline containing BSA.

DPV measurements of serotonin oxidation peak potential in high KCl HEPES-buffered saline (3.2 Experimental methods) containing 50 mg ml^{-1} of Bovine Serum Albumin (BSA) (to mimic the intracellular environment) were conducted as described in Chapter 2 (2.2.3.2 Differential pulse voltammetry (DPV)).

5.2.5 Analysis of the electrochemistry recordings

Oxidation of neurotransmitter content generates amperometric events. The analysis of the parameters of the intracellular events recorded with the nanotip electrodes were carried out using the IgorPro 6 routine from David Sulzer laboratory (Mosharov and Sulzer, 2005) as describe in chapter 3 (3.2.7 Analysis of the electrochemistry recordings).

5.2.6 Cluster analysis

Cluster analyses of the amperomteric data were performed as described in Chapter 4 (4.2.5 Cluster analysis).

5.2.7 Statistical analysis

Statistical analyses were performed as described in Chapter 4 (3.2.9 Statistical analysis). Bonferroni multiple-comparison correction was applied to account for the four t-tests performed to determine the effect of age on the intracellular vesicular content and extracellular release between the young and old groups and the corrected level of significance was determined to be $p = 0.0125$. Proportion of release was calculated as the percentage of the median number of molecules released per cell to the median number of molecules recorded intracellularly. All p-values are shown above the graphs.

5.3 Results

5.3.1 Detection of vesicular release and intracellular vesicular content using the nano-tip electrodes

Nano-tip electrodes, held at +750mV, were first positioned on the surface of the cell to record the kinetics of exocytotic events (**Figure 5.2 A**) and later inserted into the cell to record the content of the intracellular vesicles (**Figure 5.2 C**). Corresponding amperometric traces with events were recorded as shown in **Figure 5.2 B and D** and Faraday's law (N=Q/nF) was applied to quantify the number of molecules released by the cells and the number of molecules contained in in the intracellular vesicles of the CGCs.
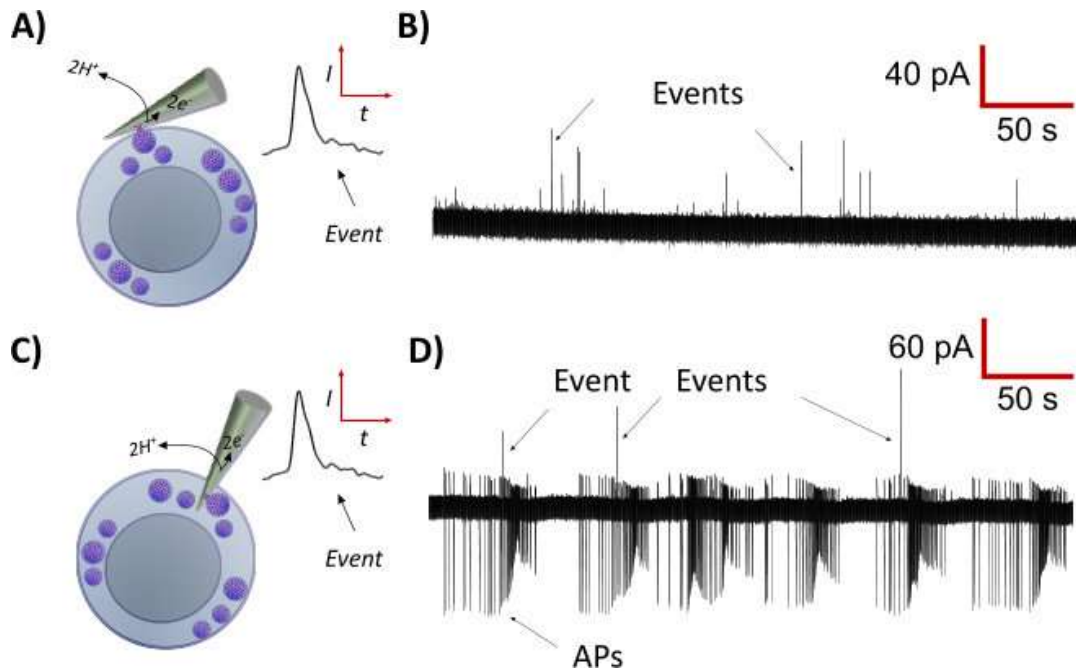
Figure 5.2 Exocytosis and vesicular content in the CGC. A) Schematic of CGC cell with nanotip disk electrode positioned on the cell membrane. B) Amperometric trace recorded with nanotip electrode positioned on the CGC with neurotransmitter release events. C) Schematic of a CGC cell with a nano tip inserted inside of the cell. D) Amperometric trace recorded with nano tip electrode inserted inside of the cell with events recorded from vesicular neurotransmitter contents (large upward deflections) and the action potentials (APs) generated by the cell (predominantly downward deflections).

Given the small size of the tip of the nano-tip electrode and the difficulty in visualising the tip under a light microscope it was important to confirm that recordings were made from the CGC and not a cell that was close by. To confirm this, intracellular recordings were made from the left CGC using an intracellular glass microelectrode in current clamp mode. Sample action potentials are shown for two different cells on a slow time base (**Figure 5.3 Ai/Bi**) and on a faster time base (**Figure 5.3 Ci/Di**). Extracellular action potentials receorded when the nano-tip is placed on the RCGC are shown on a slow time base in (**Figure 5.3 Aii**) and on a faster time base (**Figure 5.3 Cii**). Similarly, action potentials recorded using a nano-tip electrode placed inside the RCGC are shown on a slow timebase (**Figure 5.3 Bii**) and a fast timebase (**Figure 5.3 Dii**). Confirmation that the nano-tip electrode was recording from the CGC was shown by

the simultaneous action potentials recorded in the LCGC with the glass microelectrode and the RCGC with the nano-tip electrode (compare **Figure 5.3 Ai/Aii and Bi/Bii)** as the CGCs are the only cells in the cerebral ganglia to show this synchronous firing due to their strong electrical coupling. The same is observed when the nano-tip is positioned inside of the cell (**Figure 5.3 Bi and Bii**). Sample intracellular action potentials from the traces shown in **Figure 5.3 Ai and Bi** are shown on a faster time base in **Figure 5.3 Ci and Di**. Recordings of the CGC action potential using the nano-tip electrode placed on the surface (**Figure 5.3 Cii**) and inside the CGC (**Figure 5.3 Dii**) shows that extracellular recordings of the action potential tend to have a smaller amplitude and are much briefer events compared to the action potentials insice of the CGC. This difference was used to distinguish between extracellular release events and those recroded inside the CGC.
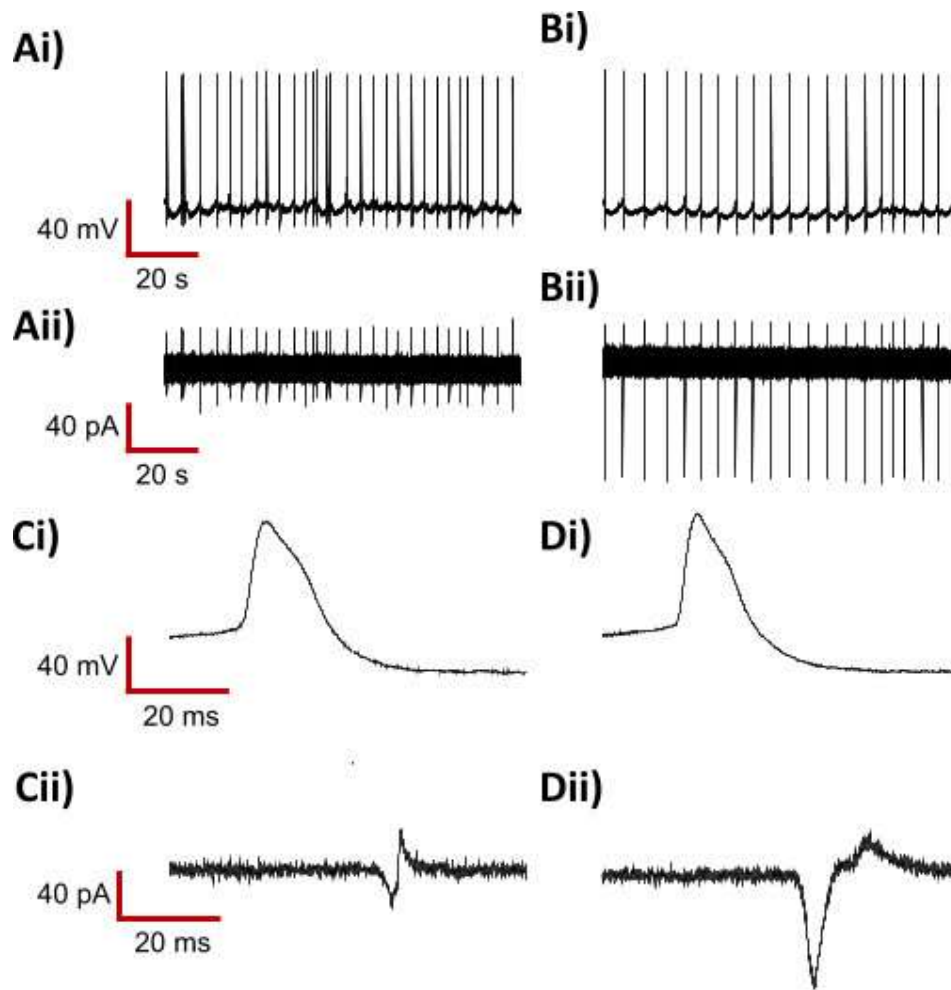
Figure 5.3 Action potentials waveforms of the extracellular and intracellular recordings. *Ai) Typical trace of action potentials recorded with a classical intracellular electrode from the LCGC. Aii) Corresponding amperometric trace of extracellular recording with action potentials recorded with the nano-tip. Bi) Trace with action potentials recorded with electrophysiology from the LCGC. Bii) Corresponding amperometric trace of intracellular recording with action potentials. Ci) and Di) electrophysiological action potential recorded from the LCGC. Cii) Action potential waveform from an extracellular amperometric recording and Dii) Action potential waveform from intracellular amperometric recording.*

DPV experiments of the serotonin oxidation peak potential recorded in HEPES-buffered saline to mimic the extracellular environment and in a high K+ HEPES + BSA to more closely mimic the CGC cytoplasm are shown in **Figure 5.4 A**. Increasing the concentration of K$^+$ ions (10mM KCl) in the recording solution and adding BSA caused a significant rightward shift in the serotonin oxidation potential **Figure 5.4 B**. Because of this the potential of the nano-tip electrodes was increased to +850 mV and +950 mV.
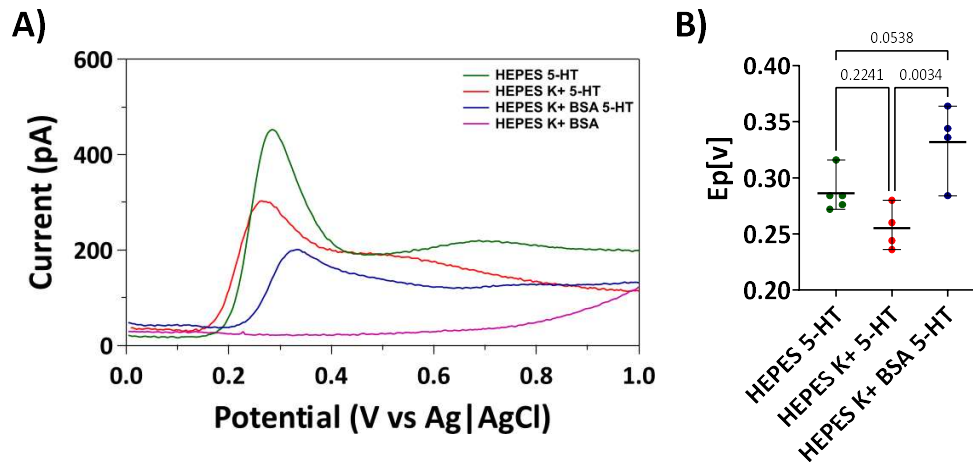
Figure 5.4 Oxidation peak potential of serotonin in different environments. *A) DPVs of serotonin oxidation peak potential in HEPES-buffered saline, high KCl HEPES-buffered saline and high KCl HEPES-buffered saline containing 50mg/ml BSA. B) Serotonin oxidation peak potential in HEPES-buffered saline (n = 5), high KCl HEPES-buffered saline (n = 4) and high KCl HEPES-buffered saline containing 50mg/ml BSA (n = 4). One-way ANOVA with Sidak multiple comparisons test.*

Increasing the oxidation potential from +750 mV to +850 mV in the young and old led to a significant increase in the number of molecules oxidized per event detected on the nano-tip (**Figure 5.5 A and B**). Increasing the potential from +750 mV to +950 mV also significantly increased the number of molecules oxidised from ruptured vesicles in the recordings from young CGCs, although these values were not significantly different from +850 mV (**Figure 5.5 A**). Similar increases to +950 mV in the old failed to show a significant difference from events recorded from +750 or +850 mV in old (**Figure 5.5 B**). Based on these findings only events recorded at +850 and +950 mV were considered to

have optimised mass transfer at the electrode and therefore only events recorded at these potentials were considered for analysis.

A)

B)
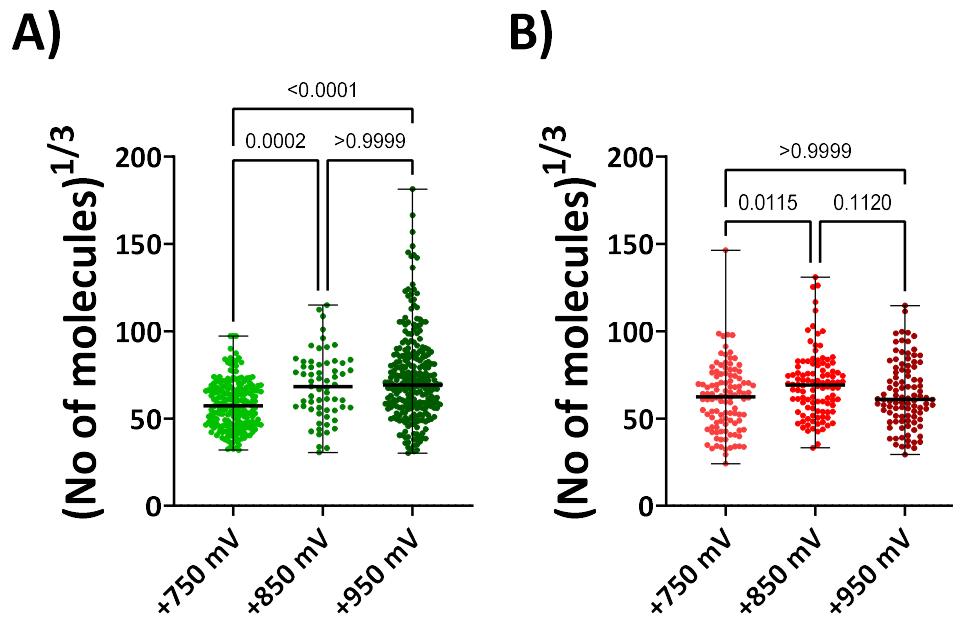
Figure 5.5 Increases in the oxidation potential increased the cube root of number of molecules oxidised per vesicle recorded in both young and old CGCs. *A) Cube root of number of molecules oxidized per vesicle in the young with increase of oxidation potential from +750 to +850 and +950 mV. B) Cube root of number of molecules oxidized per vesicles at +750, +850 and +950 mV in the old (young: +750 mV, n = 206; +850 mV, n = 63; +950 mV, n = 262; old: +750 mV, n = 110; +850 mV, n = 106; +950 mV, n = 99, Kruskal-Wallis tests).*

5.3.2   Effect of age on intracellular vesicular content and release

Age did not change the content of 5-HT in the intracellular vesicles (**Figure 5.6 A)**. Increasing age significantly increased the number of molecules of 5-HT released by the old CGCs (**Figure 5.6 B**).
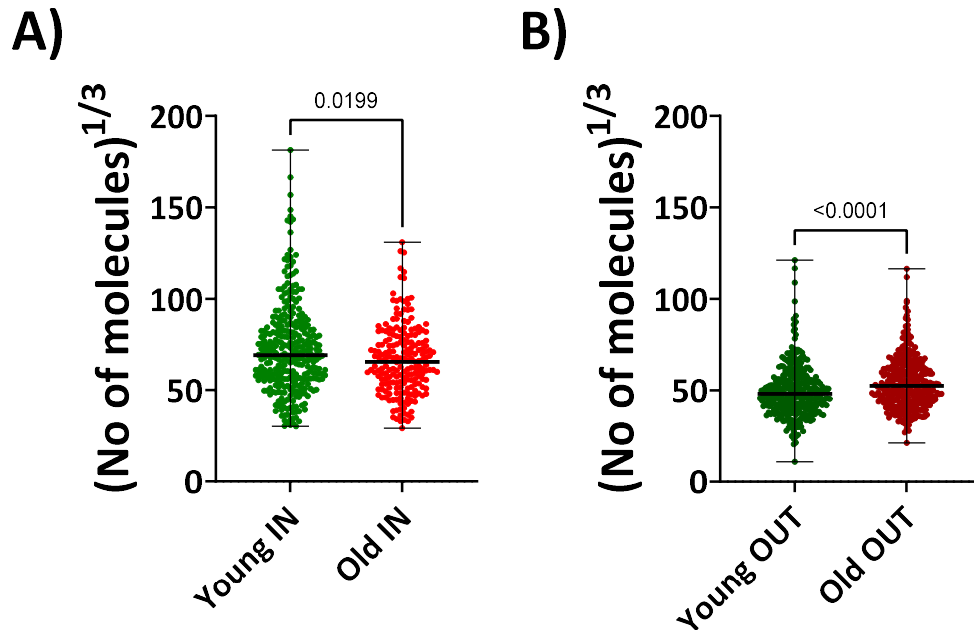
Figure 5.6 Effect of age on vesicular content of the CGCs. *A) Comparison of the number of molecules in intracellular vesicles oxidized at + 850 and 950 mV between young and old CGCs (young n = 325; old n = 205, Mann-Whitney test). B) Comparison of the number of molecules in released from young and old CGCs (young n = 338; old n =344, Mann-Whitney test).*

5.3.3 Effect of age on the proportion of neurotransmitter released by the CGCs

Comparing the number of molecules of 5-HT released from the young CGCs to the number of molecules oxidized inside of the cells, showed that the intravesicular content is significantly higher compared to that released by the cells (**Figure 5.7 A**). Similar in the old significantly more molecules of serotonin are oxidized inside of the cells compared to the molecules released by the cells (**Figure 5.7 B**). Analysis of the proportion of transmitter released in young showed that on average 40.2 % of the transmitter per vesicle is released upon fusion with the CGC membrane. In contrast, in

the old 74.3% of the vesicular contents are released on average per fusion event. (**Figure 5.7 C**).
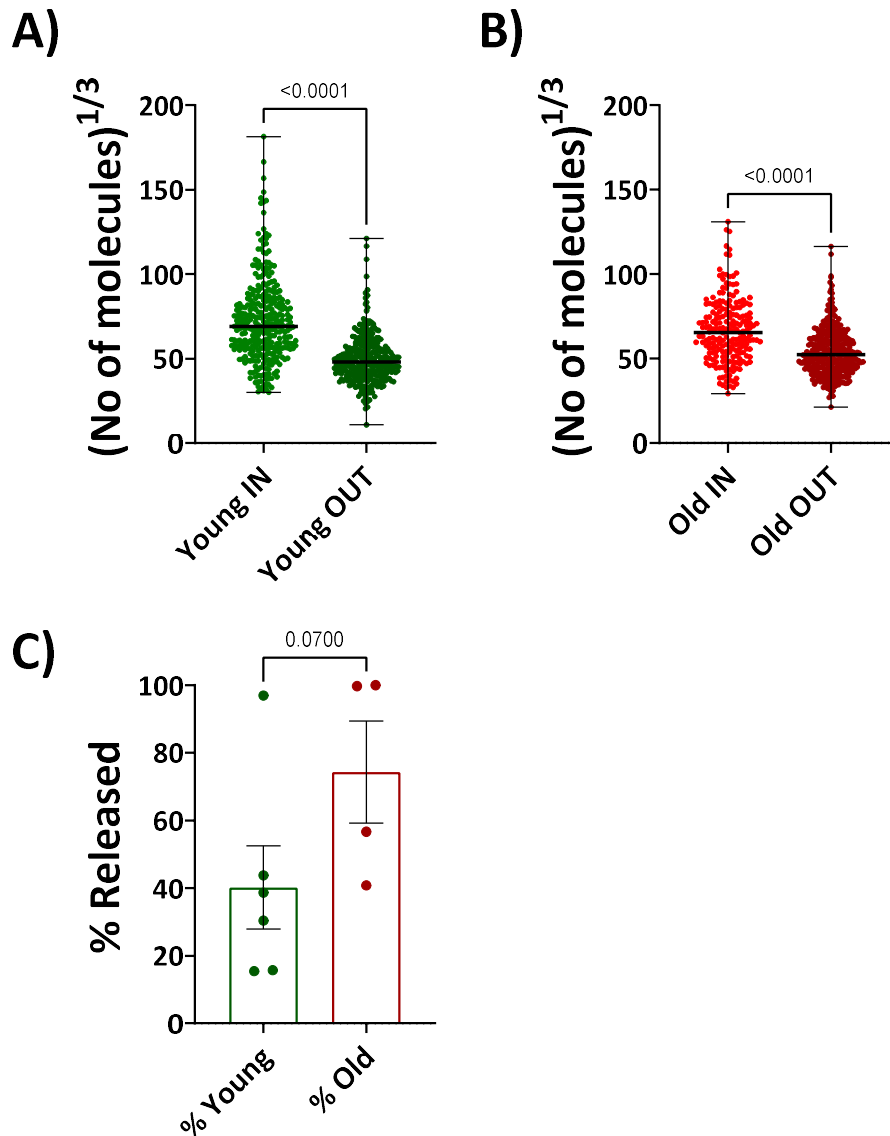
Figure 5.7 Intravesicular 5-HT content of young and old CGCs is higher than the 5-HT released by the cells. *A) Comparison of the number of molecules oxidized inside of the young CGCs to the number of molecules released per cells (IN n = 325, OUT n = 338, Mann-Whitney test). B) Comparison of the number of molecules oxidized inside of the old CGCs to the number of molecules released by the cells (IN n = 205, OUT n = 344, Mann-Whitney test). C) Percentage of neurotransmitter released by the young and old CGCs (young n = 6, old n = 4, paired t-test).*

5.3.4 Cluster analysis of vesicular release events and intracellular vesicles recorded using nano-tip electrodes.

Clustering was used to identify possible sub-pools of events based on SCA and IVIEC. First, release events and intracellular content events were clustered based on the cube root of the number of molecules associated with the events and then based on log-transformed data of the parameters describing the event's kinetics. In all cases the BIC was used to predict the possible number of clusters that can best describe the data and clustering was performed using the Gaussian mixture model algorithm.

5.3.4.1 Identification of vesicular release sub-pools

5.3.4.1.1 Identification of distinct clusters based on the cube root of number of molecules released by the young and old CGCs

ΔBIC were calculated for each possible mixture of gaussian models, which could be describing the young and old datasets. The model with the lowest ΔBIC in the young was 2 (**Figure 5.8 A**), making this the best candidate and there were no other models with a ΔBIC < 10 that could also be considered potential candidates. The model with the lowest ΔBIC in the old was also 2 (**Figure 5.8 B**), however a model with 3 clusters is also likely, suggested by the ΔBIC of 7. These data suggest the existence of two pools of vesicles released by the young and the old, and a possible model with 3 pools in the old, which is less likely.
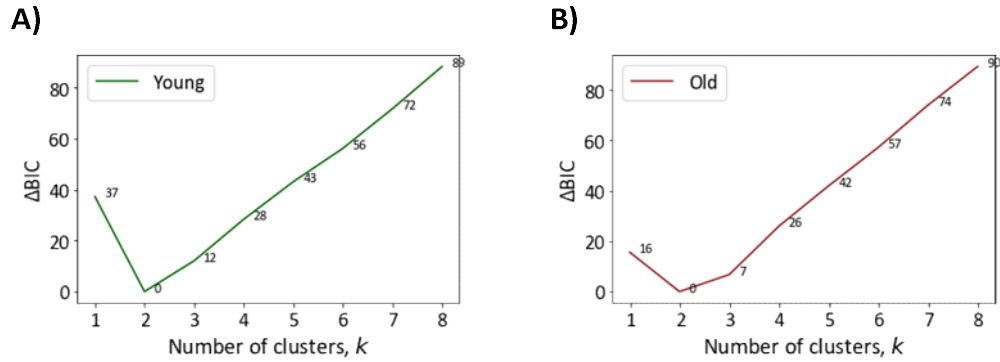
Figure 5.8 ΔBIC suggests that the events released by both the young and old CGCs are best described as coming from two clusters/populations of vesicles. Using the cube root of the number of molecules of the release events the ΔBIC of young (A) and old (B) shows that a model of 2 clusters best describes the data in both, however a model of 3 clusters in the old also falls into the ΔBIC < 10 criteria for likeliness.

Based on the recommendations from the BIC, which suggests 2 clusters as the most likely model in both groups, and using the Gaussian mixture algorithm, the release events were clustered into two clusters (**Figure 5.9 A and B**). As with the release events recorded by the 10 μm disc electrodes, the clustering of the release events recorded with the nano-tip electrodes showed an age-related decrease in the percentage of events in Cluster 1, which decreased from 88.8 % in the young to 71.5 % in the old (**Figure 5.9 A and B**). Additionally, an age-related increase in the percentage of events fitted in Cluster 2, was observed, which has increased from 11.2 % in the young to 28.5 % in the old (**Figure 5.9 A and B**).
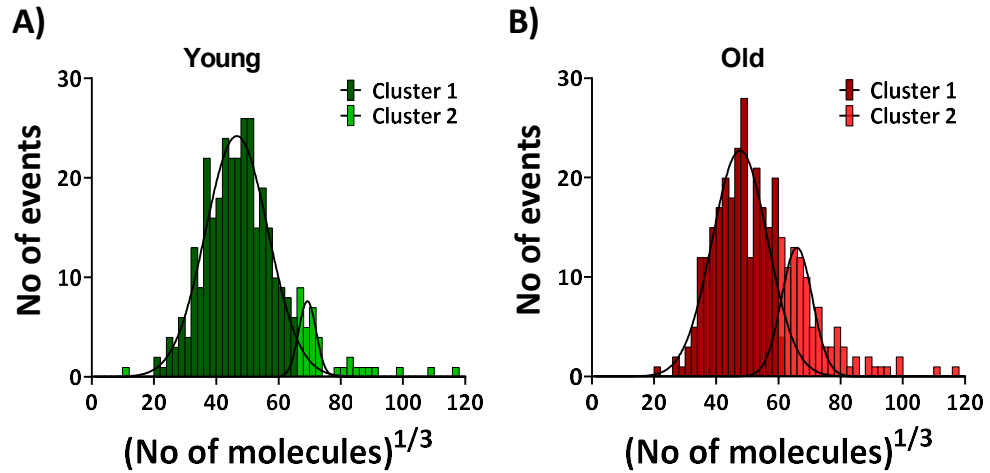
Figure 5.9 Increasing age decreases the percentage of events in the first cluster and increases the percentage of events in the second cluster. A) Histogram plot of the two clusters of events released by (A) the young CGCs (88.8 % in cluster 1 (300 events, mean = 110764 molecules), 11.2 % in cluster 2 (38 events, mean = 495876 molecules)) and (B) the old CGCs (71.5 % in cluster 1 (246 events, mean = 112658 molecules), 28.5 % in cluster 2 (98 events, mean = 390980 molecules)).

Typical example of events from the two clusters in both young and old and comparisons of the content of release and the release parameters of the events can be seen in **Figure 8.1** in the **8.1.1 Clustering of the release events based on the cube root of molecules** section of the Appendix.

To determine which of the parameters of the release events best described the number of molecules released by the events, an ordinary linear regression model was utilized. The regression model again showed that in both groups, all event parameters can predict the molecules released by the events (**Table 5-1**).

	Young (p – value)	Young β-coefficient	Old (p – value)	Old β-coefficient
t1/2[ms]	< 0.0001	-0.9063	<0.0001	-1.3747
Imax [pA]	< 0.0001	3.7392	<0.0001	3.3899
Rise (25-75) [ms]	< 0.0001	0.8025	<0.0001	0.9273
Fall (75-25) [ms]	< 0.0001	0.4841	<0.0001	0.4894

Table 5-1 Result of the Ordinary linear regression model showing that all parameters of the events can significantly account for the molecules released by the events. The algorithm was applied on the log-transformed values of the parameters.

Utilizing the BIC on the event parameters showed that in both age groups the most likely number of clusters that best describes the release events is 2 (**Figure 5.10**).
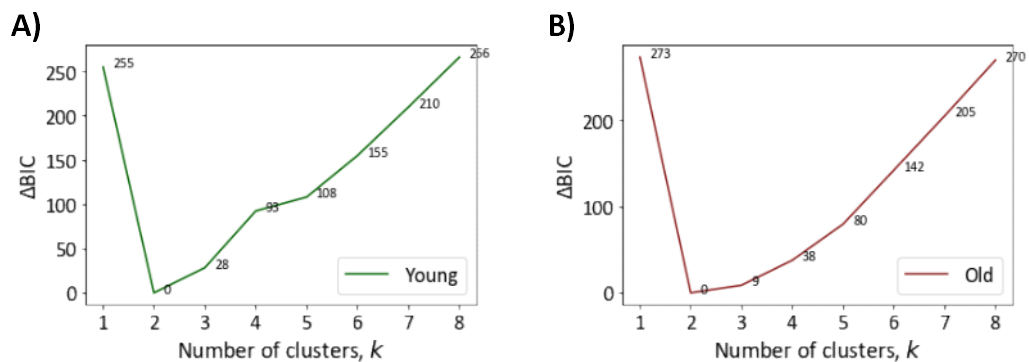
Figure 5.10 ΔBIC on the log-transformed data of t-half, I-max, t-rise and t-fall suggests two clusters of events in both groups. A) young and B) old.

Based on the results of the BIC, the events from both age groups were clustered into two clusters. The clustering showed that in the young, 55 % of the events fit in one cluster (Cluster 1) and 45 % of the events in another (Cluster 2) (**Figure 5.11 A**). In the old, 65.7 % of the events fit in one cluster (Cluster 1) and 34.3 % in another (Cluster 2) (**Figure 5.11 B**).
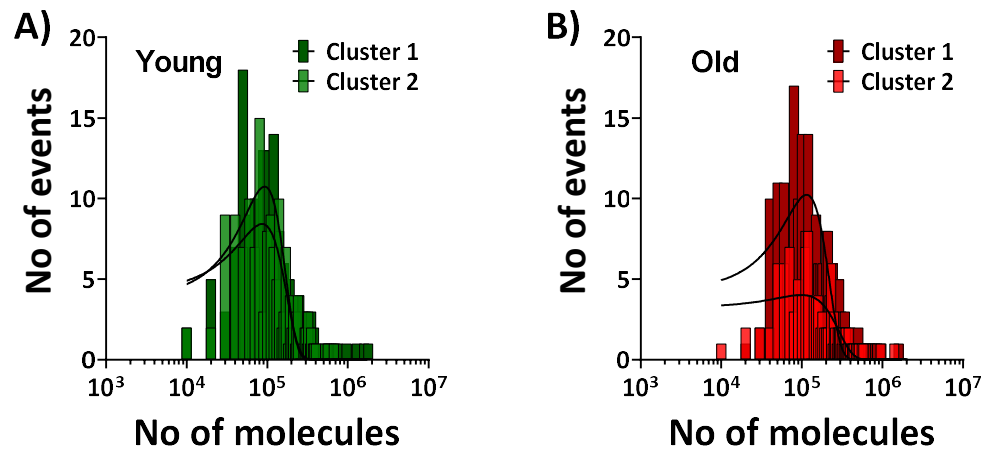
Figure 5.11 Cluster analysis of the release events from young and old CGCs in two distinct clusters. *A) Histogram plot of the two clusters of events released by (A) the young CGCs (55 % in cluster 1 (186 events), 45 % in cluster 2 (152 events)) and (B) the old CGCs (65.7 % in cluster 1 (226 events), 34.3 % in cluster 2 (118 events)).*

Typical events of the two clusters in both young and old and comparisons of the content of release and the release parameters of the events can be seen in **Figure 8.2** in the **8.1.2 Clustering of the release events based on the log-transformed values of event parameters** section of the Appendix.

5.3.4.2 Identification of intracellular vesicular content sub-pools

5.3.4.2.1 Identification of distinct vesicular content sub-pools based on the cube root of number of molecules of the intracellular events.

The BIC was used to identify possible sub-pools of vesicles based on the cube root of molecules contained in the events recorded intracellularly. The ΔBIC results in the young suggested that the most likely model of clusters is 2 (**Figure 5.12 A**). The ΔBIC results in the old suggested that a model of 1 or a model of 2 clusters was the best fit of the data (**Figure 5.12 B**).
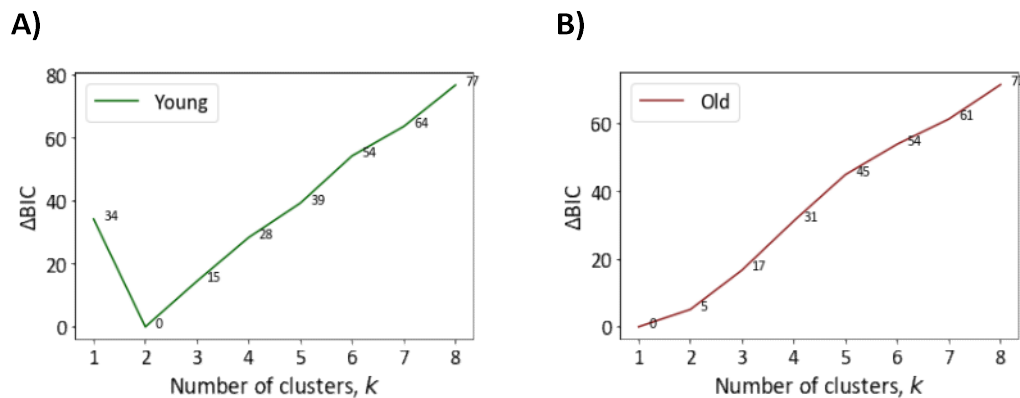
Figure 5.12 ΔBIC suggests that a model of 2 clusters best describes the intracellular events of the young CGCs, whereas two models one of one cluster and one of 2 clusters are likely to be a good description of the number of clusters in which the events of the old CGCs can be fit. *A) ΔBIC of young. B) ΔBIC of old.*

Based on the BIC results and using the Gaussian mixture model, the young group of events was clustered into two clusters, whereas for the old both models of one and two clusters were explored. Clustering the events of the young CGCs into two clusters generates Cluster 1, containing 84.6 % of the events and Cluster 2, containing 15.4 % of the events (**Figure 5.13 A**). One cluster of the intracellular events in the old is shown in **Figure 5.13 B**. Clustering the event of the old CGCs into two clusters generates Cluster 1, containing 66.3% of the events and Cluster 2 containing 33.7 % of the events (**Figure 5.13 C**).
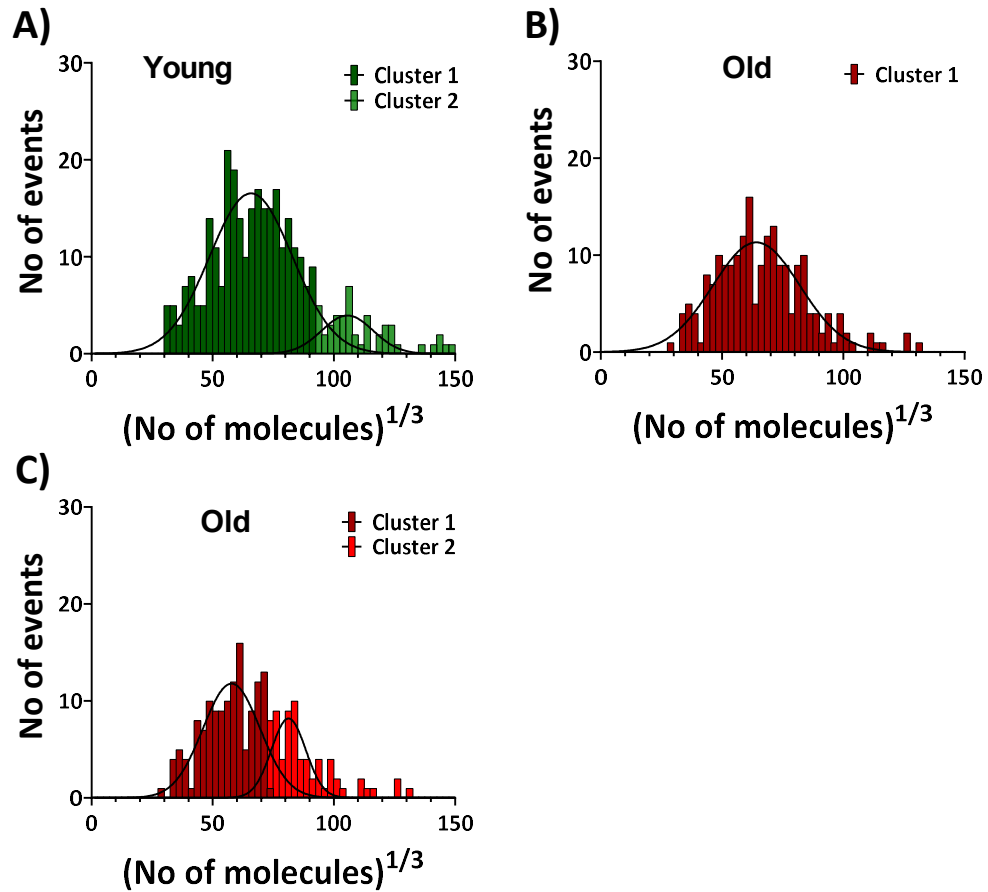
Figure 5.13 Cluster analysis of the intracellular events. *A) Histogram plot of the two clusters of intracellular events generated in the young CGCs (84.6 % in Cluster 1, n = 275, mean = 313619 molecules; 15.4 % in Cluster 2, n = 50, mean = 1677960 molecules). B) Histogram plot of a single cluster in old (n = 205, mean = 374883 molecules). C) Histogram plot of the two clusters of intracellular events (66.3 % in Cluster 1, n = 136, mean = 195567 molecules; 33.7 % in Cluster 2, n = 69, mean = 728319 molecules).*

Clustering of the intracellular events of the young CGCs into two clusters and the intracellular events of the old into one cluster showed no significant difference between the molecular content in Cluster 1 in the young and the only cluster (Cluster 1) in the old (**Figure 5.14 A**). When both the intracellular events of the young and the old CGCs are clustered into two clusters, a comparison of young and old showed

significant decreases in the number of molecules for both Cluster 1 and Cluster 2 (**Figure 5.14 B**).
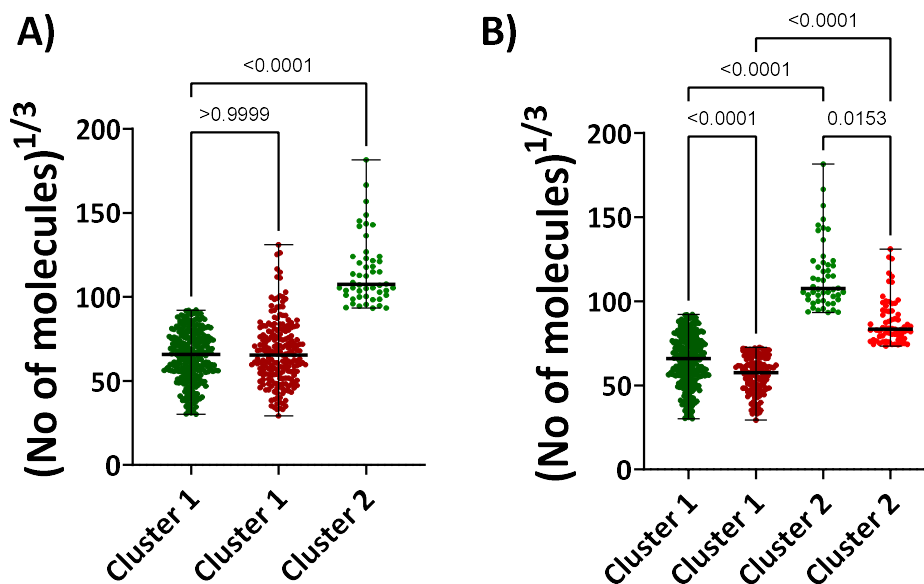
Figure 5.14 Two clustering outcomes based on the used model. *A) Comparison of the clusters generated in the young and the old when clustering intracellular events of the young CGCs into two clusters and the intracellular event of the old CGCs into one cluster (Young Cluster 1 n = 275, Cluster 2 n = 50; Old Cluster 1 n = 205). B) Comparison of the clusters generated in the young and the old when both groups of events are clustered into two clusters (Young Cluster 1 n = 275, Cluster 2 n = 50; Old Cluster 1 n = 136, Cluster 2 n = 69, Kruskal-Wallis tests).*

Comparisons of the parameters of the events, based on the clustering model used can be seen in **Figure 8.3** in the **8.1.3 Clustering of the intracellular events based on the cube root of the molecules of the events** section of the Appendix for a model of two clusters in the young and one in the old, and in **Figure 8.4** in the **8.1.3 Clustering of the intracellular events based on the cube root of the molecules of the events** section of the Appendix for a model of two clusters in both the young and the old group.

Events were next clustered according to their kinetics. Applying the linear regression model showed that all parameters contributed significantly to the molecular content of the events in both the young and old groups. (**Table 5-2**).

	Young (p − value)	Young β-coefficient	Old (p − value)	Old β-coefficient
t1/2[ms]	< 0.0001	-1.1592	<0.0001	-1.1584
Imax [pA]	< 0.0001	3.8524	<0.0001	3.6051
Rise (25-75) [ms]	< 0.0001	0.6131	<0.0001	0.7253
Fall (75-25) [ms]	< 0.0001	0.5180	<0.0001	0.6308

Table 5-2 The results of the Ordinary linear regression model showed that all parameters of the intracellular events can account significantly for the molecular content of the events. The algorithm was applied on the log-transformed values of the parameters.

Applying the BIC showed that, a model of 3 clusters can best describe the events in the young CGCs (**Figure 5.15 A**), whereas a model of 2 clusters can best describe the events in the old CGCs (**Figure 5.15 B**).
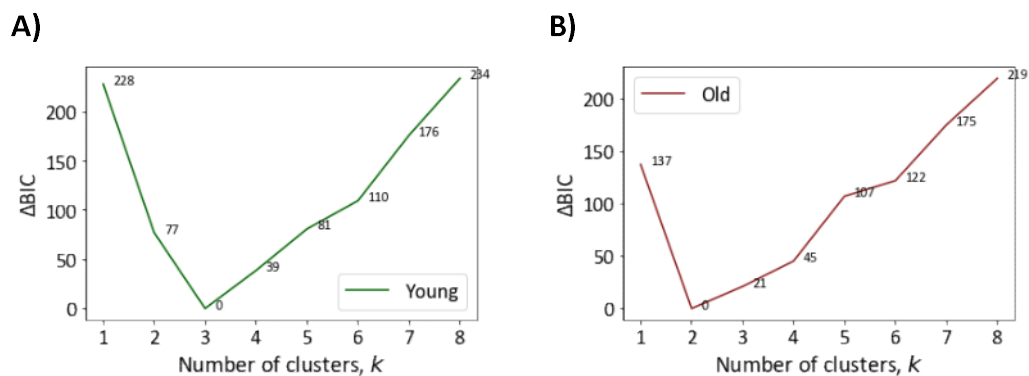
Figure 5.15 ΔBIC on the log-transformed combined data of t-half, I-max, t-rise and t-fall suggests three clusters of events as most likely model in the young A) and two clusters of events as the most likely modes in the old B).

Clustering of the events from the young CGCs into three clusters and the events of the old CGCs into two clusters, as suggested by the BIC, fitted most of the events, 52.3 % of the events in young and 67.8 % of the events in the old in the first Cluster (Cluster 1) (**Figure 5.16 A and B**). 28.5 % of the events in the young CGCs and 32.2 % of the events in the old CGCs were fitted in a second cluster (Cluster 2), and the remaining of the events in the young CGCs (9.2 %) were fitted in the third cluster (Cluster 3) (**Figure 5.16 A and B**).
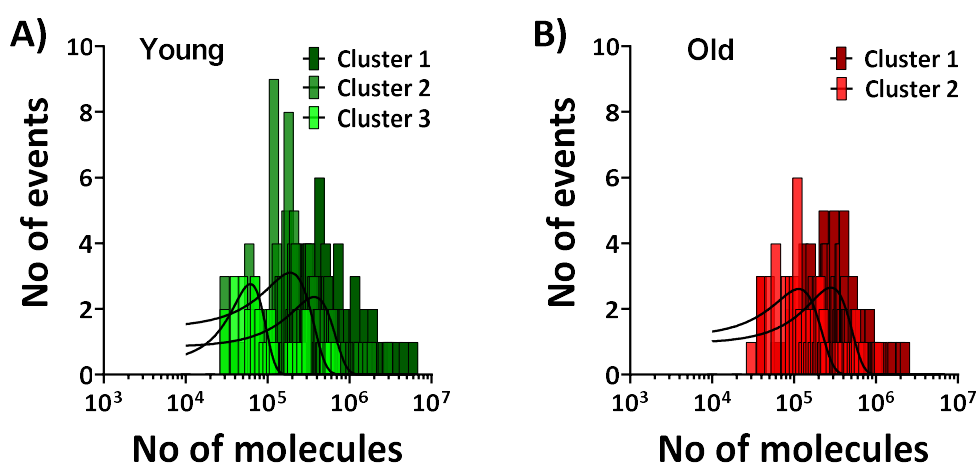
Figure 5.16 Cluster analysis of the intracellular events of young and old. A) Histogram plot of the three clusters of events in the young CGCs, 52.3 % in cluster 1 (170 events), 28.5 % in cluster 2 (125 events) and 9.2 % in cluster 3 (30 events). B) Histogram plot of the two clusters of events in the old CGCs, 67.8 % in cluster 1 (139 events) and 32.2 % in cluster 2 (66 events).

Typical events representing all identified clusters of events in the young (green) and the old (red) CGCs are shown in **Figure 5.17 A**. As with the release events, the events in Cluster 1 from both the young and the old CGCs have a larger amplitude (**Figure 5.17 D**), contain the largest quantity of 5-HT (**Figure 5.17 B**) have the largest half width (**Figure 5.17 C**) and the slowest fall time (**Figure 5.17 F**) compared to the events in Cluster 2. For both clusters (Cluster 1 and 2) the content of 5-HT is larger in the young CGCs compared to the old CGC (**Figure 5.17 B**), however the events of the old CGCs,

have a significantly higher amplitude compared to the young (**Figure 5.17 D**). Significant differences between the events of the young and the old CGCs are also observed in the half width (**Figure 5.17 C**), rise time (**Figure 5.17 E**) and fall time (**Figure 5.17 F**) of the events in Cluster 1.
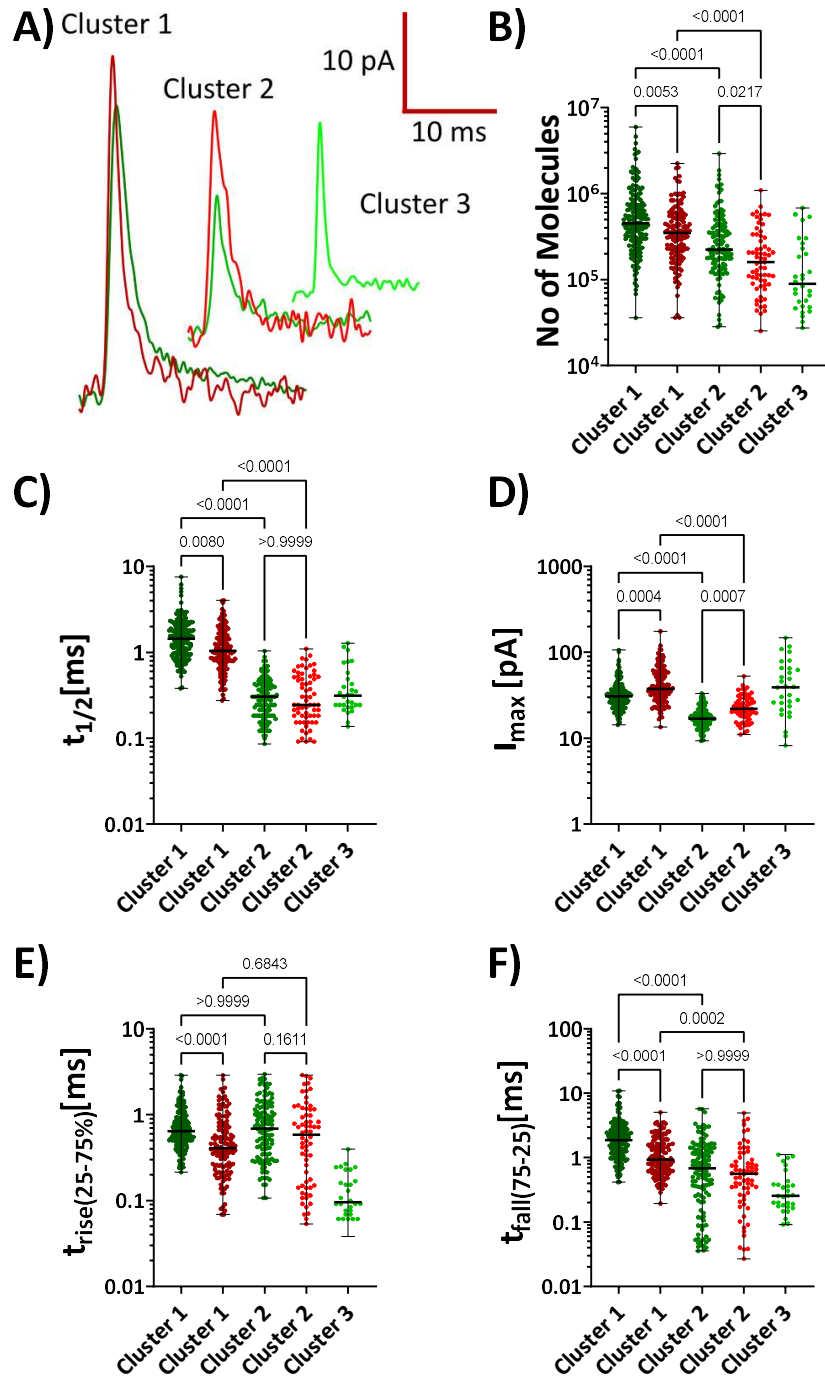
Figure 5.17 Intracellular clusters of events in the young and old CGCs. *A) Sample events from young (green) and old (red) CGCs for each of the clusters. (B-F) Plots comparing the properties of the intracellular events. B) Number of molecules, C) Half width, D) Imax, E) Rise time and F) Fall time (young cluster 1 n = 170, cluster 2 n = 125, cluster 3 n = 30, old cluster 1 n = 139, cluster 2 n =66, Kruskal-Wallis tests).*

5.4 Summary and discussion

In this chapter nano-tip electrodes were used to investigate the serotonin content of the intracellular vesicles in both the young and old CGCs, to cluster the data and to compare the content of an average vesicle to the number of molecules of serotonin released per event. Using the nano-tip sensors, release was seen to be significantly greater in the old CGCs and cluster analysis predicted two clusters of release events, consistent with the data published in Chapter 4 using the 10 µm sensor. Analysis of the intracellular content of the vesicles showed that old vesicles contained less oxidisable 5-HT than the young. Cluster analysis on this data strongly inferred that the young CGC soma contained one more cluster of vesicles than the old. Combining the data obtained using IVIEC with that obtained using SCA showed that the proportion of 5-HT released from the vesicles was significantly higher in the old CGCs when compared to the young.

5.4.1 Effect of age on the 5-HT content of the release events measured using the nanotip sensor.

Like the release recorded with the 10 µm disc electrode in chapter 4, measuring release with the nano-tip electrodes showed that significantly more serotonin was released by the old CGCs per release event. The results of the BIC suggested the likely existence of 2 clusters of release events in each clustering model for each age group. Clustering using the cube root of molecules produced two clusters of similar features to those observed in chapter 4 with the disc electrode. I.e., the cluster with the highest number of events had the smallest number of molecules and the percentage of events in this cluster decreased with age, whereas the percentage of events in the other cluster with larger events increased. Clustering using the log-transformed data, also produced two clusters with similar properties to the clusters observed when release was recorded using the 10 µm disc electrodes. That is, a cluster of events with a larger amplitude and half-width and a cluster of events with a shorter amplitude and half

width. These data are reassuring as they show that very similar data can be obtained using both the nano-tip and the 10 µm sensors (Gu et al., 2020b) and reassured us that our experiments were reproducible between different experiments and batches of snails.

5.4.2 Effect of age on the CGC's intracellular vesicular content and the proportion of 5-HT released.

Intracellular content was detected using an oxidation potential of +750 mV. However, previous literature has shown that increasing the electrode potential to higher voltages (+900 mV) increases the number of events observed (Lovrić et al., 2016) and that the intracellular biological matrix of proteins can influence the oxidation of serotonin therefore requiring greater oxidation potentials to achieve efficient mass transfer (Fagan-Murphy et al., 2012). This was also confirmed in the CGC by showing that increasing the potential from +750 mV to +850 mV led to a significant increase of the number of molecules of 5-HT oxidised in the cytoplasm of both the young and the old CGC somas. Increasing the potential to +950 mV failed to further increase the number of serotonin molecules oxidised at the sensor. These observations suggest that a holding potential of +850 mV is required to optimise the oxidation of the 5-HT at the sensor. Using the combined data obtained at +850 and +950 mV, vesicles in old CGCs were shown, on average, not to significantly change their 5-HT content.

5.4.3 Populations of intracellular vesicular sub-pools

As in the previous chapter, cluster analyses were applied to the events recorded intracellularly. Using both the cube root of molecules and the log-transformed data of the kinetics of the events.

Applying the BIC to the cube root of molecules of the intracellular events, generated a model of 2 clusters in the young and 1 or 2 clusters in the old. The first model of 2 clusters in the young and 1 in the old suggests a difference between the content of

serotonin in the young and the old CGCs, due to the second cluster of larger events in the young, whereas the second model of 2 clusters in both young and old suggests a difference in the content between the two age groups due to significantly more molecules of serotonin in both of the young clusters. As both models are likely, at this point it is hard to determine, which model is correct. The first model could represent a pool of two types of vesicles (small and large), with the existence of only the pool of smaller vesicles in the old. Whereas the second model would suggest the existence of both small and large vesicles in both groups, like the clustering models observed with the release events.

Decreased intracellular 5-HT content in the old CGCs could be due to one or more of the following reasons:

a) Decrease in serotonin synthesis or an increase in serotonin metabolism.

In the brain, serotonin is synthesised from the essential amino acid L-tryptophan, which is supplied through the diet and transported into the nerve cells by active transport. In the serotonergic neurons, L-tryptophan is converted to 5-hydroxytryptophan by the enzyme tryptophan hydroxylase (TPH), which is the rate limiting step in the synthesis of 5-HT. This reaction is followed by the decarboxylation of 5-hydroxytryptophan (5-HTP) to 5-hydroxytryptamine (5-HT) by the L-amino acid decarboxylase (ADDC) enzyme (Höglund et al., 2019). The mRNA of the neuronal form of the TPH enzyme, TPH2, is significantly decreased with age in the human dorsal and medial raphe nuclei (Bach-Mizrachi et al., 2006). An age-related decrease in expression of TPH2 is suggested in the neural and neurointermediate lobes of the pituitary of rats (Saland et al., 1993), however, no age-related changes in TPH2 expression are observed in SAMP8 mice (Pérez-Cáceres et al., 2013), rats (Timiras et al., 1984) or humans (Klöppel et al., 2001). The expression/activity of TPH in *Lymnaea* has not been directly examined, however, the production of 5-HTP from tryptophan was shown not to change with age in the region of the CNS containing the CGCs (Morgan et al., 2021), suggesting that changes in TPH activity could not explain the observed changes in vesicular content seen with increasing age.

In the nervous system, 5-HT is metabolised by the enzyme monoamine oxidase (MAO), which is expressed in two forms, MAO_A and MAO_B (O'Carroll et al., 1983). The MAO_B is more common is 5-HT containing neurons, but has a lower affinity for 5-HT, whereas the MAO_A expression is shown in glial cells and has a higher affinity for 5-HT (Fitzgerald et al., 1990, Westlund et al., 1988). Some studies have shown an age-associated increase in expression or activity of the two MAO forms (Shih, 1979, Sparks et al., 1991), that may be brain region dependent, while others have shown no significant changes (Nicotra et al., 2004, Volchegorskii et al., 2001). Like TPH, the expression/activity of MAO enzymes in *Lymnaea* has also not been directly examined, however, as 5-HTP was shown not to change with age in the region of the CNS containing the CGCs (Morgan et al., 2021), any changes in expression or activity of MAO enzymes are likely not the cause of the observed changes in vesicular content seen the CGCs with increasing age.

b) Decrease of the expression or activity of VMAT

5-HT is transported into vesicles by vesicular monoamine transporters (VMAT) (R. G. Johnson, 1988, Schuldiner et al., 1995). VMAT actively removes neurotransmitters from the cell cytosol to the vesicles, a process that is coupled with the movement of 2 protons from the vesicle to the cytosol. The intra-vesicular proton gradient necessary for this transport is generated by the vesicular H^+- ATPase (Yaffe et al., 2018). It has been shown that the quantal size and volume of vesicles in cultured dopaminergic PC12 cells can be increased by incubating the cells with the dopamine precursor L-3,4-dihydroxyphenylalanine (L-DOPA) or decreased using the high-affinity competitive inhibitor reserpine and these changes have been attributed mostly to changes in the volume of the halo surrounding the dense core of the dense-core vesicles (Colliver et al., 2000). An age-related decrease of the density of VMAT has been observed in some regions of the rats' brain such as the nucleus accumbens, the olfactory tubercle, the substantia nigra pars compacta and ventral tegmental area, however no changes are seen in the striatum (Leroux-Nicollet and Costentin, 1991). An age-associated decrease of the rate at which VMAT-2 transports dopamine have been observed in vesicles of rat striata (Volz et al., 2009). These observations suggest that the decrease in the intravesicular content in the old CGCs could be caused either by a decrease of VMAT

density at single vesicles or a decrease of the rate at which it transports 5-HT into the vesicles (Hermann et al., 2020), but further work is needed to confirm this.

It has been suggested that during IVIEC, the neurotransmitter inside of the vesicles escapes through a pore which opens between the vesicle and the surface of the electrode following vesicle adsorption to the electrode (Li et al., 2018, Lovrić et al., 2016). This suggests that different types of vesicles when opening on the intracellular electrode might be producing events of different kinetics, similar to those recorded during release. Therefore, the intracellular events recorded from the young and old CGCs were also clustered based on the kinetics of the events. The BIC suggested that the events in the young CGCs can be best fitted into three clusters, whereas the events in the old CGCs can be best fitted into two clusters. Clustering the events in both age groups, produced two main clusters which exhibited corresponding properties to the clusters produced by the clustering of the release data. That is, a cluster of events with larger molecular content, larger half width, larger amplitude and a slower fall time, and a cluster of events with smaller molecular content, shorter half width and amplitude and faster fall time. An additional third cluster was observed in the young, but not in the old that probably reflects a population of SCVs as this cluster contained the smallest number of molecules of 5-HT. However, confirmation of these findings would require an electron microscopy study of the CGC soma in young and old cells. The similarities between the clusters of the release events and the intracellular events suggest that the clusters are formed by vesicles of corresponding properties, most likely determined by the intra-vesicular content.

As mentioned earlier, the large dense-core vesicles contain a protein matrix, which is composed of the acidic proteins (chromogranins) between which the neurotransmitter of the cell is compacted (Taupenot et al., 2003). In some dense-core vesicle, the dense core is surrounded by an additional compartment, termed the halo, occupied predominantly by the solubilized neurotransmitter (Omiatek et al., 2010, Colliver et al., 2000). Based on these observations, Oleinick et al. (2015) have proposed a theoretical model (**[Equation** *1*),

$$q_{slow} \xrightleftharpoons[k_2]{k_1} q_{fast} \xrightarrow{k_p^{diff}} q_{out}$$
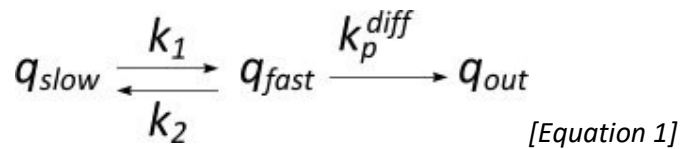
<div align="right">*[Equation 1]*</div>

which describes the release/diffusion kinetics from the two intra-vesicular compartments, the dense-core (a slow-release compartment) and the halo (a fast-release compartment). In this equation, the q_{slow} and q_{fast} are the quantities of transmitter released from the slow and the fast-releasing compartments, q_{out} is the quantity released, k_1 and k_2 the rate constants featuring the exchange of the transmitter between the two compartments, and k_p^{diff} is a pseudo-rate constant of release/diffusion through the pore. Based on this model, a faster rate of release and diffusion are expected for the neurotransmitter in the halo, whereas the neurotransmitter in the matrix will have to diffuse to the fast compartment (the halo) before it diffuses through the pore and is released.

Ren et al. (2020) has shown that treating PC12 cells with zinc can change both the size and the volume of both vesicular compartments the dense-core and the halo. In particular, zinc treatment increases the diameter and the volume of the dense core but decreases the diameter of the vesicles and its volume and the volume of the halo, as measured from TEM images. These changes appear to affect the kinetics of the release events, by enlarging the duration of the pre-spike foot and the duration of the spike itself, however, zinc treatment also decreases the maximum size of the radius of the pore formed between the vesicular and the cell membranes, possibly by disturbing the lipid composition of the cell membrane (Ren et al., 2019). Therefore, it is not possible to determine how changes in the intra-vesicular compartments alone would have affected the kinetics of the release events. Overall, the percentage of neurotransmitter molecular content in the two compartments – the dense core and the halo, in vesicles extracted form chromaffin cells of bovine adrenal glands has been measured to be 32% in the halo and 68% in the dense core (He and Ewing, 2022). As mentioned above, chromogranins, the main proteins of the dense core, can have a crucial role in both storage and exocytosis of catecholamines. Knock-out of chromogranin A in mouse chromaffin cells significantly increases the amplitude of the release events, measured with amperometry, additionally causing the cells to release 41% less catecholamines

(Montesinos et al., 2008). This suggests that events with higher amplitude and less contents would correspond to clear vesicles or vesicles with possibly smaller dense core, whereas events with lower amplitude and possibly larger content of neurotransmitters would represent LDCV.

The observations that the size and volume of the two intra-vesicular compartments can vary and that knocking-out the main protein of the matrix can increase the amplitude of the events suggests that the two clusters of corresponding intracellular and release events in both the young and the old CGCs could represent vesicles of different structure. Specifically, the events with the larger amplitude, larger half width and larger transmitter content might represent vesicles with a larger size/volume of the halo compartment. This cluster is characterised by fast diffusion kinetics, leading to events with higher amplitudes. Whereas events with a smaller amplitude, half width and molecular content might represent vesicles with a smaller halo, and more transmitter stored in the dense core, which is characterised by slower kinetics and therefore could produce smaller events.

5.4.4 Ageing increases the proportion of transmitter released.

Having quantified the transmitter content of the intracellular vesicles and measured the release profile of the different events in the same cells, it was possible to calculate the proportion of transmitter released from an average vesicle and determine how this changed with increasing age. Comparing the percentage of serotonin released by the young CGCs to the percentage of serotonin released by the old CGCs showed that the fraction of release increased with increasing age, from an average of 40.15 % released by the young to 74.31 % in the old CGCs. This is the first report demonstrating that the natural ageing process changes the proportion of release at the vesicular level. It is important to note that part of this increase in the proportion of transmitter released is due to a decrease in the transmitter content of the intracellular vesicles in aged CGCs. However, this reduction cannot totally explain the change observed with increasing age meaning that the release process is also affected in aged CGCs consistent with the changes described in chapter 4.

The first study to directly compare the percentage of release by measuring release using single cell amperometry and measuring vesicular content using electrochemical cytometry of isolated vesicles from cultured PC12 cell was conducted by Omiatek et al. (2010). The authors showed that only 40 % of transmitter content is released by the PC 12 cells. A slightly higher percentage (64 %) of release, is observed from the same cell line with the first application of IVIEC with nano-tip electrodes (Li et al., 2015b). A few other studies, which have applied IVIEC and SCA have shown that like PC 12 cells, other cells such as mouse pancreatic beta cells and bovine chromaffin cells also show partial release. In particular, mouse pancreatic beta cells release ~34 % of their content (Hatamie et al., 2021), whereas bovine chromaffin cells release ~53 % of their content (Majdi et al., 2017). In all these studies, the proportion of release from the used cells appear very similar to what was observed in the young CGCs. It is possible that the increase in the proportion of transmitter released with age by the CGCs, is a response to a decrease in the total number of vesicles in the cell. A significant reduction of the total number of presynaptic vesicles and vesicles in the resting pool have been observed in the CA1 area of the hippocampus of aged Wistar rats experiencing impaired cognitive function (Lomidze et al., 2021). Previous studies have shown that the proportion of release in PC12 cells increases following incubation with drugs, such as zinc that facilitate learning and memory (Ren et al., 2017) and decreases when exposed to drugs, such as cocaine, that impair learning and memory (Zhu et al., 2019). Given the CGC is a cell that is involved in long-term memory formation, the results described in this thesis suggest that plasticity at the level of the single vesicle maybe reduced with increasing age. Indeed, previous work has shown that aged *Lymnaea* fail to learn to associate two chemical stimuli as well as their younger counterparts (Hermann et al., 2007, Watson et al., 2013) and it is possible that part of this deficit is due to impaired plasticity at the level of the individual vesicle.

In summary, ageing reduced the number of clusters of intracellular vesicles, the transmitter content of the vesicles and increased the proportion of transmitter released. The age-related increase in the proportion of transmitter released cannot be solely explained by the decreased intracellular content of age CGC vesicles. Therefore, additional changes must be occurring that consistently affect the release process of

both clusters. As mentioned in the previous chapter, in addition to the proteins facilitating/regulating transmitter release, several lipids have been shown to affect the kinetics of release, by influencing the pore formed between the vesicle and the cell membrane (Uchiyama et al., 2007, Wang et al., 2010). Therefore, in the next chapter the effect of age on the lipid composition of the CNS of young and old *Lymnaea* will be investigated.

6 Effects of age on CNS Lipid composition

6.1 Introduction

The previous chapters showed that ageing slowed the kinetics of the release events, increased the amount of transmitter released per event and increased the proportion of transmitter released from an individual vesicle. This chapter explores how ageing alters the expression of membrane lipids and the potential of these changes to explain the effects of age on vesicular release dynamics.

6.1.1 Membrane lipid structure

Lipids have a modular structure, characterised by large number of lipid components that can be combined to form a diverse range of lipid classes. Depending on their role in the organism, lipids can be categorised as stores of energy in the form of fat (Gurr and Harwood, 1991) or as the main components of the structure of the cell and organelle membranes (Cooper, 2000). The most abundant lipids in the cell plasma membrane are the phospholipids. They are constructed of a glycerol backbone with two hydrophobic fatty acids attached to it via ester bonds at the sn-1 and sn-2 carbons and a hydrophilic head group, such as choline, ethanolamine, serine, inositol or glycerol, attached to the sn-3 carbon by a phosphodiester linkage (**Figure 6.1**).

1-palmitoyl-2-oleoyl-3-phosphoethanol
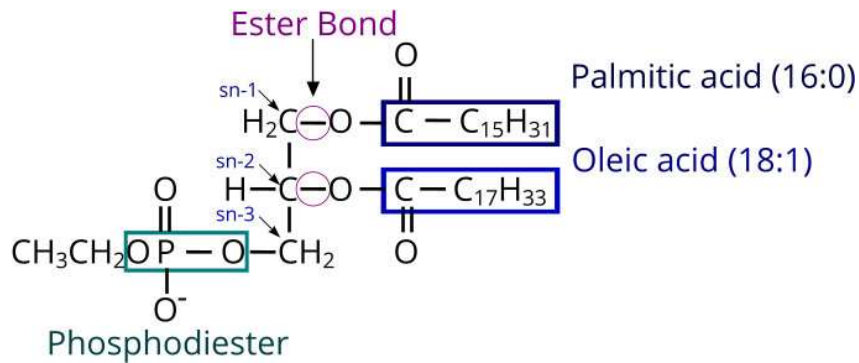
Figure 6.1 Phospholipid (1-palmitoyl-2-oleoyl-sn-glycero-3-phosphoethanol) with two fatty acid chains esterified to the sn-1 and sn-2 carbon atoms of the glycerol backbone and an ethanolamine head group linked with phosphodiester bond to the sn-3 carbon atom of the glycerol backbone.

The headgroup of the phospholipid defines the class of the lipid, with the main classes being: phosphatidic acid (PA, with no additional group attached to the phosphate) phosphatidylcholine (PC, with choline as the head group), phosphatidylethanolamine (PE, with ethanolamine as the head group), phosphatidylserine (PS, with serine as the head group), phosphatidylinositol (PI, with inositol as the head group) and phosphatidylglycerol (PG, with glycerol as the head group). The associated fatty acid chains define its saturation. Fatty acids with no double bonds, between the carbon atoms of the chain, are termed saturated fatty acids. Fatty acids with one double bond are termed monounsaturated fatty acids (MUFA), whereas fatty acids with two or more double bonds are termed polyunsaturated fatty acids (PUFA). In addition to the glycerophospholipids described above, two other lipid classes are characterised by having two fatty acid chains. One of these are glycerophospholipids known as plasmanyls and plasmenyls. These two lipid classes differ from the other classes of phospholipids by the type of sn-1 bond between the glycerol backbone and the fatty acid. In the case of the plasmanyls, this bond is an alkyl ether bond and in the case of the plasmenyls, the bond is a vinyl ether bond. As in the other type of phospholipids, they can have different head groups such as choline or ethanolamine. Another lipid class is the sphingolipids, which is composed of a long-chain sphingosine base with, a fatty acid connected to it and a head group that is predominantly a choline. A final

major group of lipids in cell membranes are the sterols, such as cholesterol. A diagram illustrating the structure of these different classes of lipid is shown below (**Figure 6.2**) (Fahy et al., 2005, Skowronska-Krawczyk and Budin, 2020).
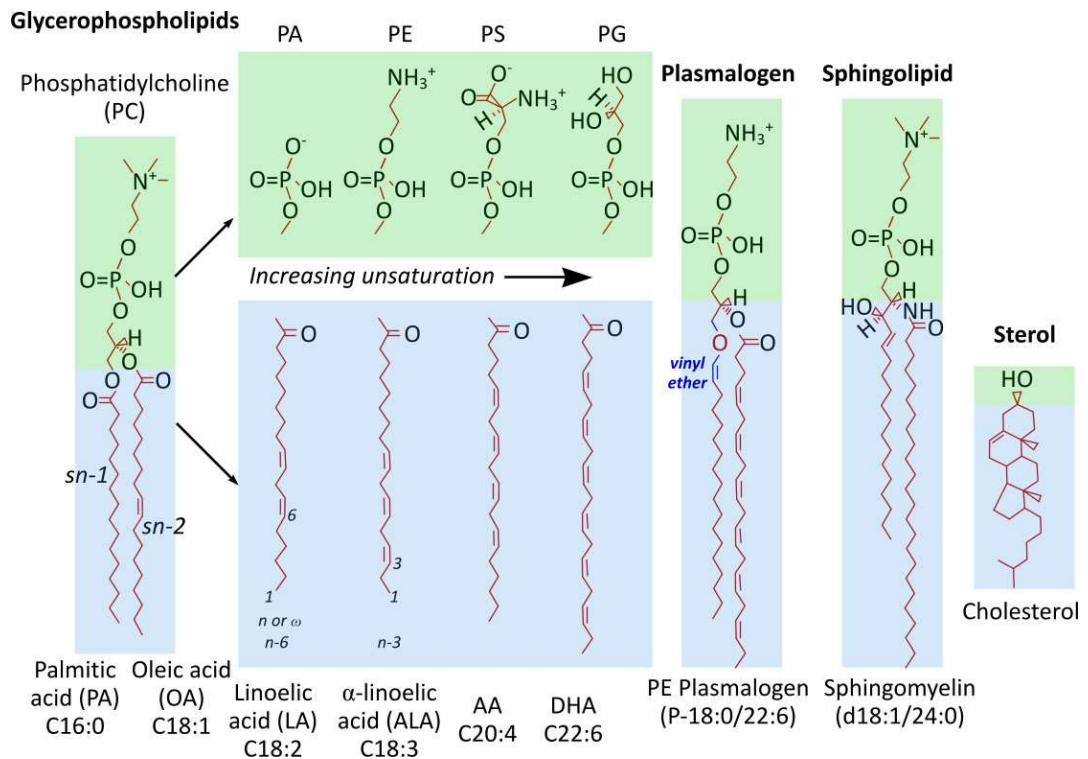
Figure 6.2 Structure of lipids. *Glycerophospholipids are composed of a two hydrophobic fatty acid chains attached to a glycerol backbone on the sn-1 and sn-2 carbons and hydrophilic head group, attached with a phosphodiester linkage to the sn-3 carbon. Based on the head group linked to the phosphate at the sn-3 carbon, the lipids can be classified as phosphatidylcholine (PC), if the head group is choline, phosphatidylethanolamine if the head group is ethanolamine, phosphatidylserine (PS) if the head group is serine, phosphatidylglycerol (PG) if the head group is glycerol and phosphatidylinositols (PI) if the head group is inositol. If no additional group is attached to the phosphate at the sn-3 carbon, the lipid is known as phosphatidic acid (PA). Glycerophospholipids can also have fatty acid connected to the sn-1 position by a vinyl ether bond and are known as plasmanyls or plasmenyls. Other two major classes of lipids are the sphingolipids, such as sphingomyelin and the sterols, such as cholesterol.*

Besides being stores of energy or building blocks of the membrane, lipids can also be precursors of signalling molecules. These include PA and diacylglycerol (DAG), which is

formed by the dephosphorylation of PA (Ridgway, 2016). Lyso-phospholipids and arachidonic acid (AA), which are formed by the hydrolysis of phospholipids, by phospholipases such as phospholipase A2 (Brown et al., 2003) and inositol-1, 4, 5-triphosphate (IP$_3$) which is released by the hydrolysis of phosphoinositol$_{4,5}$-biphosphate (PIP$_2$) (Lee and Rhee, 1995, Steelman et al., 2015).

6.1.2 Role of lipids in regulating vesicular release

Neurotransmitter release from intracellular vesicles is dependent on the ability of the lipid membrane of the vesicle to merge with the plasma membrane. How and where this happens is dictated by the topological arrangement of the lipids composing the membranes (Piomelli et al., 2007) and its effect on the positioning of the SNARE protein machinery (Milovanovic and Jahn, 2015). Lipid arrangement and packing in the membrane is dependent on the type of the lipid, the length of the fatty acid chains and their saturation, and the compatibility between the lipid's head group and tail (Piomelli et al., 2007). Lipids with symmetric head and tails, which have a cylindrical shape tend to pack tightly, whereas lipids with asymmetrical shapes such as a cone (small head and larger and unsaturated tails) or an inverse cone (larger head group and smaller saturated tails or a single tail) tend to pack more loosely (**Figure 6.3 A and B**). In addition to the degree of packing, the shape of the lipids can also influence the curvature of the membrane. The cone shaped lipids tend to give a negative curvature of the lipid layer, whereas inverse cone shaped lipids tend to give a positive curvature of the lipid layer (Dowhan et al., 2008). Transiently formed negatively curved monolayers facilitate the first phase of the formation of a fusion pore between the plasma membrane and a fusing vesicle. This is followed by pore opening and widening, which is helped by the presence of a positively curved monolayer (**Figure 6.3 C**) (Piomelli et al., 2007).
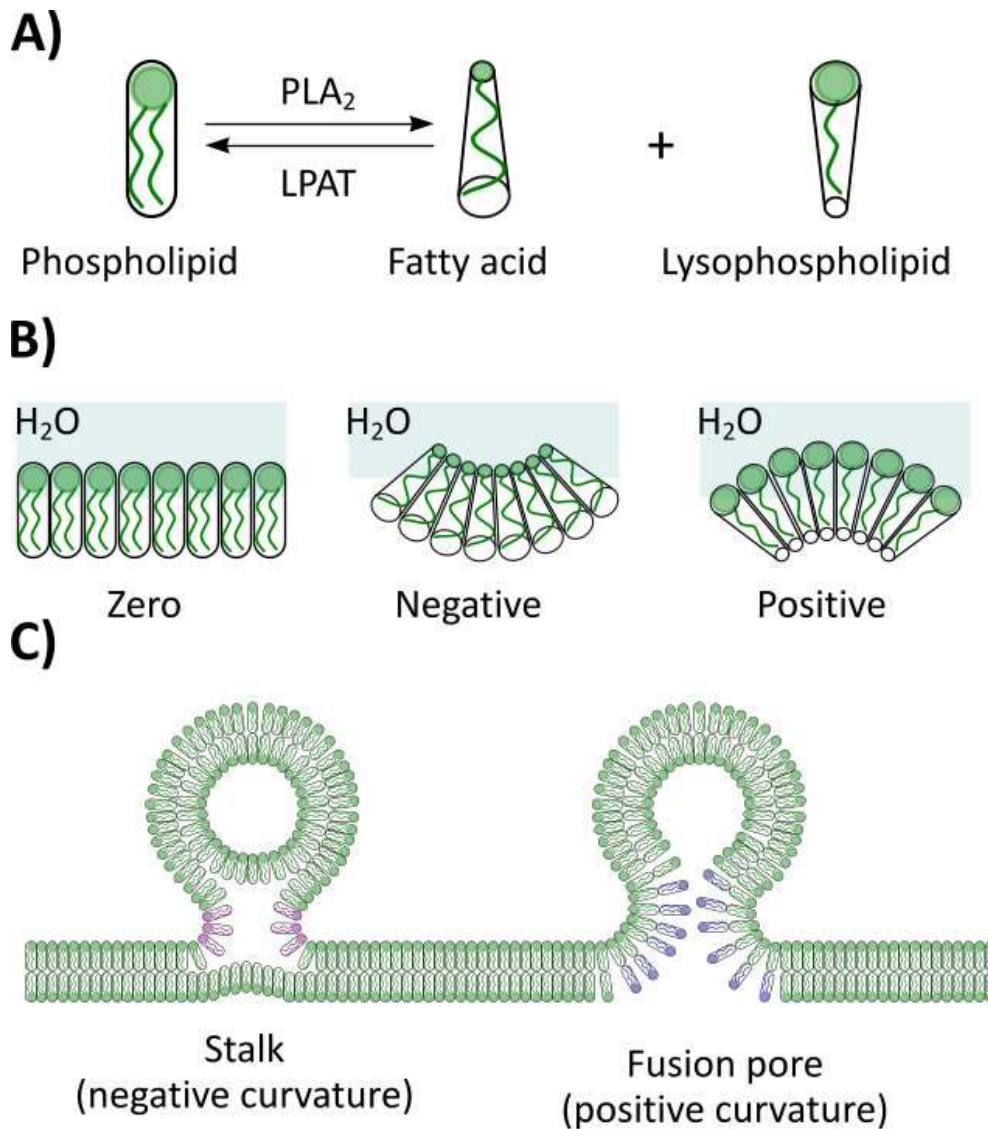
Figure 6.3 Lipids of different shapes and their effect on membrane curvature. A) *Phospholipids of conical shape can be modified by enzymes such as phospholipase A2, which converts the phospholipid into two lipids, one of conical and one of inverse conical shape. The opposite process is facilitated by lysophospholipid acyl transferases, which produces a lipid of a cylindrical shape. B) Lipids of different geometries can produce stable planar monolayers, such as in the case of cylindrical lipids, or monolayers of negative or positive curvature. C) Fusing lipid membranes undergo two steps of pore formation. During the first step, aggregation of lipids of conical shape facilitates the formation of a fusion stalk, which is followed by a pore opening and widening facilitated by the aggregation of lipid of inverted conical shape. Figure adopted from Piomelli et al. (2007).*

In addition to the modulation of membrane curvature, lipids of different shapes and size can promote the formation of membrane compartments of different viscosities, an example of which are the lipid rafts. Lipid rafts are mainly comprised of cholesterol and sphingomyelin, which cluster in the membrane forming discrete regions (Simons and Ikonen, 1997). It is believed that SNARE proteins, both on the cell membrane and the vesicle, associate with the lipid rafts and therefore the composition of the lipid rafts indirectly regulates the exocytotic process of neurotransmitter release (Chamberlain et al., 2001, Chamberlain and Gould, 2002, Gil et al., 2005, Salaün et al., 2004, Wang et al., 2019). Removal of cholesterol, from preparations of plasma membranes and isolated release ready native cortical secretory vesicles, significantly decreased the rate and the kinetics of vesicle fusion (Churchward et al., 2005). Similarly, cholesterol reduction in cultured neurons impairs synaptic vesicle exocytosis (Linetti et al., 2010). The ratio of SM/cholesterol also seems to be an important factor for membrane fusion as an increase of the level of SM in model vesicle systems dramatically reduces the fusion process (Haque et al., 2001).

Another lipid class, which is highly compartmentalized and has an effect on membrane fusion is the phosphoinositides, especially phosphatidyl-inositol 4,5-diphosphate (PI(4,5)P2) (Di Paolo et al., 2004). Several observations have inferred a role for the inositides in regulating exocytosis. PI(4,5)P2 has been shown to accumulate in syntaxin clusters and this accumulation correlates with exocytotic activity (Aoyagi et al., 2005). Co-localization of syntaxin 1 with PI(4,5)P2 in PC12 cells also appears to be essential for Ca^{2+}-dependent exocytosis (Aoyagi et al., 2005). Finally, binding of synaptotagmin, a protein located on the vesicle, with phosphoinositides in a calcium-dependent manner (Schiavo et al., 1996) suggests a bridging role of the lipid between the two lipid bilayers, which facilitates fusion (Wenk and De Camilli, 2004).

The direct effect of lipids, such as PC, Lyso PC, PE, PI, PS and AA on the release kinetics and quantity of molecules released by PC 12 and chromaffin cells have also been demonstrated in several experiments that have explored changes in the lipid composition of the whole cell membrane or only its inner or outer leaflets (Amatore et al., 2006, Aref et al., 2020, Gu et al., 2019, Gu et al., 2020a, Uchiyama et al., 2007).

In particular, repetitive stimulation of exocytosis from PC 12 cells with high potassium saline has shown a relative decrease of ~ 40 % of the abundance of PCs, and relative increase in the abundance of PE and PI of ~ 40 % and ~ 30 %, respectively after 6 stimulation pulses (Gu et al., 2020a). These changes in cell membrane composition are correlated to a significant increase of the number of molecules of neurotransmitter released by the cells and a significant increase in the proportion of molecules released, due to a decrease in the intravesicular contents and a significant increase in the half width of the release events. The latter is possibly due to a longer lasting fusion pore (Gu et al., 2019). Short incubation (3min) of chromaffin cells with LysoPC and AA, only caused changes to the lipid composition of the outer leaflet of the cell membrane. LysoPC and AA have an opposite effect on the content and dynamics of vesicular release. LysoPC increased the quantity of transmitter release and the amplitude of the release events but decreased the rise time and the width of the events. Conversely, AA decreased the quantity of transmitter release and the amplitude of the events, but increased the rise time and the width of the events (Amatore et al., 2006). Longer incubation of PC 12 cells (3 days) with PS, PC, PI, PE and SM have shown that some of these lipids can influence either the kinetics of release or the content of release or both. PC significantly increased the transmitter content released by the cells in addition to decreasing the rise time of the events and increasing the width of the events and their fall time. Incubation with SM significantly increased the rise time of the events, whereas PE decreased the width of the events and their fall time. PI and PS do not appear to significantly affect any of the release parameters (Uchiyama et al., 2007). Lipid changes targeted to the inner cell membrane layer and intracellular vesicles of chromaffin cells, have been achieved by nano-injections of PC, PE and LysoPC. In these experiments, incubation with PE significantly increased the number of molecules released by the cell by increasing all parameters of the events (amplitude, width and rise and fall time), whereas PC and LysoPC significantly decreased the molecules released by the cell by decreasing the amplitude and the width of the events. In addition incubation of PC12 cells with PE increased the intracellular content of the vesicles (at 90% confidence interval), measured using IVIEC, however, this appears to be an indirect effect, probably caused by an effect on the cellular machinery involved in the neurotransmitter packaging and storage, as the increase

was not observed when neurotransmitter content of isolated vesicles was measured (Aref et al., 2020).

Exocytosis of vesicles can also be affected by the signalling role of lipids such as PA, DAG, AA and sphingosine. Due to its conical shape, PA is believed to alter membrane architecture (Kooijman et al., 2003, Kooijman et al., 2005) and therefore promote membrane fusion. PA is also noted to bind the SNARE protein syntaxin 1A, and this interaction is believed to regulate membrane fusion energetics (Lam et al., 2008). DAG on the other hand, indirectly regulates the release process owing to its ability to activate protein kinase C (PKC) which phosphorylates various SNARE proteins (Barclay et al., 2003, de Jong et al., 2016). DAG also binds Munc 13-1, to modulate secretory output by increasing the release competent pool of vesicles (Bauer et al., 2007). Like PA and DAG, AA and sphingosine can also interact with the SNARE proteins and therefore modulate exocytosis (Darios et al., 2009, Garcia-Martinez et al., 2018, Rickman and Davletov, 2005). In bovine adrenal chromaffin cells, both AA and sphingosine increase the speed of opening of the fusion pore, the amplitude of the release events and the number of catecholamine molecules released per event (García-Martínez et al., 2013).

6.1.3 Effect of age on lipids

The concentration and localization of lipids in brain membranes change with increasing age. A summary of some of the lipids that change with age in different areas of the human brain, the rodent brain and cultured neurons is given by Ledesma et al. (2012). In brief, cholesterol and sphingomyelin are increased with age (24 months old) in the total rodent brain compared to younger rats (6 months), whereas PC, PE, PS, PI and PA seem not to be affected significantly by the ageing process (Aureli et al., 2000). In contrast, cholesterol is decreased with age in the human hippocampus (Söderberg et al., 1990), human cortex (Svennerholm et al., 1994), cultured hippocampal neurons (Martin et al., 2008, Sodero et al., 2011) and rodent synaptosomes (Sodero et al., 2011). Age also appears to affect the distribution of cholesterol between the exofacial

and cytofacial leaflets of the synaptic plasma membrane, increasing it twofold in the exofacial leaflet (Igbavboa et al., 1996). Increased sphingomyelin (in the rodent brain, rodent synaptosomes, cultured neurons) and its precursors ceramide (rodent cortex, rat cerebellar granule cells) and sphingosine are also observed with increasing age (Aureli et al., 2011, Cutler et al., 2004, Giusto et al., 1992, Prinetti et al., 2001, Trovò et al., 2011, Valsecchi et al., 1996, Yamamoto et al., 2008). The levels of some fatty acid chains such as the PUFAs, arachidonic acid (AA) and docosahexaenoic acid (DHA) have been shown to decrease with increasing age, along with total PUFA content (Favrelière et al., 2000, López et al., 1995, McGahon and Lynch, 1996, Ulmann et al., 2001). Similarly, a decrease of phosphoinositides is observed in the synaptosomes from rodent brains (Zambrzycka, 2004).

The age-related changes in the level of different membrane lipids presented above can influence the curvature of the plasma and vesicle membranes and therefore their ability to merge and form fusion pores, through which neurotransmitter can be released (Jahn and Südhof, 1999). Additionally, changes of the composition of the membranes can indirectly influence exocytosis by affecting the SNARE complex of proteins facilitating the neurotransmitter release process. A lipid bilayer model presented by Ledesma et al. (2012) describes the changes of mature membranes with age (**Figure 6.4**).

Inverted cone shaped converted into cone upon Ca^{2+} binding: PI(4,5)P2

Cone shaped: ceramide

Small polar head group: cholesterol

Cylinder shaped: sphingomyelin

Inverted cone shaped: gangliosides
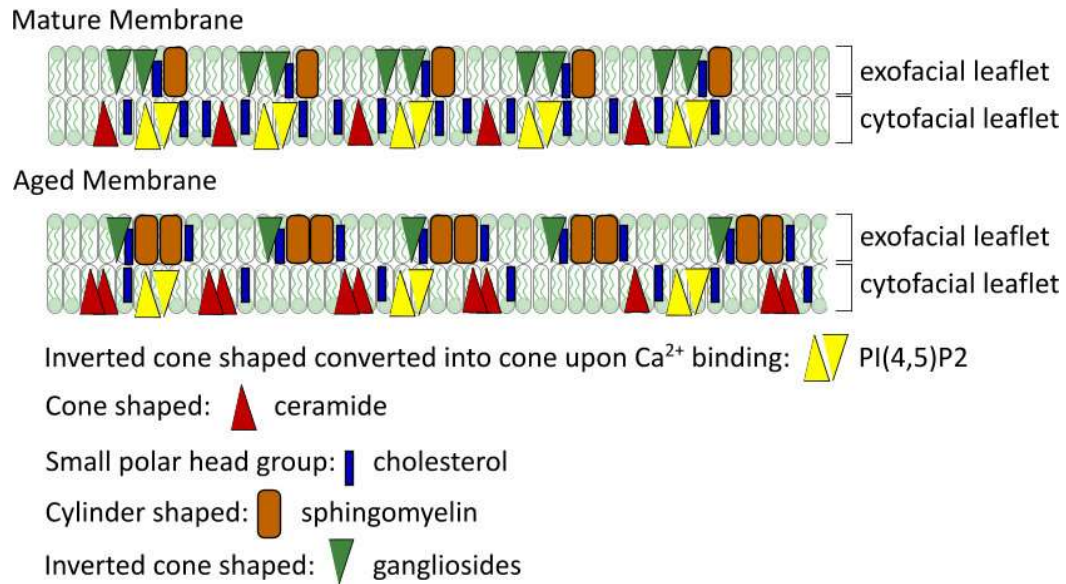
Figure 6.4 Model of the age-related changes of lipid membranes. *With age the level of SM is increased, which is shown as an increase of SM on the exofacial leaflet of the membrane. SM increase is accompanied by a decrease of gangliosides. In addition, the level of ceramide is increased, and this is shown as an increase of the lipid on the cytofacial leaflet. PI(4,5)P2 localized on the cytofacial leaflet is decreased, which is similar for cholesterol, which is spread between the two leaflets, rather than being concentrated at the cytofacial leaflet such as in mature membranes. Figure adopted form Ledesma et al. (2012).*

An age-related decrease of cholesterol and PI(4,5)P2 from the cytofacial leaflet could influence the negative curvature of the membrane, which is required during the initial steps of fusion pore formation. In addition, changes in the ratio of SM/cholesterol could influence membrane fluidity and the colocalization of SNARE proteins. This can also be influenced by the accumulation of ceramides on the cytofacial leaflet (Ledesma et al., 2012).

Changes with age in the levels of fatty acids such as arachidonic acid (AA) and docosahexaenoic acid (DHA) (Favrelière et al., 2000, López et al., 1995, McGahon and Lynch, 1996, Ulmann et al., 2001) can have an effect on the SNARE release machinery and therefore indirectly modulate exocytosis (Darios et al., 2009, Garcia-Martinez et al., 2018, Rickman and Davletov, 2005). Additionally, they could also

directly affect the kinetics of release events, decreasing the rise time and increasing the fall time, and increase the neurotransmitter molecules released per event (García-Martínez et al., 2013). Similarly, an age-related decrease of phosphoinositides as observed in the synaptosomes from rodent brains (Zambrzycka, 2004) can interfere with the phosphoinositides facilitation of the fusion process (Wenk and De Camilli, 2004).

As indicated in Chapter 4, the ageing process slows the kinetics of neurotransmitter release from the soma of the CGC. Ageing has also been shown to increase the activity of phospholipase A2. This would increase the production of free fatty acids such as AA and lysophospholipids (Farooqui and Horrocks, 2006, Watson et al., 2013), both of which would affect membrane curvature and therefore exocytosis (Dowhan et al., 2008, Piomelli et al., 2007). In addition, AA can act as a signalling molecule further influencing the release process (Rickman and Davletov, 2005). Therefore, considering the importance of the lipid composition of the plasma membrane for the normal process of neurotransmitter release and the indirect regulation of the exocytotic process by lipids, it is important to understand how the lipid composition of the *Lymnaea* CNS changes with age and if any observed changes could account for the age-related changes in neurotransmitter release from the CGC. This chapter will therefore test the hypothesis that age-related changes in CNS membrane lipid composition can explain the changes in vesicular release kinetics observed with increasing age.

6.2 Methods

6.2.1 Lipid extraction

CNSs from young (3-4 months) and old (10-12 months) *Lymnaea* were dissected and pooled into samples containing 5 CNSs each. Lipids were extracted from samples using the Bligh and Dyer protocol (Bligh and Dyer, 1959). Dissected CNSs were homogenised on ice in 800 µl of 0.9% NaCl. A 10 µl mixture of internal standards (SPLASH LipidoMIX Internal Standard – 3307707, Avanti Polar Lipids, Alabaster, Alabama, 35007-9105, USA) was added to the samples before the extraction of the lipids. Briefly, the extraction process is as follows: 1 ml of chloroform ($CHCl_3$) is added to the CNS homogenate and the mixture is vortexed for 1 min. Following this 2ml of MeOH is added to the homogenate and the mixture is vortexed for another minute. Then a further 1 ml of $CHCl_3$ is added again and the mixture is vortexed, and this is followed by the addition of 1 ml of H_2O and another minute of vortexing. The sample is then centrifuged for 10 min at 1500 RPM, leading to the separation of the sample in three phases. The lower organic phase of the sample is collected and then dried under N_2 stream and stored at -20°C until it is used for mass spectrometry (**Figure 6.5**).
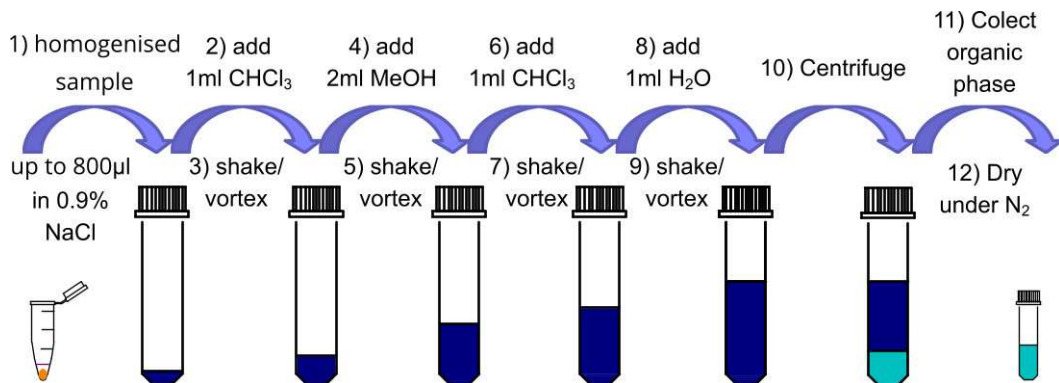
Figure 6.5 Schematic of the Bligh and Dyer protocol for lipids extraction.

6.2.1 High performance liquid chromatography-mass spectrometry (HPLC-MS)

HPLC-MS of the lipid 'samples is performed on a hybrid quadrupole Orbitrap mass spectrometer (Q Exactive, ThermoScientific UPLC HSS T3 Column (100Å, 1.8 μm, 2.1 mm X 100 mm, Waters Corporation) with a solvent gradient consisting of solvent A ;(60:40 v/v); water (Hypergrade for LC-MS, LiChrosolv®, MerckKGaA): acetonitrile (MSsuprasolve®, Sigma Aldrich) and 10% (m/v) ammonium formate (99.995%, Sigma Aldrich) and solvent B; (90:10) isopropanol (Optima™LC/MS Grade, Fisher Scientific): acetonitrile (MSsuprasolve®, Sigma Aldrich) and 10% (m/v) ammonium formate (99.995%, Sigma Alrich) at a flow rate of 200 μL/min. For the first 30s the flow is diverted to waste and the gradient is started with 0% B (0-1 min), then increased to 100% B over 53 min, held at 100% B for 3 min and then lowered back to 0% B in 1 min and equilibrated for 9 min. The column is kept in the column oven at 40°C and the samples are stored at 4°C in the autosampler. 5 μl of each sample is injected with the use of μL pick-up injection twice and analysed by mass spectrometry in the positive and negative mode, respectively with the use of heated electrospray ionization (HESI). Spray voltage is set to 3500 V for positive mode and -3500 V for negative mode, sheath gas set to 45 au, auxiliary gas set to 8 au, sweep gas set to 1 au and probe temperature set to 350°C. The temperature of the capillary is 320°C and S-Lens is set to 50. The acquisition of the MS data is carried in a data dependent manner with full scan profile MS spectra (250-1, 200 m/z) recorded at a resolution of 140,000@200 m/z followed by the fragmentation of the top 10 most abundant precursor ions. Dynamic exclusion is set to 10 s and charge exclusion set for unassigned and slightly charged species. Automatic gain control (AGC) target is set to 1×10^6 with a maximum injection time of 50 ms for full scan. Fragmentation of precursor ions is performed by higher-energy collisional dissociation (HCD) with a normalized stepped collision energy of 25 and 30, with a default charge state of 1. MS/MS scans are recorded in profile mode and performed at a resolution of 17,500@200 m/z with an AGC target value of 1×10^5 and a maximum injection time of 100 ms using an isolation window of 1.0 m/z.

6.2.2 Data processing, lipids identification and data analysis

Spectral data are initially processed using the MZmine (Pluskal et al., 2010) software which enables the relative quantitative comparison of the detected species by filtering the spectral data, detecting the peaks corresponding to the fragmented compounds, aligning corresponding pecks across the samples and normalizing for the systematic error by adjusting the intensities within each run of the samples (Bahja et al., 2022).

The identification of different lipid species is achieved with the use of the LipiDex software suite (NCQBCS, Coon Lab 4462, Madison WI, USA) (Hutchins et al., 2018). The software uses the mzXML format of the raw data files, the conversion of which is made using the Proteowizard software package (Proteowizard, Palo Alto, CA 94304, USA) and the peak tables generated by the MZmine to identify the peaks detected in the mass spectrum.

Relative quantitative comparisons of the identified lipids were performed based on the known concentrations of the lipid's standards added to the samples and the pack areas of the lipid standard and the identified lipid. The calculated lipids concentrations were then normalized to the weight of the samples.

Differences between groups were assessed using unpaired Student's t-test when two groups were compared or two-way ANOVA with Sidak post-hoc test for multiple comparisons. Bonferroni multiple-comparison correction was applied to account for the 17 t-tests performed to determine the effect of age on the total lipid class between the young and old groups and the corrected level of significance was determined to be $p = 0.0029$. Data is represented as means ± SEM, p-values are shown above the graphs.

6.3 Results

To investigate the lipid composition of the CNS of *Lymnaea*, total CNS lipids from young and old snails were extracted and identified using mass spectrometry. Analysis of the major lipid classes showed most were present in the CNS of *Lymnaea*. These included SM, PI, CE, PS, PC, PC(OH), PA, PE, PE(OH), PG, TG, Alkanyl-TG, LysoPC, LysoPE, LysoPI, LysoPS, Plasmanyl-PC, Plasmenyl-PC, Plasmanyl-PE and Plasmenyl-PE. The work presented below shows quantitative age-related differences in a subset of these lipids which were run with their corresponding lipid standard.

The most abundant lipids in the young CNS are PC (32.5 %), Plasmanyl-PC (27.99 %), Plasmenyl-PE (10.16 %) and PE (7.17 %) (**Figure 6.6, A**), whereas the most abundant lipids in the old CNS are CE (43.20 %), PC (22.03 %), Plasmanyl-PC (16.99 %) and Plasmenyl-PE (5.54 %) (**Figure 6.6, B**).

A)

0.95% Plasmenyl-PC	
0.06% Alkanyl-TG	
6.43% CE	
0.32% PS	
10.16% Plasmenyl-PE	
0.01% SM	
1.05% TG	
0.36% LysoPC	
1.23% LysoPE	
32.50% PC	
1.59% PC(OH)	
7.17% PE	
0.03% PE(OH)	
0.16% PG	
27.99% Plasmanyl-PC	5.86% PI
4.14% Plasmanyl-PE	

B)

0.71% Plasmenyl-PC	
0.04% Alkanyl-TG	
43.20% CE	
0.26% PS	
5.54% Plasmenyl-PE	
0.01% SM	
0.71% TG	
0.21% LysoPC	
0.45% LysoPE	
22.03% PC	
0.42% PC(OH)	
5.46% PE	
0.01% PE(OH)	
0.15% PG	
16.99% Plasmanyl-PC	1.78% PI
2.04% Plasmanyl-PE	
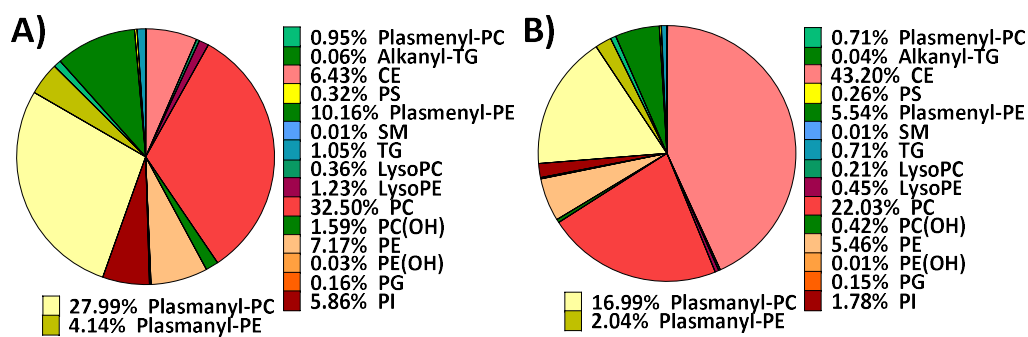
Figure 6.6 Percentage lipids in the whole CNS. *A) Young and B) Old.*

6.3.1 Sphingomyelin (SM)

Age significantly increased the total concentration of sphingomyelin (**Figure 6.7**, **A**) and this appeared to be due to changes in the predominant lipid species: SM d39:1 (71.81% of total SM lipids in young and 72.84 % in old, **Figure 6.7 B**), SM d40:1 (3.99 % in young and 6.27 % in old, **Figure 6.7, B**) and SM d41:1 (19.29 % in young and 16.74 %

in old, **Figure 6.7**, **B**), whose concentration is significantly increased in the CNS of old snails (**Figure 6.7 C**, p < 0.0001 Species, p = 0.0001 Age, p < 0.0001 Interaction).
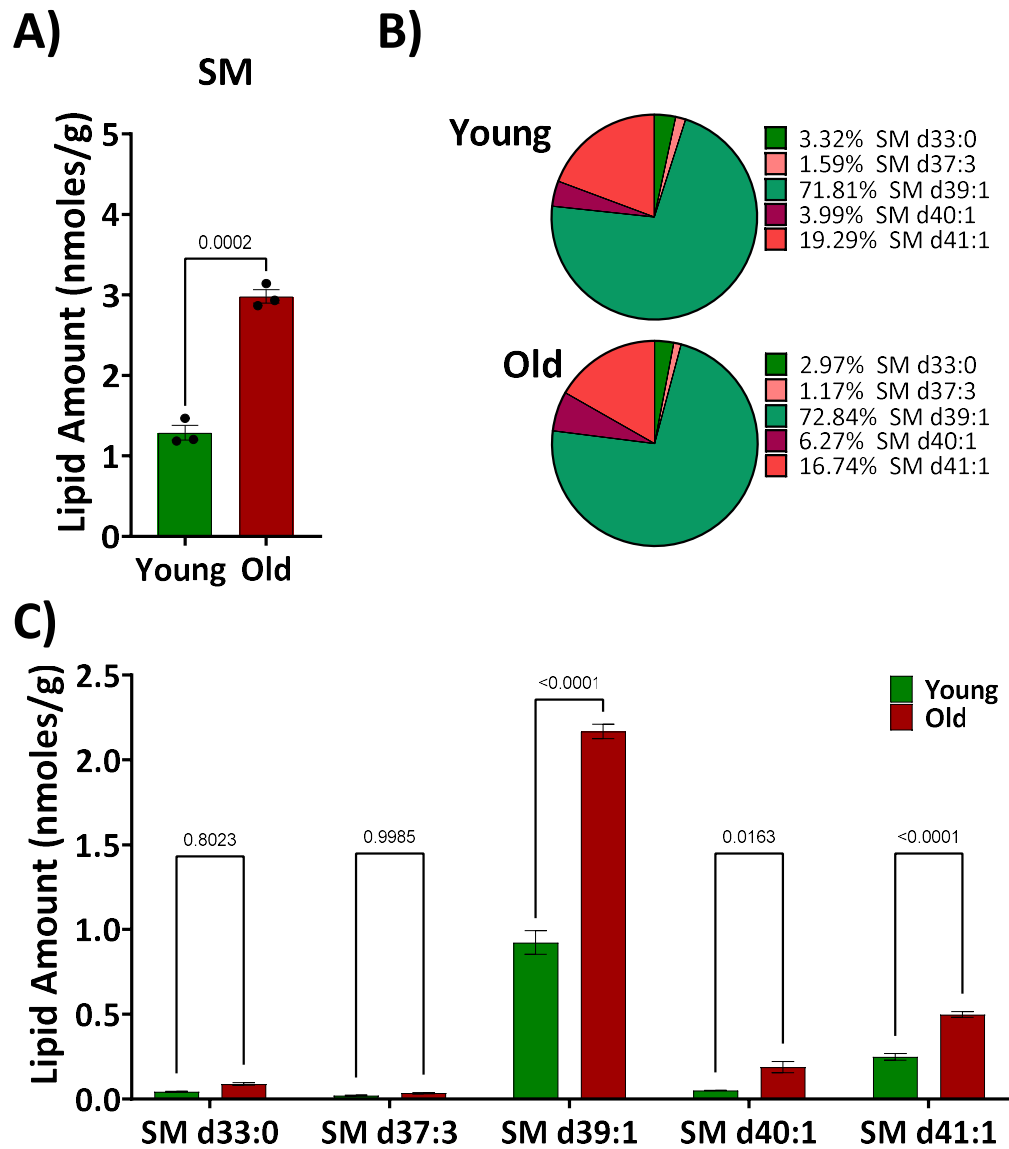
Figure 6.7 The concentration of sphingomyelin is significantly increased by age. *A) Total concentration of sphingomyelin in the CNS of young and old Lymnaea (unpaired t-test). B) Percentage of the total sphingomyelin of the identified SM species. C) Changes of the concentration of different SM species. N = 3 for young and n = 3 for old (Two-way ANOVA with Sidak multiple comparisons test).*

6.3.2 Phosphatidylinositol (PI)

In contrast to SM, PI was not significantly chanted with increasing age (**Figure 6.8 A**). The percentage of the most abundant PI lipid PI 38:4 was decreased from 65.61 % in the young to 51.42 % in the old (**Figure 6.8**, **B**). The molar concentration of this lipid was also significantly decreased with age (**Figure 6.8 C**, $p < 0.0001$ Species, $p = 0.0001$ Age, $p < 0.0001$ Interaction). Although LysoPI could not be quantified due to the lack of a standard in the mix that was used, expression increased with age consistent with the reduction in PI.
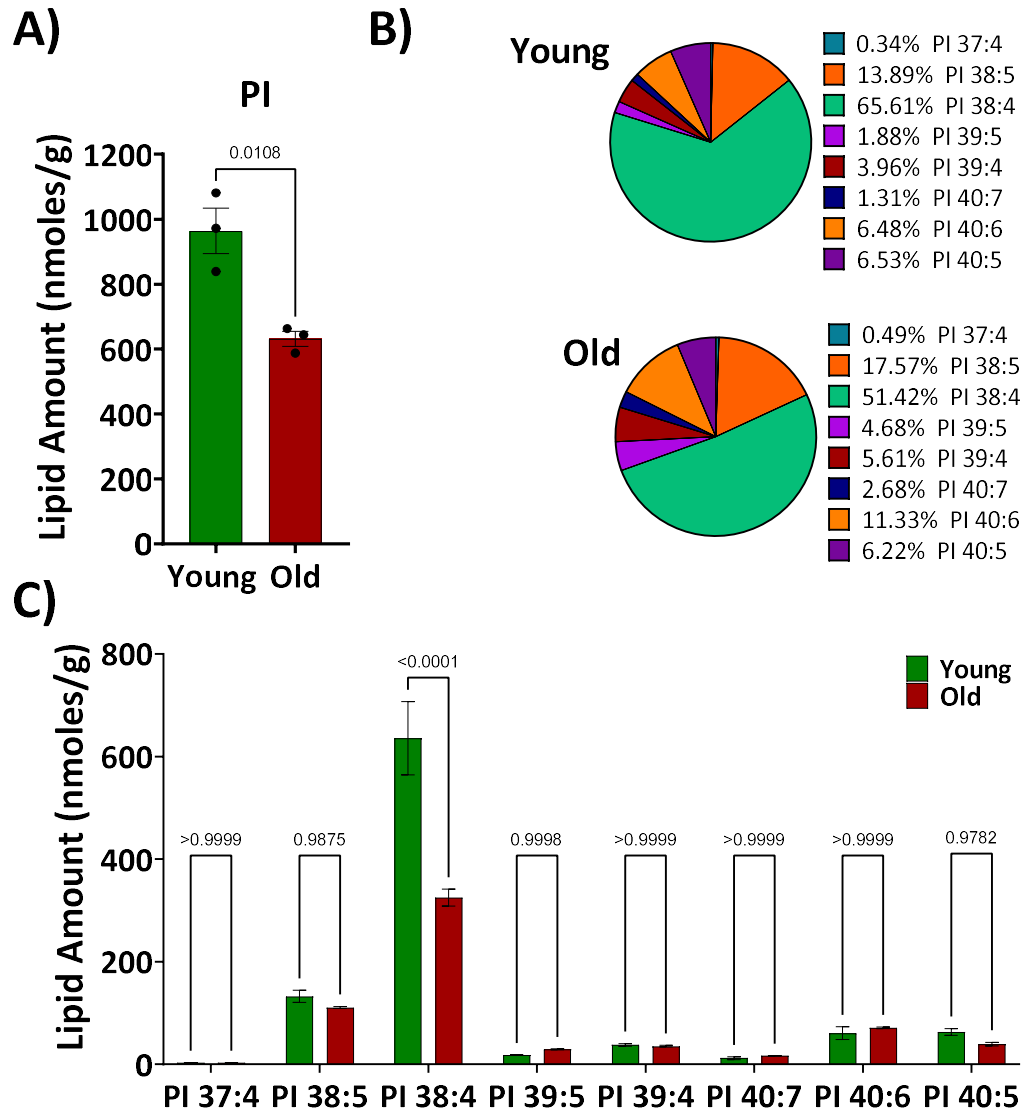
Figure 6.8 The total concentration of phosphatidylinositol is not changed significantly by age, however the most abundant PI lipid species (PI 38:4) was decreased by age. A) Total concentration of all phosphatidylinositol species in the CNS of young and old Lymnaea (unpaired t-test). B) Percentage PI species from total PI in the CNS of young and old Lymnaea. C) Changes of the concentration of different PI species. N = 3 for young and n = 3 for old (Two-way ANOVA with Sidak multiple comparisons test).

6.3.3 Cholesteryl ester (CE)

Another lipid class which is significantly affected with age is the CE. The concentration of total cholesteryl esters is significantly increased in the CNS of old *Lymnaea* (**Figure 6.9**, **A**). The most abundant lipid species of this class is CE 22:4, which is 59.47 % of the total CE lipids in the young and 58.76 % of the total CE lipids in the old (**Figure 6.9 B**). The CE species, which are significantly increased with age are: CE 20:1, CE 20:2, CE 20:3, CE 20:4, CE 20:5, CE 22:2, CE 22:4, CE 22:5 and CE 24:4 (**Figure 6.9 C,** $p < 0.0001$ Species, $p < 0.0001$ Age, $p < 0.0001$ Interaction).
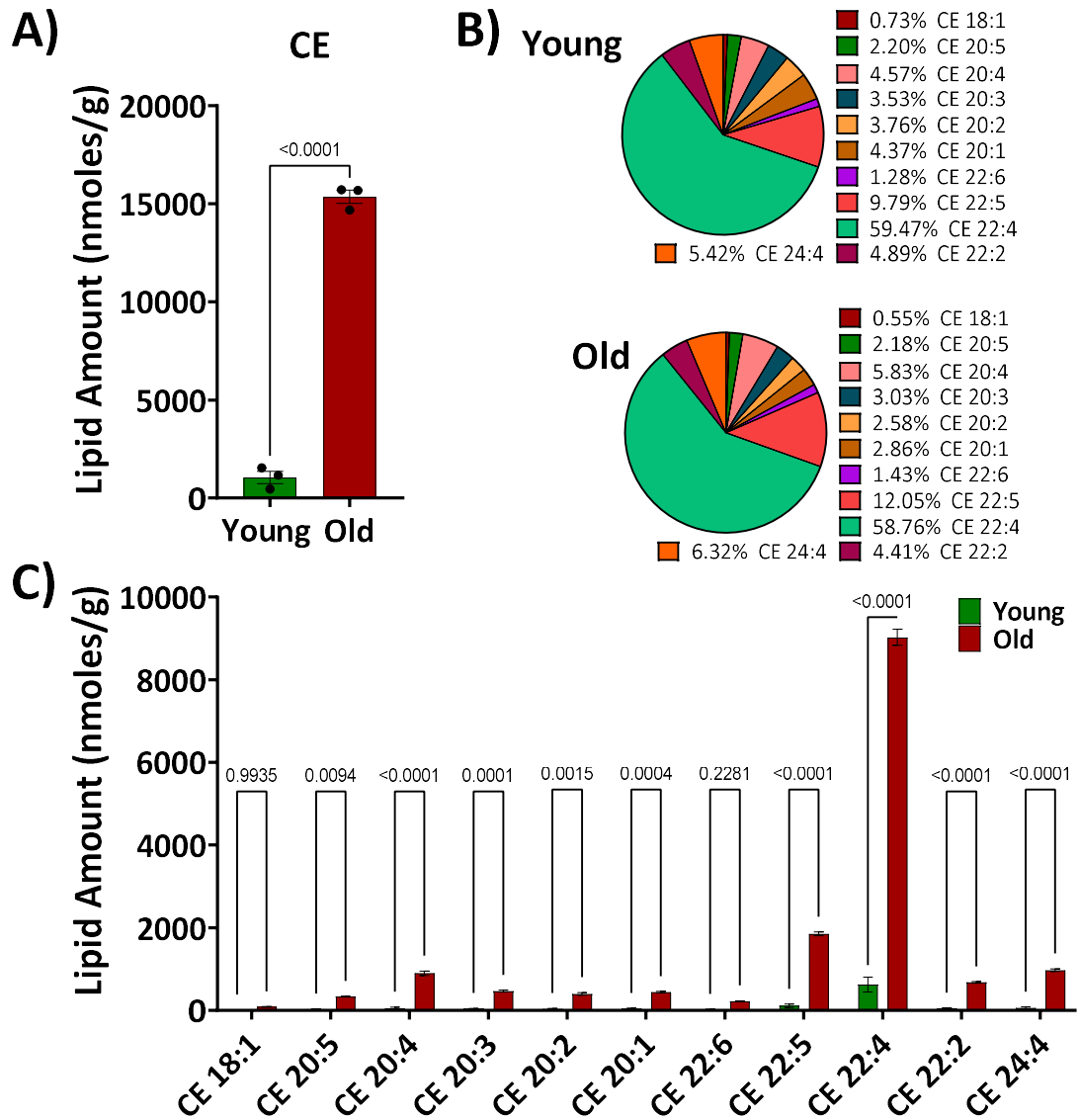
Figure 6.9 The total concentration of Cholesteryl ester is significantly increased by age. *A) Total concentration of all cholesteryl ester species in the CNS of young and old Lymnaea (unpaired t-test). B) Percentage CE species from total CE in the CNS of young and old Lymnaea. C) Changes of the concentration of different CE species. N = 3 for young and n = 3 for old (Two-way ANOVA with Sidak multiple comparisons test).*

6.3.4 Phosphatidylcholine (PC), Plasmanyl-PC, Plasmenyl-PC and PC(OH)

The total concentration of the three classes of lipids with choline as a head group: Phosphatidylcholine, plasmanyl PC and plasmenyl PC are not significantly changed by age (**Figure 6.10 A, B and C**), and no significant change is observed in the PC(OH) (**Figure 6.10**, **D**). 130 species of PC were identified and quantified, and the 10 most abundant species are shown in **Table 8-1** in the **8.2.1 Phosphatidylcholine** section of the Appendix. 12 of the 130 species are significantly increased by age (Appendix, **8.2.1 Phosphatidylcholine**, **Table 8-2**). 47 species of Plasmanyl PC were identified and the 10 most abundant species are shown in **Table 8-3** in the **8.2.2 Plasmanyl PC** section of the Appendix. 7 of the 47 species are significantly increased by age (Appendix, **8.2.2 Plasmanyl PC**, **Table 8-4**). 16 species of plasmenyl PC were identified and the percentage of each species are shown in **Table 8-5** in the **8.2.3 Plasmenyl PC** section of the Appendix. 3 of the 16 species are significantly increased by age (Appendix, **8.2.3 Plasmenyl PC**, **Table 8-6**). 45 species of PC(OH) were also identified and the percentage of the 10 most abundant species are shown in **Table 8-7** in the **8.2.4 PC(OH)** section of the Appendix. 4 of the 45 species are significantly decreased by age (Appendix, **8.2.4 PC(OH)**, **Table 8-8**).

A) PC

B) Plasmanyl-PC

C) Plasmenyl-PC
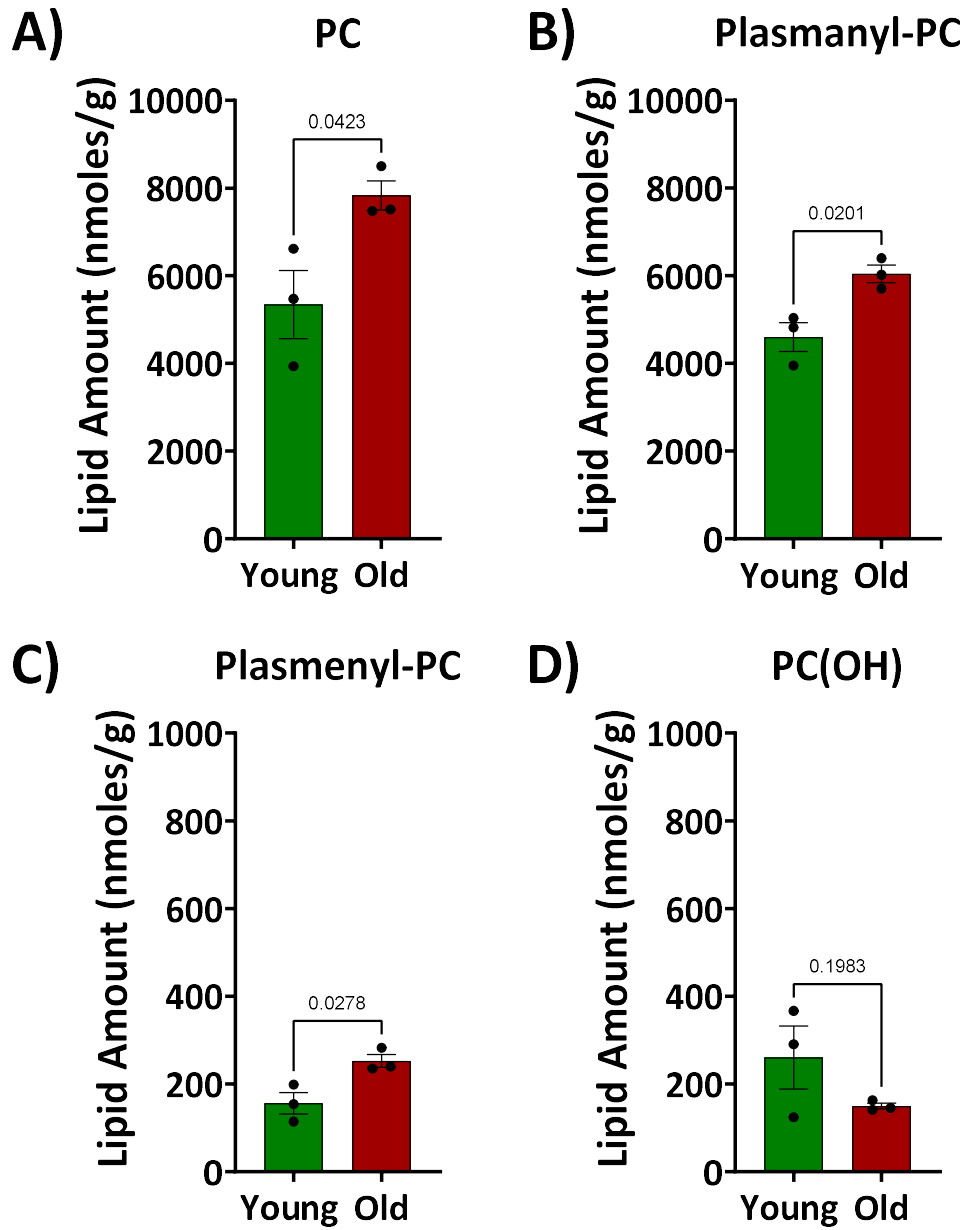
D) PC(OH)

Figure 6.10 The total composition of Phosphatidylcholine, Plasmanyl Phosphatidylcholine, Plasmenyl Phosphatidylcholine and PC(OH) are not siginficantly changed by age. A) Total concentration of PC in the CNS of young and old Lymnaea. B) Total concentration of Plasmanyl PC in the CNS of young and old Lymnaea. C) Total concentration of Plasmenyl PC in the CNS of young and old Lymnaea. D) Total concentration of PC(OH) in the CNS of young and old Lymnaea. N = 3 for young and n = 3 for old, unpaired t-tests.

6.3.5 Lyso-phosphatidylcholine

The total concentration of lyso-phosphatidylcholine also does not change significantly with increasing age (**Figure 6.11**, **A**). The two most abundant phospholipids of this class are lyso-PC 16:0, 36.72 % in the young and 33.28 % in the old, and lyso-PC 18:1, which is 20.24 % of the total lipid class in the young and 17.99 % in the old (**Figure 6.11**, **B**). Two of the Lyso-PC species are significantly increased by age: Lyso-PC 16:0 and Lyso-PC 20:2 (**Figure 6.11 C**, $p < 0.0001$ Species, $p < 0.0001$ Age, $p < 0.0001$ Interaction).
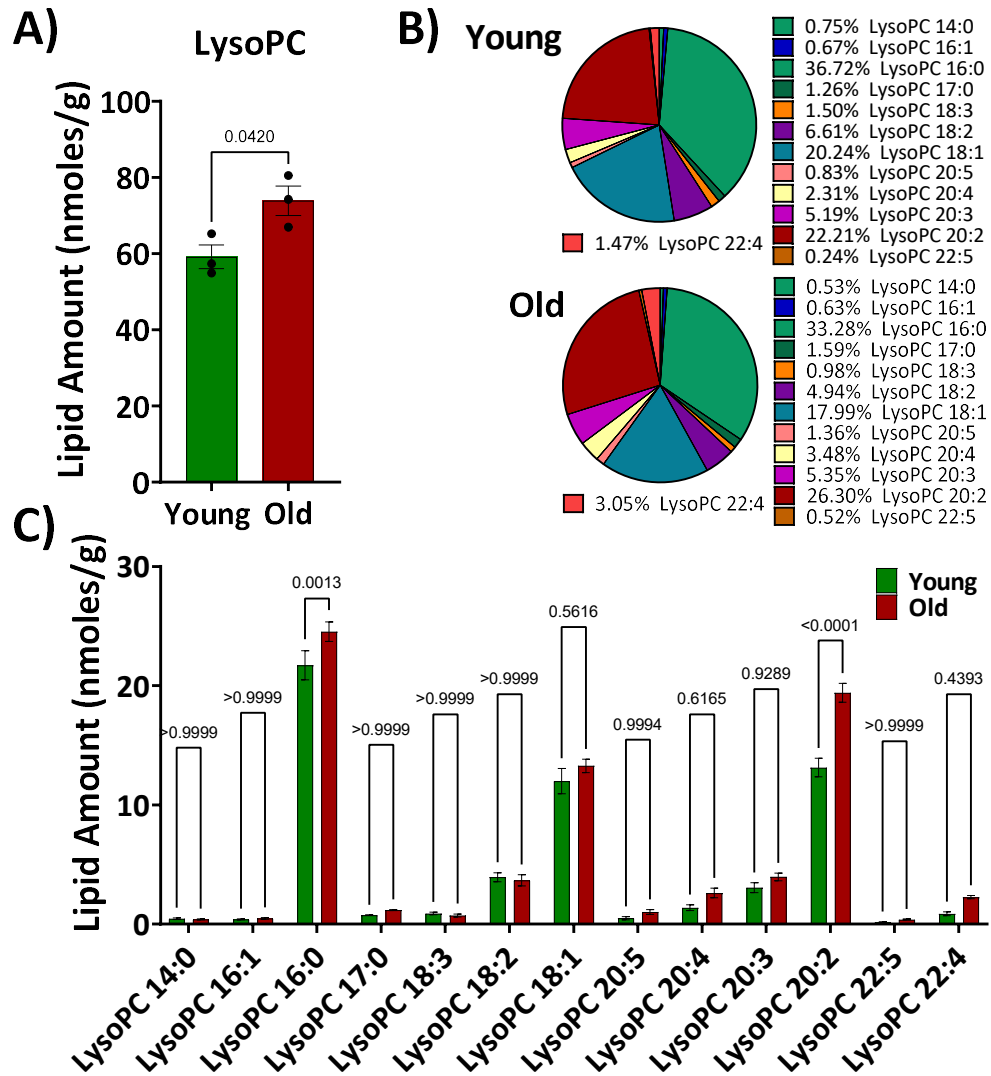
Figure 6.11 The concentration of total Lyso PC does not change with age, however two lyso PC species are significantly increased by age. *A) Total lyso PC concentration in young and old CNS (unpaired t-test). B) Percentage Lyso-PC species from total Lyso-PC in the CNS of young and old Lymnaea. C) Changes of the concentration of different Lyso-PC species. N = 3 for young and n = 3 for old (Two-way ANOVA with Sidak multiple comparisons test).*

6.3.6 Phosphatidylethanolamine (PE), Plasmanyl-PE, Plasmenyl-PE and PE(OH)

No significant age-related changes were observed in the total concentration of the three classes of lipids with ethanolamine as a head group: Phosphatidylethanolamine, Plasmanyl PE, Plasmenyl PE or PE(OH) (**Figure 6.12 A, B, C and D**). 56 species of PE were identified and quantified, and the 10 most abundant species are shown in **Table 8-9** of **8.2.5 PE** section (see Appendix). 3 of the 56 species are significantly increased by age (Appendix, **8.2.5 PE, Table 8-10**) 20 species of Plasmanyl PE were identified and the 10 most abundant species are shown in **Table 8-11** of **8.2.6 Plasmanyl PE** section of the Appendix. 2 of the 20 species are significantly changed by age, one of them Plasmanyl-PE O-16:0_22:4 is significantly increased and the other Plasmanyl-PE O-38:4 significantly decreased (Appendix, **8.2.6 Plasmanyl PE, Table 8-12**). 30 species of Plasmenyl PE were identified and the percentages of the 10 most abundant species are shown in **Table 8-13**, **8.2.7 Plasmenyl PE** section of the Appendix. 2 of the 30 species, Plasmenyl-PE P-16:0_22:4 and Plasmenyl-PE P-38:1, are significantly increased by age (Appendix, **8.2.7 Plasmenyl PE, Table 8-14**) 2 species of PE(OH) were identified. PE[OH] OH-31:4, which is 20.28 % of the total content in the young and 3.77 % of the total content in the old and PE[OH] OH-40:7, which is 79.72 % of the total content in the young and 96.23 % of the total content in the old. None of the two lipids species is significantly influenced by the normal aging ($p = 0.0008$ Species, $p = 0.3247$ Age, $p = 0.6207$ Interaction).
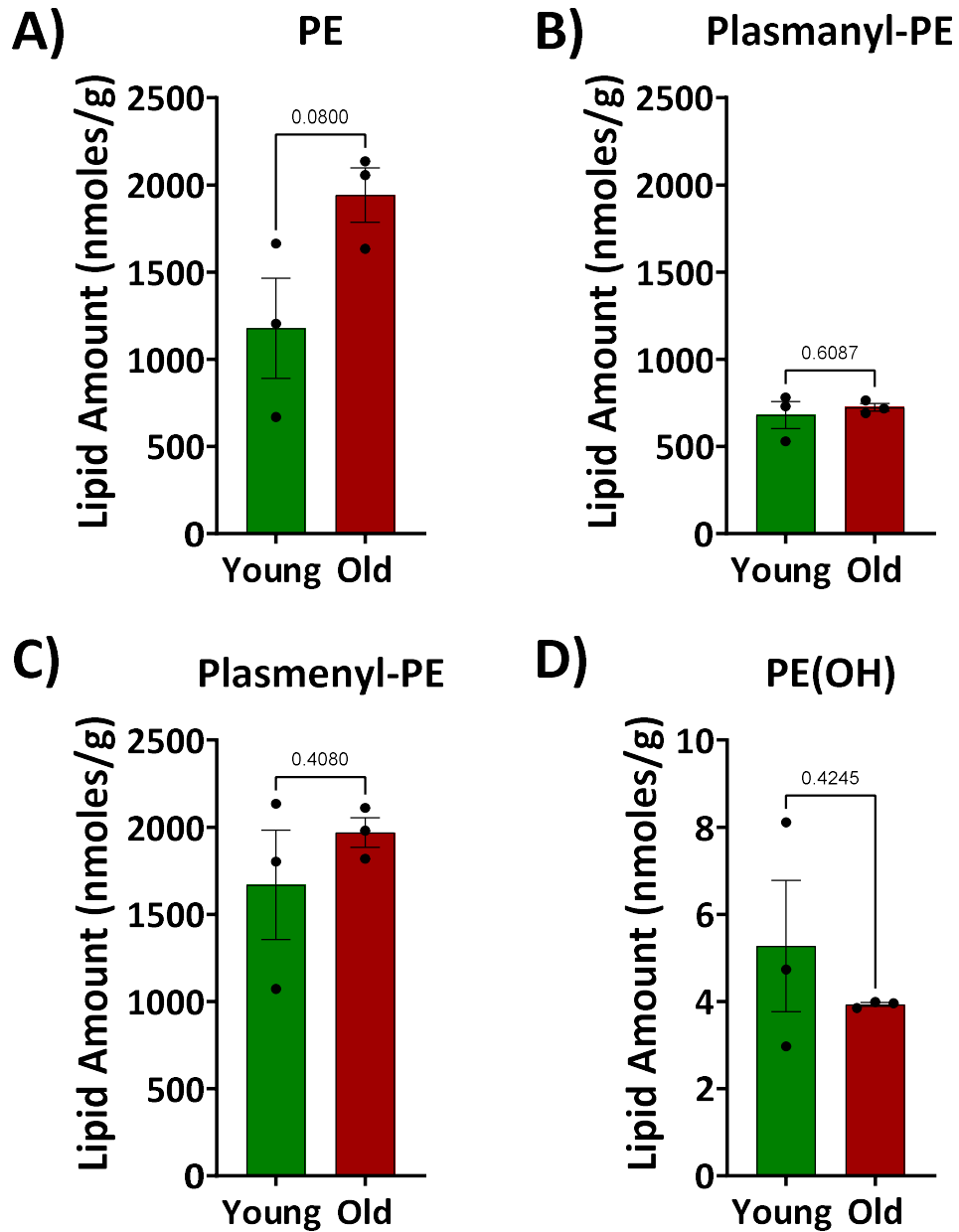
Figure 6.12 There are no significant changes in the total concentrations of PE, Plasmanyl PE, Plasmenyl PE and PE(OH) in the CNS of young and old Lymnaea. *A) Total concentration of PE, B) Plasmanyl PE and C) Plasmenyl PE and D) PE(OH) in the CNS of young and old Lymnaea. N = 3 for young and n = 3 for old, unpaired t-tests.*

6.3.7 Lyso-phosphatidylethanolamine (Lyso-PE)

In contrast to the Phosphatidylethanolamine, Plasmanyl PE and Plasmenyl, which showed a non-significant increase in their total concentration with increasing age, the total concentration of lyso-PE in the CNS of *Lymnaea* decreased with age, however this is not significant (**Figure 6.13 A**). The three most abundant lyso-PEs are Lyso-PE 18:0, which is 21.61 % of total lipid class in the young CNS and 30.26 % in the old, lyso-PE 22:4, which is 24.76 % of the total lipid class in the young CNS and 11.98% in the old and lyso-PE 20:2, which is 15.95 % of the total lipid class in the young CNS and 24.48 % in the old (**Figure 6.13 B**). Although the total concentration of lyso-PE is not significantly changed with age, one of its species significantly decreased with increasing age: Lyso-PE 22:4 (**Figure 6.13 C**, $p < 0.0001$ Species, $p = 0.0260$ Age, $p = 0.0003$ Interaction).
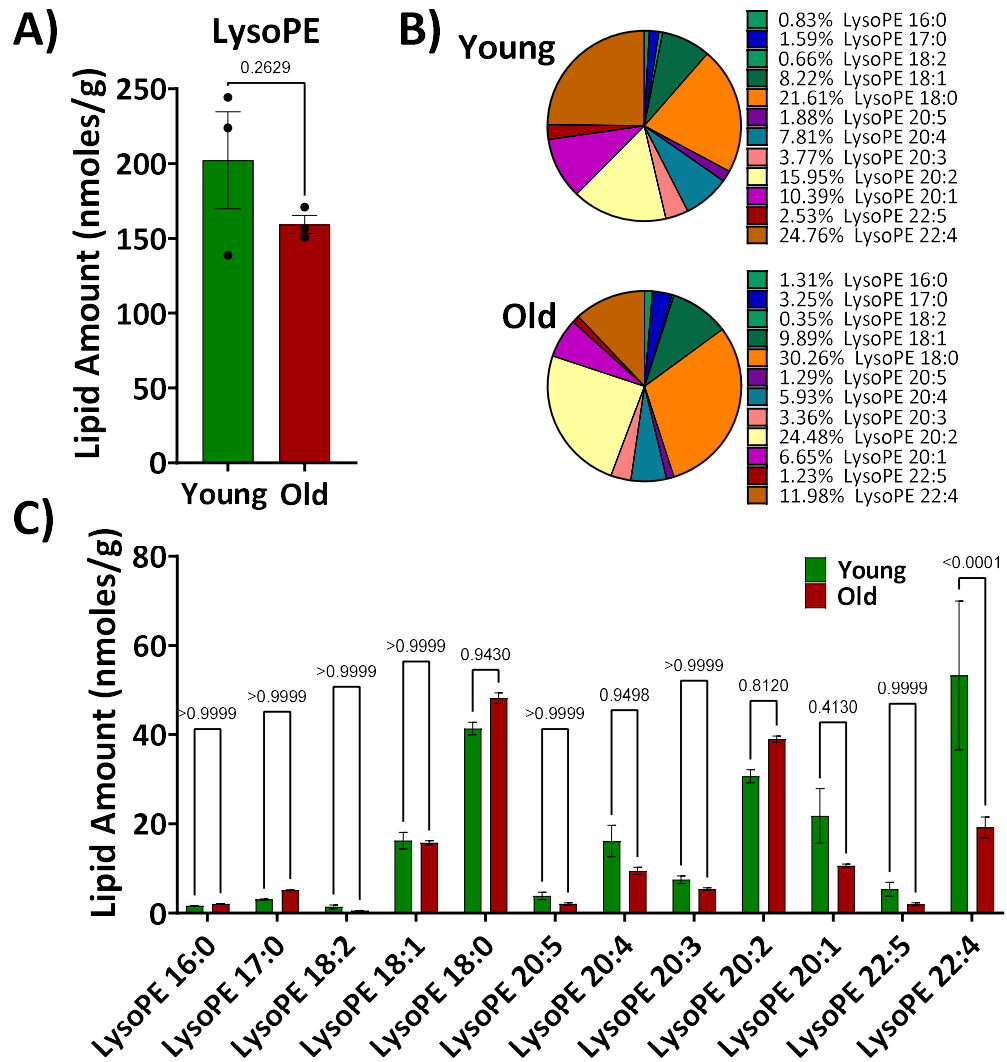
Figure 6.13 The concentration of one lyso PE species is significantly decreased with age. *A) Total lyso-PE concentration in young and old CNS (unpaired t-test). B) Percentage Lyso-PE species from total Lyso-PE in the CNS of young and old Lymnaea. C) Changes of the concentration of different Lyso-PE species. N = 3 for young and n = 3 for old (Two-way ANOVA with Sidak multiple comparisons test).*

6.3.8 Phosphatidylserine (PS)

The total concentration of PS does not change with age in the CNS of *Lymnaea* (**Figure 6.14 A**). Five species of the lipid were identified and the two most abundant of them are PS 20:4_20:1, which is 59.46 % of the total lipid class in the CNS of the young *Lymnaea* and 58.45% of the total lipid in the old, and PS 20:4_20:2, which is 17.60 % of the total lipid class in the young and 18.93 % of the total lipid class in the old (**Figure 6.14 B**). Again, although the increase of the concentration of the total lipid class is not significant with age, one of the PS species, PS 20:4_20:1, is significantly increased by age (**Figure 6.14 C**, $p < 0.0001$ Species, $p = 0.0004$ Age, $p = 0.0086$ Interaction).
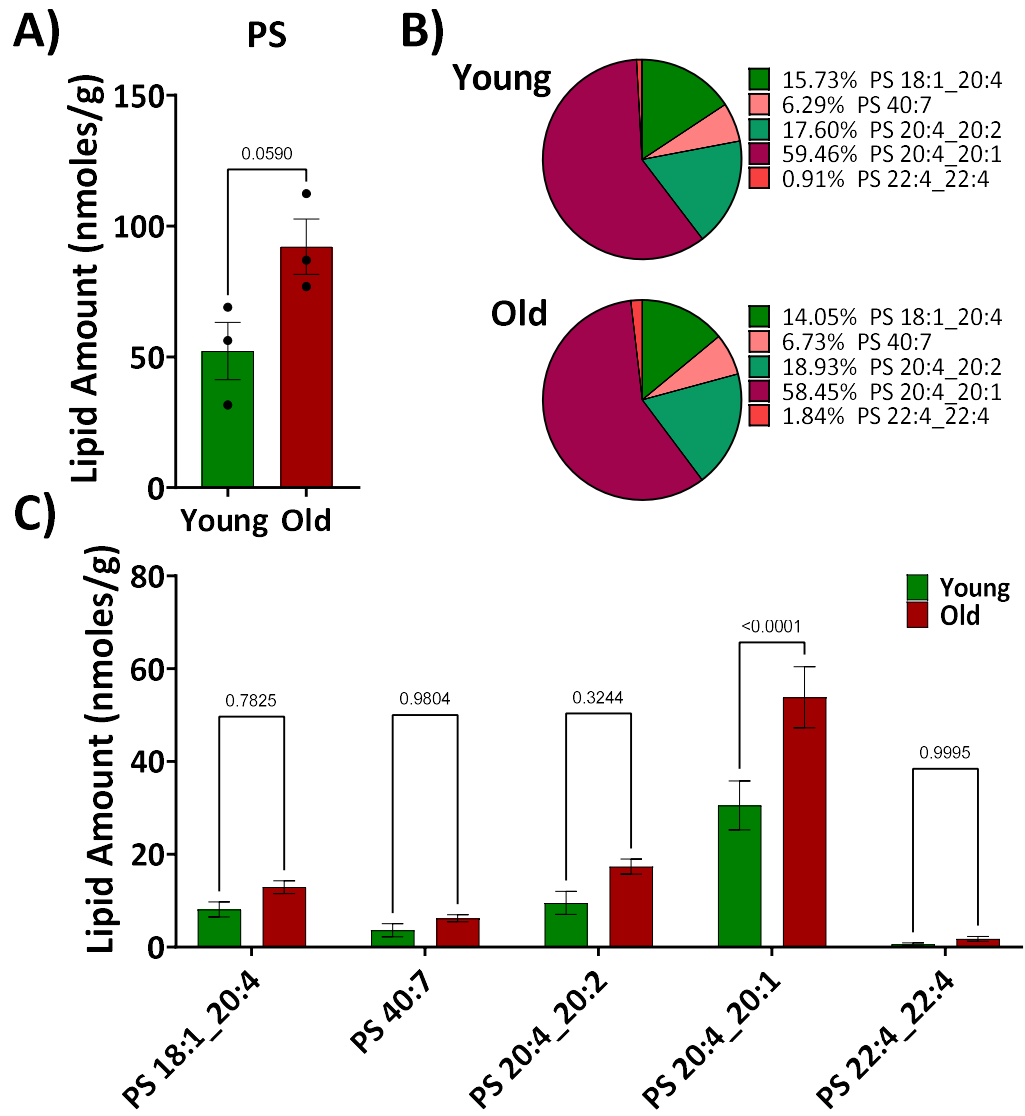
Figure 6.14 The concentration of three PS species is significantly increased with age.

A) Total PS concentration in young and old CNS (unpaired t-test). B) Percentage PS species from total PS in the CNS of young and old Lymnaea. C) Changes of the concentration of different PS species. N = 3 for young and n = 3 for old (Two-way ANOVA with Sidak multiple comparisons test).

6.3.9 Triglyceride (TG), Alkanyl-TG and Phosphatidylglycerol (PG)

TG, Alkanyl-TG and PG also do not change significantly with age (**Figure 6.15 A, B and C**). 107 species of TG were identified and quantified, and the 10 most abundant species are shown in **Table 8-15** in the **8.2.8 TG** section of the Appendix. Only 10 of the 107 species are significantly increased by age (Appendix, **8.2.8 TG**, **Table 8-16**). 21 species of Alkanyl-TG were identified and quantified, the 10 most abundant species are shown in **Table 8-17** the **8.2.9 Alkanyl-TG** section in the Appendix. 4 of the 21 species are significantly increased by age (Appendix, **8.2.9 Alkanyl-TG**, **Table 8-18**). 32 species of PG were identified and quantified, and the 10 most abundant species are shown in **Table 8-19** of the **8.2.10 PG** section of the Appendix. 7 of the 32 species are significantly increased by age (Appendix, **8.2.10 PG**, **Table 8-20**).
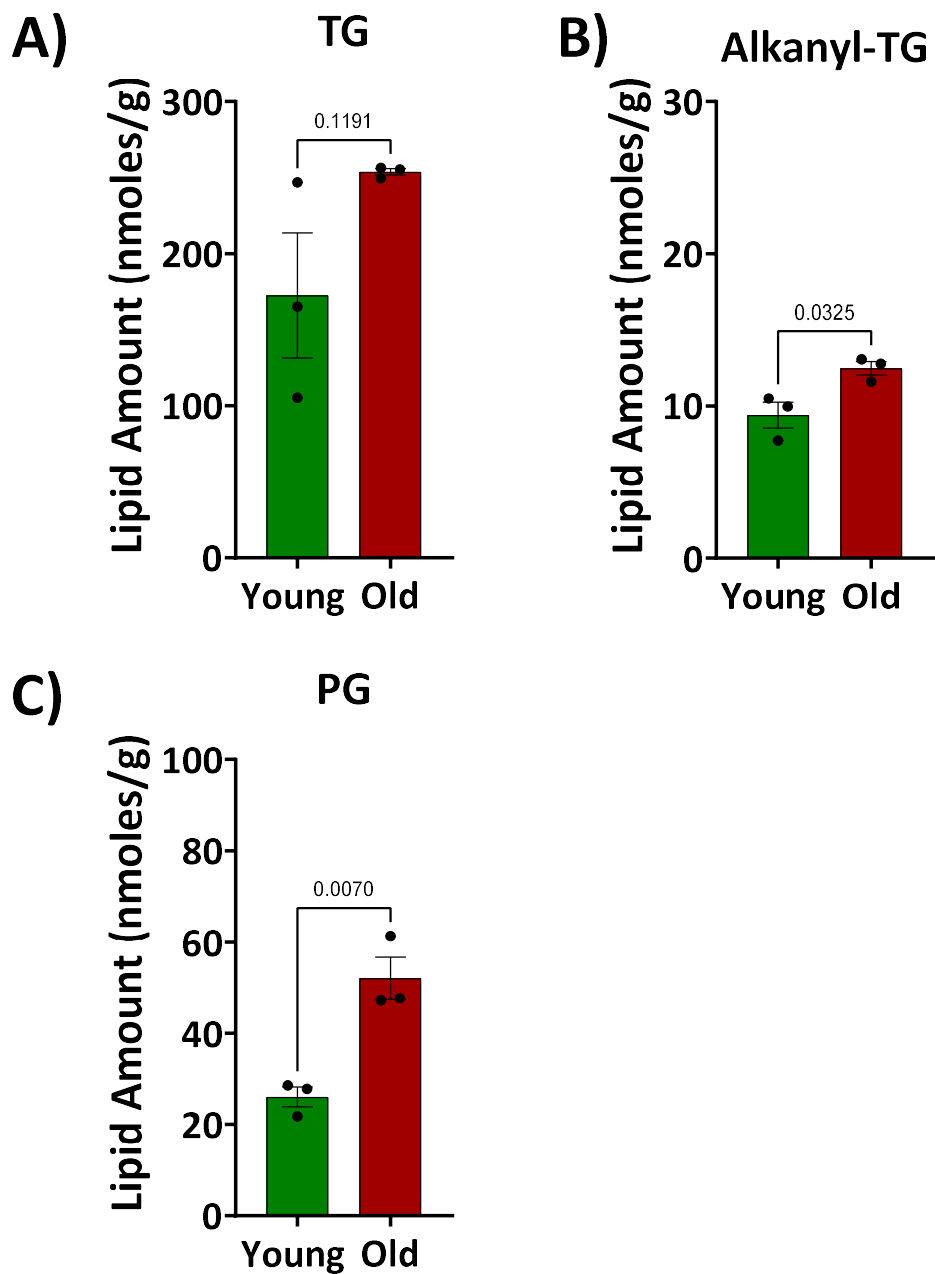
Figure 6.15 Age has no significant effect on the total concentration of Phosphatidylglycerol, and Alkanyl-TG, and Triglycerides. *A) Total concentration of TG. B) Total concentratin of Alkanyl-TG. C) Total concentration of PG. N = 3 for young and n = 3 for old, unpaired t-tests.*

6.4 Summary and discussion

In this chapter the lipid content of the whole *Lymnaea* CNS has been quantified in both young and old CNS. Clear age-related increases were observed in the total concentration of SM and CE lipid classes. Age related changes are also observed in the different lipid species, including a decrease of PI 38:4, an increase of 12 PC species (PC 16:1_16:0, PC 16:0_20:5, PC 16:0_20:4, PC 18:2_18:1, PC 18:1_20:5, PC 38:5, PC 18:2_20:3, PC 16:0_22:4, PC 40:7, PC 20:4_20:2, PC 40:5 and PC 42:6), an increse in two Lyso-PC species (LysoPC 16:0, LysoPC 20:2), an increase in 7 Plasmanyl-PC species (Plasmanyl-PC O-16:0_16:1, Plasmanyl-PC O-16:0_17:1, Plasmanyl-PC O-16:0_18:1, Plasmanyl-PC O-36:5, Plasmanyl-PC O-36:4, Plasmanyl-PC O-38:5 and Plasmanyl-PC O-16:0_22:4), an increase in 3 Plasmenyl-PC species (PC O-32:1, PC O-35:3, and PC O-36:5), an increase in 3 PE species (PE 17:1_22:2, PE 40:7 and PE 20:4_20:2), an increase (Plasmanyl-PE O-16:0_22:4) and decrease (Plasmanyl-PE O-38:4) in Plasmanyl-PE species, an increase in two Plasmenyl-PE species (Plasmenyl-PE P-16:0_22:4, Plasmenyl-PE P-38:1), an increase in 10 TG species (TG 53:1, TG 54:5, TG 54:4, TG 56:7, TG 56:6, TG 56:5, TG 58:8, TG 58:7, TG 58:5, TG 60:9), an increase in 4 Alkanyl-TG species (Alkanyl-TG O-52:1, Alkanyl-TG O-16:0_17:0_20:1, Alkanyl-TG O-16:0_20:3_20:1, Alkanyl-TG O-16:0_20:1_22:4) and an increse in 7 PG species (PG 16:0_16:0, PG 16:0_17:0, PG 17:0_18:1, PG 16:0_20:5, PG 16:0_20:4, PG 20:5_20:4, PG 20:4_20:4).

6.4.1 Changes ester lipids (SM, PI, PC and Lyso-PC)

6.4.1.1   Increase in SM

The age-related increase in SMs observed in *Lymnaea*'s CNS are consistent with changes observed in mammalian systems. An increase of SM is observed in the total rodent brain (Giusto et al., 1992), rodent synaptosomes (Yamamoto et al., 2008) and cultured hippocampal neurons (Trovò et al., 2011) with increasing age. These

observations suggest that a common mechanism of lipids modifications, perturbed by age, might be influencing their availability in both vertebrate and invertebrate systems.

The SM lipids are synthesised by the sphingomyelin synthase (SMS) enzyme, which transfers a phosphorylcholine from PC onto a ceramide generating SM and diacylglycerol (DAG). SMS is also able to catalyse the opposite reaction, regulating in opposite directions the level of the DAG and ceramide (Huitema et al., 2004). In addition SMs are also degraded to ceramide and PC by three different families of sphingomyelinases (SMases), acid (aSMases), neutral (nSMases) and alkaline SMases, based on the optimal pH the enzymes require to function (**Figure 6.16**) (Milhas et al., 2010).
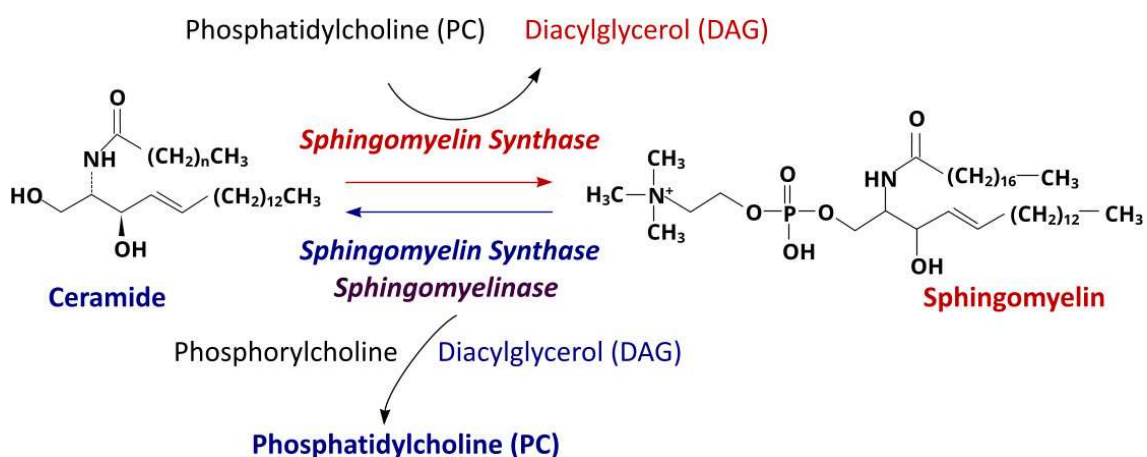
Figure 6.16 Sphingolipids metabolism. *SM is synthesised by SMS from ceramide and PC and metabolised by SMS and SMase.*

As SMS is the enzyme catalysing the production of SM, the increase of SM availability with age could be a consequence of a change in the availability or the activity of SMS, therefore favouring the reaction of SM production. An age-related increase in the production and accumulation of ceramide (Cutler et al., 2004) could also lead to the increase of SM production. Alternatively, the age-related increase of SM, could be a consequence of a change in the expression or activity of SMases, leading to accumulation of SM. For example, a five-fold increase in SM in the brain is observed in 7 months old mice in which the aSMase has been knocked out (Scandroglio et al., 2008). Not much is known about the effect of age on the expression or activity on any of the three types of SMases or SMS, however altered SM metabolism (decrease of

SMs and increase of ceramides) has been related to the neuropathogenesis of Alzheimer's disease (Haughey et al., 2010). As the SMs together with cholesterol are a major components of lipid rafts (Simons and Ikonen, 1997), with which proteins of the vesicular release machinery interact, they can have an effect on the vesicular release of transmitters (Chamberlain et al., 2001, Chamberlain and Gould, 2002, Gil et al., 2005, Salaün et al., 2004, Wang et al., 2019). Increase of SM in PC 12 cells following 3 days incubation with the lipid, significantly increases the rise time and the half width of the release amperometry events recorded from the cells (Uchiyama et al., 2007). Similarly, increase in the SM/PC species following zinc treatment of the same cell line also leads to a significant increase in the half width and fall time of the observed exocytotic amperometry events (Ren et al., 2019). Based on these observations, it is plausible to hypothesise that the age-related increase of SMs in the CNS of *Lymnaea* is contributing to the observed changes in the release dynamics, specifically the increase in the rise and fall time of the events and their half width, and therefore contributing to the increase of serotonin release by the old CGCs. Additionally, the increase of SM could lead to an increase or decrease in ceramide, as a product of SM hydrolysis, or if used in the synthesis of SM. It has been demonstrated that a threefold increase in ceramide (C24:0) and more than a hundred fold increase in C24:0 galactosylceramide are observed in homogenates form cerebral cortex of 25 months-old mice, compared to 3 months old mice (Cutler et al., 2004). In the presence of SM, ceramide, tends to self-aggregate, segregating in microdomains/rafts and therefore could also influence the membrane permeability and curvature (van Blitterswijk et al., 2003). Therefore, it would be interesting for future studies to quantify ceramide and determine its role in the dynamics and quantity of vesicular release.

6.4.1.2   Decrease in PI

Although the total concentration of PI does not change significantly with age, the most abundant PI lipid (PI 38:4) is significantly decreased with age. Age-related decrease in PI in the CNS of old *Lymnaea*, is consistent with a decrease of PI observed in synaptosomes of aged rodent brains (Zambrzycka, 2004) and like the SM, PI has also been related to the regulation of exocytosis (Aoyagi et al., 2005, Wenk and De Camilli,

2004). The PIs are phospholipids with a head group of the cyclic polyol *myo*-inositol. Due to the *myo*-inositol free hydroxy groups at different positions, PIs can be readily phosphorylated, resulting in seven different phosphorylated forms (Falkenburger et al., 2010). Two of the PI forms, the PI(4)P and PI(4,5)P_2 are the most abundant PIs species in the Golgi and vesicles membranes (Wenk and De Camilli, 2004). The accumulation of PI(4,5)P_2 in syntaxin clusters in PC 12 cells has been correlated to the accumulation of LDCVs and exocytosis activity (Aoyagi et al., 2005). Similarly, the less-abundant PI lipid, the PI(3,4,5)P_3 has been observed to concentrate with Syntaxin 1A at the neuromuscular synapse of *Drosophila* larva. At this synapse, a reduction of PI(3,4,5)P_3 levels leads to dispersion of Syntaxin 1A and reduced neurotransmitter release (Khuong et al., 2013). An effect of PI(4,5)P_2 on the size of the releasable pool of vesicles is also observed in chromaffin cells, in which scaling of the amount of the lipid leads to scaling of the pool of releasable vesicle (Milosevic et al., 2005). Direct effect of PI on vesicular release kinetics has been observed in PC 12 cells, in which a decrease of PI due to zinc treatment has been correlated to an increase of the half width and fall time of the amperometry events recorded during exocytosis of catecholamine molecules (Ren et al., 2019).

These observations suggests that the age-related decrease of the PI lipid in the CNS of *Lymnaea* might be related to a decrease in the number of available releasable vesicles, and the increase in the parameters, such as the half with and fall time of the release events. As mentioned in Chapter 5, the increase in the number of molecules released by the old CGCs could be a compensatory mechanism to a possible decrease of the number of releasable vesicles in the soma of the cell and this could be related to the decrease of PIs.

6.4.1.3   PC, Lyso-PC and PE

PCs are the most abundant lipids in the young *Lymnaea* CNS, comprising 32.5 % of all lipids and the concentration of 12 PC lipid species is increased with age. The abundance of the PCs in the CNS of *Lymnaea* is similar to observations made in

mammalian cells membranes, in which the PCs and the PEs are the most abundant, with the PCs comprising ~ 40-50 % of the total lipids (van der Veen et al., 2017). In mammalian cells, synthesis of both the PCs and the PEs occur by a similar pathway, involving the phosphorylation of the choline and ethanolamine by the enzymes choline kinase (CK) and ethanolamine kinase (EK). This is followed by the conversion of phosphocholine and the phosphoethanolamine into CDP-choline and CDP-ethanolamine, by the enzymes cytidylyltransferase (CT) and CTP:phosphoethanolaminecytidylyltransferase (ET) respectively. CDP-choline and CDP-ethanolamine are transferred to DAG by the ER membrane proteins CDP-choline:1,2-diacylglycerol cholinephosphotransferase (CPT) and the dual-specificity protein CDP-choline:1,2-diacylglycerol choline/ethanolamine phosphotransferase (CEPT) to form PC an PE. Alternatively, PC can be formed from PE conversion by phosphatidylethanolamine N-methyltransferase (PEMT), whereas PE can also be formed from PS by the decarboxylation of PS by phosphatidylserine decarboxylase (PSD) (**Figure 6.17**) (van der Veen et al., 2017).
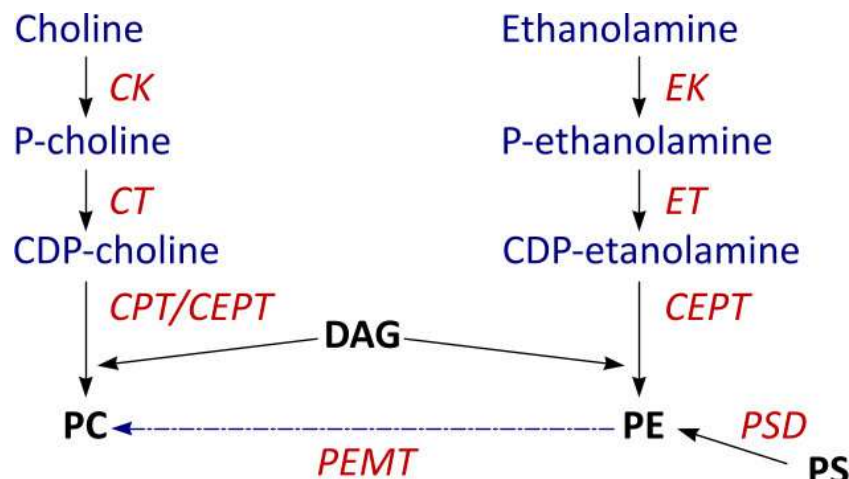
Figure 6.17 Biosynthesis of PC and PE. *PC and PE are synthesised by the transfer of CDP-choline and CDP-ethanolamine to a DAG molecule, by the enzymes CPT and CEPT. PE can be converted to PC by PEMT, and PE can also be synthesised from PS, by the enzyme PSD.*

Conversely, PC and PE can be hydrolysed by the Phospholipases A1/2, C and D (PLA, PLC and PLD) enzymes to generate Lyso-PC/PE, DAG, and phosphatidic acid (PA) (**Figure 6.18**) (Joensuu et al., 2020).
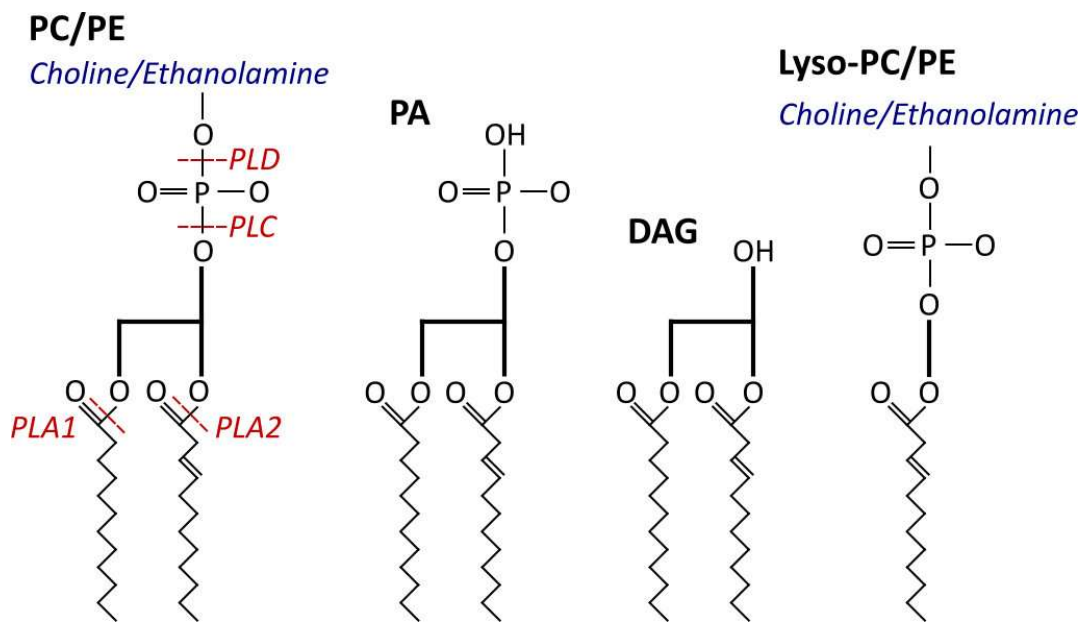
Figure 6.18 Hydrolysis of PC and PE. *Phospholipase A, C and D hydrolyse PC and PE to produce PA, DAG and Lyso-PC and Lyso-PE.*

An age-related increase of some of the PC species (PC 14:0_16:0, PC 16:0_16:0, PC 16:0_18:2, PC 16:0_22:6) is observed either in mitochondrial or microsomal membranes collected from human cerebellum and motor cortex, whereas others are decreased (PC 16:0_20:1, PC 16:0_20:4, PC 16:0_22:4, PC 18:0_18:1, PC 18:0_20:4, PC 18:1_22:6) (Hancock et al., 2022). Similarly, changes of PC species are also observed in the aged mice model of Alzheimer's disease, where an increase is observed in the PC 18:1_20:4 species and a decrease is observed in the PC 18:0_20:4 species (Emre et al., 2021). Due to the multiple pathways through which PC lipids can be produced, either from the transfer of CDP-choline to DAG, from PE or from SM, it is hard to determine which pathway might be affected by age leading to the increase of some of the PC species observed in the CNS of *Lymnaea*. As total PEs do not change significantly with age in the whole *Lymnaea* CNS, it is likely that they do not contributing to the observed age-related increase in PCs.

Like other lipids, PCs have also been shown to have an influence on the quantity and kinetics of transmitter release. Specifically, incubation of PC 12 cells for 3 days with the PC lipids has led to a significant decrease in the transmitter released per vesicle, despite a small, but significant increase of the diameters of the vesicles, as observed

with electron microscopy. The decrease of transmitter release appears to be a result of a decrease of the amplitude and rise time of the events, although an increase of their fall time and half-with is observed (Uchiyama et al., 2007). A correlation between changes in PC amount and the kinetics of the release events is also observed in the same cells following treatment with zinc. In these experiments, an increase of PCs is correlated to an increase in the half with and fall time of the exocytotic events (Ren et al., 2019). The changes in the dynamics of release observed with an increase in PCs in PC 12 cells, specifically, the increase of the half with and fall time of the events are similar to the changes in release observed in the CGCs with age. These observations suggest a common effect of the PC lipid on the release process from different cells. However, unlike in the PC 12 cells, in which the number of molecules released by the cells is decreased with the increase of the PC lipid, in the CGCs this effect is the opposite. The age-related increase of some of the PC species in the CNS of *Lymnaea* correlates to an increase of the amount of serotonin released by the CGCs. This distinction is possibly determined by the effect that the age-related change in all other lipids exerts on the cell and vesicle membranes and therefore on release. In parallel to the increase of PC, two lyso-PCs species (LysoPC 16:0, LysoPC 20:2) are also increased in the aged snail CNSs. As mentioned above, PCs are hydrolysed by the phospholipases A1/2 to produce lyso-PC. An age-associated increase in the activity of PLA2 is observed in the brains of aged *Lymnaea*, leading to a significant increase in the release of PLA2-dependent free fatty acids (FFA) (Watson et al., 2013). The increased activity of PLA2 would also increase the production of Lyso-PC lipids (Farooqui and Horrocks, 2006) observed in the CNS of old *Lymnaeas*. Increases in Lyso-PCs adds a high positive curvature to lipid membranes and changes their elasticity, therefore influencing the ability of vesicle and cell membranes to fuse (Fuller and Rand, 2001, Piomelli et al., 2007). To test this hypothesis, several studies have explored how lyso-PC can alter the kinetics of the release events. Incubating chromaffin cells with lyso-PC increased the number of molecules of transmitter per release event (Amatore et al., 2006). However, intracellular nano injection of Lyso-PC into the same cell type decreased the number of molecules released by the cells per release event (Aref et al., 2020). These observations suggest that an increase of the Lyso-PC at different leaflets of the cell membrane can have different effects. The observed correlation of an increased Lyso-

PC species in the CNS of old snails and the increased number of molecules released by the old CGCs suggests that Lyso-PC could be one of the lipid components influencing the age-related change in transmitter release, possibly by an increase of the Lyso-PC localised to the outer membrane of the cell.

6.4.2 Changes in CE

The CEs were the most abundant lipids in the old *Lymnaea* CNS, increasing from 6.43 % of the total lipids' composition in the young to 43.20 % in the old. CEs are a way for cells to modulate their cholesterol levels and a way of transporting cholesterol in the blood stream. Excessive cholesterol is esterified by the enzyme acyl-CoA:cholesterol acyltransferase (ACAT) to CEs. CEs can be hydrolysed back to cholesterol by the enzyme CE Hydrolase (**Figure 6.19**) (Liscurn, 2002).
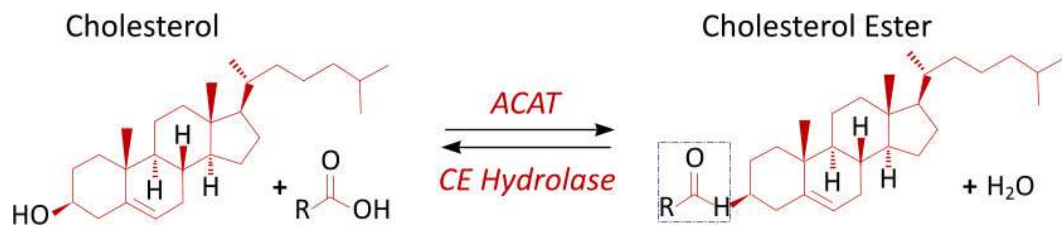
Figure 6.19 Cholesterol ester esterification and hydrolysis.

CEs are usually stored in lipid droplets (LDs) together with triacylglycerols (TAGs) and it has been shown that all brain cell types form LDs (Farmer et al., 2020). A few studies have shown age-dependent accumulation of LDs in different cells and brain regions. An increase of LDs is observed in microglia cell in both mice and human brains (Marschallinger et al., 2020). Although neurons do not usually accumulate LD due to active turnover of TAGs favouring lipolysis, some stressors such as neuronal excitotoxicity and neurodegeneration have been observed to lead to LD accumulation (Islimye et al., 2022). In a C. eleganse model of excitotoxicity, neuronal LD dynamics have been related to the regulation of PUFA availability, suggesting that PUFAs generated from TAG lipolysis or de-novo synthesise may be incorporated into membrane phospholipids, either maintaining cell membrane function in normal conditions or promoting neurodegeneration in stress conditions (Yang et al., 2020).

It is possible that the age-related increase in CEs in the CNS of *Lymnaea* is a result of increased cholesterol, or changes in the expression or activity of the ACAT and the CE hydrolase enzymes. The ACAT is coded by two different genes, ACAT1 and ACAT2, where ACAT1 is predominantly expressed in normal human tissue (Chang et al., 2009). Immunohistochemical staining for ACAT1 in human brain tissue has shown that the enzyme is present in neurons, but not in glial cells (Sakashita et al., 2000). A significant age-related increase in cholesterol esters, in 24-months old male Sparague-Dawley rats, has been correlated to a significant increase of the steady state mRNA of ACAT enzyme and significant reduction of the mRNA expression of CE Hydrolase (Mulas et al., 2005). The increase of CEs could be reflective of changes in cholesterol levels in the old CNS, although how cholesterol is affected by age in the CNS of the snails is unknown as our mass spectrometer was unable to detect cholesterol using the methodology described. If cholesterol levels in the CNS are affected, then these can modulate both the presynaptic and the postsynaptic properties of neurotransmission. A depletion of cholesterol in cultures of hippocampal neurons reduces significantly the amplitude of evoked excitatory postsynaptic currents (eEPSC) of NMDA and AMPA receptors, whereas physiological levels of cholesterol in neurons appear important for the propagation of action potentials and the attenuation of spontaneous vesicular release (Korinek et al., 2020). Additionally, increased cholesterol efflux, induced by cholesterol acceptors leads to impairment of LTP in CA 1 synapses of 3-4 months Wistar rats (Koudinov and Koudinova, 2001). Conversely, an increase of cholesterol in PC 12 cells due to repetitive stimulation of exocytosis with a high potassium saline (Gu et al., 2020a) correlated with a significant increase in the number of molecules released by the cells and a significant increase if the fraction of molecules released (Gu et al., 2019).

These observations suggest that the age-related increase of CE in Lymnaea, might be a consequence of increased levels of cholesterol, which could be influencing neurotransmission between neurons including the number of molecules released and the kinetics of the release events from the CGC soma. This could be one of the reasons for the increased number of molecules released by the cells with age. However, as mentioned earlier, the mass spectrometry method used to detect lipids was unable to

detect cholesterol, therefore the relationship between changes of CE and cholesterol is unclear and additional studies would be required to further investigate the matter.

6.4.3 Changes in Ether lipids (Plasmanyl-PC, Plasmenyl-PC, Alkanyl-TG)

27.99 % of the total lipids in the young CNS of *Lymnaea* were accounted by the ether lipid Plasmanyl-PC, which decreased to 16.99 % in old CNS. Similarly, around 20 % of the lipids in mammalian cells are accounted for by ether lipids and higher levels (20 - 50 %) have been detected in the human brain (Braverman and Moser, 2012, Paul et al., 2019, Lessig and Fuchs, 2009). The ether lipids differ from the glycerophospholipids by the link at the sn-1 position between the glycerol backbone and the fatty acid chain, which is an ether or vinyl ester, instead of an ester link, as in the diacyl-phospholipids. There are two types of ether phospholipids, plasmanyls and plasmenyls (also known as plasmalogens), which differ in the moiety which forms the ether bond. This is an alkyl in the case of the plasmanyls and alkenyl in the case of the plasmenyls. The plasmalogens are synthesized within the peroxisomes and the ER, where an acyl-chain of dihydroxyacetone phosphate (DHAP) is replaced by an alkyl-chain at the sn-1 position, by the alkyl-DHAP synthase enzyme. This process is followed by the reduction of a ketone group by the alkyl-DHAP reductase enzyme and the final generation of an alkyl-glycerophosphate (alkyl-GP) (**Figure 6.20**) (Lee, 1998).
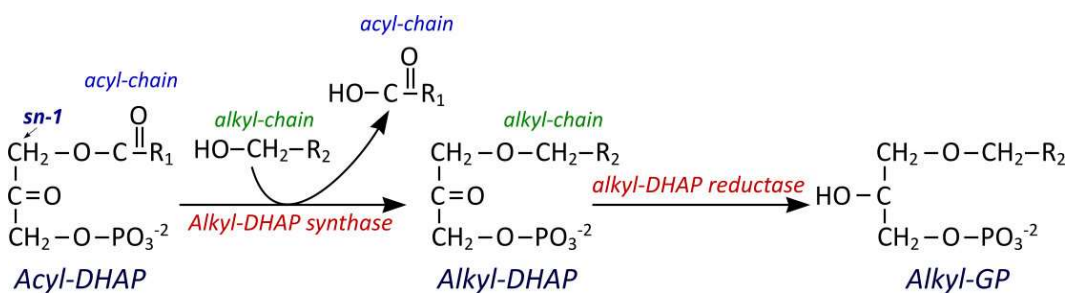
Figure 6.20 Synthesis of ether lipids. *Ether lipids are synthesized from dihydroxyacetone phosphate on which an acyl-chain is replaced by an alkyl-chain by the alkyl-DHAP synthase, followed by a ketone group reduction by alkyl-DHAP reductase and the formation of an alkyl-glycerophosphate.*

A few enzymes (alkyl-GP acyltransferase, alkylacyl-GP phosphohydrolase, alkylacyl-G:CDP-choline (CDP-ethanolamine) choline (ethanolamine) phosphotransferase) convert the alkyl-GP into the major glycerophospholipids alkylacyl-GPC and alkylacyl-GPE. In addition, alkylacyl-GPE can be directly converted to alkylacyl-GPC through base exchange (Lee, 1998). In the nervous system of mammals, PE plasmalogens are the most enriched lipid of all ether lipids (30 mol%), whereas PC plasmalogens only show a trace amounts (Dorninger et al., 2017). This slightly differs from what was observed in the CNSs of *Lymnaea*, in which the plasmanly-PC (which have a simple ether bond at the sn-1 instead of the vinyl-ether of plasmenyls) appeared to be the most abundant ether lipid (~28 % in the young, and ~17 % in the old) followed by PE plasmalogens (PE-plasmenyl, ~ 10 % in the young and 5.5 % in the old). Although the percentage of PE plasmalogens was decreased with age, the total amount of the lipid concentration remained unchanged probably due to both a significant increase (Plasmanyl-PE O-16:0_22:4) and decrease (Plasmanyl-PE O-38:4) in Plasmanyl-PE species and an increase in two Plasmenyl-PE species (Plasmenyl-PE P-16:0_22:4, Plasmenyl-PE P-38:1). Seven Plasmanyl-PC and 3 Plasmenyl PC lipid species were significantly increased by age. Although not much is known about the effect that the ether PC lipids could have on the properties and functions of lipid membranes, a reduction of ether lipids biosynthesis has been related to changes in neurotransmitter release. It has been demonstrated that deficiency of ether lipids in isolated murine terminals decreases both glutamate and acetylcholine release (Brodde et al., 2012). Based on these observations it is possible that an increase in ether lipid species, as observed with age in the CNS of *Lymnaea*, might have the opposite effect, therefore suggesting that the increase in ether PC lipids (plasmanyl PC and plasmenyl PC species) might be contributing to the observed increase in transmitter release.

Like ester lipids, ether lipids contain a PUFA in the sn-2 position, which can be released by the action of plasmalogen specific phospholipase A2 (PLA2), generating lysoplasmalogens and free PUFA, predominantly arachidonic acid and docosahexaenoic acid, that can participate in cell signalling pathways. In particular AA is used in the synthesis of eicosanoids and prostaglandins, essential for immune function and DHA is a precursor to anti-inflammatory mediators (Paul et al., 2019). Due

to their structure (an acyl chain at the sn-2 position and alkyl-chain at the sn-1 position without the carbonyl group) it has been shown that they can exhibit stronger hydrogen bonding between the head groups, therefore possibly affecting the membrane structure and potential difference, compared to the ester glycerophospholipids (Farooqui and Horrocks, 2001, Lohner et al., 1991). Based on this observation it is possible that the age-related increase in plasmanyl-PC and plasmenyl-PC lipid species in the CNS of *Lymnaea*, has an effect on the membrane properties of the cells including the CGCs, which could be one of the reasons for the observed increase in the duration of the events released by old CGCs and the increase of the number of molecules released by the cells. As the alkanyl-TG is synthesised predominantly from plasmanyl-PC (Schooneveldt et al., 2022), it is possible that the age-related increase in alkanyl-TG lipid species in the CNS of *Lymnaea* is also due to increase of plasmanyl-PC species.

Overall, the observed age-related changes in the lipids of the CNS of *lymnaea* can have multiple effects on neurotransmitter release (Ledesma et al., 2012). The age-related increase of the number of molecules released by the old CGCs could be a result of the increase of cholesterol, observed as an increase of CEs, and the increase of lyso-PC species. An increase of both lipids has been shown to correlate to increased content of transmitter release from PC or chromaffin cells (Adams et al., 2015, Amatore et al., 2006, Gu et al., 2020a). However, it must be emphasised that these changes are observed in the total lipids CNS composition, which includes lipids of all membranes, including the membrane of neurons, glial cells, intracellular organelles, and lipid droplets. Therefore, future work will be needed to investigate the effect of age on the lipids of the membranes of individuals cells, including the CGCs and how this might relate to the kinetics and the quantity of the released neurotransmitters.

7   General discussion and future work

7.1   General discussion

The aim of this thesis was to determine the effect of age on the intracellular vesicular content, the release content, and the kinetics of release from the CGCs and how they relate to changes in *Lymnaea's* CNS lipids composition.

In chapter 2 of this thesis carbon fibre nano-tip and micro electrodes were fabricated and characterised for the measurement of neurotransmitter release and intracellular vesicular content. The electrodes were characterised to determine their sensitivity and stability. The disc electrodes were subjected to cleaning procedures to remove any layers of biological material acquired on the tip during the experiments and only successfully clean electrodes were used repeatedly. Nano-tip electrodes were only used once as a single use blunted the tip making it difficult to penetrate the cell membrane of subsequent cells.

In chapter 3, electrochemical recordings of serotonin release from the CGCs of young and old snails were performed using the 10 μm carbon fibre disc electrodes. Two types of release were recorded - spontaneous and ionomycin evoked release. Spontaneous release from both young and old CGCs was observed at similar frequencies, however ionomycin significantly increased the number of release events in 10 minutes in the young group. No changes in the kinetics of the release events or the number of molecules released per event were observed between the spontaneous and ionomycin triggered release in both groups. Comparisons of the release from the soma of the CGCs of young and old snails showed a significant increase of the number of molecules released per event with age. This was due to increases in the rise and fall time of the events and their half width. Cluster analysis of the data predicted two populations of release events in both the young and old CGCs. For any given age group, these two populations could be due to a single population of vesicles fusing and releasing in two different modes or two distinct populations of intracellular vesicles fusing and

releasing some or all their contents. In terms of the age-related changes, the observed increase in neurotransmitter release could be due to an increase in the level of transmitter stored in the vesicles or changes in the release kinetics or release from another pool of vesicles with different release dynamics and neurotransmitter concentration.

To refine the model further, nano-tip electrodes were used to determine the intracellular content of the vesicles in young and old CGCs, and a cluster analysis performed to determine how many populations of vesicles were predicted to be present and whether this was altered by increasing age. Vesicles in the soma of the young CGCs contained significantly more molecules of 5-HT than in the old CGCs. Additionally, significantly larger number of molecules of 5-HT were present in the intracellular vesicles than were released in both age groups, showing that release from the young and old CGCs is partial. Analysis of the proportion of transmitter released showed that the proportion of release is significantly lower in the young, strongly suggesting that the old vesicles are having to release more of their content to maintain homeostasis in the CNS. Given that drugs that can increase learning and memory formation also increase the proportion of transmitter released from individual vesicle (Dong et al., 2014, Ren et al., 2017), these data strongly suggest that release is not as plastic in the old compared to the young. Cluster analysis using the distributions of the number of molecules comprising the vesicles or the kinetics of events as vesicle 'popped' on the intracellular sensor showed that there was one more cluster of vesicles in the young CGC soma compared with the old CGCs (2 vs 1 using molecules for the clustering and 3 vs 2 using the kinetics of the events). Given that the release events in both young and old could be assigned to two clusters, the simplest model is one in which two clusters of intracellular vesicles are giving rise to two clusters of release events in both young and old CGCs (**Figure 7.1 A and B**).
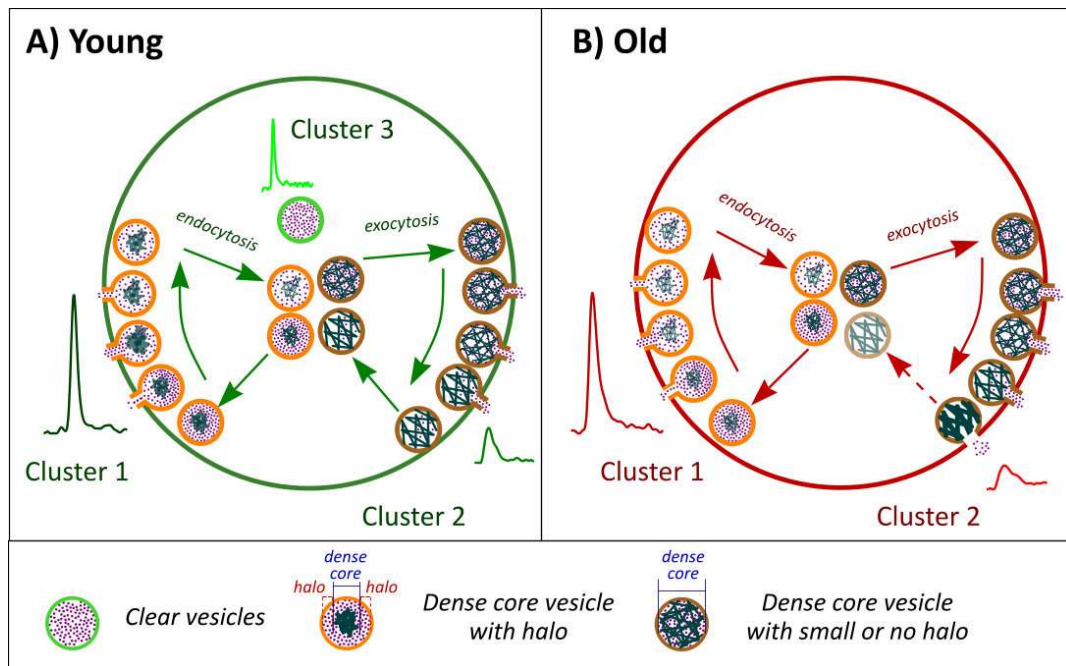
Figure 7.1 Proposed model of vesicular content and release from the CGC of young and old Lymnaea. *A) Young CGCs contain three pools of vesicles (clear vesicles – CV, Dense core vesicles (DCV) with a halo, and DCV with small or no halo. Only two of the three pools are released into two different modes of release. B) Old CGCs contain only two pools of vesicles (DCV with halo and DCV with no halo) and both are released in similar modes as young.*

So, what are the clusters related to? Clearly serotonergic neurons have been shown to contain both LDCVs and SCVs (Bruns et al., 2000, Bruns and Jahn, 1995) and work on the monoaminergic PC12 cells or bovine chromaffin cells has shown that they can contain more than one population of LDCVs (Adams and Harkins, 2014). Therefore, the emerging model suggests that the CGC soma in both young and old has two distinct populations of LDCVs and that the young have an additional cluster that contains the lowest number of molecules of 5-HT and is therefore most likely a population of SCV. So why do the old not have a population of SCVs? The most well studied synapse that explores how ageing affects vesicular content is the rodent neuromuscular junction. This work has shown that SCVs are decreased significantly with increasing age (Fahim and Robbins, 1982, Jang and Van Remmen, 2011), providing a precedent for the central data of this thesis.

If the emergent model is true and two populations of vesicles that release to generate two populations of release events, in both young and old CGCs, then whatever is causing the old to release more molecules of transmitter is affecting both populations of vesicles equally. This could be age-related changes to the SNARE complexes that facilitate vesicle fusion with the membrane (Hatanpää et al., 1999, Jacobsson et al., 1998, Shimohama et al., 1998, Orock et al., 2020, VanGuilder et al., 2010) or it could be age-related changes in the membrane lipids (Ledesma et al., 2012). To explore this further chapter 6 examined how the ageing process affected membrane lipids in the CNS of *Lymnaea*. Ageing increased SM, CE, PC, plasmanyl PC, plasmenyl PC, lyso-PC, PE, plasmanyl PE, plasmenyl PE, PS, PG and TG or some of their species and decreased PI, lyso PE (in particular lyso PE 22:2), and Plasmanyl-PE O-38:4). These changes are consistent with age-related changes in a range of vertebrates including mice and rats (Giusto et al., 1992, Trovò et al., 2011, Zambrzycka, 2004) and based on previous work the changes observed could affect the dynamics of vesicular release in a way that is similar to the effects of increasing age (Amatore et al., 2006, Aref et al., 2020, Gu et al., 2019, Gu et al., 2020a, Ren et al., 2019). Therefore, alterations in membrane lipids are likely to play a part in the effects of age on vesicular release dynamics but it cannot be excluded that other factors such as age-related changes in intracellular Ca^{2+} dynamics, or alterations in membrane proteins also have an effect.

7.2 Future work

Future work that should be considered can include:

- Identification of a stimulus/behaviour that consistently releases 5-HT from the soma of CGCs.

In this thesis different stimuli were applied to trigger release, however from all used stimuli, only the ionophore Ionomycin triggered release in the young CGCs. Future work should look at the identification of a behaviour or stimulus, or a combination of stimuli that can consistently trigger the release of serotonin from the CGCs.

- Map the targets of somatic 5-HT release.

Mapping the targets of somatic serotonin release would allow to determine the function of release and how it is affected by age.

- Perform electron microscopy to confirm the presence of different clusters of vesicles in young and old CGC soma.

Electron microscopy of the CGCs of young and old *Lymnaea* would allow to provide information of the morphological properties of the vesicles inside of the CGCs and their localisation to the cell membrane and release sites.

- Identify the lipids that are present in both the plasma and vesicular membranes.

Identifying the lipids of the cell and vesicular membranes of young and old CGCs would allow stronger predictions about the role that age-related changes in lipids have on vesicular release dynamics.

- Manipulate membrane lipids.

To ensure causation of the changes of membrane lipids, membrane lipids would need to be manipulated either through the diet or through intracellular injection and their effects on vesicular release examined.

8 Appendix

8.1 Clustering of events recorded with the nano-tip electrodes

8.1.1 Clustering of the release events based on the cube root of molecules

Typical events within each cluster in the young and old (**Figure 8.1 A**). Comparison of the content released by the two clusters and the kinetics of the release events (**Figure 8.1 B, C, D E and F**).
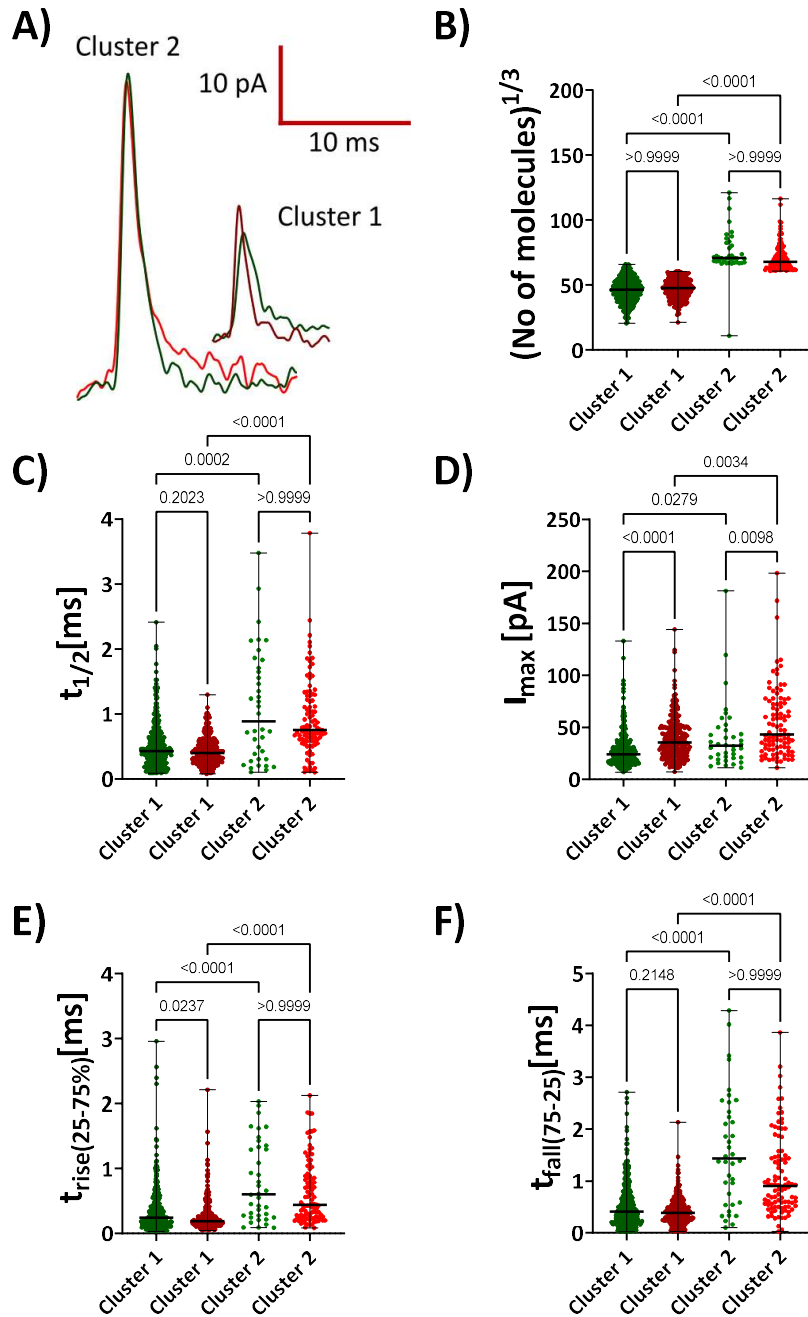
Figure 8.1 Both clusters of release events are differentially affected by age. *A) Sample release events from young (green) and old (red) for each of the two clusters. (B-F) Plots comparing the effect of age on the properties of the release events from each of the clusters. B) Number of molecules, C) Half width, D) Imax, E) Rise time and F) Fall time (young cluster 1 n = 300, cluster 2 n = 38; old cluster 1 n = 246, cluster 2 n = 98, Kruskal-Wallis test).*

8.1.2 Clustering of the release events based on the log-transformed values of event parameters

Typical events within each cluster in the young and old (**Figure 8.2 A**). Comparison of the content released by the two clusters and the kinetics of the release events (**Figure 8.2 B, C, D, E, and F)**.
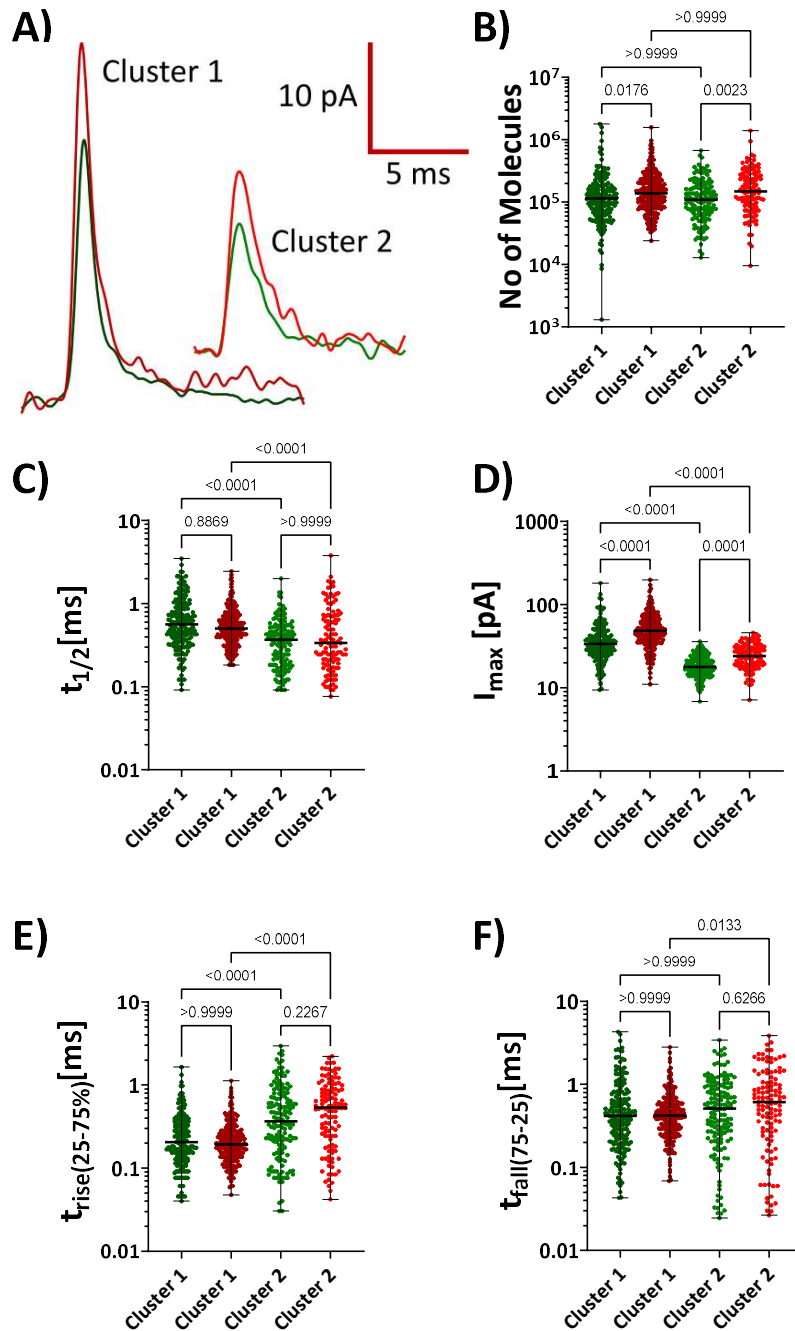
Figure 8.2 Both clusters of release events are differentially affected by age. *A) Sample release events from young (green) and old (red) for each of the two clusters. (B-F) Plots comparing the effect of age on the properties of the release events from each of the clusters. B) Number of molecules, C) Half width, D) Imax, E) Rise time and F) Fall time (young cluster 1 n =186, cluster 2 n = 152; old cluster 1 n = 226, cluster 2 n =118, Kruskal-Wallis test).*

8.1.3 Clustering of the intracellular events based on the cube root of the molecules of the events

Comparison of the kinetics of the intracellular events of the young and old CGCs clustered using a model of two clusters in the young and a model of one cluster in the old (**Figure** *8.3* **A, B, C and D)**.
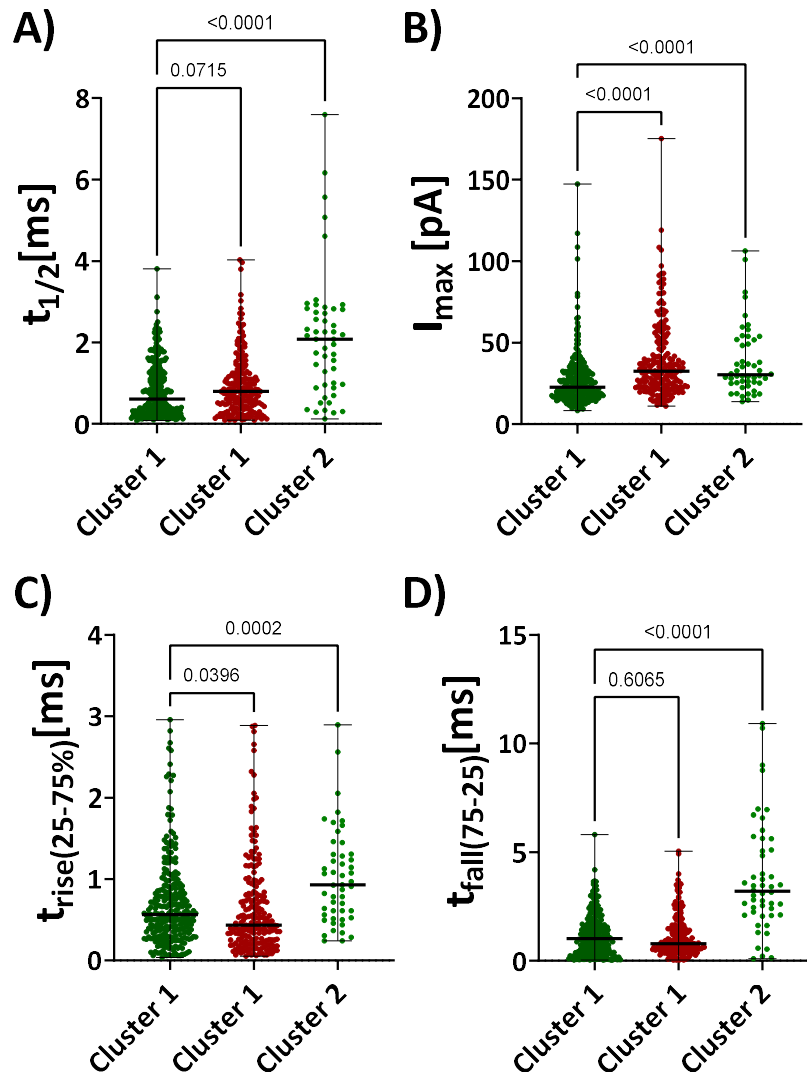
Figure 8.3 Age affects the parameters of the events in Cluster 1. *Plots comparing the effect of age on the properties of the intracellular events from each of the clusters, A) Half width, B) Imax, C) Rise time and D) Fall time. Young Cluster 1 n = 275, Cluster 2 n = 50, Old Cluster 1 n = 205, Kruskal-Wallis test.*

Comparison of the kinetics of the intracellular events of the young and old CGCs clustered using a model of two clusters in the young and a model of two cluster in the old **(Figure *8.4* A, B, C and D)**.
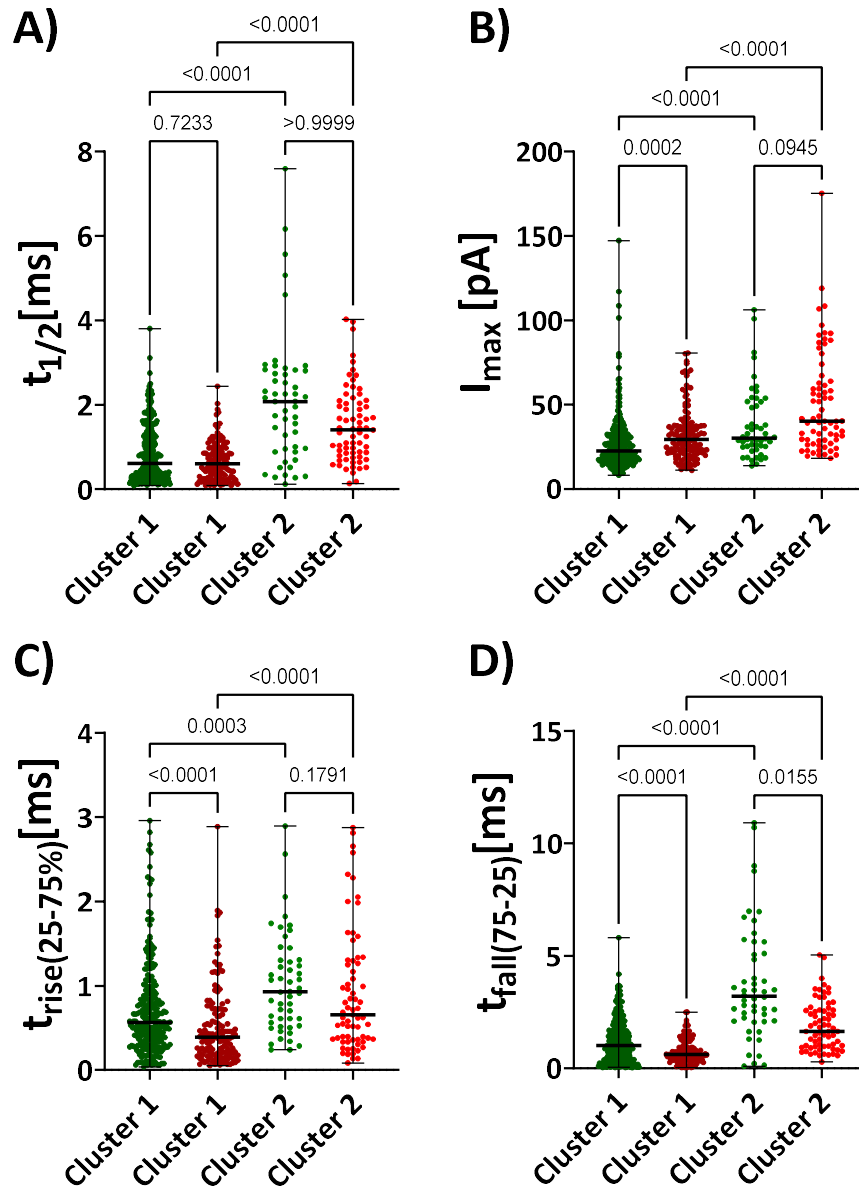
Figure 8.4 Age affects the parameters of the events in both Cluster 1 and Cluster 2. *Plots comparing the effect of age on the properties of the intracellular events from each of the clusters, A) Half width, B) Imax, C) Rise time and D) Fall time. Young Cluster 1 n = 275, Cluster 2 n = 50, Old Cluster 1 n = 136, Cluster 2 n = 69, Kruskal-Wallis test.*

8.2 Effect of age on lipid composition

8.2.1 Phosphatidylcholine

Lipid Class	% Total lipid class in Young	% Total lipid class in Old
PC 16:1_16:0	8.72	8.58
PC 16:0_18:3	5.03	3.51
PC 16:0_18:2	8.07	5.87
PC 16:0_18:1	7.21	4.63
PC 36:4	3.80	3.24
PC 18:2_18:1	5.20	4.32
PC 16:0_20:1	2.93	2.05
PC 38:5	3.99	4.95
PC 38:4	5.07	3.14
PC 18:1_20:2	2.51	1.84

Table 8-1 The 10 most abundant PC species in the CNS of young and old Lymnaea.

Lipid class	Mean concentration in young (nM per g of tissue)	Mean concentration in old (nM per g of tissue)	p-value
PC 16:1_16:0	447.1829	668.0941	<0.0001
PC 16:0_20:5	113.8831	251.9228	<0.0001
PC 16:0_20:4	156.7136	231.9462	0.0002
PC 18:2_18:1	273.3449	337.9479	0.0049
PC 18:1_20:5	92.66725	241.8149	<0.0001
PC 38:5	221.3645	386.4969	<0.0001
PC 18:2_20:3	187.6982	243.4389	0.0464
PC 16:0_22:4	115.7387	184.3728	0.0016
PC 40:7	136.3086	327.9012	<0.0001
PC 20:4_20:2	131.5939	296.5951	<0.0001
PC 40:5	116.77	193.9499	0.0001
PC 42:6	66.88794	176.6188	<0.0001

Table 8-2 PC species significantly increased in the CNS old Lymnaea (p < 0.0001, Species; p < 0.0001, Age; p < 0.0001, Interaction).

8.2.2 Plasmanyl PC

Lipid Class	% Total lipid class in Young	% Total lipid class in Old
Plasmanyl-PC O-16:0_14:0	6.11	3.81
Plasmanyl-PC O-16:0_15:0	3.69	3.34
Plasmanyl-PC O-16:0_16:1	7.89	8.28
Plasmanyl-PC O-16:0_16:0	5.12	4.68
Plasmanyl-PC O-16:0_17:1	4.01	4.61
Plasmanyl-PC O-34:3	9.52	6.85
Plasmanyl-PC O-16:0_18:1	26.31	22.48
Plasmanyl-PC O-35:1	2.78	2.86
Plasmanyl-PC O-36:4	9.07	11.46
Plasmanyl-PC O-16:0_22:4	6.69	9.80

Table 8-3 The 10 most abundant Plasmanyl PC species in the CNS of young and old Lymnaea.

Lipid class	Mean concentration in young (nM per g of tissue)	Mean concentration in old (nM per g of tissue)	p-value
Plasmanyl-PC O-16:0_16:1	364.0093	499.9489	<0.0001
Plasmanyl-PC O-16:0_17:1	183.6323	278.3486	<0.0001
Plasmanyl-PC O-16:0_18:1	1199.735	1357.601	<0.0001
Plasmanyl-PC O-36:5	90.84157	224.6989	<0.0001
Plasmanyl-PC O-36:4	422.1527	692.3161	<0.0001
Plasmanyl-PC O-38:5	110.268	219.6477	<0.0001
Plasmanyl-PC O-16:0_22:4	310.5688	592.5942	<0.0001

Table 8-4 Plasmanyl PC species significantly increased in the CNS old Lymnaea ($p < 0.0001$, Species; $p < 0.0001$, Age; $p < 0.0001$, Interaction)

8.2.3 Plasmenyl PC

Lipid Class	% Total lipid class in Young	% Total lipid class in Old
PC O-29:0	0.71	0.67
PC O-30:1	0.21	0.21
PC O-31:1	0.78	0.83
PC O-32:2	3.63	3.42
PC O-32:1	42.63	36.14
PC O-33:2	11.28	8.23
PC O-34:4	0.82	0.96
PC O-34:2	3.92	3.98
PC O-35:3	7.51	9.54
PC O-35:2	8.24	4.02
PC O-36:5	16.37	28.46
PC O-37:2	2.16	1.52
PC O-38:6	1.04	1.19
PC O-39:1	0.31	0.24
PC O-40:7	0.16	0.29
PC O-40:6	0.19	0.29

Table 8-5 The 10 most abundant Plasmenyl PC species in the CNS of young and old Lymnaea.

Lipid class	Mean concentration in young (nM per g of tissue)	Mean concentration in old (nM per g of tissue)	p-value
PC O-29:0	1.084241	1.712494	>0.9999
PC O-30:1	0.325042	0.54036	>0.9999
PC O-31:1	1.208194	2.124694	>0.9999
PC O-32:2	5.694181	8.711354	0.9998
PC O-32:1	64.38042	91.49158	<0.0001
PC O-33:2	17.44613	20.8029	0.9992
PC O-34:4	1.342477	2.423586	>0.9999
PC O-34:2	6.083745	10.0356	0.9949
PC O-35:3	11.86111	24.12071	0.0201
PC O-35:2	12.56963	10.0686	>0.9999
PC O-36:5	27.6626	71.72028	<0.0001
PC O-37:2	3.273441	3.834188	>0.9999
PC O-38:6	1.76929	3.022912	>0.9999
PC O-39:1	0.475356	0.620081	>0.9999
PC O-40:7	0.276469	0.729956	>0.9999
PC O-40:6	0.343151	0.748909	>0.9999

Table 8-6 Plasmenyl PC species significantly increased in the CNS old Lymnaea (p < 0.0001, Species; p < 0.0001, Age; p < 0.0001, Interaction).

8.2.4 PC(OH)

Lipid Class	% Total lipid class in Young	% Total lipid class in Old
PC[OH] OH-34:2	11.38	4.69
PC[OH] OH-34:1	13.27	1.63
PC[OH] OH-34:0	4.05	0.02
PC[OH] OH-36:5	4.02	4.30
PC[OH] OH-36:4	7.66	7.24
PC[OH] OH-36:3	10.04	6.81
PC[OH] OH-36:2	4.11	3.47
PC[OH] OH-38:5	3.48	3.71
PC[OH] OH-38:4	3.13	3.26
PC[OH] OH-38:3	6.13	6.96

Table 8-7 The 10 most abundant PC(OH) species in the CNS of young and old Lymnaea.

Lipid class	Mean concentration in young (nM per g of tissue)	Mean concentration in old (nM per g of tissue)	p-value
PC[OH] OH-34:2	31.83244	7.020116	>0.9999
PC[OH] OH-34:1	42.81727	2.442759	>0.9999
PC[OH] OH-36:3	29.2214	10.21828	>0.9999

Table 8-8 PC(OH) species significantly increased in the CNS old Lymnaea (p < 0.0001, Species; p = 0.0005, Age; p < 0.0001, Interaction).

8.2.5 PE

Lipid Class	% Total lipid class in Young	% Total lipid class in Old
PE 18:1_18:1	1.18	0.08
PE 18:1_20:4	4.31	4.51
PE 18:0_20:5	5.10	4.54
PE 18:0_20:4	30.05	19.10
PE 38:3	4.00	5.37
PE 38:2	1.31	0.50
PE 20:4_20:2	8.96	10.37
PE 40:5	6.22	5.79
PE 40:4	4.89	4.00
PE 40:3	2.24	1.38

Table 8-9 The 10 most abundant PE species in the CNS of young and old Lymnaea.

Lipid class	Mean concentration in young (nM per g of tissue)	Mean concentration in old (nM per g of tissue)	p-value
PE 17:1_22:2	27.0828	96.0308	0.0027
PE 40:7	68.1853	284.7966	<0.0001
PE 20:4_20:2	117.3501	200.0859	<0.0001

Table 8-10 PE species significantly increased in the CNS old Lymnaea (p < 0.0001, Species; p < 0.0001, Age; p < 0.0001, Interaction).

8.2.6 Plasmanyl PE

Lipid Class	% Total lipid class in Young	% Total lipid class in Old
Plasmanyl-PE O-16:0_18:1	1.14	1.02
Plasmanyl-PE O-16:0_20:4	3.98	6.53
Plasmanyl-PE O-16:0_20:1	4.68	4.29
Plasmanyl-PE O-38:4	70.12	59.82
Plasmanyl-PE O-16:0_22:4	6.14	11.60
PE O-38:2	1.79	2.79
Plasmanyl-PE O-38:1	1.04	0.87
Plasmanyl-PE O-18:0_22:4	1.82	2.26
Plasmanyl-PE O-40:2	2.42	2.10
Plasmanyl-PE O-42:4	2.85	2.29

Table 8-11 The 10 most abundant Plasmanyl PE species in the CNS of young and old Lymnaea.

Lipid class	Mean concentration in young (nM per g of tissue)	Mean concentration in old (nM per g of tissue)	p-value
Plasmanyl-PE O-16:0_18:3	1.772073	1.427152	>0.9999
Plasmanyl-PE O-16:0_18:2	2.521924	2.916005	>0.9999
Plasmanyl-PE O-34:1	1.836087	3.417966	>0.9999
Plasmanyl-PE O-16:0_18:1	7.55204	7.422269	>0.9999
Plasmanyl-PE O-36:5	3.226099	5.546795	>0.9999
Plasmanyl-PE O-16:0_20:4	27.59008	47.4062	0.8774
Plasmanyl-PE O-36:3	2.182659	2.22256	>0.9999
PE O-36:2	3.140608	2.127931	>0.9999
Plasmanyl-PE O-16:0_20:1	31.18313	31.05013	>0.9999
Plasmanyl-PE O-36:1	3.958892	7.767803	>0.9999
Plasmanyl-PE O-18:0_20:5	0.553074	2.889235	>0.9999
Plasmanyl-PE O-16:0_22:5	7.233006	15.65801	>0.9999
Plasmanyl-PE O-38:4	476.2051	433.0823	0.0101
Plasmanyl-PE O-16:0_22:4	42.52346	84.12867	0.0153
PE O-38:2	12.02928	20.2584	>0.9999
Plasmanyl-PE O-38:1	6.793027	6.295621	>0.9999
Plasmanyl-PE O-38:1	1.154551	2.703358	>0.9999
Plasmanyl-PE O-18:0_22:4	12.64642	16.33395	>0.9999
Plasmanyl-PE O-40:2	16.48894	15.18516	>0.9999
Plasmanyl-PE O-42:4	19.53049	16.58911	>0.9999

Table 8-12 Plasmanyl PE species significantly increased in the CNS old Lymnaea (p <

0.0001, Species; p = 0.4073, Age; p = 0.1018, Interaction).

8.2.7 Plasmenyl PE

Lipid Class	% Total lipid class in Young	% Total lipid class in Old
Plasmenyl-PE P-16:0_18:1	4.04	2.77
Plasmenyl-PE P-16:0_20:4	9.91	12.10
Plasmenyl-PE P-16:0_20:3	2.72	2.06
PE O-36:2	2.77	1.66
Plasmenyl-PE P-36:1	7.48	5.24
Plasmenyl-PE P-38:4	4.46	2.37
Plasmenyl-PE P-16:0_22:4	25.08	27.70
Plasmenyl-PE P-38:1	7.41	10.72
Plasmenyl-PE P-18:0_22:4	16.10	10.76
Plasmenyl-PE P-40:4	4.01	5.36

Table 8-13 The 10 most abundant Plasmenyl PE species in the CNS of young and old

Lymnaea.

Lipid class	Mean concentration in young (nM per g of tissue)	Mean concentration in old (nM per g of tissue)	p-value
Plasmenyl-PE P-16:0_22:4	423.8168	545.2519	<0.0001
Plasmenyl-PE P-38:1	118.0093	211.5519	0.0022

Table 8-14 Plasmenyl PE species significantly increased in the CNS old Lymnaea (p <

0.0001, Species; p = 0.0177, Age; p = 0.0006, Interaction).

8.2.8 TG

Lipid Class	% Total lipid class in Young	% Total lipid class in Old
TG 50:1	2.53	1.23
TG 52:3	3.17	1.74
TG 52:2	3.57	1.89
TG 52:1	3.54	2.40
TG 53:1	2.29	2.44
TG 54:4	5.34	4.64
TG 54:3	4.02	2.53
TG 54:2	3.86	2.20
TG 56:4	3.33	2.68
TG 56:3	2.65	1.69

Table 8-15 The 10 most abundant TG species in the CNS of young and old Lymnaea.

Lipid class	Mean concentration in young (nM per g of tissue)	Mean concentration in old (nM per g of tissue)	p-value
TG 53:1	3.498902	6.182798	0.0345
TG 54:5	4.470868	7.219339	0.0249
TG 54:4	9.124361	11.77169	0.0413
TG 56:7	2.643364	5.254657	0.0492
TG 56:6	5.657929	9.871009	<0.0001
TG 56:5	7.192925	11.22743	<0.0001
TG 58:8	2.378569	5.510644	0.0031
TG 58:7	4.716324	7.481645	0.0228
TG 58:5	4.54691	8.522967	<0.0001
TG 60:9	1.617999	4.639396	0.0058

Table 8-16 TG species significantly increased in the CNS old Lymnaea ($p < 0.0001$, Species; $p < 0.0001$, Age; $p < 0.0001$, Interaction).

8.2.9 Alkanyl-TG

Lipid Class	% Total lipid class in Young	% Total lipid class in Old
Alkanyl-TG O-50:1	5.90	4.83
Alkanyl-TG O-16:0_17:0_18:1	4.02	3.87
Alkanyl-TG O-52:2	6.41	5.44
Alkanyl-TG O-52:1	14.47	13.03
Alkanyl-TG O-16:0_17:0_20:1	5.36	6.30
Alkanyl-TG O-54:3	6.00	4.56
Alkanyl-TG O-16:0_18:1_20:1	9.65	7.39
Alkanyl-TG O-16:0_18:0_20:1	4.07	2.89
Alkanyl-TG O-16:0_20:3_20:1	6.77	7.37
Alkanyl-TG O-16:0_20:1_20:1	4.77	4.57

Table 8-17 The 10 most abundant Alkanyl-TG species in the CNS of young and old Lymnaea.

Lipid class	Mean concentration in young (nM per mg of tissue)	Mean concentration in old (nM per mg of tissue)	p-value
Alkanyl-TG O-52:1	1.334889	1.626096	0.0117
Alkanyl-TG O-16:0_17:0_20:1	0.495151	0.785973	0.0119
Alkanyl-TG O-16:0_20:3_20:1	0.654634	0.918013	0.035
Alkanyl-TG O-16:0_20:1_22:4	0.519178	1.800914	<0.0001

Table 8-18 Alkanyl-TG species significantly increased in the CNS old Lymnaea ($p < 0.0001$, Species; $p < 0.0001$, Age; $p < 0.0001$, Interaction).

8.2.10 PG

Lipid Class	% Total lipid class in Young	% Total lipid class in Old
PG 31:0	4.11	2.61
PG 15:0_16:0	2.75	2.42
PG 32:1	2.34	1.61
PG 16:0_16:0	27.16	23.90
PG 16:0_17:0	3.61	4.20
PG 16:0_18:2	3.72	1.97
PG 17:0_18:1	6.87	8.14
PG 16:0_20:5	4.93	6.61
PG 16:0_20:4	9.22	12.30
PG 16:0_20:3	9.02	5.03

Table 8-19 The 10 most abundant PG species in the CNS of young and old Lymnaea.

Lipid class	Mean concentration in young (nM per g of tissue)	Mean concentration in old (nM per g of tissue)	p-value
PG 16:0_16:0	6.926687	12.42711	<0.0001
PG 16:0_17:0	0.936869	2.192537	0.0156
PG 17:0_18:1	1.767007	4.285888	<0.0001
PG 16:0_20:5	1.324246	3.432251	<0.0001
PG 16:0_20:4	2.46113	6.411469	<0.0001
PG 20:5_20:4	0.586396	2.557405	<0.0001
PG 20:4_20:4	0.44165	1.931835	0.0013

Table 8-20 PG species significantly increased in the CNS old Lymnaea ($p < 0.0001$, Species; $p < 0.0001$, Age; $p < 0.0001$, Interaction).

9 References

ADAMS, D. J., ARTHUR, C. P. & STOWELL, M. H. 2015. Architecture of the Synaptophysin/Synaptobrevin Complex: Structural Evidence for an Entropic Clustering Function at the Synapse. *Sci Rep,* 5**,** 13659.

ADAMS, R. & HARKINS, A. 2014. PC12 Cells that Lack Synaptotagmin I Exhibit Loss of a Subpool of Small Dense Core Vesicles. *Biophysical journal,* 107**,** 2838-49.

AGNATI, L. F., FUXE, K., ZOLI, M., OZINI, I., TOFFANO, G. & FERRAGUTI, F. 1986. A correlation analysis of the regional distribution of central enkephalin and beta-endorphin immunoreactive terminals and of opiate receptors in adult and old male rats. Evidence for the existence of two main types of communication in the central nervous system: the volume transmission and the wiring transmission. *Acta Physiol Scand,* 128**,** 201-7.

AHMAD, A. & DEY, L. 2007. A k-mean clustering algorithm for mixed numeric and categorical data. *Data & Knowledge Engineering,* 63**,** 503-527.

ALABI, A. A. & TSIEN, R. W. 2012. Synaptic vesicle pools and dynamics. *Cold Spring Harb Perspect Biol,* 4**,** a013680.

ALBERINI, C. M., BAMBAH-MUKKU, D. & CHEN, D. Y. 2012. *Memory consolidation and its underlying mechanisms*, World Scientific Publishing.

ALBILLOS, A., DERNICK, G., HORSTMANN, H., ALMERS, W., ALVAREZ DE TOLEDO, G. & LINDAU, M. 1997. The exocytotic event in chromaffin cells revealed by patch amperometry. *Nature,* 389**,** 509-12.

ALÉS, E., TABARES, L., POYATO, J. M., VALERO, V., LINDAU, M. & ALVAREZ DE TOLEDO, G. 1999. High calcium concentrations shift the mode of exocytosis to the kiss-and-run mechanism. *Nature Cell Biology,* 1**,** 40-44.

ALEXANDER JR, J., AUDESIRK, T. E. & AUDESIRK, G. J. 1984. One-trial reward learning in the snail Lymnea stagnalis. *Journal of neurobiology,* 15**,** 67-72.

ALEXANDER JR, J. E., AUDESIRK, T. E. & AUDESIRK, G. J. 1982. Rapid, nonaversive conditioning in a freshwater gastropod: II. Effects of temporal relationships on learning. *Behavioral and neural biology,* 36**,** 391-402.

ALTEN, B., GUZIKOWSKI, N. J., ZURAWSKI, Z., HAMM, H. E. & KAVALALI, E. T. 2022. Presynaptic mechanisms underlying GABAB-receptor-mediated inhibition of spontaneous neurotransmitter release. *Cell Reports,* 38**,** 110255.

ÁLVAREZ DE TOLEDO, G., MONTES, M., MONTENEGRO, P. & BORGES, R. 2018. Phases of the exocytotic fusion pore. *FEBS Lett,* 592**,** 3532-3541.

AMATORE, C., ARBAULT, S., BOURET, Y., GUILLE, M., LEMAÎTRE, F. & VERCHIER, Y. 2006. Regulation of Exocytosis in Chromaffin Cells by Trans-Insertion of Lysophosphatidylcholine and Arachidonic Acid into the Outer Leaflet of the Cell Membrane. *ChemBioChem,* 7**,** 1998-2003.

ANANTHARAM, A., AXELROD, D. & HOLZ, R. W. 2010a. Polarized TIRFM reveals changes in plasma membrane topology before and during granule fusion. *Cell Mol Neurobiol,* 30**,** 1343-9.

ANANTHARAM, A., ONOA, B., EDWARDS, R. H., HOLZ, R. W. & AXELROD, D. 2010b. Localized topological changes of the plasma membrane upon exocytosis visualized by polarized TIRFM. *J Cell Biol,* 188**,** 415-28.

ANDREAE, LAURA C. & BURRONE, J. 2015. Spontaneous Neurotransmitter Release Shapes Dendritic Arbors via Long-Range Activation of NMDA Receptors. *Cell Reports,* 10**,** 873-882.

ANDREAE, L. C. & BURRONE, J. 2018. The role of spontaneous neurotransmission in synapse and circuit development. *J Neurosci Res,* 96**,** 354-359.

AOYAGI, K., SUGAYA, T., UMEDA, M., YAMAMOTO, S., TERAKAWA, S. & TAKAHASHI, M. 2005. The activation of exocytotic sites by the formation of phosphatidylinositol 4, 5-bisphosphate microdomains at syntaxin clusters. *Journal of Biological Chemistry,* 280**,** 17346-17352.

ARCHER, D. A., GRAHAM, M. E. & BURGOYNE, R. D. 2002. Complexin regulates the closure of the fusion pore during regulated vesicle exocytosis. *J Biol Chem,* 277**,** 18249-52.

AREF, M., RANJBARI, E., ROMIANI, A. & EWING, A. G. 2020. Intracellular injection of phospholipids directly alters exocytosis and the fraction of chemical release in chromaffin cells as measured by nano-electrochemistry. *Chemical science,* 11**,** 11869-11876.

ARUNDELL, M., PATEL, B. A., STRAUB, V., ALLEN, M. C., JANSE, C., O'HARE, D., PARKER, K., GARD, P. R. & YEOMAN, M. S. 2006. Effects of age on feeding behavior and chemosensory processing in the pond snail, Lymnaea stagnalis. *Neurobiol Aging,* 27**,** 1880-91.

ASHTON, A. C. & USHKARYOV, Y. A. 2005. Properties of synaptic vesicle pools in mature central nerve terminals. *Journal of Biological Chemistry,* 280**,** 37278-37288.

ATLURI, P. P. & REGEHR, W. G. 1998. Delayed release of neurotransmitter from cerebellar granule cells. *J Neurosci,* 18**,** 8214-27.

AUDESIRK, G. 1985. Amine-containing neurons in the brain of Lymnaea stagnalis: Distribution and effects of precursors. *Comparative Biochemistry and Physiology Part A: Physiology,* 81**,** 359-365.

AUDESIRK, T. E., ALEXANDER JR, J. E., AUDESIRK, G. J. & MOYER, C. M. 1982. Rapid, nonaversive conditioning in a freshwater gastropod: I. Effects of age and motivation. *Behavioral and neural biology,* 36**,** 379-390.

AURELI, M., LOBERTO, N., LANTERI, P., CHIGORNO, V., PRINETTI, A. & SONNINO, S. 2011. Cell surface sphingolipid glycohydrolases in neuronal differentiation and aging in culture. *Journal of neurochemistry,* 116**,** 891-899.

AURELI, T., DI COCCO, M. E., CAPUANI, G., RICCIOLINI, R., MANETTI, C., MICCHELI, A. & CONTI, F. 2000. Effect of Long-Term Feeding with Acetyl-L-Carnitine on the Age-

Related Changes in Rat Brain Lipid Composition: A Study by 31P NMR Spectroscopy. *Neurochemical Research,* 25**,** 395-399.

BACH-MIZRACHI, H., UNDERWOOD, M. D., KASSIR, S. A., BAKALIAN, M. J., SIBILLE, E., TAMIR, H., MANN, J. J. & ARANGO, V. 2006. Neuronal Tryptophan Hydroxylase mRNA Expression in the Human Dorsal and Median Raphe Nuclei: Major Depression and Suicide. *Neuropsychopharmacology,* 31**,** 814-824.

BACH, M. E., BARAD, M., SON, H., ZHUO, M., LU, Y.-F., SHIH, R., MANSUY, I., HAWKINS, R. D. & KANDEL, E. R. 1999. Age-related defects in spatial memory are correlated with defects in the late phase of hippocampal long-term potentiation in vitro and are attenuated by drugs that enhance the cAMP signaling pathway. *Proceedings of the national academy of sciences,* 96**,** 5280-5285.

BAHJA, J., STEWART, N. A. & DYMOND, M. K. 2022. Oxidative stress is inhibited by plant-based supplements: A quantitative lipidomic analysis of antioxidant activity and lipid compositional change. *Advances in Redox Research,* 6**,** 100054.

BAI, J., WANG, C. T., RICHARDS, D. A., JACKSON, M. B. & CHAPMAN, E. R. 2004. Fusion pore dynamics are regulated by synaptotagmin*t-SNARE interactions. *Neuron,* 41**,** 929-42.

BAL, M., LEITZ, J., REESE, A. L., RAMIREZ, D. M., DURAKOGLUGIL, M., HERZ, J., MONTEGGIA, L. M. & KAVALALI, E. T. 2013a. Reelin mobilizes a VAMP7-dependent synaptic vesicle pool and selectively augments spontaneous neurotransmission. *Neuron,* 80**,** 934-46.

BAL, M., LEITZ, J., REESE, A. L., RAMIREZ, D. M., DURAKOGLUGIL, M., HERZ, J., MONTEGGIA, L. M. & KAVALALI, E. T. 2013b. Reelin mobilizes a VAMP7-dependent synaptic vesicle pool and selectively augments spontaneous neurotransmission. *Neuron,* 80**,** 934-946.

BARCLAY, J. W., CRAIG, T. J., FISHER, R. J., CIUFO, L. F., EVANS, G. J., MORGAN, A. & BURGOYNE, R. D. 2003. Phosphorylation of Munc18 by protein kinase C regulates the kinetics of exocytosis. *J Biol Chem,* 278**,** 10538-45.

BARNES, C., RAO, G. & HOUSTON, F. 2000. LTP induction threshold change in old rats at the perforant path–granule cell synapse. *Neurobiology of aging,* 21**,** 613-620.

BARRIA, A., DERKACH, V. & SODERLING, T. 1997a. Identification of the Ca2+/calmodulin-dependent protein kinase II regulatory phosphorylation site in the α-amino-3-hydroxyl-5-methyl4-isoxazole-propionate-type glutamate receptor. *Journal of Biological Chemistry,* 272**,** 32727-32730.

BARRIA, A., MULLER, D., DERKACH, V., GRIFFITH, L. C. & SODERLING, T. R. 1997b. Regulatory phosphorylation of AMPA-type glutamate receptors by CaM-KII during long-term potentiation. *Science,* 276**,** 2042-2045.

BAUER, C. S., WOOLLEY, R. J., TESCHEMACHER, A. G. & SEWARD, E. P. 2007. Potentiation of exocytosis by phospholipase C-coupled G-protein-coupled receptors requires the priming protein Munc13-1. *J Neurosci,* 27**,** 212-9.

BENJAMIN, P. 1989. Snail feeding oscillator: the central pattern generator and its control by modulatory interneurons. *Neuronal and cellular oscillators***,** 173-214.

BERBERIAN, K., TORRES, A. J., FANG, Q., KISLER, K. & LINDAU, M. 2009. F-actin and myosin II accelerate catecholamine release from chromaffin granules. *J Neurosci,* 29**,** 863-70.

BERTRAND, P. P. 2006. Real-time measurement of serotonin release and motility in guinea pig ileum. *The Journal of Physiology,* 577**,** 689-704.

BIRTHELMER, A., LAZARIS, A., SCHWEIZER, T., JACKISCH, R. & CASSEL, J. C. 2003a. Presynaptic regulation of neurotransmitter release in the cortex of aged rats with differential memory impairments. *Pharmacology Biochemistry and Behavior,* 75**,** 147-162.

BIRTHELMER, A., STEMMELIN, J., JACKISCH, R. & CASSEL, J. C. 2003b. Presynaptic modulation of acetylcholine, noradrenaline, and serotonin release in the hippocampus of aged rats with various levels of memory impairments. *Brain Research Bulletin,* 60**,** 283-296.

BŁASZCZYK, J. W. 2020. Energy Metabolism Decline in the Aging Brain-Pathogenesis of Neurodegenerative Disorders. *Metabolites,* 10.

BLIGH, E. G. & DYER, W. J. 1959. A rapid method of total lipid extraction and purification. *Canadian journal of biochemistry and physiology,* 37**,** 911-917.

BLISS, T. V., GARDNER-MEDWIN, A. & LØMO, T. 1973. Synaptic plasticity in the hippocampal formation. *Macromolecules and behaviour,* 193**,** 203.

BLISS, T. V. & LØMO, T. 1973. Long-lasting potentiation of synaptic transmission in the dentate area of the anaesthetized rabbit following stimulation of the perforant path. *The Journal of physiology,* 232**,** 331-356.

BLITZER, R. D., CONNOR, J. H., BROWN, G. P., WONG, T., SHENOLIKAR, S., IYENGAR, R. & LANDAU, E. M. 1998. Gating of CaMKII by cAMP-regulated protein phosphatase activity during LTP. *Science,* 280**,** 1940-1943.

BOCKAERT, J., FOZARD, J. R., DUMUIS, A. & CLARKE, D. E. 1992. The 5-HT4 receptor: a place in the sun. *Trends Pharmacol Sci,* 13**,** 141-5.

BOER, H., SCHOT, L., STEINBUSCH, H., MONTAGNE, C. & REICHELT, D. 1984. Co-existence of immunoreactivity to anti-dopamine, anti-serotonin and anti-vasotocin in the cerebral giant neuron of the pond snail Lymnaea stagnalis. *Cell and tissue research,* 238**,** 411-412.

BORIC, K., MUÑOZ, P., GALLAGHER, M. & KIRKWOOD, A. 2008. Potential adaptive function for altered long-term potentiation mechanisms in aging hippocampus. *Journal of Neuroscience,* 28**,** 8034-8039.

BRAVERMAN, N. E. & MOSER, A. B. 2012. Functions of plasmalogen lipids in health and disease. *Biochim Biophys Acta,* 1822**,** 1442-52.

BREDT, D. S. & NICOLL, R. A. 2003. AMPA receptor trafficking at excitatory synapses. *Neuron,* 40**,** 361-379.

BRICKMAN, A. & STERN, Y. 2009. Aging and memory in humans.

BRODDE, A., TEIGLER, A., BRUGGER, B., LEHMANN, W. D., WIELAND, F., BERGER, J. & JUST, W. W. 2012. Impaired neurotransmission in ether lipid-deficient nerve terminals. *Hum Mol Genet,* 21**,** 2713-24.

BROWN, W. J., CHAMBERS, K. & DOODY, A. 2003. Phospholipase A2 (PLA2) enzymes in membrane trafficking: mediators of membrane shape and function. *Traffic,* 4**,** 214-21.

BRUNS, D. & JAHN, R. 1995. Real-time measurement of transmitter release from single synaptic vesicles. *Nature,* 377**,** 62-5.

BRUNS, D., RIEDEL, D., KLINGAUF, J. & JAHN, R. 2000. Quantal release of serotonin. *Neuron,* 28**,** 205-20.

CAI, H., REIM, K., VAROQUEAUX, F., TAPECHUM, S., HILL, K., SØRENSEN, J. B., BROSE, N. & CHOW, R. H. 2008. Complexin II plays a positive role in Ca2+-triggered exocytosis by facilitating vesicle priming. *Proc Natl Acad Sci U S A,* 105**,** 19538-43.

CANAS, P. M., DUARTE, J. M., RODRIGUES, R. J., KÖFALVI, A. & CUNHA, R. A. 2009. Modification upon aging of the density of presynaptic modulation systems in the hippocampus. *Neurobiology of aging,* 30**,** 1877-1884.

CARAFOLI, E. 2010. The fateful encounter of mitochondria with calcium: how did it happen? *Biochimica et Biophysica Acta (BBA)-Bioenergetics,* 1797**,** 595-606.

CASSON, R. J. & FARMER, L. D. 2014. Understanding and checking the assumptions of linear regression: a primer for medical researchers. *Clinical & Experimental Ophthalmology,* 42**,** 590-596.

CASTILLO, P. E. 2012. Presynaptic LTP and LTD of excitatory and inhibitory synapses. *Cold Spring Harbor perspectives in biology,* 4**,** a005728.

CHAMBERLAIN, L. H., BURGOYNE, R. D. & GOULD, G. W. 2001. SNARE proteins are highly enriched in lipid rafts in PC12 cells: implications for the spatial control of exocytosis. *Proceedings of the National Academy of Sciences,* 98**,** 5619-5624.

CHAMBERLAIN, L. H. & GOULD, G. W. 2002. The vesicle-and target-SNARE proteins that mediate Glut4 vesicle fusion are localized in detergent-insoluble lipid rafts present on distinct intracellular membranes. *Journal of Biological Chemistry,* 277**,** 49750-49754.

CHANG, C. W., CHIANG, C. W. & JACKSON, M. B. 2017. Fusion pores and their control of neurotransmitter and hormone release. *J Gen Physiol,* 149**,** 301-322.

CHANG, C. W., HUI, E., BAI, J., BRUNS, D., CHAPMAN, E. R. & JACKSON, M. B. 2015. A structural role for the synaptobrevin 2 transmembrane domain in dense-core vesicle fusion pores. *J Neurosci,* 35**,** 5772-80.

CHANG, T. Y., LI, B. L., CHANG, C. C. & URANO, Y. 2009. Acyl-coenzyme A:cholesterol acyltransferases. *Am J Physiol Endocrinol Metab,* 297**,** E1-9.

CHANTURIYA, A., CHERNOMORDIK, L. V. & ZIMMERBERG, J. 1997. Flickering fusion pores comparable with initial exocytotic pores occur in protein-free phospholipid bilayers. *Proc Natl Acad Sci U S A,* 94**,** 14423-8.

CHEFER, V. I., THOMPSON, A. C., ZAPATA, A. & SHIPPENBERG, T. S. 2009. Overview of brain microdialysis. *Current protocols in neuroscience,* Chapter 7**,** Unit7.1-Unit7.1.

CHEN, B. T., PATEL, J. C., MORAN, K. A. & RICE, M. E. 2011. Differential calcium dependence of axonal versus somatodendritic dopamine release, with characteristics of both in the ventral tegmental area. *Front Syst Neurosci,* 5**,** 39.

CHEN, G. & EWING, A. G. 1995. Multiple classes of catecholamine vesicles observed during exocytosis from the Planorbis cell body. *Brain Research,* 701**,** 167-174.

CHEN, S. & KUCERNAK, A. 2002. The Voltammetric Response of Nanometer-Sized Carbon Electrodes. *The Journal of Physical Chemistry B,* 106**,** 9396-9404.

CHIANG, H. C., SHIN, W., ZHAO, W. D., HAMID, E., SHENG, J., BAYDYUK, M., WEN, P. J., JIN, A., MOMBOISSE, F. & WU, L. G. 2014. Post-fusion structural changes and their roles in exocytosis and endocytosis of dense-core vesicles. *Nat Commun,* 5**,** 3356.

CHOW, R. H., VON RÜDEN, L. & NEHER, E. 1992. Delay in vesicle fusion revealed by electrochemical monitoring of single secretory events in adrenal chromaffin cells. *Nature,* 356**,** 60-63.

CHURCHWARD, M. A., ROGASEVSKAIA, T., HÖFGEN, J., BAU, J. & COORSSEN, J. R. 2005. Cholesterol facilitates the native mechanism of Ca2+-triggered membrane fusion. *Journal of cell science,* 118**,** 4833-4848.

CLAYTON, D. A., MESCHES, M. H., ALVAREZ, E., BICKFORD, P. C. & BROWNING, M. D. 2002. A hippocampal NR2B deficit can mimic age-related changes in long-term potentiation and spatial learning in the Fischer 344 rat. *Journal of Neuroscience,* 22**,** 3628-3637.

COLGAN, L. A., CAVOLO, S. L., COMMONS, K. G. & LEVITAN, E. S. 2012. Action potential-independent and pharmacologically unique vesicular serotonin release from dendrites. *J Neurosci,* 32**,** 15737-46.

COLGAN, L. A., PUTZIER, I. & LEVITAN, E. S. 2009. Activity-Dependent Vesicular Monoamine Transporter-Mediated Depletion of the Nucleus Supports Somatic Release by Serotonin Neurons. *The Journal of Neuroscience,* 29**,** 15878-15887.

COLLIVER, T. L., PYOTT, S. J., ACHALABUN, M. & EWING, A. G. 2000. VMAT-Mediated Changes in Quantal Size and Vesicular Volume. *The Journal of Neuroscience,* 20**,** 5276-5282.

COMBS, C. A. & SHROFF, H. 2017. Fluorescence microscopy: a concise guide to current imaging methods. *Current protocols in neuroscience,* 79**,** 2.1. 1-2.1. 25.

COOPER, G. 2000. Structure of the plasma membrane. *Pages 529–540 in The Cell: A Molecular Approach.* Sinauer Assoc., Sunderland, MA.

COUSIN, M. A. & ROBINSON, P. J. 1999. Mechanisms of Synaptic Vesicle Recycling Illuminated by Fluorescent Dyes. *Journal of Neurochemistry,* 73**,** 2227-2239.

CRAIK, F. I. & ROSE, N. S. 2012. Memory encoding and aging: A neurocognitive perspective. *Neuroscience & Biobehavioral Reviews,* 36**,** 1729-1739.

CRAWFORD, D. C. & KAVALALI, E. T. 2015. Molecular Underpinnings of Synaptic Vesicle Pool Heterogeneity. *Traffic,* 16**,** 338-364.

CUMMINGS, D. D., WILCOX, K. S. & DICHTER, M. A. 1996. Calcium-dependent paired-pulse facilitation of miniature EPSC frequency accompanies depression of EPSCs at hippocampal synapses in culture. *J Neurosci,* 16**,** 5312-23.

CUTLER, R. G., KELLY, J., STORIE, K., PEDERSEN, W. A., TAMMARA, A., HATANPAA, K., TRONCOSO, J. C. & MATTSON, M. P. 2004. Involvement of oxidative stress-induced abnormalities in ceramide and cholesterol metabolism in brain aging and Alzheimer's disease. *Proceedings of the National Academy of Sciences,* 101**,** 2070-2075.

DARIOS, F., WASSER, C., SHAKIRZYANOVA, A., GINIATULLIN, A., GOODMAN, K., MUNOZ-BRAVO, J. L., RAINGO, J., JORGACEVSKI, J., KREFT, M., ZOREC, R., ROSA, J. M., GANDIA, L., GUTIÉRREZ, L. M., BINZ, T., GINIATULLIN, R., KAVALALI, E. T. & DAVLETOV, B. 2009. Sphingosine facilitates SNARE complex assembly and activates synaptic vesicle exocytosis. *Neuron,* 62**,** 683-94.

DAWKINS, M. 1974. Behavioural analysis of coordinated feeding movements in the gastropodLymnaea stagnalis (L.). *Journal of comparative physiology,* 92**,** 255-271.

DE-MIGUEL, F. F., LEON-PINZON, C., NOGUEZ, P. & MENDEZ, B. 2015. Serotonin release from the neuronal cell body and its long-lasting effects on the nervous system. *Philosophical Transactions of the Royal Society B: Biological Sciences,* 370**,** 20140196.

DE-MIGUEL, F. F., SANTAMARÍA-HOLEK, I., NOGUEZ, P., BUSTOS, C., HERNÁNDEZ-LEMUS, E. & RUBÍ, J. M. 2012. Biophysics of active vesicle transport, an intermediate step that couples excitation and exocytosis of serotonin in the neuronal soma. *PLoS One,* 7**,** e45454.

DE JONG, A. P. & FIORAVANTE, D. 2014. Translating neuronal activity at the synapse: presynaptic calcium sensors in short-term plasticity. *Front Cell Neurosci,* 8**,** 356.

DE JONG, A. P. H., MEIJER, M., SAARLOOS, I., CORNELISSE, L. N., TOONEN, R. F. G., SØRENSEN, J. B. & VERHAGE, M. 2016. Phosphorylation of synaptotagmin-1 controls a

post-priming step in PKC-dependent presynaptic plasticity. *Proceedings of the National Academy of Sciences,* 113**,** 5095-5100.

DE KOCK, C. P., CORNELISSE, L. N., BURNASHEV, N., LODDER, J. C., TIMMERMAN, A. J., COUEY, J. J., MANSVELDER, H. D. & BRUSSAARD, A. B. 2006. NMDA receptors trigger neurosecretion of 5-HT within dorsal raphe nucleus of the rat in the absence of action potential firing. *J Physiol,* 577**,** 891-905.

DEDKOVA, E., SIGOVA, A. & ZINCHENKO, V. 2000. Mechanism of action of calcium ionophores on intact cells: ionophore-resistant cells. *Membr cell biol,* 13**,** 357-368.

DEITCHER, D. L., UEDA, A., STEWART, B. A., BURGESS, R. W., KIDOKORO, Y. & SCHWARZ, T. L. 1998. Distinct requirements for evoked and spontaneous release of neurotransmitter are revealed by mutations in the Drosophila gene neuronal-synaptobrevin. *J Neurosci,* 18**,** 2028-39.

DEL CASTILLO, J. & KATZ, B. 1954. Quantal components of the end-plate potential. *J Physiol,* 124**,** 560-73.

DERKACH, V. A., OH, M. C., GUIRE, E. S. & SODERLING, T. R. 2007. Regulatory mechanisms of AMPA receptors in synaptic plasticity. *Nature Reviews Neuroscience,* 8**,** 101-113.

DERNICK, G., GONG, L. W., TABARES, L., ALVAREZ DE TOLEDO, G. & LINDAU, M. 2005. Patch amperometry: high-resolution measurements of single-vesicle fusion and release. *Nat Methods,* 2**,** 699-708.

DHARA, M., YARZAGARAY, A., MAKKE, M., SCHINDELDECKER, B., SCHWARZ, Y., SHAABAN, A., SHARMA, S., BÖCKMANN, R. A., LINDAU, M., MOHRMANN, R. & BRUNS, D. 2016. v-SNARE transmembrane domains function as catalysts for vesicle fusion. *Elife,* 5.

DI PAOLO, G., MOSKOWITZ, H. S., GIPSON, K., WENK, M. R., VORONOV, S., OBAYASHI, M., FLAVELL, R., FITZSIMONDS, R. M., RYAN, T. A. & DE CAMILLI, P. 2004. Impaired

PtdIns (4, 5) P 2 synthesis in nerve terminals produces defects in synaptic vesicle trafficking. *Nature,* 431**,** 415-422.

DILLON, C. & GODA, Y. 2005. The actin cytoskeleton: integrating form and function at the synapse. *Annu Rev Neurosci,* 28**,** 25-55.

DINGLEDINE, R., BORGES, K., BOWIE, D. & TRAYNELIS, S. F. 1999. The glutamate receptor ion channels. *Pharmacological reviews,* 51**,** 7-62.

DISTERHOFT, J. F., MOYER JR, J. R. & THOMPSON, L. T. 1994. The Calcium Rationale in Aging and Alzheimer's Disease: Evidence from an Animal Model of Normal Aging a. *Annals of the New York Academy of Sciences,* 747**,** 382-406.

DO, C. B. & BATZOGLOU, S. 2008. What is the expectation maximization algorithm? *Nature Biotechnology,* 26**,** 897-899.

DONG, Y., NING, G., EWING, A. G. & HEIEN, M. L. 2014. Pituitary adenylate cyclase activating polypeptide modulates catecholamine storage and exocytosis in PC12 cells. *PLoS One,* 9**,** e91132.

DORNINGER, F., FORSS-PETTER, S. & BERGER, J. 2017. From peroxisomal disorders to common neurodegenerative diseases - the role of ether phospholipids in the nervous system. *FEBS Lett,* 591**,** 2761-2788.

DOWHAN, W., BOGDANOV, M. & MILEYKOVSKAYA, E. 2008. CHAPTER 1 - Functional roles of lipids in membranes. *In:* VANCE, D. E. & VANCE, J. E. (eds.) *Biochemistry of Lipids, Lipoproteins and Membranes (Fifth Edition).* San Diego: Elsevier.

DRYHURST, G. 1990. Applications of electrochemistry in studies of the oxidation chemistry of central nervous system indoles. *Chemical Reviews,* 90**,** 795-811.

DUN, N. J. & MINOTA, S. 1982. Post-tetanic depolarization in sympathetic neurones of the guinea-pig. *J Physiol,* 323**,** 325-37.

EICHENBAUM, H. 2004. Hippocampus: cognitive processes and neural representations that underlie declarative memory. *Neuron,* 44**,** 109-120.

EICHENBAUM, H., DUDCHENKO, P., WOOD, E., SHAPIRO, M. & TANILA, H. 1999. The hippocampus, memory, and place cells: is it spatial memory or a memory space? *Neuron,* 23**,** 209-226.

ELEKES, K., VORONEZHSKAYA, E. E., HIRIPI, L., ECKERT, M. & RAPUS, J. 1996. Octopamine in the developing nervous system of the pond snail, Lymnaea stagnalis L. *Acta Biol Hung,* 47**,** 73-87.

ELHAMDANI, A., AZIZI, F. & ARTALEJO, C. R. 2006. Double patch clamp reveals that transient fusion (kiss-and-run) is a major mechanism of secretion in calf adrenal chromaffin cells: high calcium shifts the mechanism from kiss-and-run to complete fusion. *J Neurosci,* 26**,** 3030-6.

ELLIOTT, C. & BENJAMIN, P. 1985. Interactions of pattern-generating interneurons controlling feeding in Lymnaea stagnalis. *Journal of neurophysiology,* 54**,** 1396-1411.

EMRE, C., DO, K. V., JUN, B., HJORTH, E., ALCALDE, S. G., KAUTZMANN, M.-A. I., GORDON, W. C., NILSSON, P., BAZAN, N. G. & SCHULTZBERG, M. 2021. Age-related changes in brain phospholipids and bioactive lipids in the APP knock-in mouse model of Alzheimer's disease. *Acta Neuropathologica Communications,* 9**,** 116.

FAGAN-MURPHY, A., WATT, F., MORGAN, K. A. & PATEL, B. A. 2012. Influence of different biological environments on the stability of serotonin detection on carbon-based electrodes. *Journal of Electroanalytical Chemistry,* 684**,** 1-5.

FAHIM, M. A. & ROBBINS, N. 1982. Ultrastructural studies of young and old mouse neuromuscular junctions. *Journal of Neurocytology,* 11**,** 641-656.

FAHY, E., SUBRAMANIAM, S., BROWN, H. A., GLASS, C. K., MERRILL, A. H., JR., MURPHY, R. C., RAETZ, C. R., RUSSELL, D. W., SEYAMA, Y., SHAW, W., SHIMIZU, T., SPENER, F., VAN MEER, G., VANNIEUWENHZE, M. S., WHITE, S. H., WITZTUM, J. L. & DENNIS, E. A. 2005. A comprehensive classification system for lipids. *J Lipid Res,* 46**,** 839-61.

FALKENBURGER, B. H., JENSEN, J. B., DICKSON, E. J., SUH, B. C. & HILLE, B. 2010. Phosphoinositides: lipid regulators of membrane proteins. *J Physiol,* 588**,** 3179-85.

FARMER, B. C., WALSH, A. E., KLUEMPER, J. C. & JOHNSON, L. A. 2020. Lipid droplets in neurodegenerative disorders. *Frontiers in neuroscience,* 14**,** 742.

FAROOQUI, A. A. & HORROCKS, L. A. 2001. Plasmalogens: workhorse lipids of membranes in normal and injured neurons and glia. *Neuroscientist,* 7**,** 232-45.

FAROOQUI, A. A. & HORROCKS, L. A. 2006. Phospholipase A$_2$-Generated Lipid Mediators in the Brain: The Good, the Bad, and the Ugly. *The Neuroscientist,* 12**,** 245-260.

FATT, P. & KATZ, B. 1950. Some observations on biological noise. *Nature,* 166**,** 597-8.

FATT, P. & KATZ, B. 1951. An analysis of the end-plate potential recorded with an intracellular electrode. *J Physiol,* 115**,** 320-70.

FATT, P. & KATZ, B. 1952. Spontaneous subthreshold activity at motor nerve endings. *The Journal of physiology,* 117**,** 109-128.

FAVRELIÈRE, S., STADELMANN-INGRAND, S., HUGUET, F., DE JAVEL, D., PIRIOU, A., TALLINEAU, C. & DURAND, G. 2000. Age-related changes in ethanolamine glycerophospholipid fatty acid levels in rat frontal cortex and hippocampus. *Neurobiology of Aging,* 21**,** 653-660.

FERNANDEZ-ALFONSO, T. & RYAN, T. A. 2008. A heterogeneous "resting" pool of synaptic vesicles that is dynamically interchanged across boutons in mammalian CNS synapses. *Brain cell biology,* 36**,** 87-100.

FERNÁNDEZ-CHACÓN, R., KÖNIGSTORFER, A., GERBER, S. H., GARCÍA, J., MATOS, M. F., STEVENS, C. F., BROSE, N., RIZO, J., ROSENMUND, C. & SÜDHOF, T. C. 2001. Synaptotagmin I functions as a calcium regulator of release probability. *Nature,* 410**,** 41-9.

FERRETTI, M. E., SONETTI, D., PARESCHI, M. C., BUZZI, M., COLAMUSSI, M. L. & BIONDI, C. 1996. EFFECT OF SEROTONIN AND NEUROPEPTIDES ON ADENYLATE CYCLASE OF THE CENTRAL NERVOUS SYSTEM AND PERIPHERAL ORGANS OF THE FRESHWATER SNAIL PLANORBARIUS CORNEUS. *Neurochemistry International,* 28**,** 417-424.

FESCE, R., GROHOVAZ, F., VALTORTA, F. & MELDOLESI, J. 1994. Neurotransmitter release: fusion or 'kiss-and-run'? *Trends Cell Biol,* 4**,** 1-4.

FISHER, R. J., PEVSNER, J. & BURGOYNE, R. D. 2001. Control of fusion pore dynamics during exocytosis by Munc18. *Science,* 291**,** 875-8.

FITZGERALD, L. W., KAPLINSKY, L. & KIMELBERG, H. K. 1990. Serotonin metabolism by monoamine oxidase in rat primary astrocyte cultures. *J Neurochem,* 55**,** 2008-14.

FONSECA, J. R. & CARDOSO, M. G. 2007. Mixture-model cluster analysis using information theoretical criteria. *Intelligent Data Analysis,* 11**,** 155-173.

FUKUNAGA, K., MULLER, D. & MIYAMOTO, E. 1995. Increased phosphorylation of Ca2+/calmodulin-dependent protein kinase II and its endogenous substrates in the induction of long term potentiation. *Journal of Biological Chemistry,* 270**,** 6119-6124.

FULLER, N. & RAND, R. P. 2001. The influence of lysolipids on the spontaneous curvature and bending elasticity of phospholipid membranes. *Biophys J,* 81**,** 243-54.

GANESANA, M., LEE, S. T., WANG, Y. & VENTON, B. J. 2017. Analytical Techniques in Neuroscience: Recent Advances in Imaging, Separation, and Electrochemical Methods. *Analytical Chemistry,* 89**,** 314-341.

GARCIA-MARTINEZ, V., GIMENEZ-MOLINA, Y., VILLANUEVA, J., DARIOS, F. D., DAVLETOV, B. & GUTIÉRREZ, L. M. 2018. Emerging evidence for the modulation of exocytosis by signalling lipids. *FEBS Lett,* 592**,** 3493-3503.

GARCÍA-MARTÍNEZ, V., VILLANUEVA, J., TORREGROSA-HETLAND, C. J., BITTMAN, R., HIGDON, A., DARLEY-USMAR, V. M., DAVLETOV, B. & GUTIÉRREZ, L. M. 2013. Lipid Metabolites Enhance Secretion Acting on SNARE Microdomains and Altering the Extent and Kinetics of Single Release Events in Bovine Adrenal Chromaffin Cells. *PLOS ONE,* 8**,** e75845.

GEPPERT, M., GODA, Y., HAMMER, R. E., LI, C., ROSAHL, T. W., STEVENS, C. F. & SÜDHOF, T. C. 1994. Synaptotagmin I: a major Ca2+ sensor for transmitter release at a central synapse. *Cell,* 79**,** 717-27.

GIL, C., SOLER-JOVER, A., BLASI, J. & AGUILERA, J. 2005. Synaptic proteins and SNARE complexes are localized in lipid rafts from rat brain synaptosomes. *Biochem Biophys Res Commun,* 329**,** 117-24.

GILBERT-JOHNS, S., MASON, R., WARD, M. & HUMBY, P. 2022. Overview of the UK population: 2020. *Office for National Statistics: Newport, UK*

GIUSTO, N. M., ROQUE, M. E. & ILINCHETA DE BOSCHERO, M. G. 1992. Effects of aging on the content, composition and synthesis of sphingomyelin in the central nervous system. *Lipids,* 27**,** 835-839.

GRABNER, C. P., PRICE, S. D., LYSAKOWSKI, A. & FOX, A. P. 2005. Mouse Chromaffin Cells Have Two Populations of Dense Core Vesicles. *Journal of Neurophysiology,* 94**,** 2093-2104.

GRIMM, A. & ECKERT, A. 2017. Brain aging and neurodegeneration: from a mitochondrial point of view. *Journal of Neurochemistry,* 143**,** 418-431.

GU, C., LARSSON, A. & EWING, A. G. 2019. Plasticity in exocytosis revealed through the effects of repetitive stimuli affect the content of nanometer vesicles and the fraction of transmitter released. *Proceedings of the National Academy of Sciences,* 116**,** 21409-21415.

GU, C., PHILIPSEN, M. H. & EWING, A. G. 2020a. Mass Spectrometric Imaging of Plasma Membrane Lipid Alteration Correlated with Amperometrically Measured Activity-Dependent Plasticity in Exocytosis. *International Journal of Molecular Sciences,* 21**,** 9519.

GU, C., ZHANG, X. & EWING, A. G. 2020b. Comparison of Disk and Nanotip Electrodes for Measurement of Single-Cell Amperometry during Exocytotic Release. *Analytical Chemistry,* 92**,** 10268-10273.

GULYÁS-KOVÁCS, A., DE WIT, H., MILOSEVIC, I., KOCHUBEY, O., TOONEN, R., KLINGAUF, J., VERHAGE, M. & SØRENSEN, J. B. 2007. Munc18-1: sequential

interactions with the fusion machinery stimulate vesicle docking and priming. *J Neurosci,* 27**,** 8676-86.

GURR, M. & HARWOOD, J. 1991. Lipids as energy stores. *Lipid Biochemistry.* Springer.

HAIN, J., ONOUE, H., MAYRLEITNER, M., FLEISCHER, S. & SCHINDLER, H. 1995. Phosphorylation modulates the function of the calcium release channel of sarcoplasmic reticulum from cardiac muscle. *J Biol Chem,* 270**,** 2074-81.

HAN, X. & JACKSON, M. B. 2005. Electrostatic interactions between the syntaxin membrane anchor and neurotransmitter passing through the fusion pore. *Biophys J,* 88**,** L20-2.

HAN, X., WANG, C. T., BAI, J., CHAPMAN, E. R. & JACKSON, M. B. 2004. Transmembrane segments of syntaxin line the fusion pore of Ca2+-triggered exocytosis. *Science,* 304**,** 289-92.

HANCOCK, S. E., FRIEDRICH, M. G., MITCHELL, T. W., TRUSCOTT, R. J. W. & ELSE, P. L. 2022. Changes in Phospholipid Composition of the Human Cerebellum and Motor Cortex during Normal Ageing. *Nutrients,* 14.

HAQUE, M. E., MCINTOSH, T. J. & LENTZ, B. R. 2001. Influence of lipid composition on physical properties and peg-mediated fusion of curved and uncurved model membrane vesicles:"Nature's own" fusogenic lipid bilayer. *Biochemistry,* 40**,** 4340-4348.

HARADA, C. N., LOVE, M. C. N. & TRIEBEL, K. L. 2013. Normal cognitive aging. *Clinics in geriatric medicine,* 29**,** 737-752.

HARATA, N. C., ARAVANIS, A. M. & TSIEN, R. W. 2006. Kiss-and-run and full-collapse fusion as modes of exo-endocytosis in neurosecretion. *J Neurochem,* 97**,** 1546-70.

HATAMIE, A., REN, L., DOU, H., GANDASI, N. R., RORSMAN, P. & EWING, A. 2021. Nanoscale Amperometry Reveals that Only a Fraction of Vesicular Serotonin Content is Released During Exocytosis from Beta Cells. *Angewandte Chemie (International ed. in English),* 60**,** 7593-7596.

HATANPÄÄ, K., ISAACS, K. R., SHIRAO, T., BRADY, D. R. & RAPOPORT, S. I. 1999. Loss of Proteins Regulating Synaptic Plasticity in Normal Aging of the Human Brain and in Alzheimer Disease. *Journal of Neuropathology & Experimental Neurology,* 58**,** 637-643.

HAUGHEY, N. J., BANDARU, V. V., BAE, M. & MATTSON, M. P. 2010. Roles for dysfunctional sphingolipid metabolism in Alzheimer's disease neuropathogenesis. *Biochim Biophys Acta,* 1801**,** 878-86.

HE, X. & EWING, A. G. 2022. Simultaneous Counting of Molecules in the Halo and Dense-Core of Nanovesicles by Regulating Dynamics of Vesicle Opening. *Angewandte Chemie International Edition,* 61**,** e202116217.

HERMANN, P. M., LEE, A., HULLIGER, S., MINVIELLE, M., MA, B. & WILDERING, W. C. 2007. Impairment of long-term associative memory in aging snails (Lymnaea stagnalis). *Behav Neurosci,* 121**,** 1400-14.

HERMANN, P. M., PERRY, A. C., HAMAD, I. & WILDERING, W. C. 2020. Physiological and pharmacological characterization of a molluscan neuronal efflux transporter; evidence for age-related transporter impairment. *Journal of Experimental Biology,* 223.

HÉRY, F. & TERNAUX, J. P. 1981. Regulation of release processes in central serotoninergic neurons. *J Physiol (Paris),* 77**,** 287-301.

HÖGLUND, E., ØVERLI, Ø. & WINBERG, S. 2019. Tryptophan metabolic pathways and brain serotonergic activity: a comparative review. Front Endocrinol 10: 158.

HUFFMAN, M. L. & VENTON, B. J. 2009. Carbon-fiber microelectrodes for in vivo applications. *Analyst,* 134**,** 18-24.

HUITEMA, K., VAN DEN DIKKENBERG, J., BROUWERS, J. F. & HOLTHUIS, J. C. 2004. Identification of a family of animal sphingomyelin synthases. *The EMBO Journal,* 23**,** 33-44.

HUTCHINS, P. D., RUSSELL, J. D. & COON, J. J. 2018. LipiDex: an integrated software package for high-confidence lipid identification. *Cell systems,* 6**,** 621-625. e5.

IGBAVBOA, U., AVDULOV, N. A., SCHROEDER, F. & WOOD, W. G. 1996. Increasing age alters transbilayer fluidity and cholesterol asymmetry in synaptic plasma membranes of mice. *Journal of neurochemistry,* 66**,** 1717-1725.

ISLIMYE, E., GIRARD, V. & GOULD, A. P. 2022. Functions of Stress-Induced Lipid Droplets in the Nervous System. *Frontiers in Cell and Developmental Biology,* 10.

IWAMOTO, M., HAGISHITA, T., SHOJI-KASAI, Y., ANDO, S. & TANAKA, Y. 2004. Age-related changes in the levels of voltage-dependent calcium channels and other synaptic proteins in rat brain cortices. *Neuroscience Letters,* 366**,** 277-281.

JACK JR, C. R., LOWE, V. J., SENJEM, M. L., WEIGAND, S. D., KEMP, B. J., SHIUNG, M. M., KNOPMAN, D. S., BOEVE, B. F., KLUNK, W. E. & MATHIS, C. A. 2008. 11C PiB and structural MRI provide complementary information in imaging of Alzheimer's disease and amnestic mild cognitive impairment. *Brain,* 131**,** 665-680.

JACKSON, B. P., DIETZ, S. M. & WIGHTMAN, R. M. 1995. Fast-scan cyclic voltammetry of 5-hydroxytryptamine. *Analytical Chemistry,* 67**,** 1115-1120.

JACOBS, B. L. & AZMITIA, E. C. 1992. Structure and function of the brain serotonin system. *Physiol Rev,* 72**,** 165-229.

JACOBSSON, G., PELTO-HUIKKO, M. & MEISTER, B. 1998. Decreased mRNA levels for exocytotic proteins in the pituitary of aged rats. *Mechanisms of ageing and development,* 101**,** 33-41.

JAFFE, E. H., MARTY, A., SCHULTE, A. & CHOW, R. H. 1998. Extrasynaptic vesicular transmitter release from the somata of substantia nigra neurons in rat midbrain slices. *J Neurosci,* 18**,** 3548-53.

JAHN, R. & SÜDHOF, T. C. 1999. Membrane Fusion and Exocytosis. *Annual Review of Biochemistry,* 68**,** 863-911.

JAIN, A. K., MURTY, M. N. & FLYNN, P. J. 1999. Data clustering: a review. *ACM Comput. Surv.,* 31**,** 264–323.

JANG, Y. C. & VAN REMMEN, H. 2011. Age-associated alterations of the neuromuscular junction. *Experimental Gerontology,* 46**,** 193-198.

JIANG, Z. J., DELANEY, T. L., ZANIN, M. P., HABERBERGER, R. V., PITSON, S. M., HUANG, J., ALFORD, S., COLOGNA, S. M., KEATING, D. J. & GONG, L. W. 2019. Extracellular and intracellular sphingosine-1-phosphate distinctly regulates exocytosis in chromaffin cells. *J Neurochem,* 149**,** 729-746.

JOENSUU, M., WALLIS, T. P., SABER, S. H. & MEUNIER, F. A. 2020. Phospholipases in neuronal function: A role in learning and memory? *Journal of Neurochemistry,* 153**,** 300-333.

KAESER, P. S. & REGEHR, W. G. 2014. Molecular mechanisms for synchronous, asynchronous, and spontaneous neurotransmitter release. *Annu Rev Physiol,* 76**,** 333-63.

KATZ, B. & MILEDI, R. 1967. Ionic Requirements of Synaptic Transmitter Release. *Nature,* 215**,** 651-651.

KAUSHALYA, S. K., DESAI, R., ARUMUGAM, S., GHOSH, H., BALAJI, J. & MAITI, S. 2008. Three-photon microscopy shows that somatic release can be a quantitatively significant component of serotonergic neurotransmission in the mammalian brain. *J Neurosci Res,* 86**,** 3469-80.

KAVALALI, E. T. 2015. The mechanisms and functions of spontaneous neurotransmitter release. *Nature Reviews Neuroscience,* 16**,** 5-16.

KAWAGOE, K. T., JANKOWSKI, J. A. & WIGHTMAN, R. M. 1991. Etched carbon-fiber electrodes as amperometric detectors of catecholamine secretion from isolated biological cells. *Analytical Chemistry,* 63**,** 1589-1594.

KELLY, R. S. & WIGHTMAN, R. M. 1986. Bevelled carbon-fiber ultramicroelectrodes. *Analytica chimica acta,* 187**,** 79-87.

KEMENES, G., ELEKES, K., HIRIPI, L. & BENJAMIN, P. R. 1989. A comparison of four techniques for mapping the distribution of serotonin and serotonin-containing neurons in fixed and living ganglia of the snail, Lymnaea. *J Neurocytol,* 18**,** 193-208.

KEMENES, I., STRAUB, V. A., NIKITIN, E. S., STARAS, K., O'SHEA, M., KEMENES, G. & BENJAMIN, P. R. 2006a. Role of delayed nonsynaptic neuronal plasticity in long-term associative memory. *Curr Biol,* 16**,** 1269-79.

KEMENES, I., STRAUB, V. A., NIKITIN, E. S., STARAS, K., O'SHEA, M., KEMENES, G. & BENJAMIN, P. R. 2006b. Role of Delayed Nonsynaptic Neuronal Plasticity in Long-Term Associative Memory. *Current Biology,* 16**,** 1269-1279.

KENNEDY, B. K., BERGER, S. L., BRUNET, A., CAMPISI, J., CUERVO, A. M., EPEL, E. S., FRANCESCHI, C., LITHGOW, G. J., MORIMOTO, R. I. & PESSIN, J. E. 2014. Aging: a common driver of chronic diseases and a target for novel interventions. *Cell,* 159**,** 709.

KHACHATURIAN, Z. S. 1989. The role of calcium regulation in brain aging: reexamination of a hypothesis. *Aging Clinical and Experimental Research,* 1**,** 17-34.

KHUONG, THANG M., HABETS, RON L. P., KUENEN, S., WITKOWSKA, A., KASPROWICZ, J., SWERTS, J., JAHN, R., VAN DEN BOGAART, G. & VERSTREKEN, P. 2013. Synaptic PI(3,4,5)P3 Is Required for Syntaxin1A Clustering and Neurotransmitter Release. *Neuron,* 77**,** 1097-1108.

KLÖPPEL, S., KOVACS, G. G., VOIGTLÄNDER, T., WANSCHITZ, J., FLICKER, H., HAINFELLNER, J. A., GUENTCHEV, M. & BUDKA, H. 2001. Serotonergic nuclei of the raphe are not affected in human ageing. *Neuroreport,* 12**,** 669-71.

KOOIJMAN, E. E., CHUPIN, V., DE KRUIJFF, B. & BURGER, K. N. 2003. Modulation of membrane curvature by phosphatidic acid and lysophosphatidic acid. *Traffic,* 4**,** 162-74.

KOOIJMAN, E. E., CHUPIN, V., FULLER, N. L., KOZLOV, M. M., DE KRUIJFF, B., BURGER, K. N. & RAND, P. R. 2005. Spontaneous curvature of phosphatidic acid and lysophosphatidic acid. *Biochemistry,* 44**,** 2097-102.

KORINEK, M., GONZALEZ-GONZALEZ, I. M., SMEJKALOVA, T., HAJDUKOVIC, D., SKRENKOVA, K., KRUSEK, J., HORAK, M. & VYKLICKY, L. 2020. Cholesterol modulates presynaptic and postsynaptic properties of excitatory synaptic transmission. *Scientific Reports,* 10**,** 12651.

KORTE, M. & SCHMITZ, D. 2016. Cellular and system biology of memory: timing, molecules, and beyond. *Physiological reviews,* 96**,** 647-693.

KOUDINOV, A. R. & KOUDINOVA, N. V. 2001. Essential role for cholesterol in synaptic plasticity and neuronal degeneration. *The FASEB Journal,* 15**,** 1858-1860.

KOVACH, P. M., CAUDILL, W. L., PETERS, D. G. & WIGHTMAN, R. M. 1985. Faradaic electrochemistry at microcylinder, band, and tubular band electrodes. *Journal of Electroanalytical Chemistry and Interfacial Electrochemistry,* 185**,** 285-295.

KUFFLER, D. P., NICHOLLS, J. & DRAPEAU, P. 1987. Transmitter localization and vesicle turnover at a serotoninergic synapse between identified leech neurons in culture. *J Comp Neurol,* 256**,** 516-26.

KUMAR, A., THINSCHMIDT, J. S., FOSTER, T. C. & KING, M. A. 2007. Aging effects on the limits and stability of long-term synaptic potentiation and depression in rat hippocampal area CA1. *Journal of neurophysiology,* 98**,** 594-601.

LAM, A. D., TRYOEN-TOTH, P., TSAI, B., VITALE, N. & STUENKEL, E. L. 2008. SNARE-catalyzed fusion events are regulated by Syntaxin1A-lipid interactions. *Mol Biol Cell,* 19**,** 485-97.

LANDFIELD, P. W., CAMPBELL, L. W., HAO, S. Y. & KERR, D. S. 1989. Aging-Related Increases in Voltage-Sensitive, Inactivating Calcium Currents in Rat Hippocampus Implications for Mechanisms of Brain Aging and Alzheimer's Disease. *Annals of the New York Academy of Sciences,* 568**,** 95-105.

LANDFIELD, P. W. & PITLER, T. A. 1984. Prolonged Ca2+-dependent afterhyperpolarizations in hippocampal neurons of aged rats. *Science,* 226**,** 1089-1092.

LANDGRAF, R. & NEUMANN, I. D. 2004. Vasopressin and oxytocin release within the brain: a dynamic concept of multiple and variable modes of neuropeptide communication. *Front Neuroendocrinol,* 25**,** 150-76.

LANG, T., BRUNS, D., WENZEL, D., RIEDEL, D., HOLROYD, P., THIELE, C. & JAHN, R. 2001. SNAREs are concentrated in cholesterol-dependent clusters that define docking and fusion sites for exocytosis. *The EMBO journal,* 20**,** 2202-2213.

LARSSON, A., MAJDI, S., OLEINICK, A., SVIR, I., DUNEVALL, J., AMATORE, C. & EWING, A. G. 2020. Intracellular Electrochemical Nanomeasurements Reveal that Exocytosis of Molecules at Living Neurons is Subquantal and Complex. *Angewandte Chemie International Edition,* 59**,** 6711-6714.

LAURI, S. E., BORTOLOTTO, Z. A., BLEAKMAN, D., ORNSTEIN, P. L., LODGE, D., ISAAC, J. T. & COLLINGRIDGE, G. L. 2001. A critical role of a facilitatory presynaptic kainate receptor in mossy fiber LTP. *Neuron,* 32**,** 697-709.

LEDESMA, M. D., MARTIN, M. G. & DOTTI, C. G. 2012. Lipid changes in the aged brain: Effect on synaptic function and neuronal survival. *Progress in Lipid Research,* 51**,** 23-35.

LEE, S. B. & RHEE, S. G. 1995. Significance of PIP2 hydrolysis and regulation of phospholipase C isozymes. *Current Opinion in Cell Biology,* 7**,** 183-189.

LEE, T.-C. 1998. Biosynthesis and possible biological functions of plasmalogens. *Biochimica et Biophysica Acta (BBA) - Lipids and Lipid Metabolism,* 1394**,** 129-145.

LENG, G. & LUDWIG, M. 2008. Neurotransmitters and peptides: whispered secrets and public announcements. *J Physiol,* 586**,** 5625-32.

LEON-PINZON, C., CERCÓS, M. G., NOGUEZ, P., TRUETA, C. & DE-MIGUEL, F. F. 2014. Exocytosis of serotonin from the neuronal soma is sustained by a serotonin and calcium-dependent feedback loop. *Front Cell Neurosci,* 8**,** 169.

LEROUX-NICOLLET, I. & COSTENTIN, J. 1991. Evolution of the Vesicular Monoamine Transporter During Ageing in the Rat Brain: a Quantitative Autoradiographic Study with

3H Dihydrotetrabenazine. *In:* LANGER, S. Z., GALZIN, A. M. & COSTENTIN, J. (eds.) *Presynaptic Receptors and Neuronal Transporters.* Pergamon.

LESSIG, J. & FUCHS, B. 2009. Plasmalogens in biological systems: their role in oxidative processes in biological membranes, their contribution to pathological processes and aging and plasmalogen analysis. *Curr Med Chem,* 16**,** 2021-41.

LI, X., DUNEVALL, J. & EWING, A. G. 2016a. Using Single-Cell Amperometry To Reveal How Cisplatin Treatment Modulates the Release of Catecholamine Transmitters during Exocytosis. *Angew Chem Int Ed Engl,* 55**,** 9041-4.

LI, X., MAJDI, S., DUNEVALL, J., FATHALI, H. & EWING, A. G. 2015a. Quantitative measurement of transmitters in individual vesicles in the cytoplasm of single cells with nanotip electrodes. *Angewandte Chemie,* 127**,** 12146-12150.

LI, X., MAJDI, S., DUNEVALL, J., FATHALI, H. & EWING, A. G. 2015b. Quantitative measurement of transmitters in individual vesicles in the cytoplasm of single cells with nanotip electrodes. *Angew Chem Int Ed Engl,* 54**,** 11978-82.

LI, X., MOHAMMADI, A. S. & EWING, A. G. 2016b. Single cell amperometry reveals curcuminoids modulate the release of neurotransmitters during exocytosis from PC12 cells. *J Electroanal Chem (Lausanne),* 781**,** 30-35.

LI, X., REN, L., DUNEVALL, J., YE, D., WHITE, H. S., EDWARDS, M. A. & EWING, A. G. 2018. Nanopore Opening at Flat and Nanotip Conical Electrodes during Vesicle Impact Electrochemical Cytometry. *ACS Nano,* 12**,** 3010-3019.

LIMA, A. S., GU, C., HU, K. & EWING, A. G. 2021. Electrochemistry at and in single cells. *Electrochemistry for Bioanalysis.* Elsevier.

LIN, M. Z. & SCHNITZER, M. J. 2016. Genetically encoded indicators of neuronal activity. *Nat Neurosci,* 19**,** 1142-53.

LINETTI, A., FRATANGELI, A., TAVERNA, E., VALNEGRI, P., FRANCOLINI, M., CAPPELLO, V., MATTEOLI, M., PASSAFARO, M. & ROSA, P. 2010. Cholesterol reduction impairs exocytosis of synaptic vesicles. *Journal of Cell Science,* 123**,** 595-605.

LISCURN, L. 2002. Chapter 15 Cholesterol biosynthesis. *New Comprehensive Biochemistry.* Elsevier.

LLANO, I., GONZÁLEZ, J., CAPUTO, C., LAI, F. A., BLAYNEY, L. M., TAN, Y. P. & MARTY, A. 2000. Presynaptic calcium stores underlie large-amplitude miniature IPSCs and spontaneous calcium transients. *Nat Neurosci,* 3**,** 1256-65.

LLINAS, R. Calcium and transmitter release in squid synapse. Society for neuroscience symposia, 1977. Society for Neuroscience Bethesda, MD, 139-160.

LLINAS, R. & NICHOLSON, C. 1975. Calcium role in depolarization-secretion coupling: an aequorin study in squid giant synapse. *Proceedings of the National Academy of Sciences,* 72**,** 187-190.

LOHNER, K., BALGAVY, P., HERMETTER, A., PALTAUF, F. & LAGGNER, P. 1991. Stabilization of non-bilayer structures by the etherlipid ethanolamine plasmalogen. *Biochim Biophys Acta,* 1061**,** 132-40.

LOMIDZE, N., ZHVANIA, M. G., TIZABI, Y., JAPARIDZE, N., POCHKHIDZE, N., RZAYEV, F. & LORDKIPANIDZE, T. 2021. Aging affects cognition and hippocampal ultrastructure in male Wistar rats. *Developmental Neurobiology,* 81**,** 833-846.

LÓPEZ, G. H., ILINCHETA DE BOSCHERO, M. G., CASTAGNET, P. I. & GIUSTO, N. M. 1995. Age-associated changes in the content and fatty acid composition of brain glycerophospholipids. *Comparative Biochemistry and Physiology Part B: Biochemistry and Molecular Biology,* 112**,** 331-343.

LOVRIĆ, J., NAJAFINOBAR, N., DUNEVALL, J., MAJDI, S., SVIR, I., OLEINICK, A., AMATORE, C. & EWING, A. G. 2016. On the mechanism of electrochemical vesicle cytometry: chromaffin cell vesicles and liposomes. *Faraday Discussions,* 193**,** 65-79.

LUDWIG, M., APPS, D., MENZIES, J., PATEL, J. C. & RICE, M. E. 2016. Dendritic Release of Neurotransmitters. *Compr Physiol,* 7**,** 235-252.

LUDWIG, M., BULL, P. M., TOBIN, V. A., SABATIER, N., LANDGRAF, R., DAYANITHI, G. & LENG, G. 2005. Regulation of activity-dependent dendritic vasopressin release from rat supraoptic neurones. *J Physiol,* 564**,** 515-22.

LUDWIG, M. & LENG, G. 2006. Dendritic peptide release and peptide-dependent behaviours. *Nat Rev Neurosci,* 7**,** 126-36.

LUDWIG, M., SABATIER, N., BULL, P. M., LANDGRAF, R., DAYANITHI, G. & LENG, G. 2002. Intracellular calcium stores regulate activity-dependent neuropeptide release from dendrites. *Nature,* 418**,** 85-9.

MACHADO, D. J., MONTESINOS, M. S. & BORGES, R. 2008. Good Practices in Single-Cell Amperometry. *In:* IVANOV, A. I. (ed.) *Exocytosis and Endocytosis.* Totowa, NJ: Humana Press.

MAEDA, T., KANEKO, S., AKAIKE, A. & SATOH, M. 1997. Direct evidence for increase in excitatory amino acids release during mossy fiber LTP in rat hippocampal slices as revealed by the patch sensor methods. *Neuroscience letters,* 224**,** 103-106.

MAGOSKI, N. S., BAUCE, L. G., SYED, N. I. & BULLOCH, A. G. 1995. Dopaminergic transmission between identified neurons from the mollusk, Lymnaea stagnalis. *J Neurophysiol,* 74**,** 1287-300.

MAJDI, S., LARSSON, A., NAJAFINOBAR, N., BORGES, R. & EWING, A. G. 2019. Extracellular ATP Regulates the Vesicular Pore Opening in Chromaffin Cells and Increases the Fraction Released During Individual Exocytosis Events. *ACS Chem Neurosci,* 10**,** 2459-2466.

MAJDI, S., NAJAFINOBAR, N., DUNEVALL, J., LOVRIC, J. & EWING, A. G. 2017. DMSO Chemically Alters Cell Membranes to Slow Exocytosis and Increase the Fraction of Partial Transmitter Released. *ChemBioChem,* 18**,** 1898-1902.

MAKHINSON, M., CHOTINER, J. K., WATSON, J. B. & O'DELL, T. J. 1999. Adenylyl cyclase activation modulates activity-dependent changes in synaptic strength and

Ca2+/calmodulin-dependent kinase II autophosphorylation. *Journal of Neuroscience,* 19**,** 2500-2510.

MALENKA, R. C. & NICOLL, R. A. 1993. NMDA-receptor-dependent synaptic plasticity: multiple forms and mechanisms. *Trends in neurosciences,* 16**,** 521-527.

MANOCHA, L. M. 2001. Carbon Fibers. *In:* BUSCHOW, K. H. J., CAHN, R. W., FLEMINGS, M. C., ILSCHNER, B., KRAMER, E. J., MAHAJAN, S. & VEYSSIÈRE, P. (eds.) *Encyclopedia of Materials: Science and Technology.* Oxford: Elsevier.

MARSCHALLINGER, J., IRAM, T., ZARDENETA, M., LEE, S. E., LEHALLIER, B., HANEY, M. S., PLUVINAGE, J. V., MATHUR, V., HAHN, O., MORGENS, D. W., KIM, J., TEVINI, J., FELDER, T. K., WOLINSKI, H., BERTOZZI, C. R., BASSIK, M. C., AIGNER, L. & WYSS-CORAY, T. 2020. Lipid-droplet-accumulating microglia represent a dysfunctional and proinflammatory state in the aging brain. *Nature Neuroscience,* 23**,** 194-208.

MARSZALEK, P. E., FARRELL, B., VERDUGO, P. & FERNANDEZ, J. M. 1997. Kinetics of release of serotonin from isolated secretory granules. I. Amperometric detection of serotonin from electroporated granules. *Biophysical Journal,* 73**,** 1160-1168.

MARTIN, K. F., MARSDEN, C. A. & CRESPI, F. 1988. In vivo electrochemistry with carbon fibre electrodes: Principles and application to neuropharmacology. *TrAC Trends in Analytical Chemistry,* 7**,** 334-339.

MARTIN, M. G., PERGA, S., TROVÒ, L., RASOLA, A., HOLM, P., RANTAMÄKI, T., HARKANY, T., CASTRÉN, E., CHIARA, F. & DOTTI, C. G. 2008. Cholesterol loss enhances TrkB signaling in hippocampal neurons aging in vitro. *Molecular biology of the cell,* 19**,** 2101-2112.

MAXIMOV, A., LAO, Y., LI, H., CHEN, X., RIZO, J., SØRENSEN, J. B. & SÜDHOF, T. C. 2008. Genetic analysis of synaptotagmin-7 function in synaptic vesicle exocytosis. *Proc Natl Acad Sci U S A,* 105**,** 3986-91.

MCCAMAN, M. W., ONO, J. K. & MCCAMAN, R. E. 1984. 5-hydroxytryptamine measurements in molluscan ganglia and neurons using a modified radioenzymatic assay. *J Neurochem,* 43**,** 91-9.

MCCORMACK, J. G., HALESTRAP, A. P. & DENTON, R. M. 1990. Role of calcium ions in regulation of mammalian intramitochondrial metabolism. *Physiological reviews,* 70**,** 391-425.

MCGAHON, B. & LYNCH, M. A. 1996. The synergism between ACPD and arachidonic acid on glutamate release in hippocampus is age-dependent. *European journal of pharmacology,* 309**,** 323-326.

MCGAUGH, J. L. 2000. Memory--a century of consolidation. *Science,* 287**,** 248-251.

MEFFERT, M. K., PREMACK, B. A. & SCHULMAN, H. 1994. Nitric oxide stimulates Ca2+-independent synaptic vesicle release. *Neuron,* 12**,** 1235-1244.

MELLANDER, L. J., TROUILLON, R., SVENSSON, M. I. & EWING, A. G. 2012. Amperometric post spike feet reveal most exocytosis is via extended kiss-and-run fusion. *Sci Rep,* 2**,** 907.

MENDEZ, J. A., BOURQUE, M. J., FASANO, C., KORTLEVEN, C. & TRUDEAU, L. E. 2011. Somatodendritic dopamine release requires synaptotagmin 4 and 7 and the participation of voltage-gated calcium channels. *J Biol Chem,* 286**,** 23928-37.

MICHEL, M., KEMENES, I., MÜLLER, U. & KEMENES, G. 2008. Different phases of long-term memory require distinct temporal patterns of PKA activity after single-trial classical conditioning. *Learning & memory,* 15**,** 694-702.

MIDORIKAWA, M. & SAKABA, T. 2017. Kinetics of Releasable Synaptic Vesicles and Their Plastic Changes at Hippocampal Mossy Fiber Synapses. *Neuron,* 96**,** 1033-1040.e3.

MILHAS, D., CLARKE, C. J. & HANNUN, Y. A. 2010. Sphingomyelin metabolism at the plasma membrane: Implications for bioactive sphingolipids. *FEBS Letters,* 584**,** 1887-1894.

MILOSEVIC, I., SØRENSEN, J. B., LANG, T., KRAUSS, M., NAGY, G., HAUCKE, V., JAHN, R. & NEHER, E. 2005. Plasmalemmal phosphatidylinositol-4, 5-bisphosphate level regulates the releasable vesicle pool size in chromaffin cells. *Journal of Neuroscience,* 25**,** 2557-2565.

MILOVANOVIC, D. & JAHN, R. 2015. Organization and dynamics of SNARE proteins in the presynaptic membrane. *Frontiers in Physiology,* 6.

MONDAY, H. R. & CASTILLO, P. E. 2017. Closing the gap: long-term presynaptic plasticity in brain function and disease. *Current opinion in neurobiology,* 45**,** 106-112.

MONTESINOS, M. S., MACHADO, J. D., CAMACHO, M., DIAZ, J., MORALES, Y. G., ALVAREZ DE LA ROSA, D., CARMONA, E., CASTAÑEYRA, A., VIVEROS, O. H., O'CONNOR, D. T., MAHATA, S. K. & BORGES, R. 2008. The Crucial Role of Chromogranins in Storage and Exocytosis Revealed Using Chromaffin Cells from Chromogranin A Null Mouse. *The Journal of Neuroscience,* 28**,** 3350-3358.

MOORE-DOTSON, J. M., PAPKE, J. B. & HARKINS, A. B. 2010. Upregulation of synaptotagmin IV inhibits transmitter release in PC12 cells with targeted synaptotagmin I knockdown. *BMC Neurosci,* 11**,** 104.

MORGAN, A. J. & JACOB, R. 1994. Ionomycin enhances Ca2+ influx by stimulating store-regulated cation entry and not by a direct action at the plasma membrane. *Biochem J,* 300 (Pt 3)**,** 665-72.

MORGAN, L. D., MOHAMMED, A., PATEL, B. A., ARUNDELL, M., JENNERT-BURTSON, K., HERNÁDI, L., OVERALL, A., BOWLER, L. D., O'HARE, D. & YEOMAN, M. S. 2021. Decreased 14-3-3 expression correlates with age-related regional reductions in CNS dopamine and motor function in the pond snail, Lymnaea. *European Journal of Neuroscience,* 53**,** 1394-1411.

MORRISON, J. H. & HOF, P. R. 1997. Life and death of neurons in the aging brain. *Science,* 278**,** 412-419.

MOSHAROV, E. V. & SULZER, D. 2005. Analysis of exocytotic events recorded by amperometry. *Nat Methods,* 2**,** 651-8.

MOSTAFAVI, H., THIYAGARAJAN, S., STRATTON, B. S., KARATEKIN, E., WARNER, J. M., ROTHMAN, J. E. & O'SHAUGHNESSY, B. 2017. Entropic forces drive self-organization and membrane fusion by SNARE proteins. *Proc Natl Acad Sci U S A,* 114**,** 5455-5460.

MULAS, M., DEMURO, G., MULAS, C., PUTZOLU, M., CAVALLINI, G., DONATI, A., BERGAMINI, E. & DESSI, S. 2005. Dietary restriction counteracts age-related changes in cholesterol metabolism in the rat. *Mechanisms of ageing and development,* 126**,** 648-654.

MÜLLER, M. S., OBEL, L. F., WAAGEPETERSEN, H. S., SCHOUSBOE, A. & BAK, L. K. 2013. Complex Actions of Ionomycin in Cultured Cerebellar Astrocytes Affecting Both Calcium-Induced Calcium Release and Store-Operated Calcium Entry. *Neurochemical Research,* 38**,** 1260-1265.

MUNDORF, M. L. & WIGHTMAN, R. M. 2002. Amperometry and Cyclic Voltammetry with Carbon Fiber Microelectrodes at Single Cells. *Current Protocols in Neuroscience,* 18**,** 6.14.1-6.14.22.

NANAVATI, C., MARKIN, V. S., OBERHAUSER, A. F. & FERNANDEZ, J. M. 1992. The exocytotic fusion pore modeled as a lipidic pore. *Biophys J,* 63**,** 1118-32.

NAVAKKODE, S., LIU, C. & SOONG, T. W. 2018. Altered function of neuronal L-type calcium channels in ageing and neuroinflammation: Implications in age-related synaptic dysfunction and cognitive decline. *Ageing Research Reviews,* 42**,** 86-99.

NEATH, A. A. & CAVANAUGH, J. E. 2012. The Bayesian information criterion: background, derivation, and applications. *Wiley Interdisciplinary Reviews: Computational Statistics,* 4**,** 199-203.

NGATCHOU, A. N., KISLER, K., FANG, Q., WALTER, A. M., ZHAO, Y., BRUNS, D., SØRENSEN, J. B. & LINDAU, M. 2010. Role of the synaptobrevin C terminus in fusion pore formation. *Proc Natl Acad Sci U S A,* 107**,** 18463-8.

NICOLL, R. A. & SCHMITZ, D. 2005. Synaptic plasticity at hippocampal mossy fibre synapses. *Nature Reviews Neuroscience,* 6**,** 863-876.

NICOTRA, A., PIERUCCI, F., PARVEZ, H. & SENATORI, O. 2004. Monoamine Oxidase Expression During Development and Aging. *NeuroToxicology,* 25**,** 155-165.

NIKITIN, E. S., VAVOULIS, D. V., KEMENES, I., MARRA, V., PIRGER, Z., MICHEL, M., FENG, J., O'SHEA, M., BENJAMIN, P. R. & KEMENES, G. 2008. Persistent sodium current is a nonsynaptic substrate for long-term associative memory. *Curr Biol,* 18**,** 1221-6.

NÚÑEZ-SANTANA, F. L., OH, M. M., ANTION, M. D., LEE, A., HELL, J. W. & DISTERHOFT, J. F. 2014. Surface L-type C a2+ channel expression levels are increased in aged hippocampus. *Aging Cell,* 13**,** 111-120.

O'CARROLL, A.-M., FOWLER, C. J., PHILLIPS, J. P., TOBBIA, I. & TIPTON, K. F. 1983. The deamination of dopamine by human brain monoamine oxidase. *Naunyn-Schmiedeberg's Archives of Pharmacology,* 322**,** 198-202.

OCORR, K. A. & BYRNE, J. H. 1986. Evidence for separate receptors that mediate parallel effects of serotonin and small cardioactive peptideB (SCPB) on adenylate cyclase in Aplysia californica. *Neuroscience Letters,* 70**,** 283-288.

OH, M. M., SIMKIN, D. & DISTERHOFT, J. F. 2016. Intrinsic hippocampal excitability changes of opposite signs and different origins in CA1 and CA3 pyramidal neurons underlie aging-related cognitive deficits. *Frontiers in systems neuroscience,* 10**,** 52.

OLEINICK, A., HU, R., REN, B., TIAN, Z.-Q., SVIR, I. & AMATORE, C. 2015. Theoretical Model of Neurotransmitter Release during In Vivo Vesicular Exocytosis Based on a Grainy Biphasic Nano-Structuration of Chromogranins within Dense Core Matrixes. *Journal of The Electrochemical Society,* 163**,** H3014-H3024.

OMIATEK, D. M., DONG, Y., HEIEN, M. L. & EWING, A. G. 2010. Only a Fraction of Quantal Content is Released During Exocytosis as Revealed by Electrochemical Cytometry of Secretory Vesicles. *ACS Chem Neurosci,* 1**,** 234-245.

OROCK, A., LOGAN, S. & DEAK, F. 2020. Age-Related Cognitive Impairment: Role of Reduced Synaptobrevin-2 Levels in Deficits of Memory and Synaptic Plasticity. *J Gerontol A Biol Sci Med Sci,* 75**,** 1624-1632.

PANG, Z. P., BACAJ, T., YANG, X., ZHOU, P., XU, W. & SÜDHOF, T. C. 2011. Doc2 supports spontaneous synaptic transmission by a Ca(2+)-independent mechanism. *Neuron,* 70**,** 244-51.

PANG, Z. P., MELICOFF, E., PADGETT, D., LIU, Y., TEICH, A. F., DICKEY, B. F., LIN, W., ADACHI, R. & SÜDHOF, T. C. 2006. Synaptotagmin-2 is essential for survival and contributes to Ca2+ triggering of neurotransmitter release in central and neuromuscular synapses. *J Neurosci,* 26**,** 13493-504.

PANNESE, E. 2011. Morphological changes in nerve cells during normal aging. *Brain Structure and Function,* 216**,** 85-89.

PARK, D. C. & BISCHOF, G. N. 2022. The aging mind: neuroplasticity in response to cognitive training. *Dialogues in clinical neuroscience*.

PARK, D. C., LAUTENSCHLAGER, G., HEDDEN, T., DAVIDSON, N. S., SMITH, A. D. & SMITH, P. K. 2002. Models of visuospatial and verbal memory across the adult life span. *Psychology and aging,* 17**,** 299.

PATEL, B., ARUNDELL, M., ALLEN, M., GARD, P., O'HARE, D., PARKER, K. & YEOMAN, M. 2006. Changes in the properties of the modulatory cerebral giant cells contribute to aging in the feeding system of Lymnaea. *Neurobiology of aging,* 27**,** 1892-1901.

PATEL, B. A. 2021. *Electrochemistry for bioanalysis*, Elsevier.

PATEL, B. A., ARUNDELL, M., PARKER, K. H., YEOMAN, M. S. & O'HARE, D. 2010. Microelectrode investigation of neuroneal ageing from a single identified neurone. *Phys Chem Chem Phys,* 12**,** 10065-72.

PATEL, J. C., WITKOVSKY, P., AVSHALUMOV, M. V. & RICE, M. E. 2009. Mobilization of calcium from intracellular stores facilitates somatodendritic dopamine release. *J Neurosci,* 29**,** 6568-79.

PAUL, S., LANCASTER, G. I. & MEIKLE, P. J. 2019. Plasmalogens: A potential therapeutic target for neurodegenerative and cardiometabolic disease. *Progress in lipid research,* 74**,** 186-195.

PEDREGOSA, F., VAROQUAUX, G., GRAMFORT, A., MICHEL, V., THIRION, B., GRISEL, O., BLONDEL, M., PRETTENHOFER, P., WEISS, R. & DUBOURG, V. 2011. Scikit-learn: Machine learning in Python. *the Journal of machine Learning research,* 12**,** 2825-2830.

PELLEGRINO DE IRALDI, A. 1992. Compartmentalization of monoaminergic synaptic vesicles in the storage and release of neurotransmitter. *Molecular Neurobiology,* 6**,** 323-337.

PÉREZ-CÁCERES, D., CIUDAD-ROBERTS, A., RODRIGO, M. T., PUBILL, D., CAMINS, A., CAMARASA, J., ESCUBEDO, E. & PALLÀS, M. 2013. Depression-like behavior is dependent on age in male SAMP8 mice. *Biogerontology,* 14**,** 165-76.

PERSOON, C. M., MORO, A., NASSAL, J. P., FARINA, M., BROEKE, J. H., ARORA, S., DOMINGUEZ, N., VAN WEERING, J. R., TOONEN, R. F. & VERHAGE, M. 2018. Pool size estimations for dense-core vesicles in mammalian CNS neurons. *The EMBO Journal,* 37**,** e99672.

PIOMELLI, D., ASTARITA, G. & RAPAKA, R. 2007. A neuroscientist's guide to lipidomics. *Nature Reviews Neuroscience,* 8**,** 743-754.

PIRGER, Z., LASZLO, Z., HIRIPI, L., HERNADI, L., TOTH, G., LUBICS, A., REGLODI, D., KEMENES, G. & MARK, L. 2010a. Pituitary Adenylate Cyclase Activating Polypeptide (PACAP) and Its Receptors Are Present and Biochemically Active in the Central Nervous System of the Pond Snail Lymnaea stagnalis. *Journal of Molecular Neuroscience,* 42**,** 464-471.

PIRGER, Z., LÁSZLÓ, Z., KEMENES, I., TÓTH, G., REGLŐDI, D. & KEMENES, G. 2010b. A homolog of the vertebrate pituitary adenylate cyclase-activating polypeptide is both necessary and instructive for the rapid formation of associative memory in an invertebrate. *Journal of Neuroscience,* 30**,** 13766-13773.

PIRGER, Z., NASKAR, S., LÁSZLÓ, Z., KEMENES, G., REGLŐDI, D. & KEMENES, I. 2014. Reversal of age-related learning deficiency by the vertebrate PACAP and IGF-1 in a novel invertebrate model of aging: the pond snail (Lymnaea stagnalis). *J Gerontol A Biol Sci Med Sci,* 69**,** 1331-8.

PLUSKAL, T., CASTILLO, S., VILLAR-BRIONES, A. & ORESIC, M. 2010. MZmine 2: modular framework for processing, visualizing, and analyzing mass spectrometry-based molecular profile data. *BMC Bioinformatics,* 11**,** 395.

POW, D. V. & MORRIS, J. F. 1989. Dendrites of hypothalamic magnocellular neurons release neurohypophysial peptides by exocytosis. *Neuroscience,* 32**,** 435-9.

PRICE, D. 2019. *Modulation of feeding and its role in appetitive memory consolidation in Lymnaea stagnalis.* University of Sussex.

PRINETTI, A., CHIGORNO, V., PRIONI, S., LOBERTO, N., MARANO, N., TETTAMANTI, G. & SONNINO, S. 2001. Changes in the lipid turnover, composition, and organization, as sphingolipid-enriched membrane domains, in rat cerebellar granule cells developing in vitro. *Journal of Biological Chemistry,* 276**,** 21136-21145.

PROFT, J. & WEISS, N. 2015. Looking for answers to L-type calcium channels in the ageing brain (Commentary on Zanos et al.). *European Journal of Neuroscience,* 42**,** 2496-2498.

PUZIANOWSKA-KUZNICKA, M. & KUZNICKI, J. 2009. The ER and ageing II: Calcium homeostasis. *Ageing Research Reviews,* 8**,** 160-172.

QUENTIN, E., BELMER, A. & MAROTEAUX, L. 2018. Somato-Dendritic Regulation of Raphe Serotonin Neurons; A Key to Antidepressant Action. *Front Neurosci,* 12**,** 982.

R. G. JOHNSON, J. 1988. Accumulation of biological amines into chromaffin granules: a model for hormone and neurotransmitter transport. *Physiological Reviews,* 68**,** 232-307.

RABASCO, S., NGUYEN, T. D. K., GU, C., KURCZY, M. E., PHAN, N. T. N. & EWING, A. G. 2022. Localization and Absolute Quantification of Dopamine in Discrete Intravesicular

Compartments Using NanoSIMS Imaging. *International Journal of Molecular Sciences,* 23**,** 160.

RAMIREZ, D. M., KHVOTCHEV, M., TRAUTERMAN, B. & KAVALALI, E. T. 2012. Vti1a identifies a vesicle pool that preferentially recycles at rest and maintains spontaneous neurotransmission. *Neuron,* 73**,** 121-134.

REIGADA, D., XED, EZ, P., XE, REZ, I., GOROSTIZA, P., VERDAGUER, A., DE ARANDA, I. G., XF, MEZ, PINEDA, O., VILARRASA, J., MARSAL, J., BLASI, J., ALEU, J. & SOLSONA, C. 2003. Control of Neurotransmitter Release by an Internal Gel Matrix in Synaptic Vesicles. *Proceedings of the National Academy of Sciences of the United States of America,* 100**,** 3485-3490.

REN, L., DOWLATSHAHI POUR, M., MALMBERG, P. & EWING, A. G. 2019. Altered Lipid Composition of Secretory Cells Following Exposure to Zinc Can Be Correlated to Changes in Exocytosis. *Chemistry – A European Journal,* 25**,** 5406-5411.

REN, L., MELLANDER, L. J., KEIGHRON, J., CANS, A. S., KURCZY, M. E., SVIR, I., OLEINICK, A., AMATORE, C. & EWING, A. G. 2016. The evidence for open and closed exocytosis as the primary release mechanism. *Q Rev Biophys,* 49**,** e12.

REN, L., OLEINICK, A., SVIR, I., AMATORE, C. & EWING, A. G. 2020. Amperometric Measurements and Dynamic Models Reveal a Mechanism for How Zinc Alters Neurotransmitter Release. *Angewandte Chemie International Edition,* 59**,** 3083-3087.

REN, L., POUR, M. D., MAJDI, S., LI, X., MALMBERG, P. & EWING, A. G. 2017. Zinc Regulates Chemical-Transmitter Storage in Nanometer Vesicles and Exocytosis Dynamics as Measured by Amperometry. *Angew Chem Int Ed Engl,* 56**,** 4970-4975.

REYMANN, K. G. & FREY, J. U. 2007. The late maintenance of hippocampal LTP: requirements, phases,'synaptic tagging','late-associativity'and implications. *Neuropharmacology,* 52**,** 24-40.

RICE, M. E., CRAGG, S. J. & GREENFIELD, S. A. 1997. Characteristics of electrically evoked somatodendritic dopamine release in substantia nigra and ventral tegmental area in vitro. *J Neurophysiol,* 77**,** 853-62.

RICE, M. E., RICHARDS, C. D., NEDERGAARD, S., HOUNSGAARD, J., NICHOLSON, C. & GREENFIELD, S. A. 1994. Direct monitoring of dopamine and 5-HT release in substantia nigra and ventral tegmental area in vitro. *Exp Brain Res,* 100**,** 395-406.

RICKMAN, C. & DAVLETOV, B. 2005. Arachidonic Acid Allows SNARE Complex Formation in the Presence of Munc18. *Chemistry & Biology,* 12**,** 545-553.

RIDGWAY, N. D. 2016. Phospholipid synthesis in mammalian cells. *Biochemistry of lipids, lipoproteins and membranes.* Elsevier.

RIZO, J. & XU, J. 2015. The Synaptic Vesicle Release Machinery. *Annu Rev Biophys,* 44**,** 339-67.

RIZZOLI, S. O. & BETZ, W. J. 2005. Synaptic vesicle pools. *Nature Reviews Neuroscience,* 6**,** 57-69.

ROBERTSON, G. S., DAMSMA, G. & FIBIGER, H. C. 1991. Characterization of dopamine release in the substantia nigra by in vivo microdialysis in freely moving rats. *J Neurosci,* 11**,** 2209-16.

RODRIGUES, S., DESROCHES, M., KRUPA, M., CORTES, J. M., SEJNOWSKI, T. J. & ALI, A. B. 2016. Time-coded neurotransmitter release at excitatory and inhibitory synapses. *Proceedings of the National Academy of Sciences,* 113**,** E1108-E1115.

ROSE, R. & BENJAMIN, P. 1979. The relationship of the central motor pattern to the feeding cycle of Lymnaea stagnalis. *Journal of Experimental Biology,* 80**,** 137-163.

ROSE, R. M. & BENJAMIN, P. R. 1981. Interneuronal Control of Feeding in the Pond Snail Lymnaea Stagnalis: II. The Interneuronal Mechanism Generating Feeding Cycles. *Journal of Experimental Biology,* 92**,** 203-228.

RUTZ, S., MAJCHRZAK, M., SIEDSCHLAG, V., BARBELIVIEN, A., HARATI, H., ROTHMAIER, A. K., FEUERSTEIN, T. J., JACKISCH, R. & CASSEL, J.-C. 2009. The modulation of striatal dopamine release correlates with water-maze performance in aged rats. *Neurobiology of Aging,* 30**,** 957-972.

SAITO, Y. 1968. A Theoretical Study on the Diffusion Current at the Stationary Electrodes of Circular and Narrow Band Types. *Review of Polarography,* 15**,** 177-187.

SAKASHITA, N., MIYAZAKI, A., TAKEYA, M., HORIUCHI, S., CHANG, C. C. Y., CHANG, T.-Y. & TAKAHASHI, K. 2000. Localization of Human Acyl-Coenzyme A:Cholesterol Acyltransferase-1 (ACAT-1) in Macrophages and in Various Tissues. *The American Journal of Pathology,* 156**,** 227-236.

SALAND, L. C., SAMORA, A., SANCHEZ, P. & CHAVEZ, G. 1993. Immunocytochemical studies of tryptophan hydroxylase, tyrosine hydroxylase, and serotonin innervation in the aging rat neurointermediate pituitary. *Exp Neurol,* 121**,** 119-26.

SALAÜN, C., JAMES, D. J. & CHAMBERLAIN, L. H. 2004. Lipid rafts and the regulation of exocytosis. *Traffic,* 5**,** 255-64.

SALIO, C., LOSSI, L., FERRINI, F. & MERIGHI, A. 2006. Neuropeptides as synaptic transmitters. *Cell and Tissue Research,* 326**,** 583-598.

SALTHOUSE, T. 2012. Consequences of age-related cognitive declines. *Annual review of psychology,* 63**,** 201-226.

SCANDROGLIO, F., VENKATA, J. K., LOBERTO, N., PRIONI, S., SCHUCHMAN, E. H., CHIGORNO, V., PRINETTI, A. & SONNINO, S. 2008. Lipid content of brain, brain membrane lipid domains, and neurons from acid sphingomyelinase deficient mice. *J Neurochem,* 107**,** 329-38.

SCHIAVO, G., GU, Q.-M., PRESTWICH, G. D., SÖLLNER, T. H. & ROTHMAN, J. E. 1996. Calcium-dependent switching of the specificity of phosphoinositide binding to synaptotagmin. *Proceedings of the National Academy of Sciences,* 93**,** 13327-13332.

SCHIKORSKI, T. & STEVENS, C. F. 1997. Quantitative Ultrastructural Analysis of Hippocampal Excitatory Synapses. *The Journal of Neuroscience,* 17**,** 5858-5867.

SCHMITZ, D., MELLOR, J., BREUSTEDT, J. & NICOLL, R. A. 2003. Presynaptic kainate receptors impart an associative property to hippocampal mossy fiber long-term potentiation. *Nature neuroscience,* 6**,** 1058-1063.

SCHOONEVELDT, Y. L., PAUL, S., CALKIN, A. C. & MEIKLE, P. J. 2022. Ether Lipids in Obesity: From Cells to Population Studies. *Frontiers in Physiology***,** 163.

SCHULDINER, S., SHIRVAN, A. & LINIAL, M. 1995. Vesicular neurotransmitter transporters: from bacteria to humans. *Physiological Reviews,* 75**,** 369-392.

SCHULZ, D., SERGEEVA, O., IANOVSKII, E., LUHMANN, H., HAAS, H. & HUSTON, J. 2004. Behavioural parameters in aged rats are related to LTP and gene expression of ChAT and NMDA-NR2 subunits in the striatum. *European Journal of Neuroscience,* 19**,** 1373-1383.

SCUTT, G., ALLEN, M., KEMENES, G. & YEOMAN, M. 2015. A switch in the mode of the sodium/calcium exchanger underlies an age-related increase in the slow afterhyperpolarization. *Neurobiol Aging,* 36**,** 2838-49.

SEABOLD, S. & PERKTOLD, J. Statsmodels: Econometric and statistical modeling with python. Proceedings of the 9th Python in Science Conference, 2010. Austin, TX, 10.25080.

SHARMA, S. & LINDAU, M. 2018. The fusion pore, 60 years after the first cartoon. *FEBS Lett,* 592**,** 3542-3562.

SHARMA, S., SINGH, N., TOMAR, V. & CHANDRA, R. 2018. A review on electrochemical detection of serotonin based on surface modified electrodes. *Biosensors and Bioelectronics,* 107**,** 76-93.

SHEN, S., GEHLERT, D. R. & COLLIER, D. A. 2013. PACAP and PAC1 receptor in brain development and behavior. *Neuropeptides,* 47**,** 421-430.

SHI, L., SHEN, Q. T., KIEL, A., WANG, J., WANG, H. W., MELIA, T. J., ROTHMAN, J. E. & PINCET, F. 2012. SNARE proteins: one to fuse and three to keep the nascent fusion pore open. *Science,* 335**,** 1355-9.

SHIH, J. 1979. Monoamine oxidase in aging human brain. *Monoamine oxidase: structure, function and altered functions.* Academic Press New York.

SHIMOHAMA, S., FUJIMOTO, S., SUMIDA, Y., AKAGAWA, K., SHIRAO, T., MATSUOKA, Y. & TANIGUCHI, T. 1998. Differential Expression of Rat Brain Synaptic Proteins in Development and Aging. *Biochemical and Biophysical Research Communications,* 251**,** 394-398.

SHIN, W., GE, L., ARPINO, G., VILLARREAL, S. A., HAMID, E., LIU, H., ZHAO, W.-D., WEN, P. J., CHIANG, H.-C. & WU, L.-G. 2018. Visualization of Membrane Pore in Live Cells Reveals a Dynamic-Pore Theory Governing Fusion and Endocytosis. *Cell,* 173**,** 934-945.e12.

SHOUDAI, K., PETERS, J. H., MCDOUGALL, S. J., FAWLEY, J. A. & ANDRESEN, M. C. 2010. Thermally active TRPV1 tonically drives central spontaneous glutamate release. *J Neurosci,* 30**,** 14470-5.

SIMONS, K. & IKONEN, E. 1997. Functional rafts in cell membranes. *Nature,* 387**,** 569-572.

SINGLETON, S. T., O'DEA, J. J. & OSTERYOUNG, J. 1989. Analytical utility of cylindrical microelectrodes. *Analytical Chemistry,* 61**,** 1211-1215.

SKOWRONSKA-KRAWCZYK, D. & BUDIN, I. 2020. Aging membranes: unexplored functions for lipids in the lifespan of the central nervous system. *Experimental Gerontology,* 131**,** 110817.

SÖDERBERG, M., EDLUND, C., KRISTENSSON, K. & DALLNER, G. 1990. Lipid compositions of different regions of the human brain during aging. *Journal of neurochemistry,* 54**,** 415-423.

SODERLING, T. R. & DERKACH, V. A. 2000. Postsynaptic protein phosphorylation and LTP. *Trends in neurosciences,* 23**,** 75-80.

SODERO, A. O., WEISSMANN, C., LEDESMA, M. D. & DOTTI, C. G. 2011. Cellular stress from excitatory neurotransmission contributes to cholesterol loss in hippocampal neurons aging in vitro. *Neurobiology of aging,* 32**,** 1043-1053.

SOKAL, R. R. 1995. The principles and practice of statistics in biological research. *Biometry***,** 451-554.

SPARKS, D. L., WOELTZ, V. M. & MARKESBERY, W. R. 1991. Alterations in Brain Monoamine Oxidase Activity in Aging, Alzheimer's Disease, and Pick's Disease. *Archives of Neurology,* 48**,** 718-721.

SQUIRE, L. R. 2004. Memory systems of the brain: A brief history and current perspective. *Neurobiology of Learning and Memory,* 82**,** 171-177.

STARAS, K., GYŐRI, J. & KEMENES, G. 2002. Voltage-gated ionic currents in an identified modulatory cell type controlling molluscan feeding. *European Journal of Neuroscience,* 15**,** 109-119.

STEELMAN, Z. A., TOLSTYKH, G. P., ESTLACK, L. E., ROTH, C. C. & IBEY, B. L. The role of PIP2 and the IP3/DAG pathway in intracellular calcium release and cell survival during nanosecond electric pulse exposures. Energy-based Treatment of Tissue and Assessment VIII, 2015. SPIE, 255-260.

STRAND, A. M. & VENTON, B. J. 2008. Flame etching enhances the sensitivity of carbon-fiber microelectrodes. *Analytical chemistry,* 80**,** 3708-3715.

STREIN, T. G. & EWING, A. G. 1992. Characterization of submicron-sized carbon electrodes insulated with a phenol-allylphenol copolymer. *Analytical Chemistry,* 64**,** 1368-1373.

SÜDHOF, T. C. 2012. Calcium control of neurotransmitter release. *Cold Spring Harbor perspectives in biology,* 4**,** a011353.

SULZER, D. & EDWARDS, R. 2000. Vesicles: equal in neurotransmitter concentration but not in volume. *Neuron,* 28**,** 1-9.

SUN, J., PANG, Z. P., QIN, D., FAHIM, A. T., ADACHI, R. & SÜDHOF, T. C. 2007. A dual-Ca2+-sensor model for neurotransmitter release in a central synapse. *Nature,* 450**,** 676-82.

SUNADA, H., LUKOWIAK, K. & ITO, E. 2017. Cerebral giant cells are necessary for the formation and recall of memory of conditioned taste aversion in Lymnaea. *Zoological science,* 34**,** 72-80.

SUTTON, M. A. & SCHUMAN, E. M. 2006. Dendritic protein synthesis, synaptic plasticity, and memory. *Cell,* 127**,** 49-58.

SVENNERHOLM, L., BOSTRÖM, K., JUNGBJER, B. & OLSSON, L. 1994. Membrane lipids of adult human brain: lipid composition of frontal and temporal lobe in subjects of age 20 to 100 years. *Journal of neurochemistry,* 63**,** 1802-1811.

TABARES, L., LINDAU, M. & ALVAREZ DE TOLEDO, G. 2003. Relationship between fusion pore opening and release during mast cell exocytosis studied with patch amperometry. *Biochemical Society Transactions,* 31**,** 837-841.

TABER, K. H. & HURLEY, R. A. 2014. Volume transmission in the brain: beyond the synapse. *J Neuropsychiatry Clin Neurosci,* 26**,** iv, 1-4.

TALEAT, Z., LARSSON, A. & EWING, A. G. 2019. Anticancer Drug Tamoxifen Affects Catecholamine Transmitter Release and Storage from Single Cells. *ACS Chemical Neuroscience,* 10**,** 2060-2069.

TANAKA, Y., HASEGAWA, A. & ANDO, S. 1996. Impaired synaptic functions with aging as characterized by decreased calcium influx and acetylcholine release. *Journal of Neuroscience Research,* 43**,** 63-70.

TARASKA, J. W. & ALMERS, W. 2004. Bilayers merge even when exocytosis is transient. *Proc Natl Acad Sci U S A,* 101**,** 8780-5.

TAUPENOT, L., HARPER, K. L. & O'CONNOR, D. T. 2003. The Chromogranin–Secretogranin Family. *New England Journal of Medicine,* 348**,** 1134-1149.

TIMIRAS, P. S., HUDSON, D. B. & SEGALL, P. E. 1984. Lifetime brain serotonin: regional effects of age and precursor availability. *Neurobiol Aging,* 5**,** 235-42.

TOBIN, V. A. & LUDWIG, M. 2007. The role of the actin cytoskeleton in oxytocin and vasopressin release from rat supraoptic nucleus neurons. *J Physiol,* 582**,** 1337-48.

TROUILLON, R. L. & EWING, A. G. 2014. Actin controls the vesicular fraction of dopamine released during extended kiss and run exocytosis. *ACS chemical biology,* 9**,** 812-820.

TROVÒ, L., VAN VELDHOVEN, P. P., MARTÍN, M. G. & DOTTI, C. G. 2011. Sphingomyelin upregulation in mature neurons contributes to TrkB activity by Rac1 endocytosis. *Journal of cell science,* 124**,** 1308-1315.

TRUETA, C., KUFFLER, D. P. & DE-MIGUEL, F. F. 2012. Cycling of dense core vesicles involved in somatic exocytosis of serotonin by leech neurons. *Front Physiol,* 3**,** 175.

TRUETA, C., MÉNDEZ, B. & DE-MIGUEL, F. F. 2003. Somatic exocytosis of serotonin mediated by L-type calcium channels in cultured leech neurones. *J Physiol,* 547**,** 405-16.

TWARKOWSKI, H. & MANAHAN-VAUGHAN, D. 2016. Loss of catecholaminergic neuromodulation of persistent forms of hippocampal synaptic plasticity with increasing age. *Frontiers in Synaptic Neuroscience,* 8**,** 30.

UCHIYAMA, Y., MAXSON, M. M., SAWADA, T., NAKANO, A. & EWING, A. G. 2007. Phospholipid mediated plasticity in exocytosis observed in PC12 cells. *Brain Res,* 1151**,** 46-54.

ULMANN, L., MIMOUNI, V., ROUX, S., PORSOLT, R. & POISSON, J.-P. 2001. Brain and hippocampus fatty acid composition in phospholipid classes of aged-relative cognitive deficit rats. *Prostaglandins, Leukotrienes and Essential Fatty Acids (PLEFA),* 64**,** 189-195.

UNDIEH, A. S. 2010. Pharmacology of signaling induced by dopamine D(1)-like receptor activation. *Pharmacol Ther,* 128**,** 37-60.

USLU, B. & OZKAN, S. A. 2007. Electroanalytical Application of Carbon Based Electrodes to the Pharmaceuticals. *Analytical Letters,* 40**,** 817-853.

VALSECCHI, M., CHIGORNO, V., NICOLINI, M. & SONNINO, S. 1996. Changes of free long-chain bases in neuronal cells during differentiation and aging in culture. *Journal of neurochemistry,* 67**,** 1866-1871.

VAN BLITTERSWIJK, W. J., VAN DER LUIT, A. H., VELDMAN, R. J., VERHEIJ, M. & BORST, J. 2003. Ceramide: second messenger or modulator of membrane structure and dynamics? *Biochem J,* 369**,** 199-211.

VAN DER KLOOT, W. & MOLGÓ, J. 1993. Facilitation and delayed release at about 0 degree C at the frog neuromuscular junction: effects of calcium chelators, calcium transport inhibitors, and okadaic acid. *J Neurophysiol,* 69**,** 717-29.

VAN DER VEEN, J. N., KENNELLY, J. P., WAN, S., VANCE, J. E., VANCE, D. E. & JACOBS, R. L. 2017. The critical role of phosphatidylcholine and phosphatidylethanolamine metabolism in health and disease. *Biochimica et Biophysica Acta (BBA) - Biomembranes,* 1859**,** 1558-1572.

VAN KEMPEN, G. T., VANDERLEEST, H. T., VAN DEN BERG, R. J., EILERS, P. & WESTERINK, R. H. 2011. Three distinct modes of exocytosis revealed by amperometry in neuroendocrine cells. *Biophys J,* 100**,** 968-77.

VANGUILDER, H. D., YAN, H., FARLEY, J. A., SONNTAG, W. E. & FREEMAN, W. M. 2010. Aging alters the expression of neurotransmission-regulating proteins in the hippocampal synaptoproteome. *J Neurochem,* 113**,** 1577-88.

VANTERPOOL, C. K., VANTERPOOL, E. A., PEARCE, W. J. & BUCHHOLZ, J. N. 2006. Advancing age alters the expression of the ryanodine receptor 3 isoform in adult rat superior cervical ganglia. *J Appl Physiol (1985),* 101**,** 392-400.

VEHOVSZKY, Á., SZABÓ, H. & ELLIOTT, C. J. H. 2005. Octopamine increases the excitability of neurons in the snail feeding system by modulation of inward sodium current but not outward potassium currents. *BMC Neuroscience,* 6**,** 70.

VELÁZQUEZ-ULLOA, N., BLACKSHAW, S. E., SZCZUPAK, L., TRUETA, C., GARCÍA, E. & DE-MIGUEL, F. F. 2003. Convergence of mechanosensory inputs onto neuromodulatory serotonergic neurons in the leech. *J Neurobiol,* 54**,** 604-17.

VERKHRATSKY, A., SHMIGOL, A., KIRISCHUK, S., PRONCHUK, N. & KOSTYUK, P. 1994. Age-dependent changes in calcium currents and calcium homeostasis in mammalian neurons. *Ann N Y Acad Sci,* 747**,** 365-81.

VERKHRATSKY, A. & TOESCU, E. C. 1998. Calcium and neuronal ageing. *Trends in neurosciences,* 21**,** 2-7.

VITALE, M. L., SEWARD, E. P. & TRIFARÓ, J. M. 1995. Chromaffin cell cortical actin network dynamics control the size of the release-ready vesicle pool and the initial rate of exocytosis. *Neuron,* 14**,** 353-63.

VOLCHEGORSKII, I. A., SHEMYAKOV, S. E., TURYGIN, V. V. & MALINOVSKAYA, N. V. 2001. Comparative analysis of age-related changes in activities of monoamine oxidase-B and antioxidant defense enzymes in various structures of human brain. *Bull Exp Biol Med,* 132**,** 760-2.

VOLZ, T. J., FARNSWORTH, S. J., ROWLEY, S. D., HANSON, G. R. & FLECKENSTEIN, A. E. 2009. Age-dependent differences in dopamine transporter and vesicular monoamine transporter-2 function and their implications for methamphetamine neurotoxicity. *Synapse,* 63**,** 147-51.

WANG, C., TU, J., ZHANG, S., CAI, B., LIU, Z., HOU, S., LIU, Z., DIAO, J., ZHU, Z.-J., LIU, C. & LI, D. 2019. Membrane association of VAMP2 SNARE motif in cells and its regulation by different lipid phases of synaptic vesicle membrane. *bioRxiv***,** 587766.

WANG, C. T., BAI, J., CHANG, P. Y., CHAPMAN, E. R. & JACKSON, M. B. 2006. Synaptotagmin-Ca2+ triggers two sequential steps in regulated exocytosis in rat PC12 cells: fusion pore opening and fusion pore dilation. *J Physiol,* 570**,** 295-307.

WANG, C. T., GRISHANIN, R., EARLES, C. A., CHANG, P. Y., MARTIN, T. F., CHAPMAN, E. R. & JACKSON, M. B. 2001. Synaptotagmin modulation of fusion pore kinetics in regulated exocytosis of dense-core vesicles. *Science,* 294**,** 1111-5.

WANG, J. 2006. Analytical electrochemistry. *New York, USA: Wiley,* 10**,** 0471790303.

WANG, N., KWAN, C., GONG, X., DE CHAVES, E. P., TSE, A. & TSE, F. W. 2010. Influence of cholesterol on catecholamine release from the fusion pore of large dense core chromaffin granules. *J Neurosci,* 30**,** 3904-11.

WANG, Y. & EWING, A. 2021. Electrochemical Quantification of Neurotransmitters in Single Live Cell Vesicles Shows Exocytosis is Predominantly Partial. *Chembiochem,* 22**,** 807-813.

WANG, Y., GU, C. & EWING, A. G. 2021. A multimodal electrochemical approach to measure the effect of zinc on vesicular content and exocytosis in a single cell model of ischemia. *QRB Discovery,* 2**,** e12.

WANG, Y., GU, C. & EWING, A. G. 2022. Single-Vesicle Electrochemistry Following Repetitive Stimulation Reveals a Mechanism for Plasticity Changes with Iron Deficiency. *Angewandte Chemie International Edition,* 61**,** e202200716.

WATSON, S. N., RISLING, T. E., HERMANN, P. M. & WILDERING, W. C. 2012. Failure of delayed nonsynaptic neuronal plasticity underlies age-associated long-term associative memory impairment. *BMC Neuroscience,* 13**,** 103.

WATSON, S. N., WRIGHT, N., HERMANN, P. M. & WILDERING, W. C. 2013. Phospholipase A2: The key to reversing long-term memory impairment in a gastropod model of aging. *Neurobiology of Aging,* 34**,** 610-620.

WEISSKOPF, M. G. & NICOLL, R. A. 1995. Presynaptic changes during mossy fibre LTP revealed by NMDA receptor-mediated synaptic responses. *Nature,* 376**,** 256-259.

WEN, H., LINHOFF, M. W., MCGINLEY, M. J., LI, G. L., CORSON, G. M., MANDEL, G. & BREHM, P. 2010. Distinct roles for two synaptotagmin isoforms in synchronous and asynchronous transmitter release at zebrafish neuromuscular junction. *Proc Natl Acad Sci U S A,* 107**,** 13906-11.

WENK, M. R. & DE CAMILLI, P. 2004. Protein-lipid interactions and phosphoinositide metabolism in membrane traffic: insights from vesicle recycling in nerve terminals. *Proceedings of the National Academy of Sciences,* 101**,** 8262-8269.

WESTERINK, R. H., KLOMPMAKERS, A. A., WESTENBERG, H. G. & VIJVERBERG, H. P. 2002. Signaling pathways involved in Ca2+- and Pb2+-induced vesicular catecholamine release from rat PC12 cells. *Brain Res,* 957**,** 25-36.

WESTERINK, R. H. S., DE GROOT, A. & VIJVERBERG, H. P. M. 2000. Heterogeneity of Catecholamine-Containing Vesicles in PC12 Cells. *Biochemical and Biophysical Research Communications,* 270**,** 625-630.

WESTLUND, K. N., DENNEY, R. M., ROSE, R. M. & ABELL, C. W. 1988. Localization of distinct monoamine oxidase A and monoamine oxidase B cell populations in human brainstem. *Neuroscience,* 25**,** 439-56.

WIGHTMAN, R. M., JANKOWSKI, J. A., KENNEDY, R. T., KAWAGOE, K. T., SCHROEDER, T. J., LESZCZYSZYN, D. J., NEAR, J. A., DILIBERTO, E. J., JR. & VIVEROS, O. H. 1991. Temporally resolved catecholamine spikes correspond to single vesicle release from individual chromaffin cells. *Proc Natl Acad Sci U S A,* 88**,** 10754-8.

WIGHTMAN, R. M., SCHROEDER, T. J., FINNEGAN, J. M., CIOLKOWSKI, E. L. & PIHEL, K. 1995. Time course of release of catecholamines from individual vesicles during exocytosis at adrenal medullary cells. *Biophysical Journal,* 68**,** 383.

WIGHTMAN, R. M., TROYER, K. P., MUNDORF, M. L. & CATAHAN, R. 2002. The association of vesicular contents and its effects on release. *Ann N Y Acad Sci,* 971**,** 620-6.

WILLIAMS, C., CHEN, W., LEE, C. H., YAEGER, D., VYLETA, N. P. & SMITH, S. M. 2012. Coactivation of multiple tightly coupled calcium channels triggers spontaneous release of GABA. *Nat Neurosci,* 15**,** 1195-7.

WITCHER, D. R., KOVACS, R. J., SCHULMAN, H., CEFALI, D. C. & JONES, L. R. 1991. Unique phosphorylation site on the cardiac ryanodine receptor regulates calcium channel activity. *J Biol Chem,* 266**,** 11144-52.

WITKOVSKY, P., PATEL, J. C., LEE, C. R. & RICE, M. E. 2009. Immunocytochemical identification of proteins involved in dopamine release from the somatodendritic compartment of nigral dopaminergic neurons. *Neuroscience,* 164**,** 488-96.

WU, Q., ZHANG, Q., LIU, B., LI, Y., WU, X., KUO, S., ZHENG, L., WANG, C., ZHU, F. & ZHOU, Z. 2019. Dynamin 1 Restrains Vesicular Release to a Subquantal Mode In Mammalian Adrenal Chromaffin Cells. *The Journal of Neuroscience,* 39**,** 199-211.

XU, J., MASHIMO, T. & SÜDHOF, T. C. 2007. Synaptotagmin-1,-2, and-9: Ca2+ sensors for fast release that specify distinct presynaptic properties in subsets of neurons. *Neuron,* 54**,** 567-581.

XU, J., PANG, Z. P., SHIN, O. H. & SÜDHOF, T. C. 2009. Synaptotagmin-1 functions as a Ca2+ sensor for spontaneous release. *Nat Neurosci,* 12**,** 759-66.

YAFFE, D., FORREST, L. R. & SCHULDINER, S. 2018. The ins and outs of vesicular monoamine transporters. *J Gen Physiol,* 150**,** 671-682.

YAMAMOTO, N., MATSUBARA, T., SATO, T. & YANAGISAWA, K. 2008. Age-dependent high-density clustering of GM1 ganglioside at presynaptic neuritic terminals promotes amyloid β-protein fibrillogenesis. *Biochimica et Biophysica Acta (BBA)-Biomembranes,* 1778**,** 2717-2726.

YANG, L., LIANG, J., LAM, S. M., YAVUZ, A., SHUI, G., DING, M. & HUANG, X. 2020. Neuronal lipolysis participates in PUFA-mediated neural function and neurodegeneration. *EMBO reports,* 21**,** e50214.

YAO, J., GAFFANEY, J. D., KWON, S. E. & CHAPMAN, E. R. 2011. Doc2 is a Ca2+ sensor required for asynchronous neurotransmitter release. *Cell,* 147**,** 666-77.

YE, D. & EWING, A. 2018. On the Action of General Anesthetics on Cellular Function: Barbiturate Alters the Exocytosis of Catecholamines in a Model Cell System. *ChemPhysChem,* 19**,** 1173-1179.

YE, D., GU, C. & EWING, A. 2018. Using Single-Cell Amperometry and Intracellular Vesicle Impact Electrochemical Cytometry To Shed Light on the Biphasic Effects of Lidocaine on Exocytosis. *ACS Chemical Neuroscience,* 9**,** 2941-2947.

YEOMAN, M. S., KEMENES, G., BENJAMIN, P. R. & ELLIOTT, C. J. 1994a. Modulatory role for the serotonergic cerebral giant cells in the feeding system of the snail, Lymnaea. II. Photoinactivation. *Journal of Neurophysiology,* 72**,** 1372-1382.

YEOMAN, M. S., PIENEMAN, A. W., FERGUSON, G. P., MAAT, A. T. & BENJAMIN, P. R. 1994b. Modulatory role for the serotonergic cerebral giant cells in the feeding system of the snail, Lymnaea. I. Fine wire recording in the intact animal and pharmacology. *Journal of Neurophysiology,* 72**,** 1357-1371.

ZALUTSKY, R. A. & NICOLL, R. A. 1990. Comparison of two forms of long-term potentiation in single hippocampal neurons. *Science,* 248**,** 1619-1624.

ZAMBRZYCKA, A. 2004. Aging decreases phosphatidylinositol-4, 5-bis-phosphate level but has no effect on activities of phosphoinositide kinases. *Pol. J. Pharmacol,* 56**,** 651-654.

ZHANG, Q., LIU, B., WU, Q., LIU, B., LI, Y., SUN, S., WANG, Y., WU, X., CHAI, Z., JIANG, X., LIU, X., HU, M., WANG, Y., YANG, Y., WANG, L., KANG, X., XIONG, Y., ZHOU, Y., CHEN, X., ZHENG, L., ZHANG, B., WANG, C., ZHU, F. & ZHOU, Z. 2019. Differential Co-release of Two Neurotransmitters from a Vesicle Fusion Pore in Mammalian Adrenal Chromaffin Cells. *Neuron,* 102**,** 173-183.e4.

ZHANG, Z., WU, Y., WANG, Z., DUNNING, F. M., REHFUSS, J., RAMANAN, D., CHAPMAN, E. R. & JACKSON, M. B. 2011. Release mode of large and small dense-core vesicles

specified by different synaptotagmin isoforms in PC12 cells. *Molecular biology of the cell,* 22**,** 2324-2336.

ZHAO, Y., FANG, Q., HERBST, A. D., BERBERIAN, K. N., ALMERS, W. & LINDAU, M. 2013. Rapid structural change in synaptosomal-associated protein 25 (SNAP25) precedes the fusion of single vesicles with the plasma membrane in live chromaffin cells. *Proc Natl Acad Sci U S A,* 110**,** 14249-54.

ZHOU, Y., WU, H., LI, S., CHEN, Q., CHENG, X.-W., ZHENG, J., TAKEMORI, H. & XIONG, Z.-Q. 2006. Requirement of TORC1 for late-phase long-term potentiation in the hippocampus. *PloS one,* 1**,** e16.

ZHOU, Z., MISLER, S. & CHOW, R. H. 1996. Rapid fluctuations in transmitter release from single vesicles in bovine adrenal chromaffin cells. *Biophysical Journal,* 70**,** 1543-1552.

ZHU, W., GU, C., DUNEVALL, J., REN, L., ZHOU, X. & EWING, A. G. 2019. Combined Amperometry and Electrochemical Cytometry Reveal Differential Effects of Cocaine and Methylphenidate on Exocytosis and the Fraction of Chemical Release. *Angew Chem Int Ed Engl,* 58**,** 4238-4242.

ZSILLA, G., ZELLES, T., MIKE, A., KÉKES-SZABÓ, A., MILUSHEVA, E. & VIZI, E. S. 1994. Differential changes in presynaptic modulation of transmitter release during aging. *International Journal of Developmental Neuroscience,* 12**,** 107-115.